

Title	A seismic study on the structural evolution of the North Celtic Sea Basin, offshore Ireland
Authors	Byrne, Keith B.
Publication date	2020-01-01
Original Citation	Byrne, K. B. 2020. A seismic study on the structural evolution of the North Celtic Sea Basin, offshore Ireland. MRes Thesis, University College Cork.
Type of publication	Masters thesis (Research)
Rights	© 2020, Keith B. Byrne. - https://creativecommons.org/licenses/by-nc-nd/4.0/
Download date	2023-05-07 16:26:29
Item downloaded from	http://hdl.handle.net/10468/11306

Ollscoil na hÉireann, Corcaigh

National University of Ireland, Cork



**A Seismic Study on the Structural Evolution of the
North Celtic Sea Basin, Offshore Ireland.**

Thesis presented by

Keith B. Byrne

for the degree of

Master by Research

University College Cork

School of Biological, Earth and Environmental Sciences.

Head of School: Prof. Andrew Wheeler

Supervisors: Dr. Patrick A. Meere & Dr. Kieran F. Mulchrone

Submitted January 2020

Acknowledgements

Thanks to Providence Resources Plc for sponsoring this research project and to the staff and consultants for numerous discussions and feedback. Particular thanks to Jakub Czarcinski for assistance with drafting several figures and to Fergal Murphy and John Donato for editorial advice. Seismic data is presented courtesy of Schlumberger Multiclient, Providence Resources Plc. and Lansdowne Oil and Gas Plc. Access to and permission to publish released seismic and well data was provided by the Department of Communications, Climate Action and Environment. The guidance and support of my supervisors Pat and Kieran was always available and always appreciated, keeping me on the straight and narrow amongst the wiggles of seismic. To Aisling, my best friend and wife, thanks for giving me the time and support to complete this research project, I may have enjoyed the research, but I recognise the sacrifices you've made along the way.

Table of Contents

Abstract	23
1 Introduction	25
2 Literature Review	29
2.1 NCSB Structural Development	29
2.1.1 NCSB Literature Review Summary	50
2.2 Faulting and Rifting	52
2.2.1 Geometry and growth of faults	52
2.2.2 Extensional Fault Models	54
2.2.3 Contractional Faults	55
2.2.4 Rifting models	56
2.2.5 Rift Geometry	59
2.3 Halokinesis and decollements.	61
3 Regional Geology of the NCSB	65
4 Hydrocarbon Exploration History	73
5 Analysis of Previous Structural Models	76
5.1 Conventional Steer's Head Geometry	77
5.2 Half Graben Geometry	82
5.3 Requirements of an updated model	88
6 Methodology	89
6.1 Seismic Data Quality	89

6.2	Seismic Database.....	94
6.3	Seismic Dataloading.....	98
6.4	Seismic Data Examples	102
6.5	Well database	113
6.6	Seismic Interpretation.....	118
6.6.1	Interpretation Stage 1	119
6.6.2	Interpretation Stage 2	120
6.6.3	Interpretation Stage 3	131
6.6.4	Interpretation Stage 4	131
6.6.5	Interpretation Stage 5	132
7	Results	137
7.1	Stratigraphy	144
7.1.1	Palaeozoic Basement.....	144
7.1.2	Triassic	147
7.1.3	Lower Jurassic.....	159
7.1.4	Upper Jurassic	164
7.1.5	Lower Cretaceous.....	170
7.1.6	Upper Cretaceous - Cenozoic	175
7.2	Faults	181
7.2.1	Morrigan Fault	184
7.2.2	Dagda Fault	187

7.2.3	Brigit Fault	187
7.2.4	Aonghus Fault	188
7.3	Basin Evolution Observations	188
8	Revised Structural Model.....	195
9	Discussion	213
9.1	Reservoir Potential	214
9.1.1	Lower Jurassic.....	214
9.1.2	Upper Jurassic	218
9.2	Source Potential.....	222
9.3	Renewed Interest	222
10	Conclusions	227
11	Recommendations For Further Study	229
	References Cited	230
	Appendix A	255
	Appendix B	258
	Appendix C	266
	Appendix D	267
	Appendix E.1	268
	Appendix E.2	268
	Appendix E.3	268
	Appendix E.4	268

Appendix E.5	268
Appendix E.6	268
Appendix F.1	269
Appendix F.2	269
Appendix F.3	269
Appendix F.4	269
Appendix F.5	269
Appendix F.6	269
Appendix G.1	270
Appendix G.2	270
Appendix G.3	270
Appendix G.4	270
Appendix G.5	270
Appendix G.6	270

Figures

Figure 1-1. Location map showing offshore sedimentary basins south of Ireland, highlighting the study area, drilled wells and relevant hydrocarbon discoveries. (Source Dept. of Communications, Climate Action & Environment).....	28
Figure 2-1. Location of COOLE profile 6 & 7 overlain on freeair gravity, showing location of NNW flexure identified by O'Reilly <i>et al.</i> (1991).....	39
Figure 2-2. COOLE seismic refraction models showing NNW basement flexure on Profile 7 (O'Reilly <i>et al.</i> , 1991), numbers shown are crustal velocities in km/s.	40
Figure 2-3. Location of SWAT and VARNET lines overlain on freeair gravity..	48
Figure 2-4. Interpretation of SWAT 5 seismic line across the NCSB. (V.F.) is the proposed location of the Variscan Front (Dyment <i>et al.</i> , 1990).....	48
Figure 2-5. Differences between fault distribution in half – and full-grabens based on data from Lake Tanganyika (Morley, 1995).	61
Figure 3-1. Freeair gravity map with regional Palaeozoic tectonic trends evident; (A) NE-SW trend, (B) W-E trend, (C) NW-SE trend.	67
Figure 3-2. Generalised lithostratigraphy of the NCSB, modified from O'Sullivan (2001).	71
Figure 3-3. Triassic to Cretaceous chronostratigraphy of the NCSB, (Copestake <i>et al.</i> , 2018).	72
Figure 4-1. Map showing location of all wells in the North Celtic Sea Basin and adjacent basins. Key wells used in this study are highlighted in red. Producing gas fields are also highlighted in pink. (Source Dept. of Communications, Climate Action & Environment; DCCAE 2019).	74

Figure 4-2. Details of hydrocarbon exploration and appraisal wells drilled per year in the NCSB. (Source Dept. of Communications, Climate Action & Environment; DCCAE 2019).....	75
Figure 5-1. Conventional graben model proposed by Tucker & Arter (1987) (general model presented) overlain over SWAT-5 seismic line. The model shows a localised Cenozoic package and an inversion fold within the Cretaceous. The Lower Jurassic thins towards the southeast, more representative of a half-graben while the Lower Cretaceous thickens to the southeast with no explanation for the change. Interpretation at the Jurassic and Triassic level do not accurately reflect the seismic data.	79
Figure 5-2. Conventional graben model proposed by Coward & Trudgill (1989) using SWAT-5 seismic line. The model incorrectly places the Top Jurassic at or close to the Base Chalk in the known wells. Faults and horizon interpretation can also be seen to cross-cut continuous seismic events at several places, in particular the Triassic interpretation in the basin centre.	80
Figure 5-3. Conventional graben model using MPCR-17 seismic line, proposed by McMahon & Turner (1998) overlain over SWAT-5 seismic line. The model interprets a basin sag phase in the Lower and Upper Cretaceous but does not show the compressional features known to exist at this level. The deeper interpretation is also inconsistent with the modern seismic data.....	81
Figure 5-4. Half graben model proposed by Petrie <i>et al.</i> (1989) (general model presented) overlain over SWAT-5 seismic line. The model interprets a half graben sediment wedge at the Triassic however the Lower and Upper Jurassic section has	

growth accommodated evenly on several faults across the basin which is inconsistent with a half graben.....	84
Figure 5-5. Half graben model proposed by Musgrove <i>et al.</i> (1995) (general model presented) overlain over SWAT-5 seismic line. The interpretation only addresses the Triassic section, but is consistent with the seismic data and the interpretation of other authors.....	85
Figure 5-6. Half graben model proposed by Rowell (1995) (general model presented) overlain over SWAT-5 seismic line. A half graben is illustrated with a Triassic and Lower Jurassic sedimentary wedge, but the Upper Jurassic and Cretaceous appears almost constant thickness across the basin.....	86
Figure 5-7. Half graben model proposed by Naylor & Shannon (2011) (general model presented) overlain over SWAT-5 seismic line. The interpretation only covers the northern basin boundary. The Cenozoic section appears to show a steer's head geometry which is inconsistent with a half graben model.	87
Figure 6-1 Example seismic line, not from NCSB, demonstrating seismic data quality is generally better in younger less compacted rocks (top right).	89
Figure 6-2. Location map with key seismic and wells highlighted. Source Dept. of Communications, Climate Action & Environment.....	93
Figure 6-3. Location map indicating seismic dataset utilised by this study. Source Dept. of Communications, Climate Action & Environment.....	97
Figure 6-4. Examples of seismic loading issues encountered, note the vertical shift in seismic events on the displayed line and boxes illustrating 4 different shotpoint to trace relationships encountered.	101

Figure 6-5. Barryroe 3D seismic data quality example, courtesy Providence Resources Plc and Lansdowne Oil and Gas Plc. Strong and continuous reflections can be identified throughout the seismic section.	104
Figure 6-6. SGC06-553689 modern 2D seismic data quality example. Strong and continuous reflections can be identified throughout the seismic section.	105
Figure 6-7. SGC06-554791 modern 2D seismic data quality example. Strong and continuous reflections can be identified throughout the seismic section.	106
Figure 6-8. SGC06-556892 modern 2D seismic data quality example. Strong reflections can be identified, but are less continuous at this location.	107
Figure 6-9. NCS81-59, original vintage processed product data quality example. Strong and continuous reflections can be identified in the shallow section only.	108
Figure 6-10. NCS81-59, reprocessed product data quality example. Strong reflections can be identified at depth that were not evident on the vintage processing.	109
Figure 6-11. NCS81-64, original vintage processed product data quality example. Strong and continuous reflections can be identified in the shallow section only.	110
Figure 6-12. NCS81-64, reprocessed product data quality example. Strong reflections can be identified at depth that were not evident on the vintage processing.	111
Figure 6-13. MPCR84-13and EM311, poor data quality examples. Significant uncertainty in the reliability of seismic reflections on these sections.	112

Figure 6-14. North – South correlation of Gamma Ray (GR) and Sonic (DT) logs from key wells on the west side of the study area, formation tops from Copestake <i>et al.</i> , 2018.....	116
Figure 6-15. North – South correlation of Gamma Ray (GR) and Sonic (DT) logs from key wells on the east side of the study area, formation tops from Copestake <i>et al.</i> , 2018.....	117
Figure 6-16. Seismic line ARC95-13 through wells 57/2-2 and 57/2-1 with GR log (green), Sonic log (blue) and formation tops (after Copestake <i>et al.</i> , 2018). Presented with and without seismic interpretation.....	122
Figure 6-17. Barryroe 3D arbitrary seismic line through well 48/24-3 with GR log (green), Sonic log (blue) and formation tops (after Copestake <i>et al.</i> , 2018). Presented with and without seismic interpretation.....	123
Figure 6-18. Barryroe 3D arbitrary seismic line through wells 48/24-1 and 48/24-3 with GR log (green), Sonic log (blue) and formation tops (after Copestake <i>et al.</i> , 2018). Presented with and without Base Cretaceous seismic interpretation.....	125
Figure 6-19. Seismic line NCS81-59 showing dipping reflectors (red) truncated by the Callovian-Oxfordian Unconformity.....	127
Figure 6-20. Seismic line ACS93-02 through wells 57/2-1 and 57/2-2 with GR log (green), Sonic log (blue) and formation tops (after Copestake <i>et al.</i> , 2018). Presented with and without seismic interpretation.....	128
Figure 6-21. Seismic line ACS93-01 through well 57/9-1 with GR log (green), Sonic log (blue) and formation tops (after Copestake <i>et al.</i> , 2018). Presented with and without seismic interpretation. Note the well encountered over 1000m (3281ft) of Triassic, containing approximately 250m (820ft) of massive halite.	130

Figure 6-22. Vintage seismic line MIL90-02 overlain on adjacent SGC06-553689, demonstrating that the vintage seismic is of sufficient quality to successfully use seismic character and overall structural style to extend the interpretation from the modern seismic data to the vintage seismic data.	133
Figure 6-23. Vintage seismic line CSN82-13 overlain on adjacent reprocessed NCS81-59, demonstrating that the vintage seismic is of sufficient quality to successfully use seismic character and overall structural style to extend the interpretation from the modern seismic data to the vintage seismic data.	134
Figure 6-24. Cross-plots of seismic isochron versus well isopach used for layer by layer depth conversion, a coefficient of determination is presented for each layer.	136
Figure 7-1. Seismic line SGC06-553689 imaging the entire NCSB, with hydrocarbon exploration well locations, without interpretation. Reproduced in a larger scale in Appendix E.1.	138
Figure 7-2. Seismic line SGC06-553689 imaging the entire NCSB with hydrocarbon exploration wells, major seismically definable stratigraphic markers and fault interpretation shown.....	139
Figure 7-3. Northwest to southeast seismic line NCS81-59 imaging the entire NCSB, with hydrocarbon exploration well locations, without interpretation. Reproduced in a larger scale in	140
Figure 7-4. Northwest to southeast seismic line NCS81-59 imaging the entire NCSB, with hydrocarbon exploration wells, major seismically definable stratigraphic markers and fault interpretation shown, courtesy Schlumberger Multiclient. (A) represents the opaque seismic character of the Paleozoic	

Basement. (B) represents the high amplitude continuous character of the Triassic. (C) indicates areas of syn-sedimentary growth within the Triassic. (D) indicates subtle change in dip of seismic reflectors at the Callovian-Oxfordian unconformity. (E) indicates areas where the Callovian-Oxfordian Unconformity is interpreted and there is no change in dip or well control. (F) indicates the areas where the Base Cretaceous is represented by the upper of two parallel reflectors in the basin centre. (G) indicates where the reflectors at (F) have thinned and coalesced as one reflector. Reproduced in a larger scale in Appendix E.4..... 141

Figure 7-5. Barryroe 3D seismic data quality example, without interpretation. Courtesy Providence Resources Plc and Lansdowne Oil and Gas Plc. Reproduced in a larger scale in Appendix E.5. 142

Figure 7-6. Barryroe 3D seismic data quality example, exhibiting imaging at depth and minor halokinesis. Courtesy Providence Resources Plc and Lansdowne Oil and Gas Plc. (D) indicates subtle change in dip of seismic reflectors at the Callovian-Oxfordian unconformity. (E) indicates areas where the Callovian-Oxfordian Unconformity is interpreted and there is no change in dip or well control. (F) indicates the areas where the Base Cretaceous is represented by the upper of two parallel reflectors in the basin centre. (G) indicates where the reflectors at (F) have thinned and coalesced as one reflector. (H) indicates areas of syn-sedimentary growth within the Cretaceous. Reproduced in a larger scale in Appendix E.6. 143

Figure 7-7. Seismic line ACS93-01 through well 57/9-1 with GR log (green), Sonic log (blue) and formation tops (after Copestake et al., 2018). Presented with and without seismic interpretation. The well encountered over 1000m (3281ft) of

Triassic, represented as a high amplitude seismic package, containing approximately 250m (820ft) of massive halite. There is an opaque seismic character within the metamorphosed carboniferous basement encountered by the well.....	145
Figure 7-8. Depth map of Top Paleozoic Basement, interpreted within the study area, contour interval 250m (820ft), well control highlighted. Faulting has a NE-SW strike and a southerly dip. The fault labelled the Morrigan Fault exhibits the greatest throw.....	146
Figure 7-9. Seismic line NCS-84 with clearly identifiable faults in yellow and evidence of growth of stratigraphy to the NW above a low angle fault which dips to the SE. Presented with and without seismic interpretation.....	150
Figure 7-10. Depth map of Top Triassic, interpreted within the study area, contour interval 250m (820ft), well control highlighted. Faults which intersect the Top Triassic are younger faults with detach within the Triassic.....	151
Figure 7-11. Isopach of the Triassic interpreted within the study area, contour interval 250m (820ft), well control highlighted. SW-NE reactivated Variscan faults accommodate Triassic extension creating 6 half grabens. Sediment thickness also changes along the strike of the half grabens suggesting both fault and paleo-topographic control on sedimentation.....	152
Figure 7-12. Seismic line NCS81-59 zoomed to 57/9-1 well, with area of halite movement (halokinesis) annotated and resulting erosion of Triassic section at the Callovian-Oxfordian unconformity which provides a date for onset of halokinesis as Lower Jurassic, courtesy Schlumberger Multiclient.....	155

Figure 7-13. Barryroe 3D Inline 58, with area of halite movement (halokinesis) annotated. Overlying faults are seen to detach within the Triassic section. Note evidence of erosion of Lower Jurassic section by the Callovian-Oxfordian unconformity.	156
Figure 7-14. Barryroe 3D Inline 135, with area of halite movement (halokinesis) annotated. Salt withdrawal within the Lower Jurassic created a local depocenter. Overlying faults are seen to detach within the Triassic section.	157
Figure 7-15. Seismic line SGC06-553689 zoomed to illustrate an area of halite movement (halokinesis). Overlying faults are seen to detach within the Triassic section.	158
Figure 7-16. Seismic Line Mil90-16 illustrating evidence of Callovian-Oxfordian Unconformity in the basin centre on vintage seismic data.	160
Figure 7-17. Depth map of Callovian-Oxfordian unconformity, interpreted within the study area, contour interval 200m (660ft), well control highlighted. The deepest area of 4700m (15,400ft) is located to the NE between the Morrigan and Dagda faults. Local high areas of 2800m (9,200ft) exist to the west adjacent to the Morrigan and Dagda Faults.	162
Figure 7-18. Isopach of the Lower Jurassic interpreted within the study area, contour interval 250m (820ft), well control highlighted. A western and Eastern isopach thick are readily identified. Note - faults are present day, any apparent thickness changes across northerly dipping faults may be an interpretation error on poor data.	163
Figure 7-19. Depth map of Base Cretaceous interpreted within the study area, contour interval 200m (660ft), well control highlighted. There are two mid-basinal	

lows of up to 2600m (8500ft). A subtle mid-basinal high is also evident following the 2200m (7200ft) contour against the Dagda fault, in the region of the 48/23-1, 48/24-1 and 48/24-3 wells; this is the Barryroe Oil Field.....	166
Figure 7-20. Isopach of the Upper Jurassic interpreted within the study area, contour interval 20m (660ft), well control highlighted. A primary depocenter is evident to the northeast between the Morrigan and Dagda Faults of up to 2,200m (7,200ft) thick. Syn-sedimentary growth is also evident across the Brigit and Aonghus Faults of 500m (1,650ft) and 300m (1,00ft) respectively.....	167
Figure 7-21. Seismic Line SGC06-556892 zoomed to illustrate growth of the Upper Jurassic section across the Aonghus Fault and the detachment within the Triassic section.....	168
Figure 7-22. Depth map of Plenus Marl interpreted within the study area, contour interval 100 metres, well control highlighted. Note the mid-basinal highs adjacent to the Dagda and Brigit Faults in the northeast of the study area caused by Cenozoic compressional reactivation.....	172
Figure 7-23. Isopach of the Lower Cretaceous interpreted within the study area, contour interval 200 metres, well control highlighted. Extension is accommodated primarily on the Morrigan, Dagda and Brigit Faults to the northeast and the Morrigan, Brigit and Aonghus Faults to the southwest.	173
Figure 7-24. Seismic Line SGC06-553689 zoomed to illustrate reverse displacement at the Plenus Marl and growth of the Lower Cretaceous section across the Dagda and Brigit Faults.....	174
Figure 7-25. Depth map of Top Chalk (Seabed/ Base Cenozoic), interpreted within the study area, contour interval 25 metres, well control highlighted. A	

Cenozoic outlier is present to the southwest of the study area, to the northeast of this the Top Chalk outcrops at the seabed.....	177
Figure 7-26. Isopach of the Upper Cretaceous (Chalk) interpreted within the study area, contour interval 100 metres, well control highlighted. Note isopach thins to the northeast against the Dagda and Bridgit faults where Upper Cretaceous was eroded.....	178
Figure 7-27. Isopach of Water Column and Cenozoic interpreted within the study area, contour interval 25 metres, well control highlighted. The water column is broadly consistent across the area at approximately 100-130m (330-430ft). The Cenozoic section is up to 200m (660ft) thick in the south west of the study area and absent to the north east.	179
Figure 7-28. Isopach map of the Upper Cretaceous section, illustrating area of reduced thickness(circled in purple) which appears to be regional in nature and not reduced by later uplift and erosion. A NW-SE shear zone is postulated which would help explain regional variations in thickness during a basin sag phase...	180
Figure 7-29. Map of the freeair gravity data in the study area. Gravity trends are indicated by red arrows and faults active within the Triassic are shown as black fault polygons. The strike of the faults appears to align with the gravity trends.	182
Figure 7-30. Map of the freeair gravity data in the study area. Gravity trends are indicated by red arrows and faults active within the Cretaceous are shown as black fault polygons. The strike of the faults appears to align with the gravity trends.	183
Figure 7-31. Seismic Line SWAT 5 with interpretation of the stratigraphy and the basin bounding Morrigan Fault. The fault becomes low angle with depth and exhibits significant offset and associated sediment deposition.....	185

Figure 7-32. Seismic Line SGC06-553689 showing the interpretation of the major faults. The basin bounding Morrigan Fault becomes low angle with depth and was active from the Triassic to Cretaceous. The antithetic Dagda, Brigit and Aonghus Faults sole out within the rotated Triassic and are active from the Upper Jurassic to the Cretaceous.	186
Figure 7-33. Isopach map of the Upper Cretaceous section, illustrating areas of inversion (circled in purple). The inversion is primarily accommodated on the Dagda Fault in the northeast and on the Brigit and Aonghus Faults to the southwest. A NW-SE shear zone is postulated which would facilitate the transfer of compression across faults.	192
Figure 7-34. Isopach map of the Lower Cretaceous section, illustrating two discrete depocenters (in red). The depocenter locations suggest rift extension is being accommodated on the Dagda Fault in the northeast and on the Brigit and Aonghus Faults to the southwest. A NW-SE shear zone is postulated which would facilitate the transfer of extension across faults.	193
Figure 7-35. Smith and Sandwell (2015) freeair gravity map, overlain by Cretaceous fault polygons, showing potential NW-SE shear zone. Gravity values are higher to the west of the potential NW-SE shear zone indicating potential changes in basement density across the shear zone.	194
Figure 8-1. Revised structural evolution model of the NCSB. (A) Pre-rift setting of Variscan thrusts. (B) Triassic rifting accommodated by reactivated Variscan thrusts as a series of half-grabens. (C) Rifting continued into the Lower Jurassic with a half-graben geometry. (D) Upper Jurassic rifting is accommodated by the northern basin bounding fault and new mid-basinal antithetic faults which detach	

within the underlying Triassic, forming a conventional graben geometry. (E)	
Lower Cretaceous extension continued as a conventional graben. (F)	
Upper Cretaceous basin sag. (G) Cenozoic compression accommodated by reactivating mid-basinal antithetic faults.	196
Figure 8-2. Structural evolution of the NCSB – Pre-rift setting showing a series of Variscan thrust bound blocks.	198
Figure 8-3. Structural evolution of the NCSB – Triassic cross section illustrating the proposed reactivation of Variscan thrusts to form a set of Triassic half grabens.	199
Figure 8-4. Structural evolution of the NCSB – Lower Jurassic cross section illustrating the continued extensional reactivation of Variscan thrusts to form a Lower Jurassic half graben. Minor halokimes is also initiated.	202
Figure 8-5. Seismic lines Porc97-68 from the Goban Spur Basin and SGC06-553689 from the NCSB, showing similar SE dipping fault style at depth.	205
Figure 8-6. Structural evolution of the NCSB – Upper Jurassic cross section illustrating renewed rifting with extension accomodated on the northern basin bounding fault and on newly developed mid-basinal antithetic faults which detach within the underlying Triassic.	206
Figure 8-7. Structural evolution of the NCSB – Lower Cretaceous cross section illustrating continued rifting with extension accomodated on the northern basin bounding fault and on the mid-basinal antithetic faults which detach within the underlying Triassic.	209

Figure 8-8. Structural evolution of the NCSB – Upper Cretaceous cross section illustrating a basin sag phase with Upper Cretaceous sediments overstepping the basin extents yielding a classic “steer’s head” geometry.....	210
Figure 8-9. Structural evolution of the NCSB – Cenozoic cross section illustrating basin wide uplift and compressional reactivation of the mid-basinal faults to yield broad anticlines and flower structures.....	212
Figure 9-1. Triassic depth structure map (present day), coloured by overlying Lower Jurassic sediment thickness. Conceptual sediment patterns related to the proposed structural model are proposed within the thickest sediment areas, with sediment controlled by the Morrigan Fault.	216
Figure 9-2. Depth map of the Callovian-Oxfordian Unconformity (top) and Lower Jurassic thickness (bottom). Structurally high areas which are coincident with thick sediment are highlighted as areas of potential interest for Lower Jurassic hydrocarbon exploration. Note - faults are present day.	217
Figure 9-3. Callovian-Oxfordian Unconformity depth structure map (present day) with syn-depositional faults, coloured by overlying Upper Jurassic sediment thickness. Conceptual sediment patterns related to the proposed structural model are proposed within the thickest sediment areas. Note the conventional graben architecture, and the thickest sediment adjacent to the Dagda Fault.	219
Figure 9-4. Depth map of the Base Cretaceous (top) and Upper Jurassic thickness (bottom). A structurally high areas which is coincident with thick sediment is highlighted as an area of potential interest for Upper Jurassic hydrocarbon exploration.....	221

Figure 9-5. Regional multi-client seismic data recently acquired by Petroleum Geo-Services (blue) and GeoPartners (yellow).....	223
Figure 9-6. Licence authorisations in 2011.....	225
Figure 9-7. Licence authorisations in 2016.....	226

Tables

Table 2-1. Sediment stratigraphy and thickness in the NCSB (after Tucker & Arter, 1987)	35
Table 2-2. Key Tectonic Events in the NCSB (after Tappin <i>et al.</i> , 1994)	43
Table 6-1. Barryroe 3D acquisition parameters; after Polarcus, 2011.....	94
Table 6-2. Barryroe 3D summary processing flow; after Polarcus, 2011.....	95

Declaration:

This is to certify that the work I am submitting is my own and has not been submitted for another degree, either at University College Cork or elsewhere. All external references and sources are clearly acknowledged and identified within the contents. I have read and understood the regulations of University College Cork concerning plagiarism and intellectual property.

Abstract

The North Celtic Sea Basin (NCSB) is one of a number of basins related to regional Mesozoic extension across north-west Europe. Previous authors have described the NCSB as having a conventional “steer’s head” geometry or alternatively a half graben geometry. Modern 2D and 3D seismic data has now allowed interpretation of faulting at depth within the NCSB. In particular it has demonstrated the importance of intra-basinal faulting and results in a robust updated structural evolution of the NCSB. Rifting is believed to have commenced in the Triassic with the development of an asymmetric simple shear rift. Extension was accommodated by several reactivated Variscan thrust faults with a detachment between the upper and lower crust at 18-20 km (11-12.5 miles) depth. Rifting continued through the Lower Jurassic and extension was accommodated primarily on the most northern of the reactivated Variscan thrusts, the Morrigan Fault. A deep extension of the Morrigan Fault has been mapped by previous authors on deep refraction seismic data as a south -easterly dipping low angle detachment. The other Variscan thrusts became locked, possibly against the granites within the Labadie Bank High – Pembrokehire Ridge to the south. Halokinesis initiated within the Lower Jurassic, caused by movement on underlying faults and differential loading of the overburden. Renewed rifting in the Upper Jurassic and Lower Cretaceous was accommodated by a symmetric pure shear rift as extension was accommodated on the Morrigan Fault and new mid-basinal normal faults, antithetic to the Morrigan Fault, resulting in a conventional full graben geometry. These antithetic faults (Dagda, Brigit and Aonghus Faults) detach in the underlying Triassic halites. The

post rift sag phase in the Upper Cretaceous yielded thick deep marine deposits which overstepped the basin bounding faults to yield a classic “steer’s head” geometry. Subsequent Alpine compression in the Oligo-Miocene and uplift in the Paleocene reactivated and reversed the mid-basin antithetic faults, creating broad mid-basinal anticlines and flower structures. These faults were preferentially reactivated as they detached in Triassic halites. Recognition of this revised structural evolution of the NCSB is critical to predicting the spatial distribution of sedimentary facies and de-risking hydrocarbon prospectivity of the basin.

1 Introduction

The North Celtic Sea Basin (NCSB) is located to the south of Ireland in approximately 100 meters (330ft) water depth (Figure 1-1). It is one of several basins related to Mesozoic regional extension, in a passive margin setting, across northwest Europe, such as the Porcupine, Rockall, Central North Sea, Faroe-Shetland, East Irish Sea basins (Dore *et al.*, 1999; Shannon, 1991). The shallow water depths, short distance to shore, regional geology and the proven elements of an active hydrocarbon system make the basin attractive for hydrocarbon exploration (Selley & Sonnenberg, 2015). Basins of similar age and geological history have proven to be prolific hydrocarbon producers, such as the North Sea (Hiscott *et al.*, 1990; Evans *et al.*, 2003), East Irish Sea (Colter, 1997), and most recently discoveries in the conjugate Jeanne D’Arc, Orphan and Flemish Pass basins offshore Canada (Cameron *et al.*, 2017; Gillis *et al.*, 2018).

The NCSB has had almost fifty years of hydrocarbon exploration with 83 exploration wells to date. Success has been poor with only the Kinsale Head, Southwest Kinsale, Ballycotton and Seven Heads gas fields on production to date (Naylor & Shannon, 2011). These fields are all shallow inversion features within the Cretaceous created by Cenozoic compression. A number of exploration wells have logged hydrocarbon within the Jurassic however their extent is either small or remains unmapped structurally and/or stratigraphically on vintage seismic datasets.

This is due in part to poor seismic imaging leading to a poor understanding of the structural framework of the basin. Modern seismic acquisition and processing techniques have yielded significant imaging improvements, particularly at depth, providing previously unseen structural detail. The recent success by Providence Resources Plc at the Barryroe oil discovery has brought renewed interest in the hydrocarbon potential of the NCSB, pers. comm. (Dr. John O’Sullivan, Providence Resources Plc), as evidenced by regional multi-client seismic acquisition in 2013 and 2015 by Petroleum Geo-Services and GeoPartners Limited respectively. Prior to this discovery the primary reservoir target for the preceding twenty years or more was the shallow Lower Cretaceous which produces at the Seven Heads, Ballycotton, SW Kinsale and Kinsale Head gas fields (Naylor & Shannon, 2011). Successful exploration of the deeper geology will rely on improved understanding of the structural history of the basin which is critical in predicting or de-risking the petroleum system elements, for instance, reservoir presence and quality.

Existing models for structural development of the NCSB are somewhat contradictory, postulating either a conventional graben (Tucker & Arter, 1987; Coward & Trudgill, 1989; McMahon & Turner, 1998) or a half graben geometry (Petrie *et al.*, 1989; Musgrove *et al.*, 1995; Rowell, 1995; Naylor & Shannon, 2011). These models are based on seismic data from predominantly early 1980’s and 1990’s with poor imaging at depth. Structural interpretations based on these models have implications on the predicted presence of various reservoir intervals.

The study aims to test the existing models of structural evolution of the NCSB against modern 2D and 3D seismic data and present the best structural model that honours all available data. The methodology is to-

- A. Access modern 2D and 3D seismic data over a study area.
- B. Overlay existing models of structural evolution on the modern seismic data and assess any gaps in the existing models.
- C. Use existing well control to provide stratigraphic constraint on an updated seismic interpretation, utilising the modern seismic data.
- D. Interpret regional fault planes to the base of the seismic data.
- E. Integrate and/or extrapolate knowledge from adjacent basins with greater well control and/or improved seismic data.
- F. Utilise interpretation of modern seismic data to propose the best fit structural model for the NCSB.

The location and extent of the current study area (Figure 1-1) is based on the availability of modern seismic data upon commencement of the project. The initial study area was 3,000 km² in extent and centred on the Barryroe 3D seismic survey with parts of the SGC06 2D seismic survey providing regional context. During the project the study area was doubled to 6,000 km² to accommodate the addition of the reprocessed NCS81 survey. This reprocessed dataset provided additional regional modern seismic data which was an underlying requirement of the study. Critically, the author provided input to the reprocessing and the final product validated the structural interpretation beyond the initial study area.

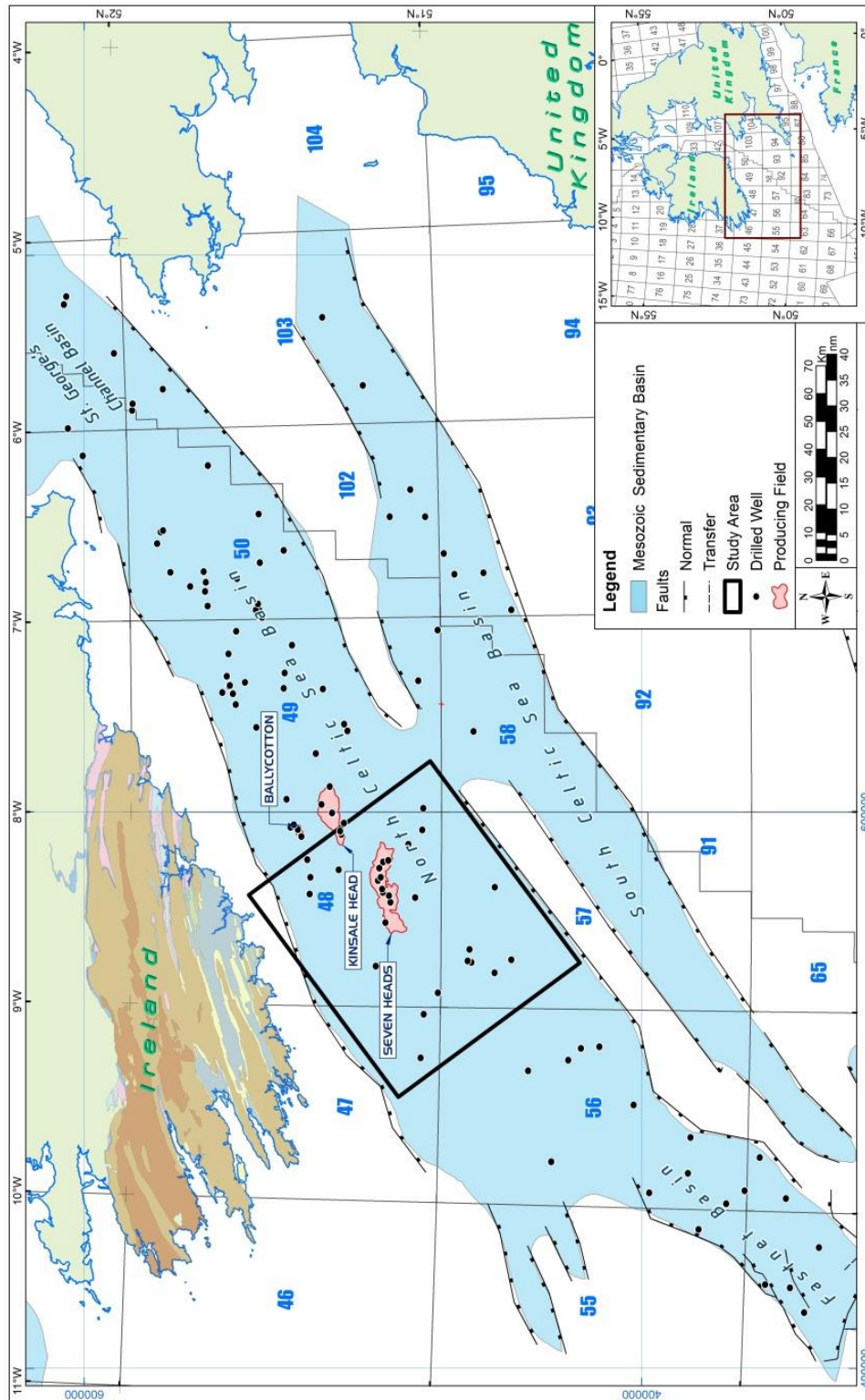


Figure 1-1. Location map showing offshore sedimentary basins south of Ireland, highlighting the study area, drilled wells and relevant hydrocarbon discoveries. (Source Dept. of Communications, Climate Action & Environment).

2 Literature Review

2.1 NCSB Structural Development

The presence of a sedimentary basin off the south coast of Ireland was first predicted using marine gravity measurements taken from submarines as far back as the 1930's and 1940's (Day & Williams, 1970). The earliest extensive gravity survey of the area was acquired in 1967, 1969 and 1970 by the University of Birmingham. Davey (1971) published the first gravity map of the area using this dataset and recognised a low gravity anomaly, trending parallel to the Irish coast, and termed it the "Southern Ireland Coastal anomaly", which is now recognised as the North Celtic Sea Basin (NCSB). The University of Birmingham also acquired seismic refraction data in 1965 and 1966 (Blundell, 1970) and published integrated seabed outcrop, gravity and seismic interpretations in 1971 (Blundell *et al.*, 1971). These early papers gave the first mapped extent and cross section images of the NCSB, predicting Neogene, Paleogene, Cretaceous, Jurassic and Permo-Triassic sediments overlying Palaeozoic basement. The first seismic surveys for hydrocarbon exploration were acquired in 1969 with the first exploration well drilled in 1970 (Chapter 4).

The first inclusion of the Celtic Sea area within regional tectono-stratigraphic studies was by Ziegler (1975 & 1982), Naylor & Mounteney (1975) and Pegrum & Mounteney (1978), who discuss the area within the regional context of North West Europe, but also within the context of the conjugate basins off North America. The presence of the underlying Caledonian NE-SW and NW-SE faults were also noted,

as were more Variscan W-E trends. Cross sections show a simple cartoon graben for both the North and South Celtic Sea Basins with halokinesis within Triassic units and the Upper Cretaceous lying unconformably over Jurassic or Lower Cretaceous sediments (Pergrum & Mounteney, 1978).

Pergrum & Mounteney (1978) proposed that the Caledonian and Variscan compressional events created a thickened crustal block which may have delayed Atlantic spreading north of the Newfoundland-Azores-Gibraltar fracture zone. The Celtic Sea, Western approaches, Porcupine and Rockall Basins were believed to represent successive attempts of the spreading ridge to breach this crustal block.

While many authors had previously identified the presence of the underlying Caledonian NE-SW and NW-SE faults, it was Robinson *et al.* (1981) that suggested the presence of these NW-SE trending strike-slip faults controlled the North Celtic Sea and Fastnet Basin extents. They further proposed that these strike-slip faults allowed the transfer of extensional movement from the NCSB area to the Porcupine Basin.

Sparker seismic profile data acquired between 1976 and 1978 and an associated programme of gravity core and dredge sampling was used by Delanty *et al.* (1981) to update the sub Quaternary geological map of the NCSB. Permo-Triassic aged red sandstones from sampling were seen to lie unconformably on Palaeozoic basement in the northwest of the basin and overlain by Upper Cretaceous which extended over the central and southern half of the NCSB. In areas east of Kinsale

Head the Upper Cretaceous units were seen to onlap directly onto Palaeozoic basement. To the southwest of the basin Tertiary and Quaternary aged sediments lie unconformably above the Upper Cretaceous, with Quaternary deposits commonly filling Pleistocene aged channels. Delanty *et al.* (1981) recognised the primary basin controlling faults as northeast-southwest trending with a series of strike slip faults trending northwest-southeast. The latest movement on these strike slip faults was proposed to be Middle Miocene based on similarly trending faults both onshore and offshore UK.

The Kinsale Head Gas Field was described by Colley *et al.* (1981) as a Palaeogene anticlinal structure with reservoirs of Aptian-Albian age. The structure is located in the axis of the NCSB and was subject to basin inversion though the mechanics were not clearly understood. There are two reservoirs, the 'A' Sand (Agone Sandstone Member of Copestake *et al.* 2018) an offshore shallow marine deposit of up to 45m (140ft) and the 'B' Sand (Bream Sandstone Member of Copestake *et al.* 2018) a shore-line deposit associated with a marine transgression of up to 4m (13ft). The gas is 'dry' and isotopically light and the source is considered to be an early oil phase which was water flushed and biodegraded producing large volumes of isotopically light methane. There is also an input from thermally generated methane from the underlying Jurassic.

Gardiner & Sheridan (1981) noted that there was no evidence of WNW-ESE "Armorican" (Variscan) structural trends within the NCSB suggesting either the Variscan structures had no influence on subsequent structural history of the NCSB

or that the structures were parallel to the Caledonian. They proposed that the position of the Variscan Front was the southern boundary of the South Celtic Sea Basin (SCSB) and not onshore southern Ireland.

The first regional geology book published which had a chapter dedicated to the Celtic Sea Basins was by Naylor & Shannon (1982), probably in response to the significant interest in the area for oil and gas exploration. At the time of publication there were 29 exploration wells drilled and a further 7 planned for the following year (1983). There is no discussion on the tectonic framework of the basin, but the stratigraphic interpretation is discussed in detail. The basement is described as Devonian and Carboniferous sedimentary rocks, uplifted and folded by the Variscan (Hercynian) orogeny and subsequently extended in the Mesozoic. Triassic sediments are predominantly continental, sourced from the surrounding Paleozoic blocks uplifted in the Variscan, with arid conditions creating evaporite sequences in the Upper Triassic. An early Jurassic transgression yielded widespread shallow marine conditions, while uplift, fault block movement and igneous activity was seen in the Middle Jurassic, returning to restricted shelf conditions in the Upper Jurassic. The Jurassic-Cretaceous boundary is commonly recognised as an unconformity, with continental deposition in the Lower Cretaceous. A major marine transgression in the Upper Cretaceous was coincident with the initiation of separation from North America. Widespread and thick chalk was deposited both within the NCSB, adjacent basins and Irish platform areas. Uplift and erosion in the Tertiary, coincident with seafloor spreading along the Reykjanes Ridge, removed significant amounts of this Cretaceous Chalk. Further uplift and erosion was seen

during the Alpine orogeny which may have removed significant amounts of Tertiary sedimentation, with only thin remnants left. At the time the available seismic data showed the North and South Celtic Sea Basins to be asymmetric with approximately 3-9km of sediment, separated by the Labadie Bank High – Permbrookshire Ridge. This ridge was well defined on available gravity data, and was reported to contain several gravity lows, probably associated with post Variscan granites, similar to those onshore (Carnsore Granite and Cornubian Massif). This agrees with early work by Day & Williams, (1970) who suggested a granite system extending from Devon and Cornwall in NE-SW orientation towards the shelf edge.

In 1983 Seismic Profilers Ltd. acquired seismic data over the basins between Ireland, UK and France on behalf of the British Institutions Reflection Profiling Syndicate (BIRPS) and Etude de la Croute Continentale Et Oceanique par Reflexion et Refraction Sismique (ECORS). The seismic data in the Celtic Sea is consists of several lines called the SWAT seismic dataset, Figure 2-3. Several publications discuss the interpretation of this SWAT seismic data, namely a southerly dipping fault or decollement beneath the NCSB that correlates well with the Variscan Front (BIRPS & ECORS, 1986; Prive, 1986; Bois *et al.*, 1988; Bois *et al.*, 1990; Dymment & Bano, 1991; Dymment *et al.*, 1990). The decollement, having a strike of 100° and a dip of 17° to the south, can be traced to 20km depth where it merges with uppermost reflectors of the lower crust. This is similar to the offshore expression of the Carrick, Lizard and Stuart thrusts of Variscan age (BIRPS & ECORS, 1986). Several other southerly dipping features are also seen and are interpreted as thrusts

or imbricated thrust zones of Variscan age, which may have been reactivated (Bois *et al.*, 1988 & 1990). The Variscan to the south of the NCSB was intruded by granite batholiths, trending along a strike of 070° (Bois *et al.*, 1990). The Moho is interpreted on this data at 28-30km depth, rising slightly beneath sedimentary basins (Prive, 1986; BIRPS & ECORS, 1986).

The Celtic Sea area began to be regularly included in discussions of regional rift development in the North Atlantic region, specifically by Masson & Miles (1986), who suggest the NCSB shared a 3-stage development with many other basins. (1) a Late Triassic – Early Jurassic rift associated with onset of rifting between Africa and North America; (2) a less active Middle Jurassic period correlated to the separation of Africa and North America (Sinemurian-Bajocian); (3) a Late Jurassic – Early Cretaceous rift associated with rifting between Iberia and Europe and later between Europe and North America.

Tucker & Arter (1987) provide a detailed description of the morphology and structural evolution of the NCSB. The basin is 300km long and 50-70km wide with a SW-NE orientation. The structural evolution is described in four stages, (1) Triassic-Jurassic interior fracture (rift), (2) Cretaceous sag (post-rift & thermal sag), (3) Early Tertiary inversion and (4) Late Tertiary sag. This differs significantly from the three stages proposed by previous authors. The authors acknowledge the Caledonian and Variscan trends within the basement but considered Triassic evaporites as the principal decollement for listric normal faults observed on available seismic data. They further propose the Triassic was deeply buried by the

Upper Jurassic and salt movement was initiated by movement on underlying faults, but the age and orientation of these underlying faults is not discussed. The stratigraphy is as per Naylor & Shannon (1982) and maximum thicknesses are proposed for the following intervals.

Epoch	Environment	Thickness (m)	Thickness (ft)
Tertiary	Marginal Marine	300	1000
Upr. Cretaceous	Deep Marine Chalk	1200	3950
Lwr. Cretaceous	Marginal Marine to Continental	2000	6550
Upr. Jurassic	Marine to Continental	1500	4900
Lwr-Mid Jurassic	Marine Carbonates & Shales	2500	8200
Triassic	Fluviatile, Lacustrine, Evaporite	3000	9850

Table 2-1. Sediment stratigraphy and thickness in the NCSB (after Tucker & Arter, 1987)

Ziegler (1987) presents a simple three stage development of the Celtic Sea similar to Masson & Miles (1986), although he states rifting may have initiated as early as the Permian and discusses a basin wide unconformity of Cenozoic age caused by intra plate stresses. It was also proposed that the NCSB trend was oblique to the Variscan trend.

The stratigraphy of the Jurassic in the area of the NCSB is described by Millson (1987) with some inference to structural development of the area. The Lower Jurassic is a thick argillaceous sequence with localised development of sandstones. The Middle Jurassic was dominantly a shallow water siliciclastic and carbonate deposition in the Aalenian to Bathonian, possibly related to a Mid-Cimmerian tectonic event, and non-marine Bathonian sequence. A major unconformity is noted

in the Oxfordian, overlain by Upper Jurassic non-marine to marginal marine sediments.

Interpretation of seismic data over the Cornubian Platform by Day *et al.*, (1989) found that the strike of Variscan thrust faults mapped on the Cornubian Platform were WSW-ENE with dextral strike slip faults trending NNW-SSE. It was therefore argued that the adjacent basins (including the NCSB) did in fact have the same trend as the Variscan thrust faults, contrary to Ziegler (1987).

Coward & Trudgill (1989) proposed that the NCSB structure changes along the strike of the basin across major NW-SE strike slip faults, particularly at its northeast end into the St. Georges Channel Basin, similar to Robinson *et al.* (1981). A McKenzie stretching model is proposed and illustrations show a conventional graben, which had evolved into a steer's head geometry by the Cretaceous. There are several southerly dipping Variscan thrusts interpreted on lines SWAT-4 & 5 of the SWAT seismic dataset (Figure 2-3) as well as a southerly dipping reflector in the mantle which is suggested to represent a mantle shear zone.

The NW-SE strike slip faults are discussed again by Petrie *et al.*, (1989) who also propose that the strike of the NCSB changes across these faults. They also suggest the main bounding fault switches from north to south across one of these NW-SE strike slip faults in the far southwest of the NCSB, approaching the Fastnet Basin, in agreement with Robinson *et al.* (1981). The basin itself is described as a half graben, developed over a reactivated southerly dipping Variscan detachment

surface. They describe three extensional events followed by passive thermal subsidence; 1) Permian-Triassic; 2) Lower Jurassic; 3) Lower Cretaceous. This is similar to that proposed by Masson & Miles (1986) and in agreement with Ziegler (1987) but suggests more rifting events than that proposed by Tucker & Arter (1987).

The application of an asymmetric simple shear (Wernicke, 1981) stretching model by Gibbs (1984) was discussed by Dymant (1989), Dymant *et al.*, (1990) and Dymant & Bano (1991). They suggest the basin's orientation (strike 060) is not consistent with reactivation of the Variscan Front (strike 100), but don't rule out local reactivation. The southerly migration of the deepest depocentre within the rift is also discussed as inconsistent with the detachment model. Lastly, using the SWAT seismic dataset (Figure 2-3) they interpret northern dipping faults which appear to offset the Variscan Front, thus indicating the Variscan Front could not have acted as a detachment later than the Triassic. A conventional graben is instead proposed based on the McKenzie (1978) stretching model, however they recognise that the lack of a detachment is inconsistent with the sediment thickness observed. Both the McKenzie and Wernicke models are noted to be inconsistent with the relatively flat Moho across the region, so they propose either a non-flat Moho prior to stretching, or a recent restoration of the Moho by lower crustal ductile flow or differentiation of the upper mantle.

The NW-SE transfer faults discussed previously (Robinson *et al.*, 1981, Coward & Trudgill, 1989, Petrie *et al.*, 1989) from gravity and seismic data were recognised by O'Reilly *et al.* (1991) on the Celtic Onshore Offshore Lithospheric Experiment (COOLE) refraction data acquired in 1985. Two COOLE lines were reviewed in the NCSB, one NW-SE line traversing the basin (profile 6, significantly west of the current study area) and one SW-NE line axially along the basin (profile 7, mid-basinal position present day, but not over the maximum depocenter), Figure 2-1. A NNW trending median flexure is interpreted as a transfer fault zone, dividing profile 7 line into two structurally independent regions within the NCSB. The authors further proposed the NCSB formed initially by simple shear (Wernicke, 1981) on a horizontal detachment between the upper and lower crust at 12 to 14km (7.5 – 8.5 miles) depth. This detachment became work hardened and extension transferred to the brittle upper crust. Crustal stretching of 1.6 is calculated and a sediment thickness of approximately 7 kilometres (4.3 miles) along the profile 7 line.

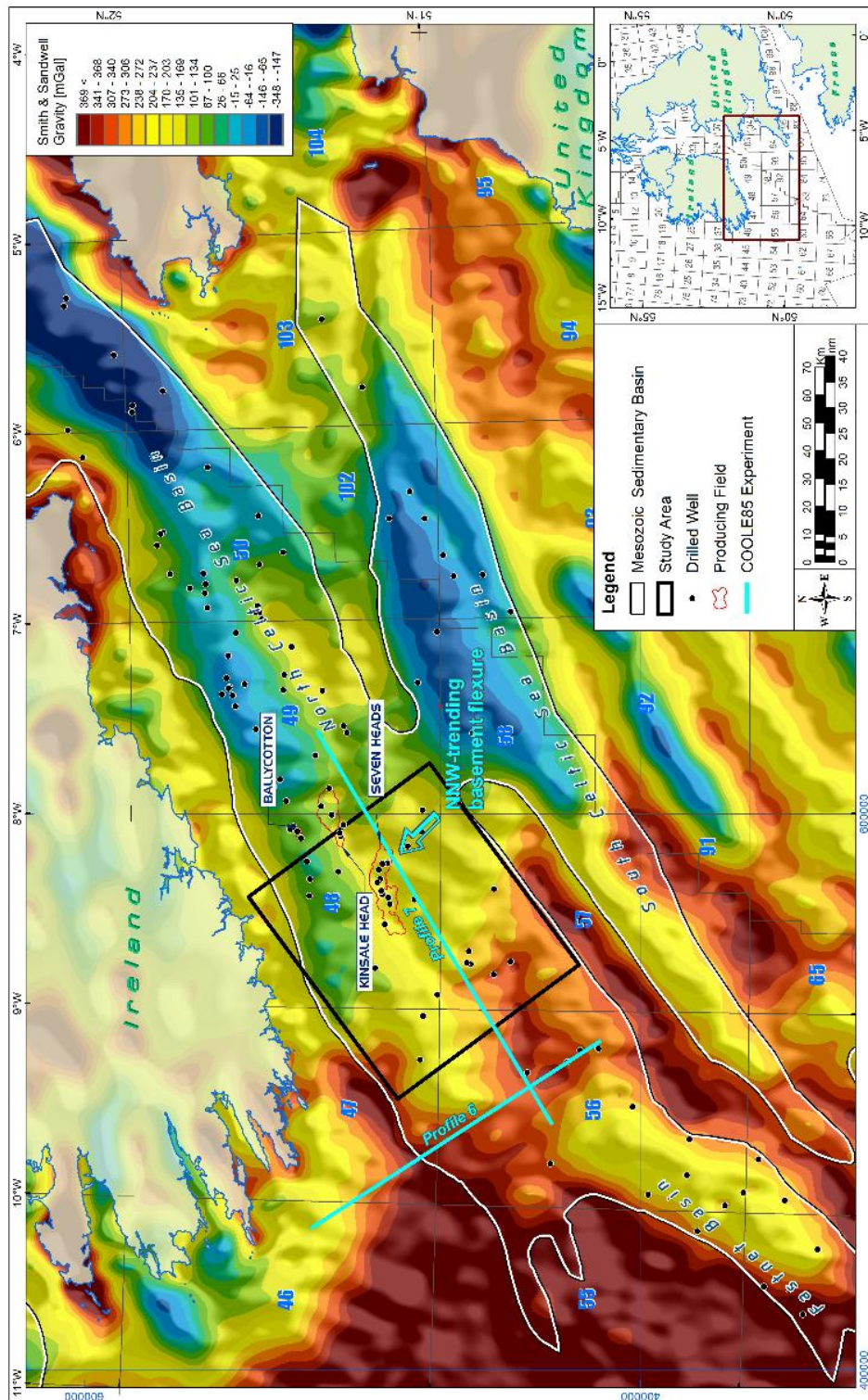


Figure 2-1. Location of COOLE profile 6 & 7 overlain on freeair gravity, showing location of NNW flexure identified by O'Reilly *et al.* (1991).

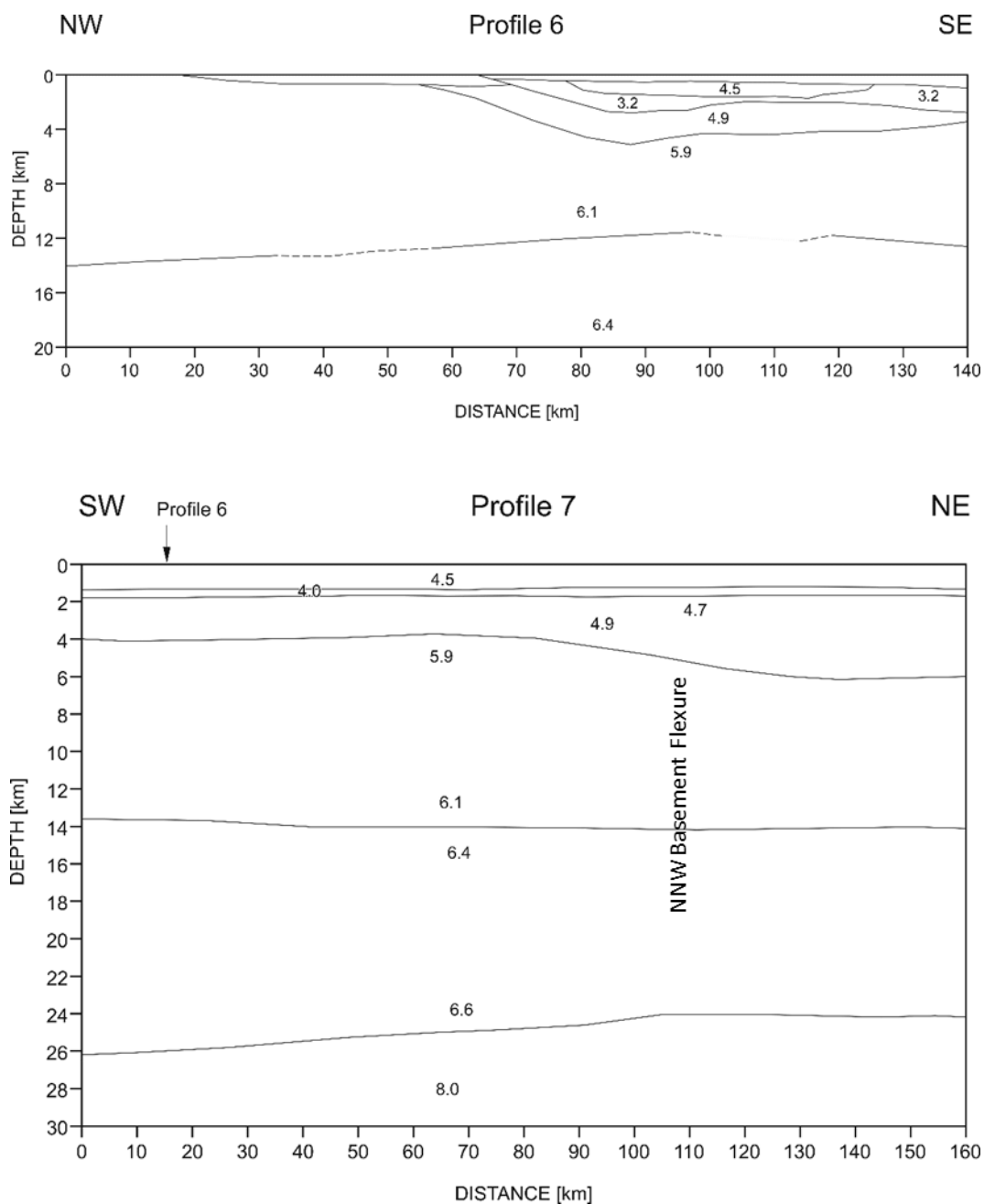


Figure 2-2. COOLE seismic refraction models showing NNW basement flexure on Profile 7 (O'Reilly *et al.*, 1991), numbers shown are crustal velocities in km/s.

An overview paper on the NCSB was published by Shannon (1991) where some of the contradictions already highlighted are mentioned, and the tectonic framework is thus briefly discussed in terms of reactivation of existing Caledonian and

Variscan structures during several rift phases and subsequent thermal sag phases. A stratigraphic summary is also discussed but is in line with previous publications (Naylor & Shannon, 1982).

Both the southerly dipping reflectors and the NW-SE strike-slip faults were examined in a regional context by Ruffell & Coward, (1992) by comparing with the Bristol Channel and onshore Wessex Basins to the east. They concluded the southerly dipping features were Variscan thrusts while the NW-SE strike slip faults allowed compartmentalisation of the Variscan thrusts. It is also proposed that during the Upper Jurassic the Variscan Front may have been reactivated as a thrust, uplifting the areas to the east (Bristol Channel and northern Wessex Basins), while further west a thrust underlying the Labadie Bank High – Pembrokeshire Ridge was reactivated, uplifting the South Celtic Sea Basin, leaving the NCSB in the foreland and preserving the Upper Jurassic section. The NW-SE strike slip faults allowed this transfer of stress across thrusts.

The far western part of the NCSB is discussed in some detail by McCann & Shannon (1993 & 1994) who propose that rifting commenced in the Triassic and had ceased by the early Cretaceous, with passive infill and thermal sag until an Eocene inversion event. They recognise three half-grabens within their study area, however critically the faults dip to the north, not to the south as seen elsewhere in the NCSB. It is proposed that this could be due to the area being separated from the rest of the NCSB by a NW-SE strike slip fault, and that a granite batholith directly to the north may have favoured the development of Variscan back thrusts which

were subsequently reactivated. They comment that the seismic data quality is too poor to speculate on the early Mesozoic evolution of the area.

A small study area was reviewed by Shannon & MacTiernan (1993) in the far northeast of the NCSB. They interpret two Triassic aged packages onlapping onto the Labadie Bank High – Pembrokeshire Ridge. The Lower package of 300-400m (1000-1300ft) high amplitude and discontinuous reflectors onlapping basement is interpreted to be Sherwood Sandstone Group (SSG) fluvial sands and shales. The upper package of 400-800m (1300-2600ft) of continuous reflectors is interpreted to be Mercia Mudstone Group shales. A localised gravity survey was also reviewed, and the Pembrokeshire Ridge was modelled to be consistent with a large high level Variscan Granite, similar to the Cornubian Massif to the south, and may have been unroofed during the Triassic providing a local sand source.

The NCSB is briefly discussed in a British Geological Survey review of the geology of the Cardigan Bay and Bristol Channel area (Tappin *et al.*, 1994). It is described as a symmetrical graben in the hanging wall of a Variscan Thrust with both pre-existing Variscan and Caledonian trends being significant in controlling the basin morphology. Using the SWAT seismic dataset they estimate the extent of crustal thinning (0.9), crustal extension (1.11) and the depth at which basin controlling faults detach (18.7km). The key tectonic events are described as:

Timing	Tectonic Event
Mid Tertiary	Alpine Compression & uplift
Early Tertiary	Thermal Sag
End Cretaceous	Thermal uplift
Late Jurassic	Rifting
Mid Jurassic	Thermal Uplift
Permo-Triassic	Rifting

Table 2-2. Key Tectonic Events in the NCSB (after Tappin *et al.*, 1994)

Musgrove *et al.* (1995) suggest the resistant thrust belt hanging walls of the Variscan form the paleotopography in the early Triassic. Their study found there was a greater chance of finding Sherwood Sandstone Group (SSG) sediments in foreland and intermontane valleys which were close to sea level. These locations were also associated with the presence of halite in the overlying Mercia Mudstone Group and thus they linked the presence of halite to the likely presence of SSG.

Within the same publication Shannon (1995) described the initial infill of the paleotopography as Permian in age, with rifting in the early Triassic creating continental dominated basins with late Triassic thermal subsidence and associated coastal sabkha or supratidal deposits. The NCSB and SCSB are suggested to be partially separated by the Labadie Bank High – Pembrokeshire Ridge at the time and the SSG was widely deposited in the western end of the NCSB while halite in the Mercia Mudstone Group was widely deposited in the SCSB.

A tectono-stratigraphic framework for the NCSB was presented by Rowell (1995) who used both the SWAT seismic dataset and 17,000 km of vintage 1980's -1990's

seismic data acquired by the oil and gas industry. He recognises influences of both Caledonian and Variscan lineaments as important in formation of the NCSB. Both Triassic NW-SE and Late Jurassic NW-SE orientated rifting reactivated SW-NE Caledonian lineaments as half-graben basin bounding faults, while WNW-ESE Variscan lineaments acted as transfer zones or minor accommodation zones. The magnitude of extension was also estimated at 80% - 100% during the Triassic and 30% during the Late Jurassic. Early Cretaceous N-S orientated rifting reactivated both pre-existing lineaments creating pull-apart geometries dominated by the Variscan trend, but extension was relatively limited. It was proposed that several sub-basins existed within the NCSB during the Jurassic and Cretaceous, controlled by reactivated Variscan thrusts. The NW-SE strike slip faults discussed by previous authors and evident on gravity data were not considered within this framework but are recognised as a Variscan Trend.

The sedimentology of the Jurassic and Lower Cretaceous interval was reviewed by Ewins & Shannon (1995) using core and well log data. They conclude the Jurassic progresses from shallow marine, estuarine and continental deposits with sedimentation controlled by passive subsidence. The Lower Cretaceous is described as being continental but becoming marine by the Albian with sedimentation controlled by fault bound subsidence. Diagenesis of these units is described as being primarily depth and temperature controlled and predominantly due to quartz overgrowths.

Kessler & Sachs (1995) describe a sequence stratigraphic study of seismic and well data from the northeast of the NCSB and St. Georges' Channel Basin. The interval of interest was the Lower and Middle Jurassic and extension is described as thermal subsidence.

A seismic stratigraphic analysis of the Lower Cretaceous was conducted by Ruffell (1995) where tectonics, eustacy and climate are considered as processes for variation in stratigraphy. In the northeast of the NCSB well data and seismic data identify coarse-grained fan delta successions which are interpreted to be related to tectonic controls. To the southwest of the NCSB, closer to the proto-Atlantic, eustatic changes are interpreted to control preservation of stratigraphy. The Lower Cretaceous is described as having an undulatory and downlapping seismic facies (possibly channelised) which passes upwards to more parallel seismic facies. This change in seismic facies is seen in the Wessex Basin and is attributed to climatic and tectonic changes.

The hydrocarbon distribution of the Lower Cretaceous 'A' Sand (Agone formation of Copestake et al., 2018) is discussed by Howell & Griffiths (1995). They suggest a Tithonian to Valanginian aged source rock for oils discovered in Barryroe area with generation and expulsion in Late Cretaceous to early Tertiary. They also conclude that shallower gas accumulations were likely charged post Cenozoic inversion.

The reservoir fairway of the Lower Cretaceous Greensand, which includes the reservoirs of the Kinsale Head Gas field, was delineated by Taber *et al.* (1995). They conclude that the reservoir quality is controlled by distance from the source with thickness controlled by paleobathymetry.

Hartley (1995) further described the sedimentology of the Lower Cretaceous Greensand of the Kinsale Head Gas Field. The reservoirs units are described as pulsed coarsening-upward units deposited in a wave-dominated shoreface environment. Minor thickness variations suggest some syn-sedimentary faulting, but this had ceased by the 'A' Sand deposition (Agone Sst Member of Copestake *et. al.* 2018). The study further suggested a southerly source for the sediment (Labadie Bank High – Pembrokeshire Ridge or the SCSB).

The 1983 drilling of the 49/9-2 well yielded the discovery of the Helvick Oil Field and Caston (1995) provided a summary of the discovery. The discovery well flowed 9901 BOPD and 7.44 MMSCFD from four sandstone reservoir intervals of Middle to Upper Jurassic age. The structure is described as a hanging wall structural high against a down-to-basin extensional fault that forms the northern margin of the NCSB. A bend in the boundary fault from NE-SW to E-W sets the updip trap to the north and west and the structure is dip closed to the south, southeast and east. The throw on the fault is interpreted to be 265-550m (870-1785ft). The recovered oil was 44° API and believed to be derived from an underlying Lower Jurassic source.

The southerly dipping reflectors imaged on the SWAT seismic lines (Figure 2-4) and discussed by several authors (BIRPS & ECORS, 1986; Bois *et al.*, 1988; Bois *et al.*, 1990; Dymment & Bano, 1991; Dymment *et al.*, 1990; Prive, 1986; Ruffell & Coward, 1992) were found to exist on commercial seismic datasets by McCann (1996). The reflector, or series of parallel reflectors almost 0.5 seconds thick, dips at 20° to the south for approximately 70 km and has a strike of 060° to 070°. It is suggested by McCann that the reflectors were formed initially during the Caledonian Orogeny but later modified by the Variscan Orogeny, thus explaining why the trend is not perfectly aligned with either the Caledonian or the Variscan. The reflectors themselves are proposed to be slivers of basement which have been thrust over each other in an imbricate fashion and thus represent a thrust zone, possibly mylonitised similar to the ENE trending mylonite zone at the northern margin of the Rosslare Complex in southeast Ireland. It was also noted that the reflectors are significantly offset and change strike between SWAT-4 and SWAT-2/3, while not discussed by McCann (1996) it's possible this is due to a NW-SE strike slip fault such as discussed by Ruffell & Coward (1992).

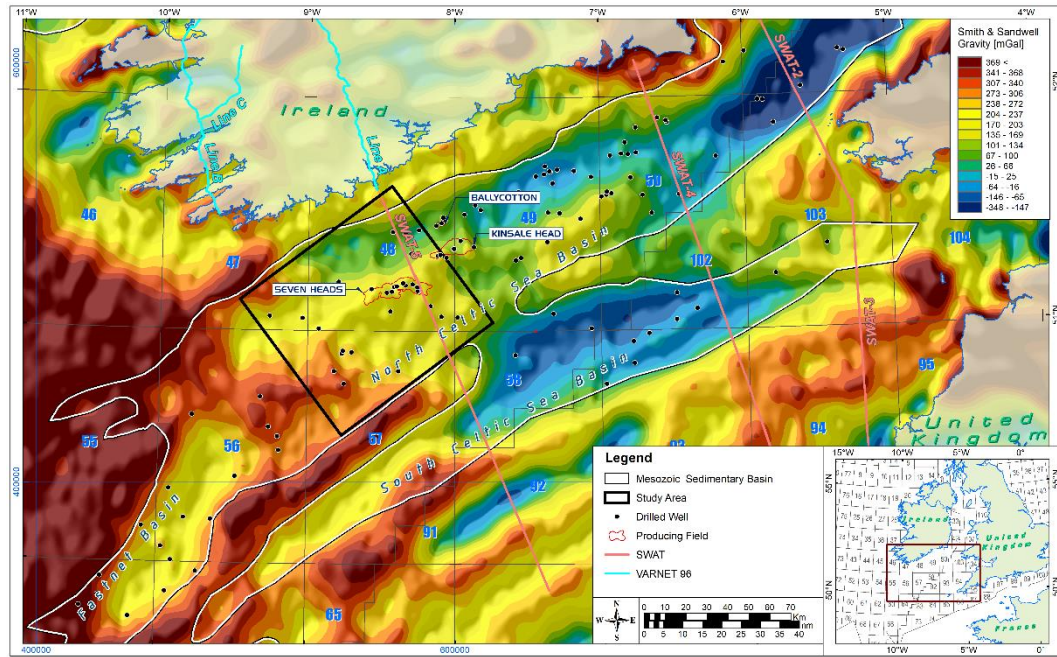


Figure 2-3. Location of SWAT and VARNET lines overlain on freeair gravity.

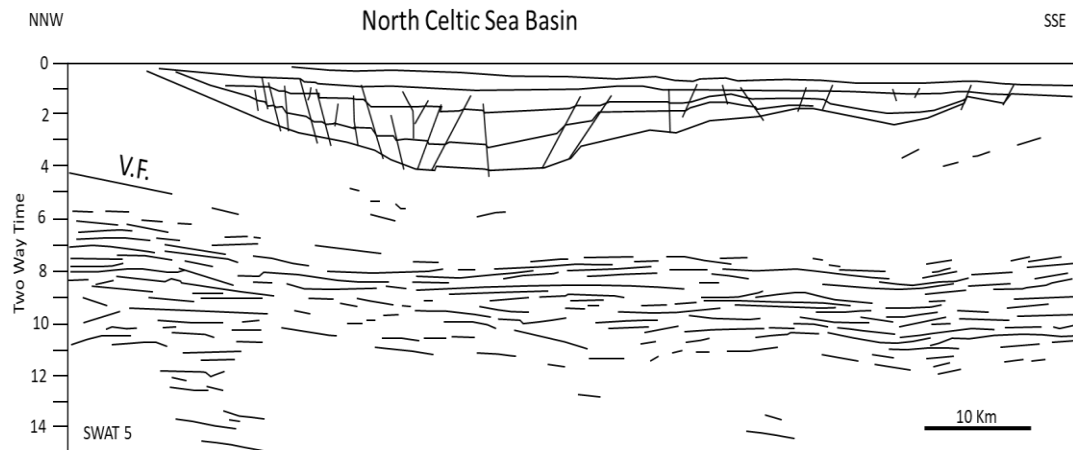


Figure 2-4. Interpretation of SWAT 5 seismic line across the NCSB. (V.F.) is the proposed location of the Variscan Front (Dyment *et al.*, 1990).

In 1996 two wide angle seismic profiles were acquired onshore Ireland as part of a multidisciplinary project (VARNET-96). One of these lines was designed as an extension of the SWAT-5 seismic line, Figure 2-3. Masson *et al.* (1998) and Landes *et al.* (2000) proposed the seismic data indicated the Variscan deformation was thin-skinned, confined to the hanging wall of a major inverted Devonian extensional fault. The W-E nature of the Variscan in the area (onshore Ireland) was deemed to be related to a rigid W-E trending basement high to the north, cored by a chain of Caledonian granites, which controlled the Variscan structural fabric. The data also showed two sub-horizontal crustal detachments (Vermeulen *et al.*, 1999; Masson *et al.*, 1998) which extend offshore beneath the NCSB. The first is at 12-14km depth (7.5 – 8.5 miles) and is a mid-crustal event related to moderate changes in ductility, while the second is at approximately 20km (12.5 miles) and represents a crustal brittle-ductile transition. The Variscan Front is stated to be the Dingle-Dungarvan Line onshore with this detachment extending beneath the NCSB at 18-20 km (11-12.5 miles) depth. It is therefore suggested that the Variscan was thin skinned, acting only in the brittle crust above this detachment and thus Mesozoic reactivation of both Caledonian SW-NE structures and Variscan W-E features was possible in controlling the NCSB evolution.

There have been no additional research papers published on the structural development of the NCSB since 2000 with the exception of chapters in regional geology texts which simply repeat or reference the above research. Regional potential field modelling of the adjacent Porcupine Basin or Atlantic Margin by Kimbell *et. al.* (2010), Welford *et. al.* (2010) and Funck *et. al.* (2016) show the

NCSB on moho depth maps (20-25Km) but there is no significant discussion of structural development, with the exception of Kimbell *et. al.* (2010) who recognise the ENE trend of the NCSB could be influenced by both Caledonain and Variscan existing structures.

2.1.1 NCSB Literature Review Summary

The literature generally agrees on 3 major phases of basin development, initiation of rifting in the Triassic-Jurassic with further rifting in the Upper Jurassic-Cretaceous and inversion in the Tertiary. There is however no consensus on the specific kinematics of the rifting within the NCSB, with both an asymmetric half graben and symmetrical conventional ‘steer’s head’ graben proposed. Seismic data quality available at the time was poor quality and structural interpretations could not be discounted. The mechanics of the mid basinal inversion were also not understood by Colley *et. al.* (1981) and remain undiscussed.

There is however general agreement on the existence of a decollement underlying the NCSB, dipping approximately 20 degrees to the south into the lower crust, often described as a zone of imbricated thrust zones. Several authors recognise the influence of existing Caledonian and Variscan basement, in particular SW-NE and NW-SE oriented lineaments though there is some disagreement on whether the lineaments are predominately Caledonian or Variscan.

With no research published on the NCSB in the last 20 years there remains a clear knowledge gap in the structural development of the NCSB. This has significant implications on the sedimentology and hydrocarbon prospectivity of the NCSB. Modern seismic data and modern seismic reprocessing has however greatly improved the quality of seismic data in the NCSB allowing for updated research.

2.2 Faulting and Rifting

The following literature review is not intended to be an exhaustive literature review, rather it is a brief synopsis on the development of research into rifting and related faulting.

2.2.1 Geometry and growth of faults

Our understanding of faulting has grown significantly in the last century, from initial outcrop observations of the early 20th century, to small scale lab experiments, and most recently the large scale yet high resolution of 2D and 3D seismic imaging. We now recognise some important relationships such as displacement variation along the length of a fault, with maximum displacement in the central part of the fault and gradually decreasing towards the tips, (Walsh & Watterson, 1988; Torabi & Berg, 2011). Also recognised is the relationship between displacement and fault damage zone width (Otsuki, 1978; Robertson, 1982; Watterson, 1986; Evans, 1990; Shipton et al., 2006; Wibberley et al., 2008; Childs et al., 2009). These relationships have been used for predictive purposes and to validate fault interpretations, however they overlook the importance of the mechanical properties of the faulted rock units which must also be considered for correct structural interpretation or prediction (Ferrill *et al.*, 2017).

A fault is generally described as a zone of brittle deformation which may exhibit fracturing, dilation, rotation of layers, dissolution and mineral precipitation. The

core of the fault is generally a narrow zone where displacement is concentrated, recognised as the top of a bell-shaped curve on crossplots of length versus displacement, as defined by Elliott (1976) and Watterson (1986). The damage zone around a fault is generally wider than the fault core thickness, representing distributed deformation (Caine *et al.*, 1996; Evans *et al.*, 1997; Mitchell & Faulkner, 2009; Faulkner *et al.*, 2010, 2011). Faults grow by accumulating displacement as strain is released by the fault, they grow in both height and length, with associated damage zone and core increases (Childs *et al.*, 2009). As strain is being accommodated, faults can interact with each other and can eventually link up, both soft linkages (where strain is transferred from one fault to another, particularly at areas where the faults overlap, called fault relays) and hard linkages (where the faults have physically connected across a breached relay to become fault segments) (Peacock & Sanderson, 1994; Childs *et al.*, 1995 & 2017; Ferrill *et al.*, 1999; Walsh *et al.*, 1999; Cowie *et al.*, 2000; Ferrill & Morris, 2001; Soliva & Benedicto, 2004; Van der Zee & Urai, 2005).

The development from soft linkages to hard linkages is a gradual process and is seen at all scales, from centimetres to kilometre, as the fault segments grow, the prior relays become curves within the coalesced fault segments. As fault segments become hard linked their displacement accumulates and again cross plots of length versus displacement continue to show a cumulative bell-shaped curve, Torabi & Berg (2011) and references therein.

The two primary end members in a range of models for the growth of fault systems are known as the “isolated fault model” where faults initiate as spatially and kinematically isolated structures (Ghalayini *et al.*, 2016; Morley, 2016; Walsh *et al.*, 2002; Nicol *et al.*, 2016), and the “constant-length coherent fault model” where a growing fault changes from rapid propagation at low strain to the accumulation of displacement without significant propagation (Morley, 2016; Curry *et al.*, 2016; Nicol *et al.*, 2016; Jackson *et al.*, 2017). The fault thickness is also increased as faults coalesce, the thickness increasing by the thickness of the relay (Wibberley *et al.*, 2008; Childs *et al.*, 2009; de Joussineau & Aydin, 2009; Ferrill *et al.*, 2016).

2.2.2 Extensional Fault Models

The term extensional or normal fault can be used for faults of any dip angle where the distance between two reference points, on opposite sides of a fault, increases perpendicular to the strike of the fault (Anderson, 1951; Price, 1966; Wise *et al.*, 1984; Groshong, 1988). They generally initiate at dips of approximately 60°, according to Coulomb fracture criterion and Anderson’s theory of faulting (Anderson, 1951), however Walsh & Watterson (1988) show that 70° is more appropriate at depths of less than 4km within the crust. Lower angle normal faults are also recognised and if the dip angle is less than 30° it is generally referred to as a low-angle fault. When a normal fault with high angle is seen to flatten to a low angle with depth it is termed a listric fault. Another type of normal fault is a detachment fault, described as a regional scale very low angle fault (Davis *et al.*, 2012).

Large scale extensional fault systems can be modelled by the domino model which is rigid and describes a series of extensional faults simultaneously rotating fault blocks, with the same dip and offset at each fault (Ransome *et al.*, 1910). The issues with this model (because it is rigid) are that there are gaps or voids in the model and indeed overlaps at the edges of the model. A simple listric fault can solve the overlap while a deformable medium (salt, clay, magma) at the base of the model can solve the void space and is itself a pre-requisite to forming a domino system. However, the listric model is not a perfect solution and creates its own space and or rigidity problems (Ramsey & Huber, 1983). A modification of this model, the soft domino model, allows for strain within the fault blocks which accommodates asymmetry in the form of variation in fault size, displacement and also internal fault block distortions (Walsh & Waterson, 1991).

2.2.3 Contractional Faults

A reverse fault (or contractional fault) is the term given to faults of any dip angle where the distance between two reference points, on opposite sides of a fault, decreases perpendicular to the strike of the fault (Norris, 1958). Extensional faults can become reactivated during compressive events, reversing the initial fault throw. At regional scales this process is termed inversion. The results can be that net extension is retained at depth while net reversal is seen up shallow, with a null point in between marking where no apparent offset is seen (Williams *et al.*, 1989). A

low-angle reverse fault is called a thrust fault and displacement on such faults can often be tens or hundreds of kilometres.

2.2.4 Rifting models

Moving from fault models to the plate tectonic scale we see extensional faults systems creating rifts. Rifts tend to form in areas where there is anisotropy in the lithosphere, generally caused by earlier deformation events (Dunbar & Sawyer, 1988; Tommasi & Vauchez, 2001; Fossen, 2016). The geometry of the rift is controlled by extensional faulting, which is itself often influenced by pre-existing fabrics, even fabrics at angles of up to 60° to the extension direction can be reactivated (Youash, 1969). At the regional scale rifts are commonly observed to be made of several segments, each tens to hundreds of kilometres long (Morley, 1995). It is also noted that studies of the constant length coherent model of fault growth have recognised a significant control of underlying structure (Paton, 2006; Jackson & Rotevatn, 2013). Transfer zones or relay ramps between boundary faults are common and can create horst blocks and tilted fault blocks (Gibbs, 1984; Gibbs, 1989; Morley, 1995) and are described by Leader (2016) and Gibbs (1989) as a primary control on sediment input into rift systems, which are widely recognised in the North Sea. The juxtaposition of structure and reservoir within these rift systems can be significant for hydrocarbon exploration (Morley, 1995). In areas of widely spaced or poor-quality seismic data the finer detail of transfer zones along rift bounding faults becomes difficult and often overlooked.

Discussions on the topic of rifting were first published by authors such as Gregory (1921), Quennell (1958, 1959), Robson (1971), Baker *et al.* (1972), McConnell (1972), Illies (1974) and Garfunkel & Bartov (1977). McKenzie (1978) described rifted basin formation from pure shear lithospheric thinning, with associated increase in heat, normal faulting of the crust and syn-rift subsidence, often referred to as the uniform rift model. After cessation of rifting the reduction in heat causes a final post-rift subsidence stage. In this model the vertical and horizontal thinning are balanced, and the upper crust deformation is brittle, while the lower crust deformation is ductile. See Dewey (1982), Kusznir & Park (1987), Barr (1987) and Kusznir *et al.* (1991) for application of this model to several sedimentary basins, demonstrating the application of the uniform model for a range of geological histories. In particular Barr (1987) incorporated the domino model of faulting into the uniform rift model of McKenzie (1978).

The uniform rift model of McKenzie continues to serve as a basis for description of various rifting phenomena (Holdsworth & Turner, 2002), namely-

- Subdivision of the stages and rift sedimentary fill into pre-rift, syn-rift and post-rift sequences.
- The shift from syn-rift to post-rift is generally recognised by an angular unconformity, particularly at the crest of tilted fault blocks.
- The post-rift sequence initiates in the rift centre and onlaps progressively onto the underlying succession in response to slow heat flow decline and thermal subsidence (lithospheric sag), thus the thickest post rift sequence is above the rift centre and generally represents over 100 Ma.

(Holdsworth & Turner, 2002)

The uniform rift model of McKenzie by its very nature generally describes a symmetrical system while Wernicke (1985) proposes a simple shear model which reflects asymmetry. The Wernicke simple shear model uses large scale low angle detachments, as recognised in the Basin-and-Range Province of the USA [Wright & Troxel (1973); McDonal (1976); Proffett (1977); Rehrig & Reynolds (1980); Davis & Hardy (1981); Wernicke (1981, 1985)]. The rifted margin that was the upper plate to the detachment is characterised by lithospheric thinning, brittle high-angle upper crustal faulting, higher flank topography and larger heat flow which consequently yields post-rift subsidence. The lower plate is characterised by less thinning of the lithosphere, more low-angle crustal faulting, lower heat flow and consequently less post-rift subsidence. Etheridge *et al.* (1989) discuss how the simple-shear model yields opposing passive margin pairs that are asymmetric and presents examples from the United States Atlantic-northwest Africa margin pairs, and southern Australia-Antarctica margin pairs.

There are several other models evolved from these two initial models such as that presented by Lister *et al.* (1986), Driscoll & Karner (1998) and Brun & Beslier (1996) as well as the higher definition provided by seismic data presented by authors such as Rosendahl *et al.* (1986), Cheadle *et al.* (1987) and Ebinger *et al.* (1987). Of significant note is the flexural cantilever model of Kusznir & Egan (1989) which accounts for isostatic behaviour, see Kusznir *et al.* (1991) for application of this model to the Northern North Sea. One of the more recent rifting models is the dynamic model of Lavier & Manatschal (2006), where they propose much of the extension of Beta (β) factors above 1.7 (greater than 170% extension)

is taken up by large concave downwards faults, where the active part of the fault is steep within the basement and the inactive part follows the top basement.

More recent summarised dynamic modelling by Manatschal *et al.* (2015) in magma poor rift systems identifies a stretching mode, where rift evolution is mainly controlled by pre-existing weakness in the upper crust, and a thinning mode where rift evolution is controlled at a lithospheric scale. Most importantly, Manatschal *et al.* (2015) indicate that inherited thermal structure and inherited weakness can control strain localisation and thus the mode and architecture of rift systems. This agrees with much of the early research on rifting, in particular by Youash (1969). Peron-Pinvidic *et al.* (2013) provide clarity of the definition of architectural elements of rifts, specifically the proximal, necking, distal and outer domains, terms which have become widely used in recent years.

2.2.5 Rift Geometry

There are two main rift basin geometries, half grabens and full or conventional grabens. The conventional graben system is generally formed under pure shear and is symmetrical with high angle faults of opposing dip on either boundary. Minor faulting is commonly concentrated in the centre of the rift where opposing dips can create horst and graben blocks (Morley, 1995), creating what could be described as a piano key of fault blocks. Typically, such a symmetrical rift can have several kilometres of post-rift sediment associated with thermal sag and are described as “Steer’s Head” geometry (Dewey, 1982; White & McKenzie, 1988).

A half graben is where extension is accommodated by one main bounding fault, asymmetrically, creating a wedge-shaped package that expands into the main fault. Half graben formation has been extensively studied in the East African rift system by authors such as Rosendahl (1987). A large rift system can be developed as a series of oppositely dipping half grabens with each half graben having a curved strike, with offset reducing away from the centre. Where one graben ends, typically an opposing half graben takes over, thus accommodating the rifting. Minor faulting within the rift is more intense towards the flexural margin (Morley, 1995). Within a half graben where the main fault is listric a roll-over occurs as the hanging wall is rotated. To achieve this, the bed length must extend, thus thinning the thickness and in general this is accommodated by counter faults (not strictly antithetic) which are listric and tend to detach in any low strength or over pressured zone in the hanging wall (Gibbs, 1984). These counter faults migrate away from the main half graben fault as extension continues and the hanging wall is further rotated. Figure 2-5 reproduced from Morley (1995) shows the primary differences between fault distribution in half and conventional grabens.

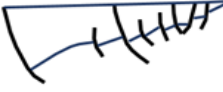
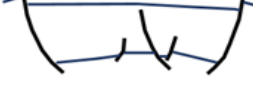
	HALF-GRABEN	FULL-GRABEN
		
Timing between major and minor faults	Minor faults are commonly abandoned prior to cessation of activity on boundary fault	Minor faults are commonly abandoned prior to cessation of activity on boundary fault
Mixture of antithetic and synthetic minor faults	Synthetic minor faults tend to be more numerous and take up the highest percentage of extension	More even mixture of minor faults dipping on both directions
Partitioning of extension between major and minor faults	Relatively high percentage of extension (20-50%) distributed on minor faults	Relatively low percentage (<20%) of extension distributed on minor faults
Minor fault spacing	Relatively closely spaced	Relatively widely spaced
Minor fault distribution	Minor faulting more intense towards flexural margin (FM). Antithetic faults more common towards FM.	Minor faults more frequent in central part of rift, less frequent approaching boundary faults

Figure 2-5. Differences between fault distribution in half – and full-grabens based on data from Lake Tanganyika (Morley, 1995).

2.3 Halokinesis and decollements.

The following literature review is a brief synopsis on the development of research into salt halokinesis and fault decollements within salt.

The mechanical properties of a rock play an important role in how it behaves during deformation, specifically folding and faulting (Ferrill *et al.*, 2017). Salt, used here to define all rock bodies composed primarily of halite (NaCl), is a rock type which deforms in a ductile or viscous fashion when subjected to stress under most geological conditions. Its low density means it is buoyant when significantly buried

by other sediments. Once movement has initiated the salt will continue to deform until the stress that initiated the flow is in equilibrium with the surrounding rocks resistance to the flow (Hudec & Jackson, 2007).

There are three stages to salt tectonics, 'reactive', 'active' and 'passive' halokinesis (Jackson & Vendeville, 1994; Harding & Huuse, 2015). Reactive halokinesis is normally initiated by differential stress, for instance at the site of localised faulting (Trusheim, 1960; Kockel, 1995; Koyi *et al.*, 1993; Vendeville & Jackson, 1993; Jackson & Vendeville, 1994) or gravity spreading (Fort & Brun, 2012); or induced by a thermal gradient (Hudec & Jackson, 2007). Salt diapirs with triangular geometries are common, located close to extensional faults (Harding & Huuse, 2015).

Active halokinesis takes over from the reactive stage when the overburden above the salt is thin and the salt itself has sufficient vertical extent to continue moving in response to differential loading of the overburden. Here the salt can push upwards into the overburden, pushing it upwards and aside (Schultz-Ela *et al.*, 1993; Jackson *et al.*, 1994).

Passive halokinesis is when the salt has reached the depositional surface (e.g. seabed) and remains there while adjacent sediments compact and subside.

Our understanding of halokinesis has been primarily developed from 2D and 3D seismic data, primary features being- canopies, walls, anticlines, rollers, pillows,

sheets, and stocks (Hudec & Jackson, 2007), which are often collectively referred to as diapirs. Often the salt features can themselves widen and ultimately collapse in environments of high extension, creating a minibasin (or depocenter) above the collapse (Vendeville & Jackson, 1992a, 1992b; Hudec & Jackson, 2007). A salt weld is the term given to the feature observed if a layer of salt thins such that the overlying and underlying section appears to touch. Commonly the lack of further available salt can trigger the collapse of diapirs discussed above.

While most halokinesis is seen in extensional environments it is also possible to initiate or modify existing salt structures during compression (Koyi, 1988; Stewart & Coward, 1995; Koyi, 1998; Sans & Koyi, 2001).

In the North Sea salt tectonics have impacted all aspects of hydrocarbon plays (trap, seal, migration, reservoir) and have been of interest since first studied in the 1950's (Trusheim, 1960). Subsequent studies (Jenyon, 1984, 1985, 1988; Remmelts, 1995, 1996; Stewart & Coward, 1995; Davison et al, 2000; Rank-Friend & Elders, 2004; Geluk et al., 2007; Stewart, 2007; ten Veen et al., 2012, Harding & Huuse, 2015) have used large well databases and 2D/3D seismic data and insights gained are transferable to frontier margins and basins. Salt is generally homogenous and thus has a transparent seismic character, the top and base are normally good seismic markers but steep flanks are normally not imaged (Stewart, 2007; Tari, 2014; Karlo, 2014; Fossen, 2016). Imaging beneath salt layers is also challenging as seismic energy is absorbed by salt, the velocity contrast causes incorrect placement of

reflectors in time and seismic ray paths are deflected by salt and often don't reach areas beneath salt structures (Stewart, 2007; Tari, 2014; Karlo, 2014).

As discussed, salt is often inherently a weak layer within a stratigraphic section. It thus plays an important role in faulting, specifically acting as a weak layer where strain is accommodated. Even thin layers of salt can act as decollement surfaces, often decoupling the faulting above and below the salt layer (Hudec & Jackson, 2007). This principle is equally valid in compressional settings, where strain is accommodated preferentially by salt layers, often associated with pre-existing faults or decollements (Jackson & Lewis, 2016). In extensional environments where there is insufficient salt available to create large diapirs the salt commonly develops as low amplitude salt rollers, which act as a decollement surface for listric faults (Hudec & Jackson, 2007).

3 Regional Geology of the NCSB

Two significant Palaeozoic orogenic events exerted significant structural control on Mesozoic basin development in the NCSB, the Caledonian Orogeny and the Variscan Orogeny (Ziegler, 1989; Petrie *et al.*, 1989; Rowell, 1995; Naylor & Shannon, 2011).

The Caledonian Orogeny (Ordovician to Early Devonian) saw the closing of the Iapetus Ocean as Ganderia/Eastern Avalonia docked with Laurentia to form Laurussia (Nance *et al.*, 2012 and references therein). A strong NE-SW Caledonian trend is observed onshore Ireland and the UK and is a primary tectonic trend in many offshore basins (Dore *et al.*, 1999).

The Variscan Orogeny (Late Carboniferous) saw the closing of the Rheic Ocean as Laurussia docked with Gondwana creating the Pangean super continent (Nance *et al.*, 2012 and reference therein). Northwest orientated convergence created local west-east striking folds and localised high-angle reverse faulting. These folds and faults are offset by northwest-southeast transfer faults representing the location of significant changes of trajectory and orientation of the main Variscan detachment (Petrie *et al.*, 1989). The more west-east Variscan trend is clearly seen in the geological outcrop onshore southern Ireland while the northwest-southeast transfers are interpreted from offsets in the northern limit of significant deformation, the Variscan Front (Figure 3-1) (Gardiner & Sheridan, 1981) and recognised by Delanty *et al.*, (1981) on sparker seismic profile data (the acoustic pulse is generated

by discharging an electrical pulse between two electrodes) with a predicted latest movement of Middle Miocene.

It is likely these large-scale transfer faults followed pre-existing lines of weakness in the basement and are thus interpreted as reactivated Caledonian strike slip structures (Kimbell *et al.*, 2005; Coward & Trudgill, 1989; Petrie *et al.*, 1989; Robinson *et al.*, 1981). Equivalent NW-SE transfers can be seen across the Atlantic Margin with the most prominent examples being the Senja Fracture Zone, the Jan Mayen Lineament and the Anton Dohrn Lineament, the former two are contiguous with transform faults in the adjacent oceanic crust (Dore *et al.*, 1999).

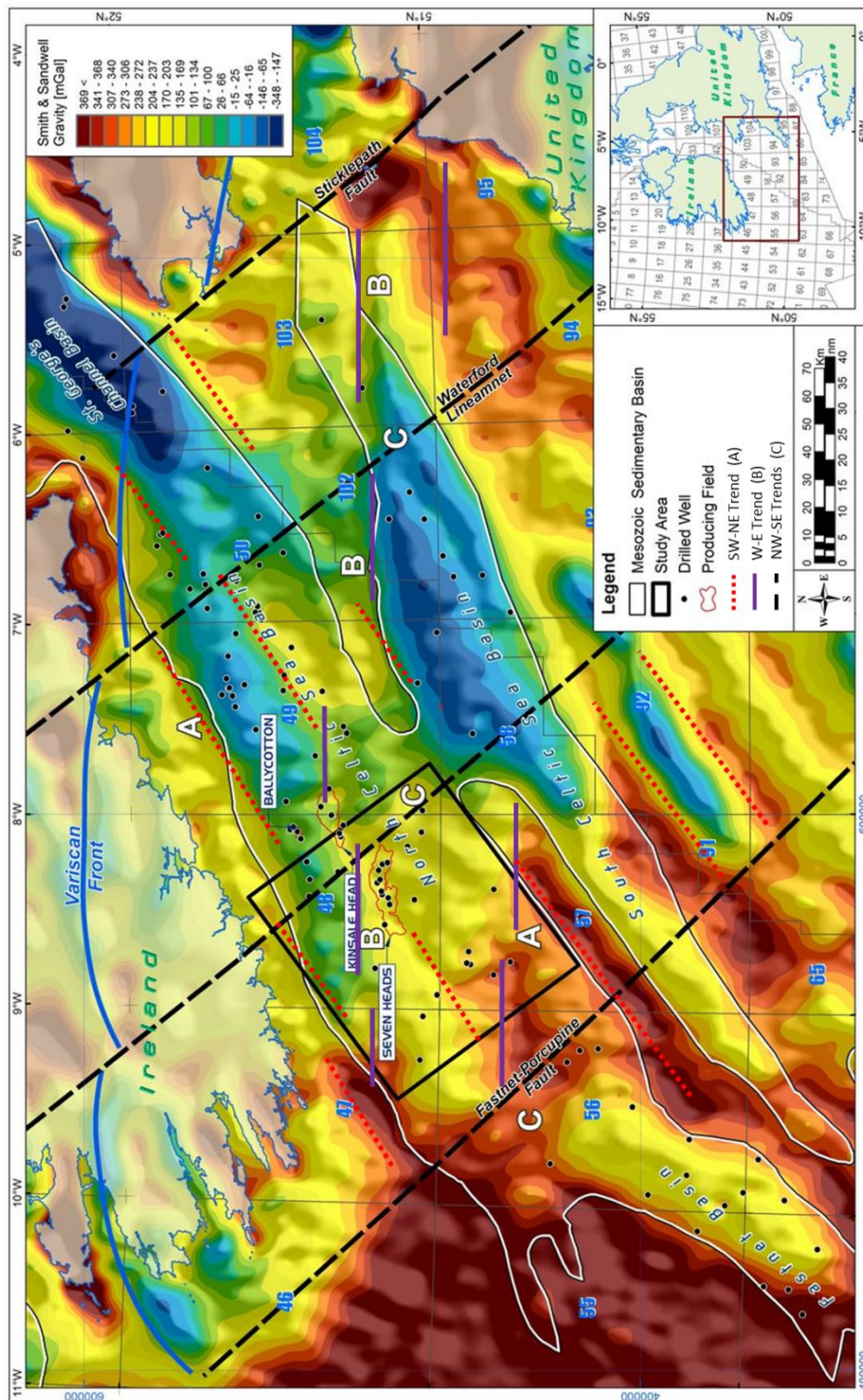


Figure 3-1. Freeair gravity map with regional Palaeozoic tectonic trends evident; (A) NE-SW trend, (B) W-E trend, (C) NW-SE trend.

The NE-SW, W-E and NW-SE Paleozoic tectonic trends are easily identified on regional gravity maps both offshore in the NCSB and onshore Ireland, indicating their control on Mesozoic basin development, shown at locations A, B and C respectively in Figure 3-1, trends are identified by Ziegler (1975 & 1982), Naylor & Mounteney (1975) and Pegrum & Mounteney (1978) and multiple subsequent authors. These regional tectonic trends are also identified along the entire Atlantic Margin from Norway to Ireland by Dore *et al.* (1999).

Petrie *et al.* (1989) discuss three phases of Mesozoic rifting in the NCSB, Triassic, Upper Jurassic and Lower Cretaceous. Tucker & Arter, (1987); Coward & Trudgill, (1989) and McMahon & Turner, (1998) describe the NCSB as having a conventional 'steer's head' geometry while other authors (Musgrove *et al.*, 1995; Rowell, 1995; Naylor & Shannon, 2011) describe how Mesozoic extension was accommodated on a large low angle normal fault that bounds the northern margin of the basin, leading to a half graben geometry.

The initial rifting phase in the Triassic and early Jurassic was accommodated along pre-existing Variscan thrust surfaces, the most northern of which, named here as the Morrigan Fault, has been mapped on deep refraction seismic data as a low angle detachment feature ((BIRPS & ECORS, 1986; McGeary *et al.*, 1987). Reactivation of Caledonian and Variscan structural features has been recognised as controlling Permian to Cretaceous rifting south of Britain (Chadwick *et al.*, 1989). Rifting in the Upper Jurassic and Lower Cretaceous created localised back rotation of fault

blocks and subsequent localised erosion at the basin flanks (for example the Helvick Field (Caston 1995)), however the centre of the NCSB was largely unaffected and a near complete Cretaceous and Jurassic interval is preserved (Shannon, 1995). There is also little seismic evidence of a Late Jurassic/Early Cretaceous uplift event (Late-Cimmerian), seen elsewhere in northwest Europe and postulated to be hot-spot related doming followed by an active rift (Underhill & Partington, 1993; Shannon, 1995). It is possible this event may be represented in the NCSB by a shift from Upper Jurassic marine facies to non-marine and lacustrine shales of the Purbeck Group (Tithonian to Berriasian). A generalised lithostratigraphic chart is presented in Figure 3-2 (after O’Sullivan, 2001) and a section of the recent lithostratigraphic chart from Copestake *et al.*, 2018 is presented in Figure 3-3.

There were two primary episodes of uplift in the Cenozoic, Paleocene and Oligo-Miocene, which have unroofed up to 900m (3000ft) of section (Murdoch *et al.*, 1995). Similar uplift timings and magnitude are seen across several basins in NW Europe and while several causes have been proposed by various authors it is likely that a combination of factors contribute, such as-

- Alpine compression as the African and European plates collided. (Murdoch *et al.*, 1995)
- Ridge-push associated with spreading along the Kolbeinsey Ridge (Dore *et al.*, 1999).
- Glaciation causing multiple erosion events of areas elevated by previous events, with further isostatic net uplift occurring during interglacial periods (Solheim *et al.*, 1996)

Scourse *et al.* (2009) describe the presence of large linear tidal sand ridges (LTSR) in the NCSB which are related to glaciation. These are the largest postulated LTSR deposits on Earth which demonstrates that glaciation could have played a significant role in NCSB Cenozoic uplift, something which to date has been largely overlooked.

These uplift events have eroded most of the Cenozoic section in the NCSB and in places significant amounts of the Upper Cretaceous. The outcrop at seabed is therefore generally Cretaceous with thin remnants of Cenozoic lithologies found preserved in the southwest of the basin (Copestake *et al.*, 2018).

The 2011 Barryroe 3D seismic survey, acquired by Providence Resources Plc., provided the first 3D seismic view of the deep basin centre, showing significant fault surfaces and evidence of minor halokinesis. Intra-basinal faulting identified in this study provides an updated understanding of the structural evolution of the NCSB. The evidence of minor halokinesis proves the presence of mobile Triassic evaporates in the basin centre, previously only proven on the basin margins (Shannon, 1995) and adjacent basins (Bulnes & McClay, 1998; Evans *et al.*, 1990) and speculated to exist onshore Ireland (Clayton *et al.*, 1986).

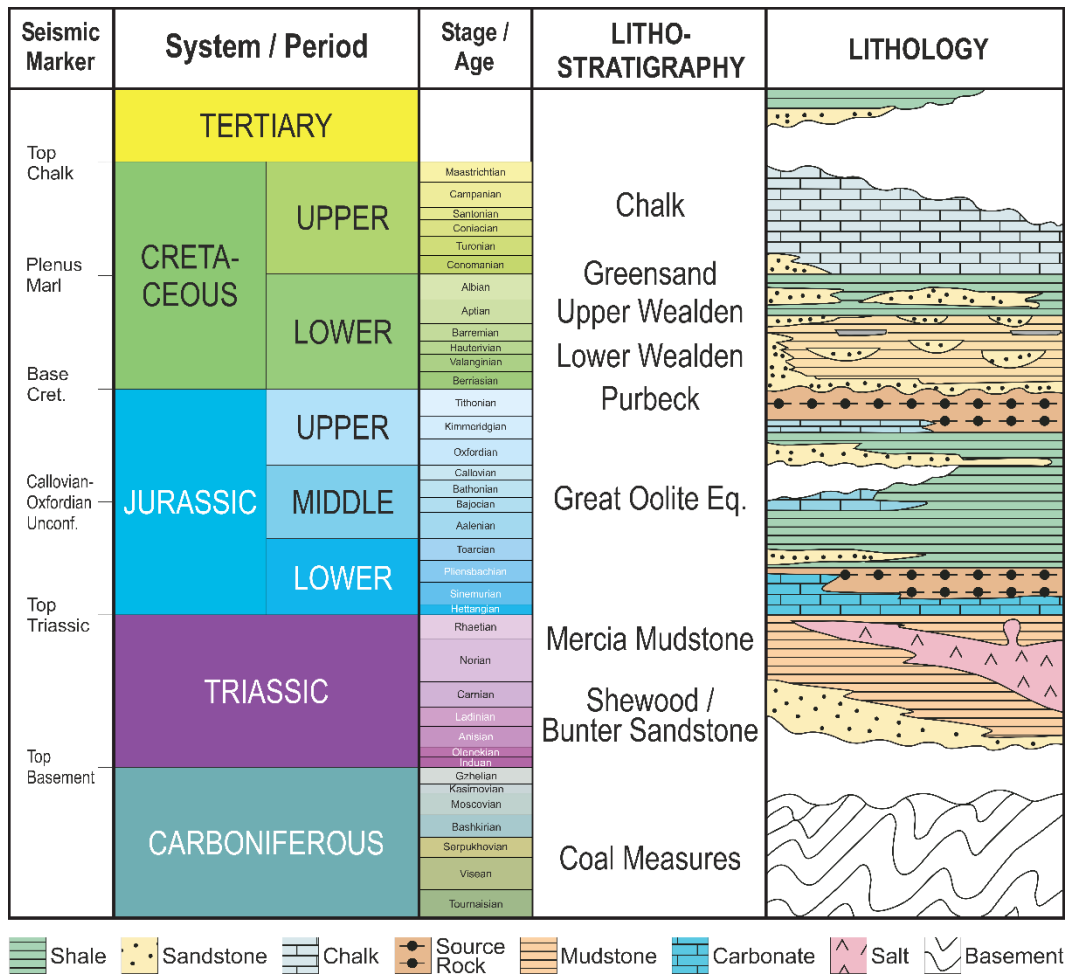


Figure 3-2. Generalised lithostratigraphy of the NCSB, modified from O’Sullivan (2001).

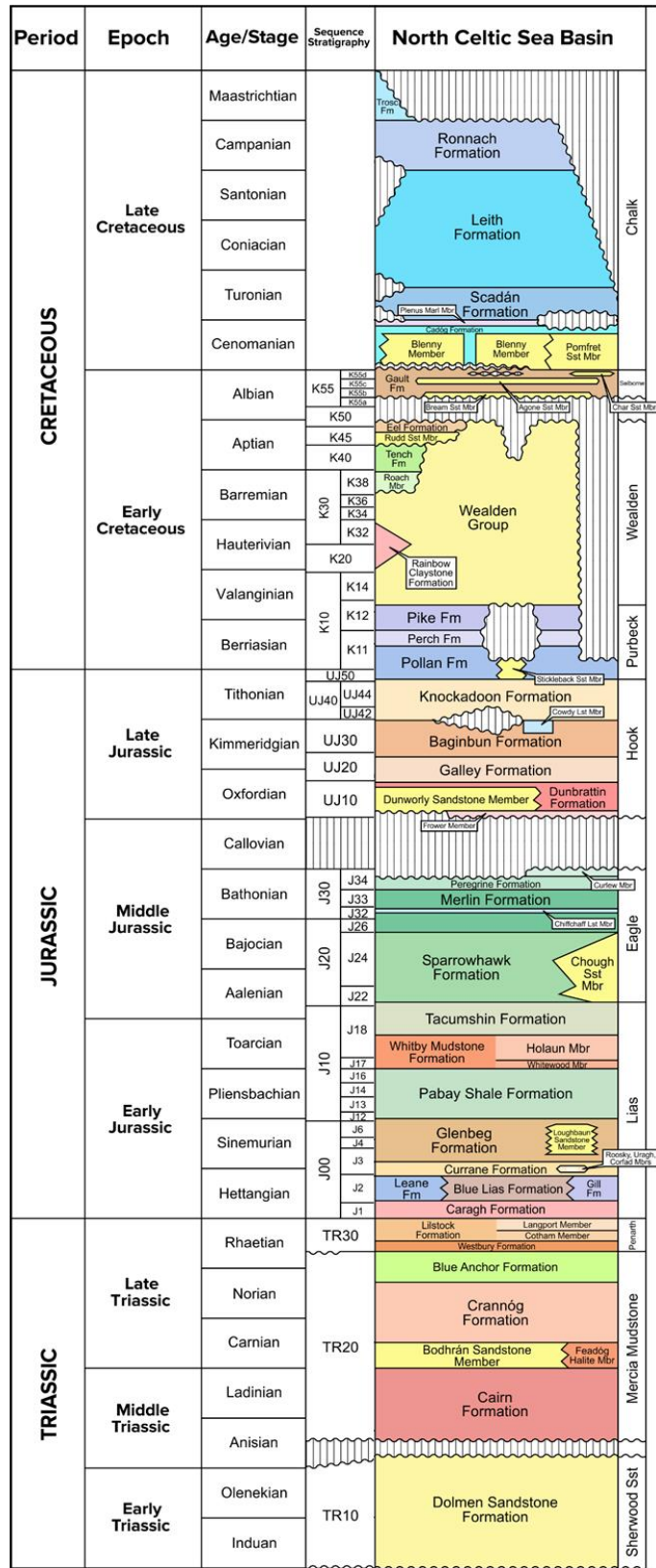


Figure 3-3. Triassic to Cretaceous chronostratigraphy of the NCSB, (Copestake *et al.*, 2018).

4 Hydrocarbon Exploration History

The history of hydrocarbon exploration in the NCSB dates back to the first seismic survey which was acquired in 1969 and the first well, 48/25-1, which was drilled by Marathon in 1970. The period through to 1995 saw significant hydrocarbon exploration with 68 exploration wells (Figure 4-2) and oil and gas discoveries at various stratigraphic levels (Shannon, 1991). Much of the previous research in the basin was conducted in the period from 1983 to 1995 when almost half the wells were drilled. Only 15 exploration and appraisal wells have been drilled in the last 20 years (Figure 4-2). A map of the exploration, appraisal and production wells is shown in Figure 4-1 and a full listing is included in Appendix A.

From the 83 exploration and appraisal wells drilled there are only 4 producing fields in the NCSB, namely Kinsale Head, Southwest Kinsale, Ballycotton and Seven Heads, a relatively poor success rate. These fields all produce from marine and fluvial sandstone reservoirs of the Lower Cretaceous (Albian to Barremian) at depths of less than 1,200m (4,000ft) and are located within or adjacent to the study area (Figure 1-1).

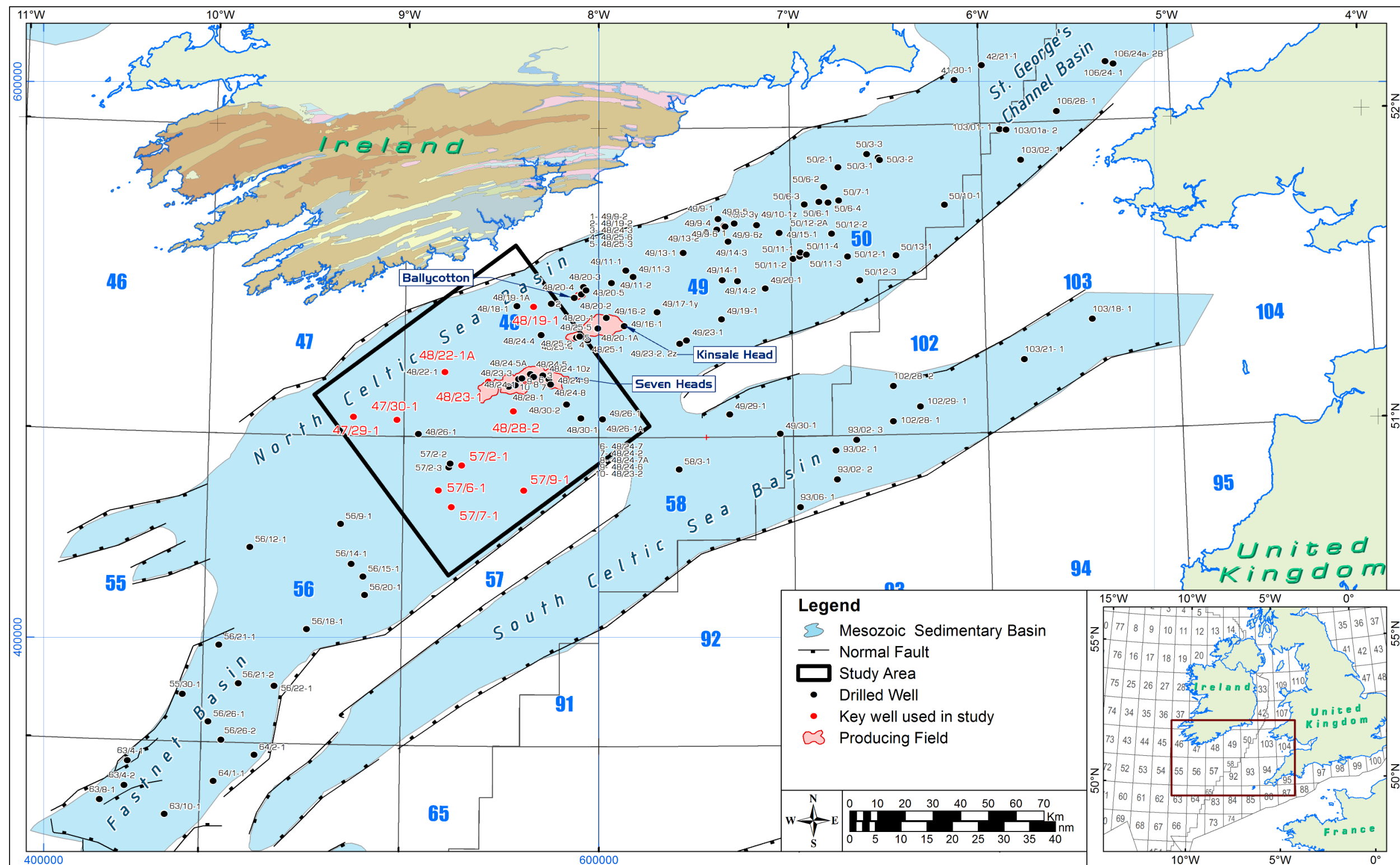


Figure 4-1. Map showing location of all wells in the North Celtic Sea Basin and adjacent basins. Key wells used in this study are highlighted in red. Producing gas fields are also highlighted in pink.

(Source Dept. of Communications, Climate Action & Environment; DCCAE 2019).

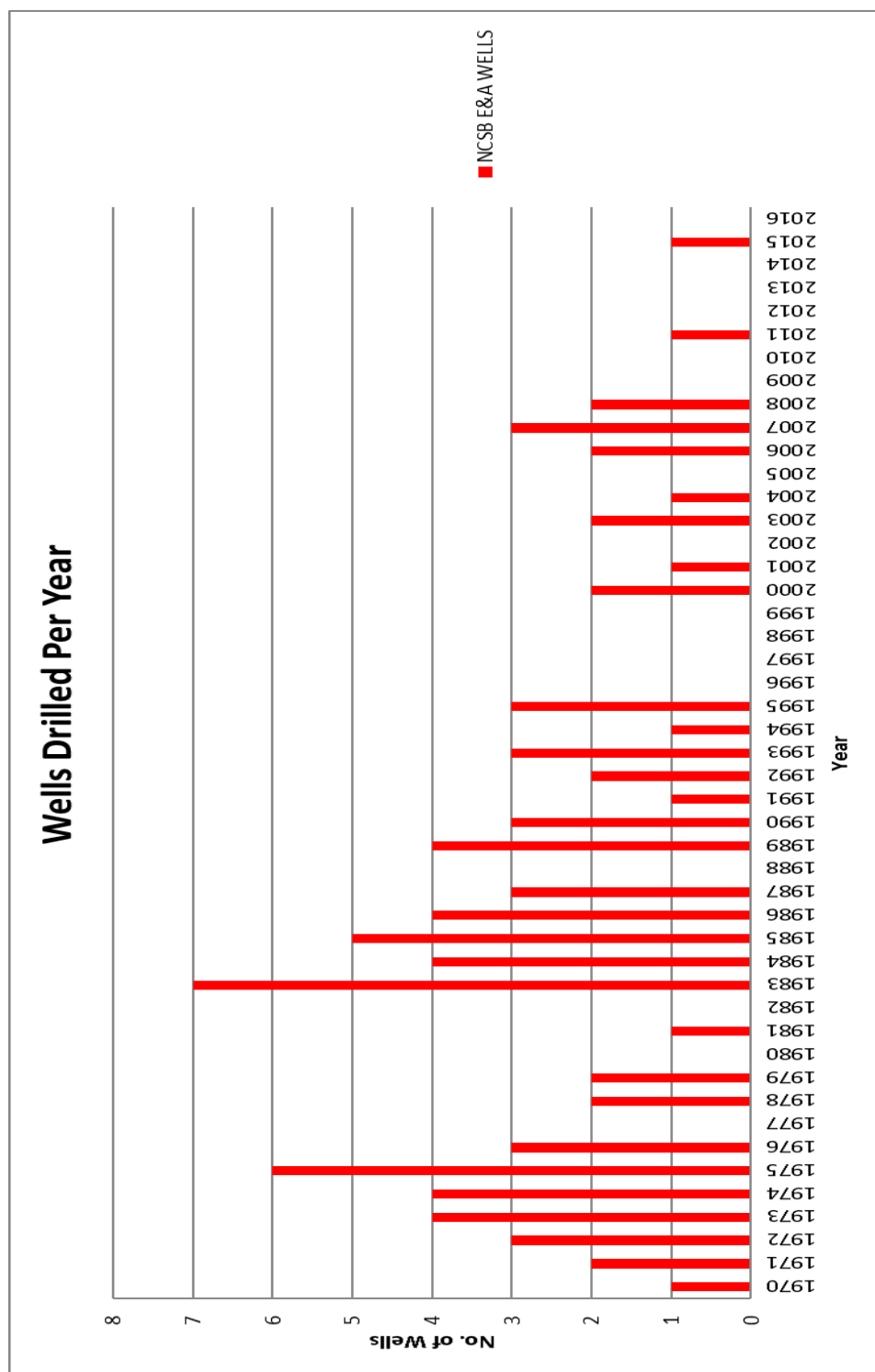


Figure 4-2. Details of hydrocarbon exploration and appraisal wells drilled per year in the NCSB. (Source Dept. of Communications, Climate Action & Environment; DCCAE 2019)

5 Analysis of Previous Structural Models

There are two alternative structural models for the NCSB described by previous authors. One is a conventional ‘steer’s head’ graben (Tucker & Arter, 1987; Coward & Trudgill, 1989; McMahon & Turner, 1998) while the other is a half graben (Petrie *et al.*, 1989; Musgrove *et al.*, 1995; Rowell, 1995; Naylor & Shannon, 2011).

Both models are viable on the vintage seismic data available at the time of their publication. Neither could be discounted due to poor deep imaging on the available seismic datasets but they have significant implications on the sedimentology and hydrocarbon prospectivity of the NCSB. Modern seismic data and modern seismic reprocessing has however greatly improved the quality of seismic data in the NCSB.

Each of the previous published illustrated models has been re-drafted and are presented here at the same scale and transposed over a common seismic line to allow an assessment of each model, and direct comparison between models. The common seismic line chosen was SWAT-5, a NW-SE orientated line through the study area, which was utilised by several previous authors as the basis for their illustrated model, Figure 2-3. The product presented is not the original raw stack data made available by BIRPS & ECORS (1986) and used by previous authors, but an updated seismic product which has been migrated to ensure correct positioning of seismic events and made available in 1999 (BIRPS, 1999). The SWAT-5 seismic line presented has comparable imaging to the modern seismic data, Figure 6-2.

5.1 Conventional Steer's Head Geometry

The model proposed by Tucker & Arter (1987) is a schematic model, not based specifically on the SWAT-5 seismic line, but appears to be heavily influenced by this line, Figure 5-1. While they describe a conventional graben, the illustration shows a Jurassic section which appears to thin towards the southeast, away from a major fault, more representative of a half graben. The Lower Cretaceous section thins to the northwest, with a thickening evident above the Labadie Bank High – Pembrokehire Ridge in the southeast, there is no explanation for this switch in sediment depocenter between the Jurassic and Lower Cretaceous. The illustrated model (Figure 5-1) does not accurately reflect the thickening of Triassic and Lower Jurassic seismic packages evident on the SWAT-5 seismic line, particularly to the southeast of the line. The model does include a localised thin package of Cenozoic above the Upper Cretaceous Chalk and shows an inversion fold within the Cretaceous, both of which represent important elements of the structural history.

The model proposed by Coward & Trudgill (1989) is a conventional graben described as having developed over a reactivated southerly dipping Variscan detachment, however no structural connection is shown between the identified Variscan detachment and the Mesozoic basin, Figure 5-2. The illustrated model also incorrectly places the Top Jurassic significantly higher than other models, at or close to, the Base Chalk in the known wells. Note, well tops are not shown at this scale, but relative position can be confirmed by review of Figure 7-6 to Figure 7-4 which are presented at a larger scale. Faults and horizon interpretation can also

be seen to cross-cut continuous seismic events at several places, in particular the Triassic interpretation in the basin centre. The illustrated model shows a roll over at the Top Jurassic in the footwall of a south-easterly dipping fault which appears to be a normal fault with associated growth in the hanging wall in the Lower Jurassic. The Upper Jurassic however appears to thin into the hanging wall. There's no discussion to justify this interpretation however it should be noted this was barely noticeable at the scale the model was originally presented at and is thus likely a drafting error.

McMahon & Turner (1998) also present a conventional graben model with a clear sag phase interpreted to be in the Lower and Upper Cretaceous (Figure 5-3). The shallow interpretation appears to be broadly robust, however the deeper interpretation is inconsistent with the seismic data on SWAT-5 as there is clear discordance between the Top Triassic interpretation and the seismic character. The model also does not clearly show the broad inversion folds evident in the Upper Cretaceous on the seismic data (modern and vintage) which are an important part of the structural history.

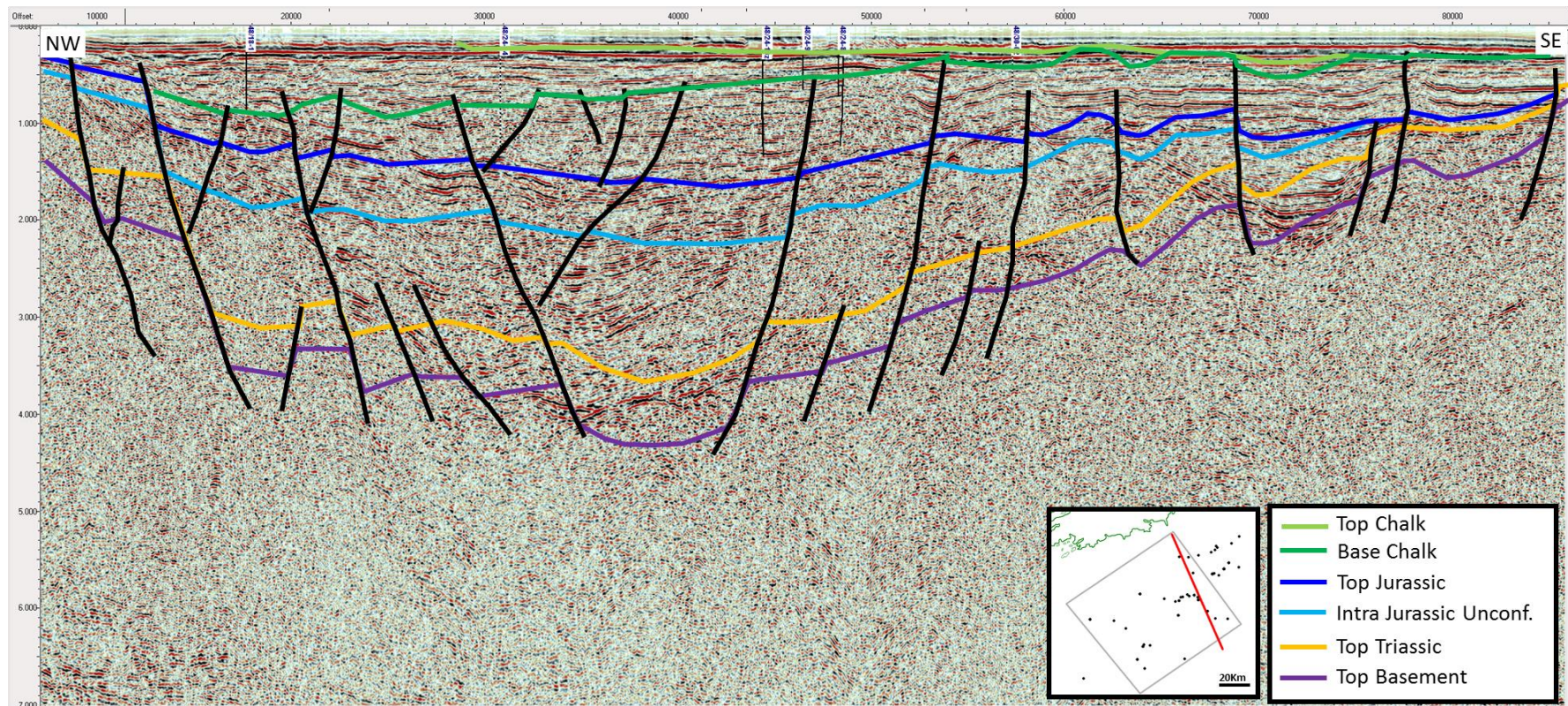


Figure 5-1. Conventional graben model proposed by Tucker & Arter (1987) (general model presented) overlain over SWAT-5 seismic line. The model shows a localised Cenozoic package and an inversion fold within the Cretaceous. The Lower Jurassic thins towards the southeast, more representative of a half-graben while the Lower Cretaceous thickens to the southeast with no explanation for the change. Interpretation at the Jurassic and Triassic level do not accurately reflect the seismic data.

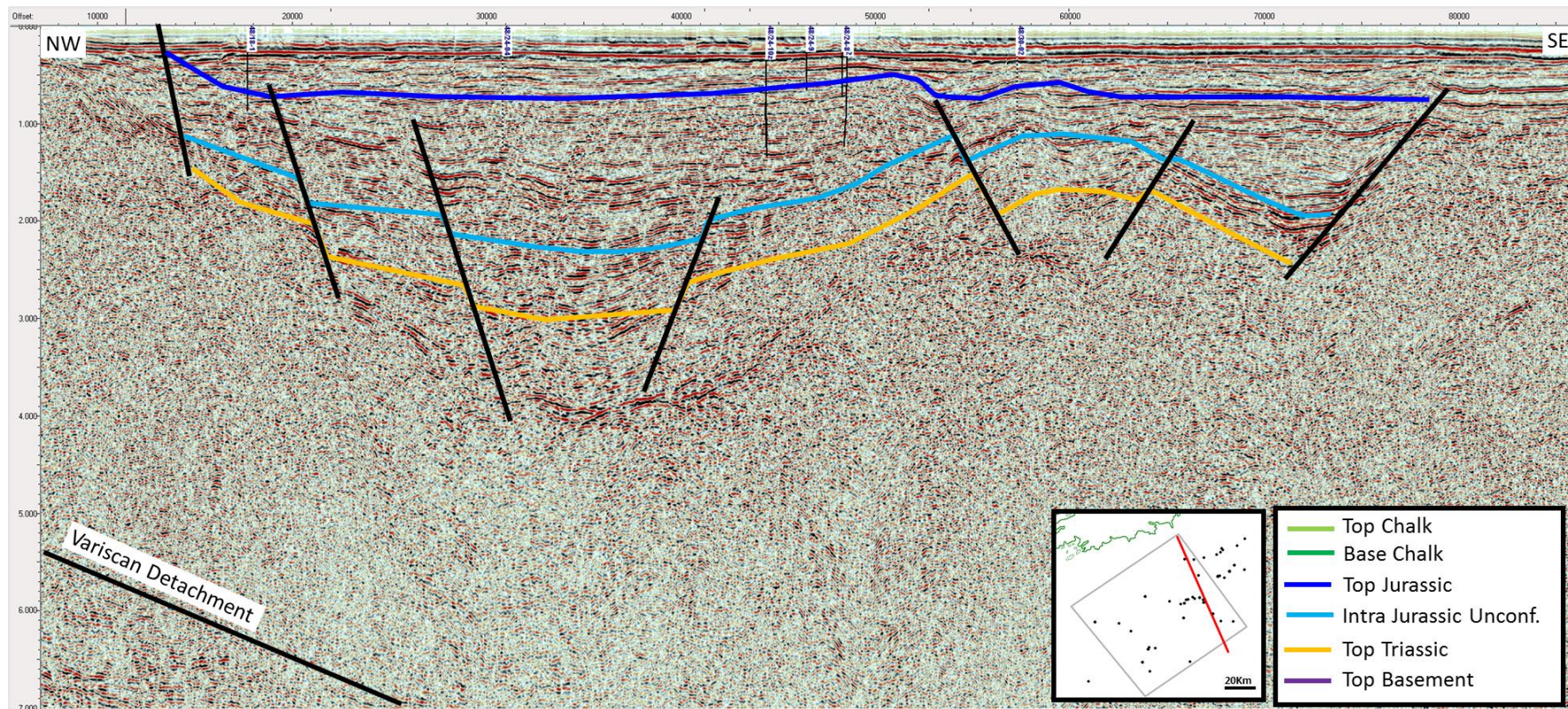


Figure 5-2. Conventional graben model proposed by Coward & Trudgill (1989) using SWAT-5 seismic line. The model incorrectly places the Top Jurassic at or close to the Base Chalk in the known wells. Faults and horizon interpretation can also be seen to cross-cut continuous seismic events at several places, in particular the Triassic interpretation in the basin centre.

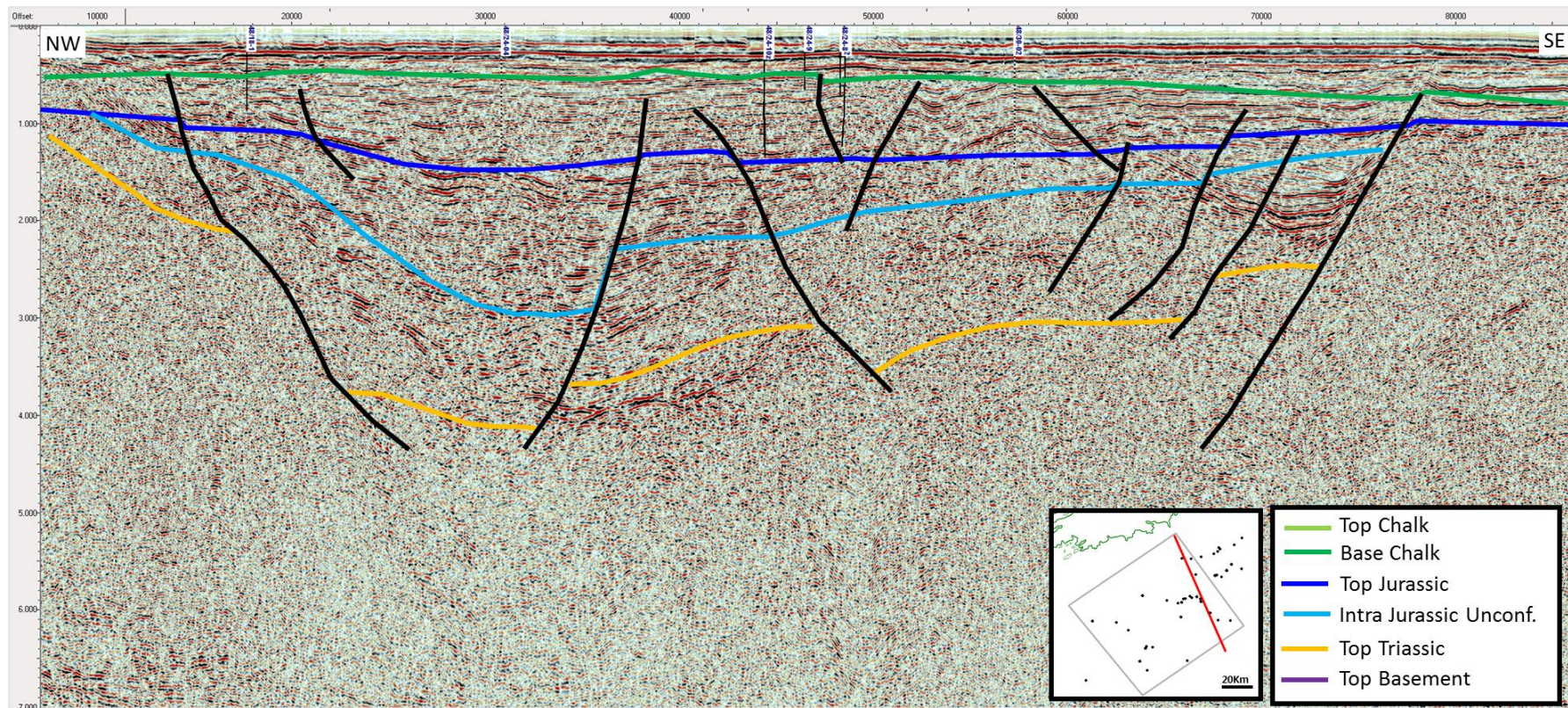


Figure 5-3. Conventional graben model using MPCR-17 seismic line, proposed by McMahon & Turner (1998) overlain over SWAT-5 seismic line. The model interprets a basin sag phase in the Lower and Upper Cretaceous but does not show the compressional features known to exist at this level. The deeper interpretation is also inconsistent with the modern seismic data.

5.2 Half Graben Geometry

The first interpretation of the NCSB as a half graben was by Petrie *et al.* (1989). They present a major south easterly dipping normal fault connecting the Mesozoic section with the underlying basement structure, Figure 5-4. This fault is described as a reactivated Variscan fault. The Triassic interval shows clear half graben geometry with a sedimentary wedge expanding to the northwest into the fault, however the Upper and Lower Jurassic interval has growth accommodated evenly on several faults across the basin. This change in structural character is not discussed by the authors. The illustrated model shows reverse movement on one of the central normal faults, acknowledging the late inversion events. As the model is not specially created at SWAT-5 there are several places where the interpretation crosscut the seismic events.

The half graben model proposed by Musgrove *et al.* (1995) deals only with the Triassic interval, and not the remainder of the sedimentary section in the NCSB. The model, shown in Figure 5-5, has been modified by applying a simple rotation to align the model with the likely present day position of the Triassic interval on SWAT-5, this is to allow comparison against other models. Clearly the model is schematic but does agree with the Triassic interpretation of many other authors.

Rowell (1995) presents a schematic illustration of a half graben model for the NCSB, Figure 5-6. The model appears to be broadly based on SWAT-5 however some interpretation is not supported by the seismic, for instance the basement

interpretation. It is also noted that the Base Chalk interpretation is significantly deeper than the well ties, note, well tops are not shown at this scale, but relative position can be confirmed by review of Figure 7-6 to Figure 7-4 which are presented at a larger scale. The Triassic and Lower Jurassic show clear half geometry with growth against a primary normal fault and thinning to the southeast away from the fault. The Upper Jurassic and Cretaceous are less dominated by the half graben geometry and appear almost constant thickness across the basin. This change in sedimentation thickness is not discussed by Rowell.

Naylor & Shannon (2011) describe the NCSB as having a half graben geometry, however they present no basin wide illustration. Figure 5-7 shows the model they present, which only covers a small portion of the NCSB. Interestingly, the Cenozoic section appears to show a steer's head geometry, where the basin sag phase has created deposits over a larger area than the original fault bounded basin, something normally associated with conventional grabens. This inconsistency is not discussed by the authors.

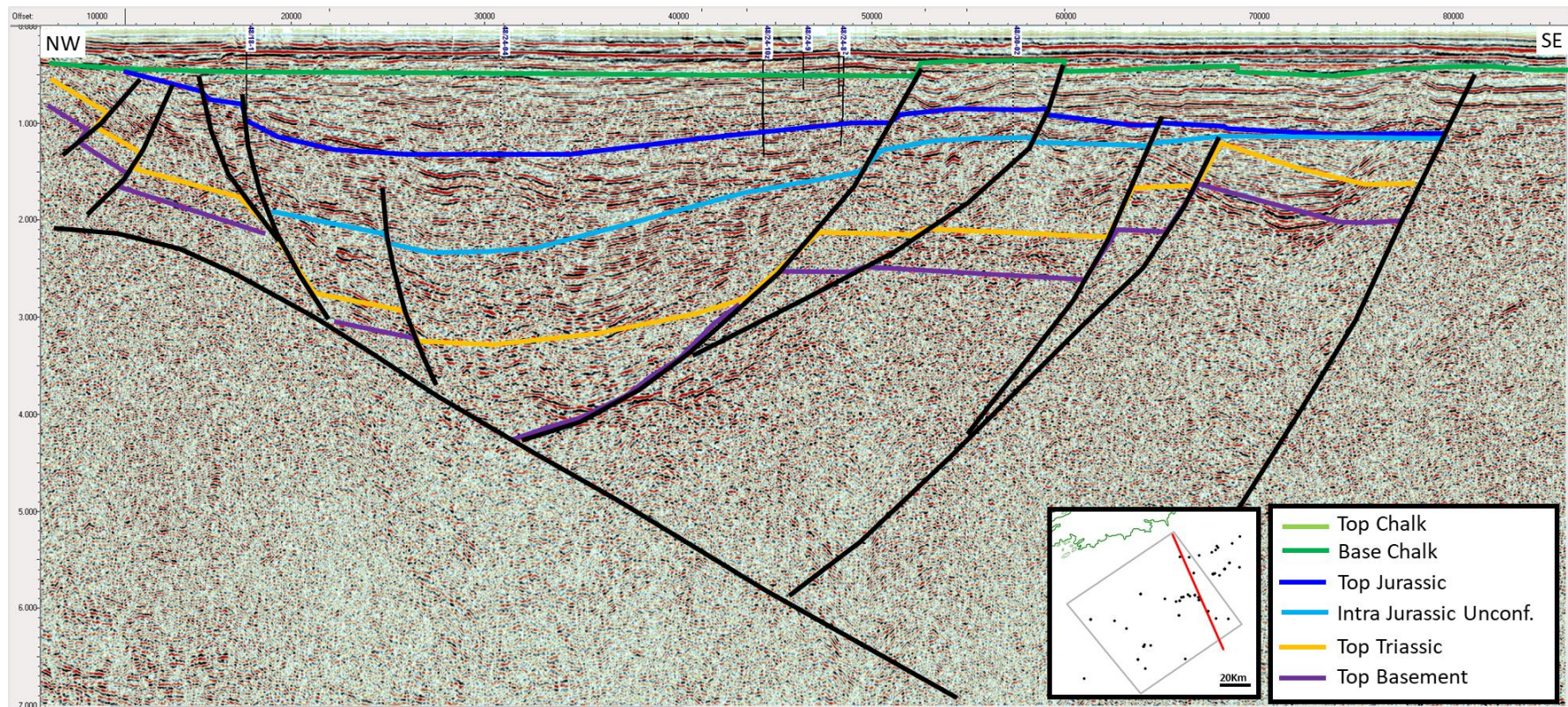


Figure 5-4. Half graben model proposed by Petrie *et al.* (1989) (general model presented) overlain over SWAT-5 seismic line. The model interprets a half graben sediment wedge at the Triassic however the Lower and Upper Jurassic section has growth accommodated evenly on several faults across the basin which is inconsistent with a half graben.

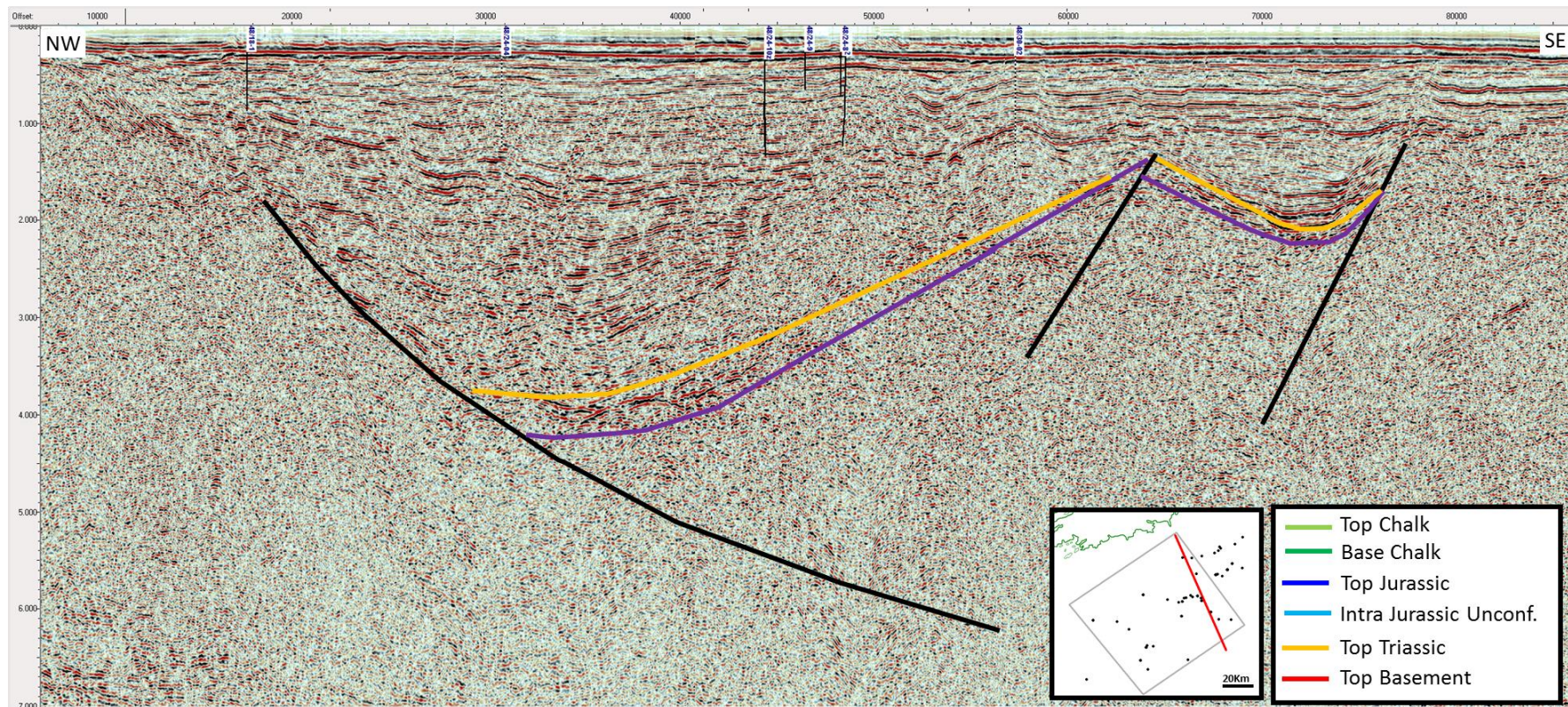


Figure 5-5. Half graben model proposed by Musgrove *et al.* (1995) (general model presented) overlain over SWAT-5 seismic line. The interpretation only addresses the Triassic section, but is consistent with the seismic data and the interpretation of other authors.

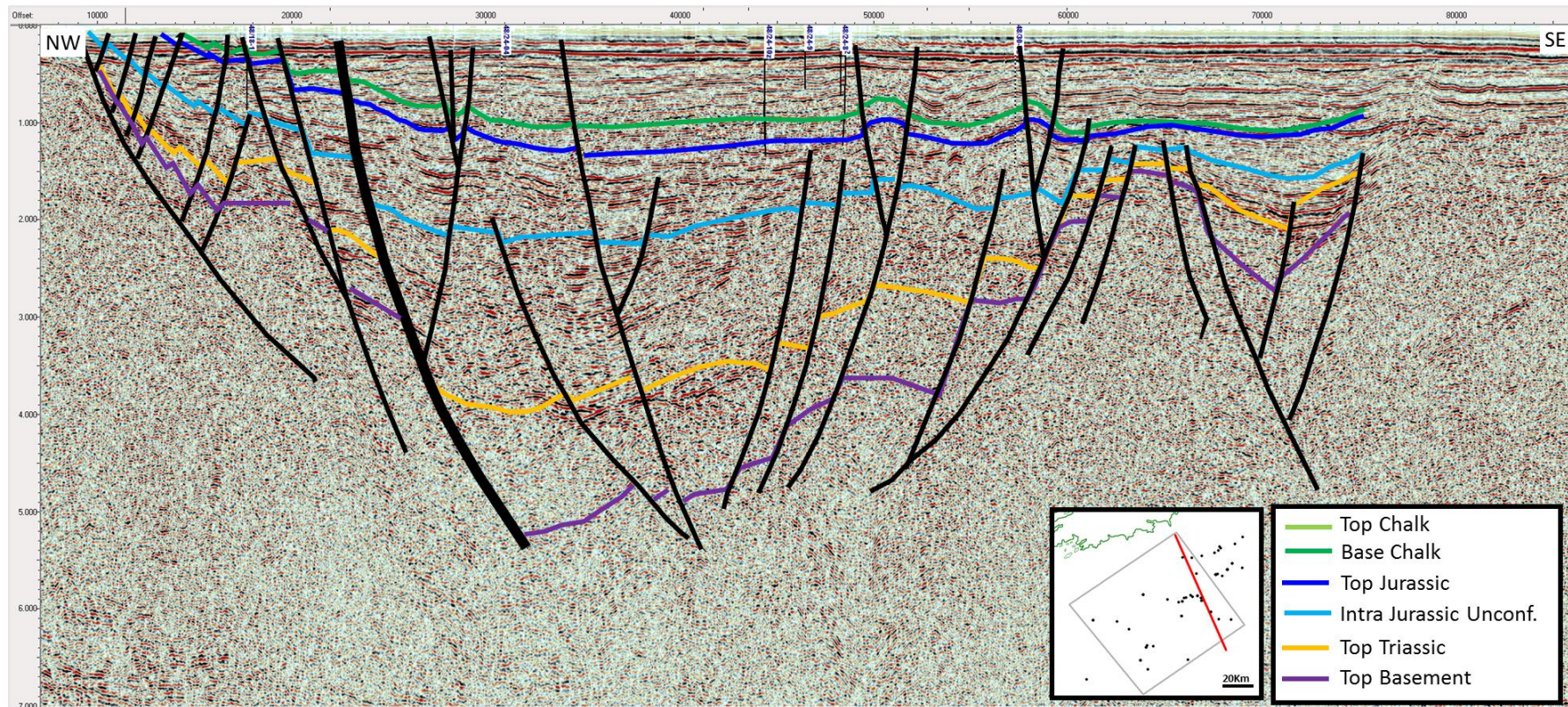


Figure 5-6. Half graben model proposed by Rowell (1995) (general model presented) overlain over SWAT-5 seismic line. A half graben is illustrated with a Triassic and Lower Jurassic sedimentary wedge, but the Upper Jurassic and Cretaceous appears almost constant thickness across the basin.

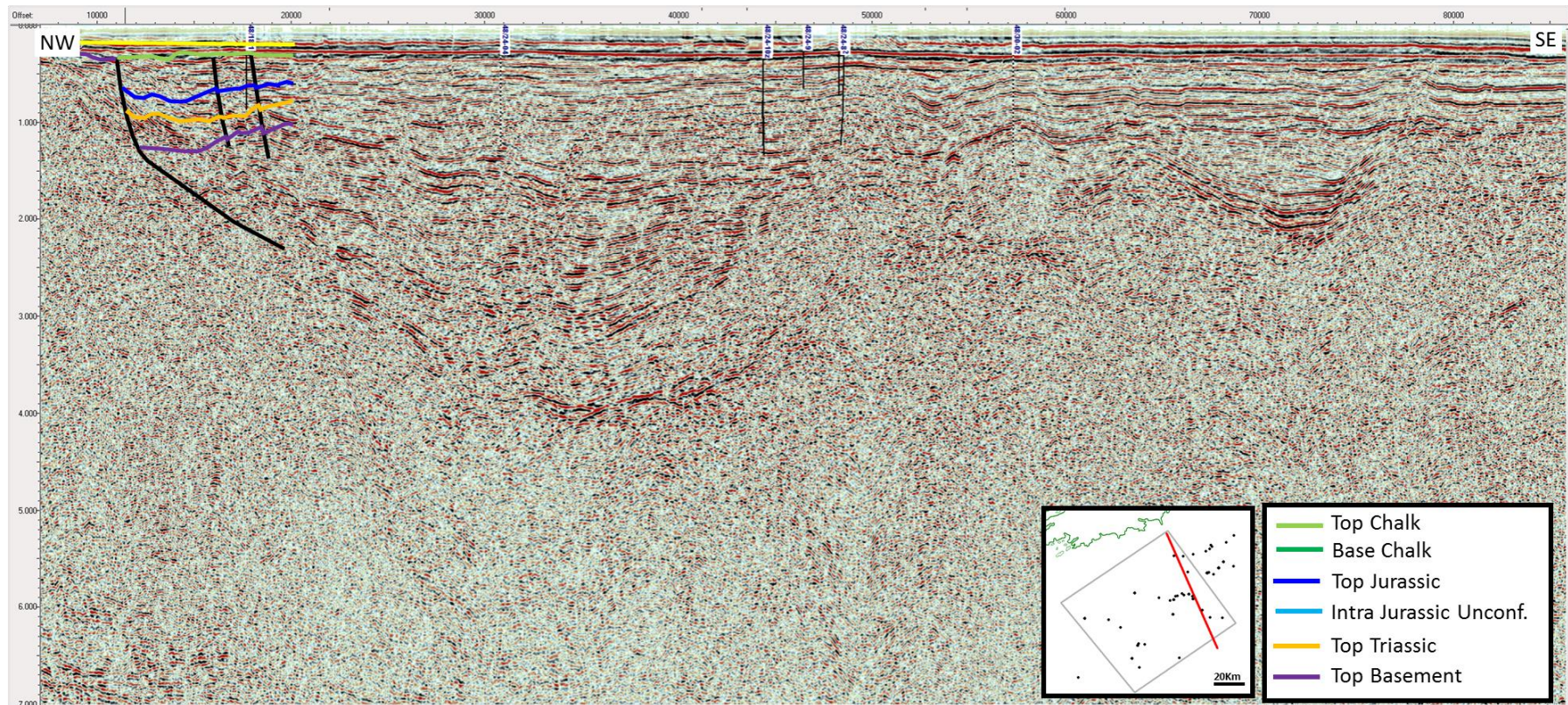


Figure 5-7. Half graben model proposed by Naylor & Shannon (2011) (general model presented) overlain over SWAT-5 seismic line. The interpretation only covers the northern basin boundary. The Cenozoic section appears to show a steer's head geometry which is inconsistent with a half graben model.

5.3 Requirements of an updated model

From analysis of the existing published structural models of the NCSB it is clear that components of each model appear to match well with SWAT-5, however there are several inconsistencies with each model. The models were also compared against several other modern seismic lines and the identified inconsistencies between the models and the seismic data were confirmed. A revised model is therefore required which utilises the modern seismic data and accurately reflects the structural development of the NCSB.

A revised model should:

- Extend over the full width of the basin.
- Tie the local and regional well control.
- Recognise and account for the thickness changes evident on the seismic.
- Connect the Mesozoic structure to the underlying Caledonian/Variscan structure.
- Illustrate the inversion structures evident in the NCSB and explain their development and location within the basin.

6 Methodology

6.1 Seismic Data Quality

The quality of seismic data is influenced by a number of factors, from the complexity of the geology that's being imaged, acquisition parameters and the processing of the data. Firstly, data acquired using a 2D method results in a series of two dimensional images of the subsurface, while data acquired using a 3D method result in a full three dimensional image (Robein, 2010; Meunier, 2011; Robinson & Clark, 2017). In general, less compacted lithological units are better imaged by seismic data than compacted units, such as basement. Figure 6-1 demonstrates typical seismic imaging of Cenozoic rocks in northwest Europe (top right) compared to underlying older basement rocks (middle left).

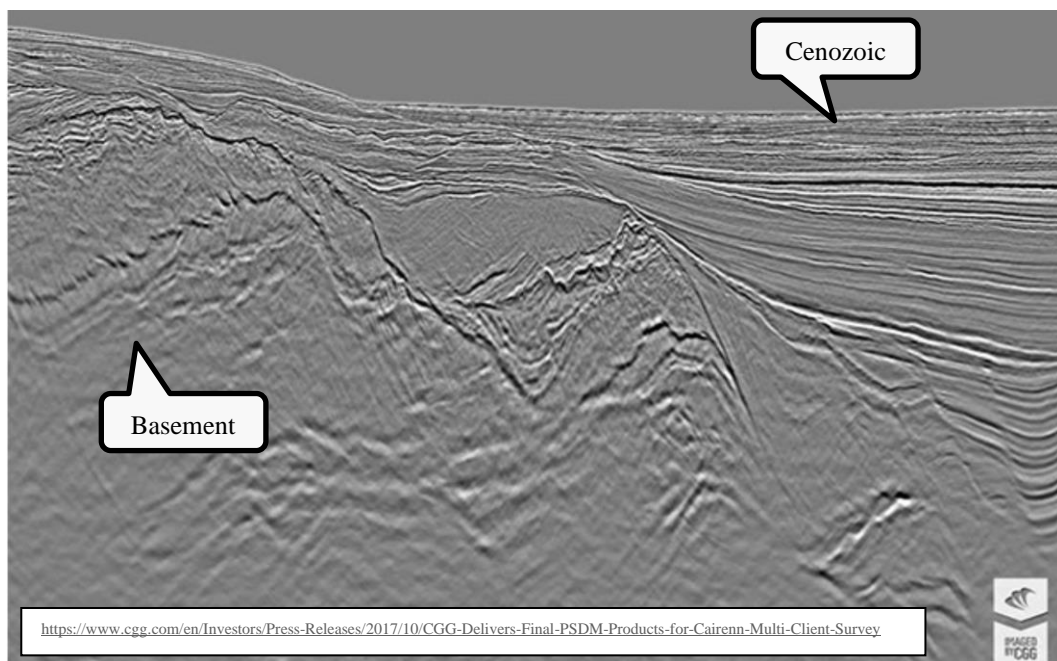


Figure 6-1 Example seismic line, not from NCSB, demonstrating seismic data quality is generally better in younger less compacted rocks (top right).

The standard seismic image has a vertical scale of time, or more specifically two-way-time (the time taken for an acoustic signal to travel down into the subsurface and return back up). Processing of the recorded data into an image of the subsurface requires an estimate of the velocity of the rocks in the subsurface. On vintage data this velocity modelling was rather simplified, however on modern data the determination of the velocity has improved significantly. The actual mathematical algorithms used to convert the recorded data into a seismic image have also improved significantly from early methods known as stacking, to modern methods known as migration (Yilmaz, 2001; Robein, 2010; Bancroft, 2007; Robinson & Clark, 2017). The migration method calculates multiple acoustic signal travel paths through the subsurface to determine the most accurate image of the subsurface. 2D data utilises migration in the 2D domain along the line length, while 3D data utilises a full three-dimensional migration to ensure the optimal imaging result (Yilmaz, 2001; Robein, 2010; Bancroft, 2007; Robinson & Clark, 2017).

As described in Chapter 3, much of the NCSB has highly compacted, high density Cretaceous Chalk lithology at the seabed, often with intense brittle fracturing. The basin is thus described geophysically as having a hard water bottom. This hard water bottom and shallow water depth creates significant issues for seismic imaging as much of the seismic energy is reflected at the seabed and can echo in the water column. This echoed energy is described as a multiple, and in the NCSB it is repeated at 0.13 second intervals (being the water depth of 100m (320ft) in two way travel time) on the seismic record, and is challenging to remove during processing (demultiple) (Weglein *et al.*, 1997; Yilmaz, 2001; Weglein & Dragoset, 2005). The

Chalk facies also attenuates high frequency energy from the propagating seismic wavelet, leaving only the lower frequencies to be recorded (Newman & Worthington, 1982; Barton, 2006; Sato & Fehler, 2009). This means the vertical resolution of the resulting seismic image will be low as vertical resolution of seismic data are directly linked to frequency of the seismic (Brown, 2011; Herron, 2011). A second multiple series is also created at the base of the chalk, with seismic energy echoing between seabed and the base of the Chalk, creating further complexity for seismic imaging. Critical advances in demultiple techniques during the processing of seismic data, have helped ensure only real data are shown in modern seismic data (often referred to as primary energy) and that multiples (echoes) are removed (Weglein *et al.*, 1997; Yilmaz, 2001; Weglein & Dragoset, 2005).

Exploration for hydrocarbons began in the late 1960's in the NCSB and the seismic data acquired in the 1970's and 1980's are generally poor quality. Seismic processing was not sufficiently advanced to migrate the recorded data to the correct subsurface position, or to tackle the significant multiple energy, as described above. It is therefore difficult to discriminate real primary subsurface reflections on this data.

Seismic data acquired in the NCSB in the 1990's and 2000's are characterised by better processing, however, the majority of the data from this period consists of small, localised datasets. These data were also generally acquired with site survey vessels and small seismic sources. These vessels were commonly used due to

higher availability and shorter mobilisation distances than conventional seismic vessels. The seismic source for the older 1970's and 1980's data was generated by large dynamite sources, or up to 30 airguns acting collectively as though they were one large instantaneous airgun. The site survey vessels which acquired the majority of the 1990's and 2000's seismic data used seismic sources with generally 4 airguns. Simply put, the seismic source for the majority of the 1990's and 2000's seismic data was approximately 10% of the size of older data. Proprietary seismic survey design modelling available to Providence Resources Plc. shows this acquisition method provides insufficient acoustic source to allow penetration of signal into the subsurface to image the entire basin fill of the NCSB (Wells, 2004).

The modern 2D and 3D data, acquired or reprocessed after 2000, have utilised large seismic sources to capture images of deep stratigraphy within the NCSB. These surveys were all acquired using conventional seismic vessels and the processed using modern processing methods, including migration and often several stages of demultiple. It should be noted that the SWAT seismic dataset acquired in 1983 utilised large seismic sources to ensure penetration of signal into the subsurface and a reprocessed seismic product was made available in 1999 (BIRPS, 1999). The SWAT-5 seismic line through the NCSB has comparable imaging to the modern seismic data, Figure 6-2.

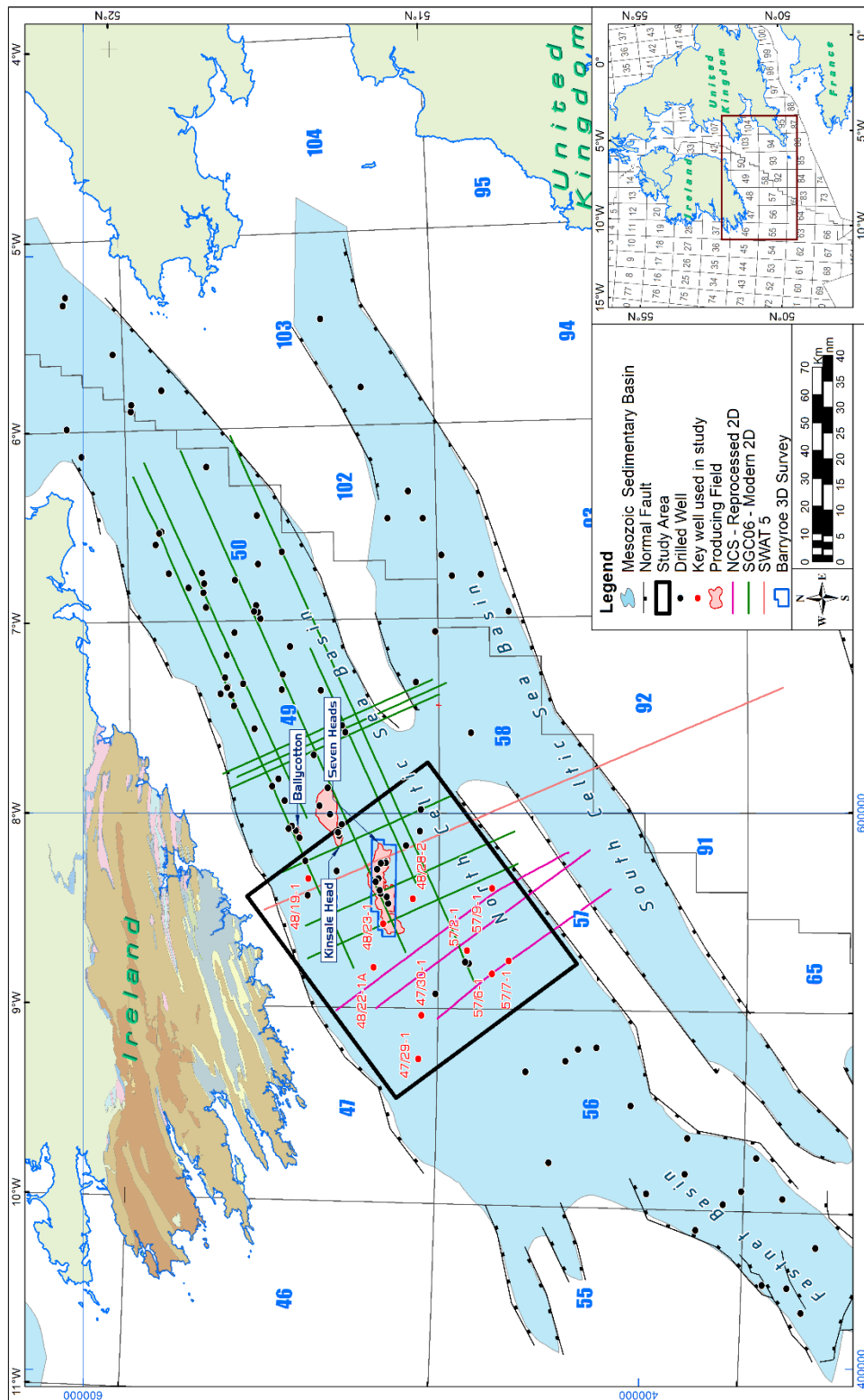


Figure 6-2. Location map with key seismic and wells highlighted. Source
Dept. of Communications, Climate Action & Environment.

6.2 Seismic Database

The primary dataset for this study consists of modern 2D and 3D seismic data which have undergone extensive processing, independently of this study. These datasets show previously unseen structural and stratigraphic detail of the entire NCSB sedimentary package which is successfully utilised in this study to propose a revised structural evolution. Figure 6-2 shows the location of modern seismic dataset and highlights the key well control.

The 3D seismic survey utilised in this study is the “Barryroe 3D” survey, which was acquired in 2011 by Providence Resources Plc. using the M/V Polarcus Samur. A total of 270 km² (104 miles²) of data was acquired and processed, as detailed in Table 6-1 and Table 6-2 (Polarcus, 2011). The survey was the second modern 3D survey in the NCSB and due to its location, provided the first 3D images of deep seismic reflectivity in the centre of the NCSB.

Streamer	Number	8
	Separation	100m (328ft)
	Depth	6m (19.7ft)
Source	Arrays	2
	Volume	69.5 litres (4240 in ³)
	Depth	7m (22.9ft)

Table 6-1. Barryroe 3D acquisition parameters; after Polarcus, 2011.

1	Shot and Channel edit, de-bubble, resample to 4ms	11	FXY random noise attenuation.
2	T ² spherical divergence correction	12	Pre-migration Time Variant Filter
3	Two passes of FXEDIT swell noise attenuation.	13	UTMOST 3D isotropic Kirchhoff Pre-STM
4	Two passes of linear noise removal - XRLIN.	14	2 nd order velocity pick post-migration.
5	Wave Equation Multiple Attenuation	15	NMO correction and A-OK velocity analysis
6	Tau-p mute, pick initial velocities	16	High resolution Radon de-multiple
7	Q compensation, Tidal Statics	17	FK dip filter
8	Fold normalisation,	18	Post stack scaling and time variant filtering
9	3D isotropic Kirchhoff Pre-STM	19	Deconvolution, gun and cable static
10	2 nd order velocity pick on migrated gather data.		

Table 6-2. Barryroe 3D summary processing flow; after Polarcus, 2011.

Upon commencement of the research, the primary 2D seismic dataset consisted of a Fugro/TGS long offset SGC06 2D survey acquired and processed in 2006 and the SWAT-5 seismic line. Subsequently, in late 2014, Schlumberger Multi-client agreed to reprocess part of the Merlin Profilers 1981 NCS 2D survey, recognising the limitation of the original processing. While the reprocessing project was focused on seismic lines within the Southern Celtic Sea Basin, three seismic lines were reprocessed in the NCSB and made available to this research project. Significant guidance and QC was provided at all stages of the processing but specific attention was paid to demultiple and the velocity model generation to ensure accurate migration of the data to the correct subsurface position. The lines were located west of the original study area, however the study area was expanded significantly to incorporate this new and vital dataset as it was seen to validate the initial work conducted on the SGC06 and SWAT-5 2D data. Additional vintage data was also incorporated within this extended area.

The SGC06, SWAT-5 and reprocessed NCS81 datasets complement the Barryroe 3D dataset, providing excellent regional tielines to regional well control, Figure 6-2. Additionally, 296 vintage 2D seismic lines from 14 surveys, covering over 7,500 km in total length, were available within the extended study area, Figure 6-3.

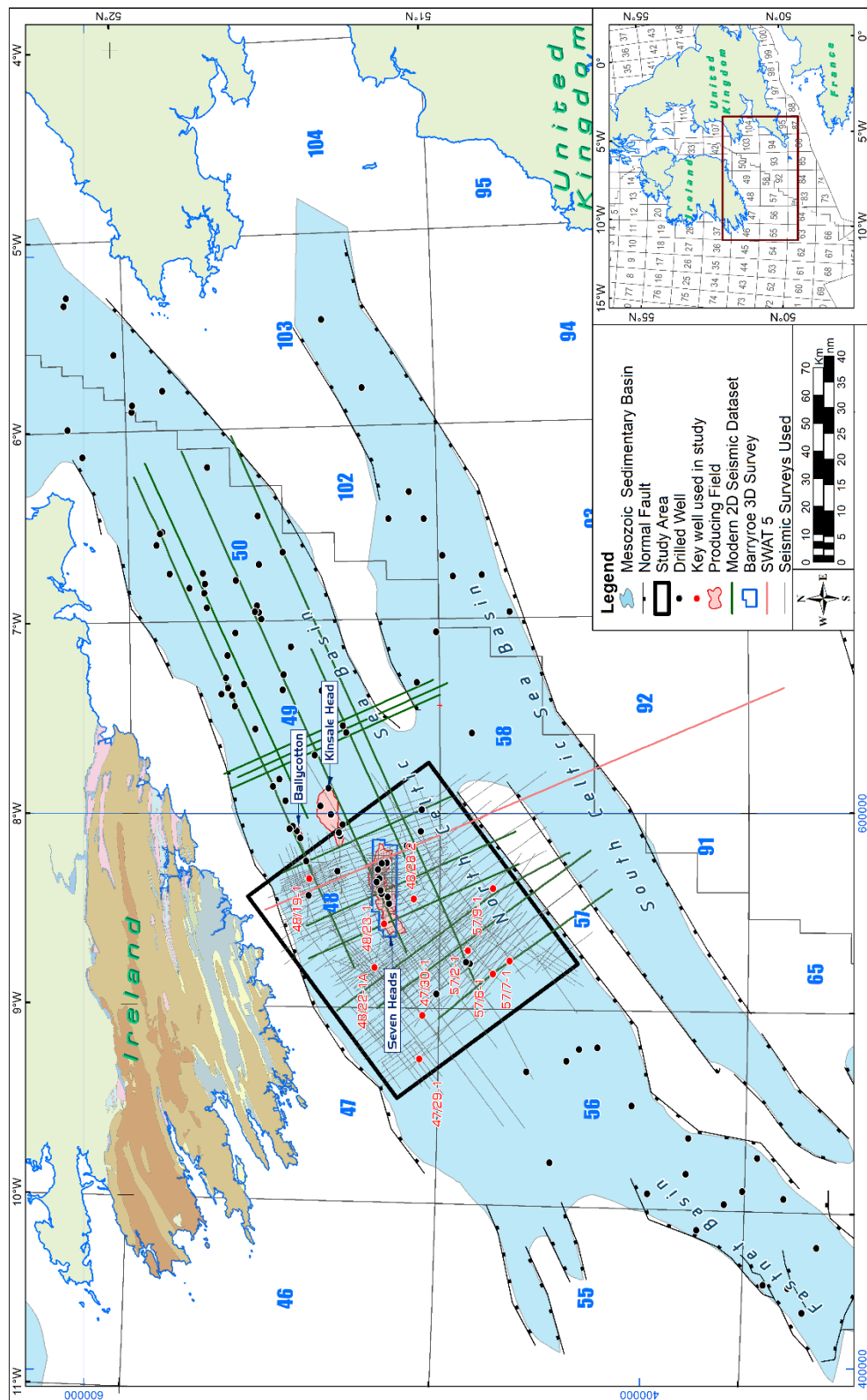


Figure 6-3. Location map indicating seismic dataset utilised by this study.

Source Dept. of Communications, Climate Action & Environment.

6.3 Seismic Dataloading

Seismic data files tend to be very large in size due to the volume of data they contain. 2D seismic data files can exceed 1Gb while 3D seismic data files can exceed 1 Tb. Due to the complexity of the data there are several components to a seismic data file, specifically a Textural Header, a Binary Header and a Trace Header.

The Textural Header contains information on the data name, date of acquisition, acquisition parameters, processing parameters, geographic location and positioning system (known as a cartographic reference system). The Binary Header file contains binary values for items such as the location number for each seismic source output (shotpoint), the number assigned to the resulting recorded data (trace), vertical sampling interval (linked to vertical resolution) and length of each piece of data (time to deepest point of data recorded). The Trace Header file contains information such as specific X, Y and Z location of the data (Hagelund & Levin, 2017).

Separately there is normally a navigation file or a loading sheet which details how to load the file into computer software programmes ensuring correct positioning of the data. It is common for this file to be missing or incomplete in data acquired prior to 2000.

The Kingdom Suite software was the chosen computer software tool chosen for the project. A total of 16 different 2D surveys required separate loading to the software and subsequent quality control (QC). If available, a navigation file was examined to review the cartographic reference system (CRS) and precise X, Y location of each survey line. Alternatively, the textural header and trace header of the seismic files were examined at length to determine the CRS and seismic line location and extents. It was common for the vintage 2D seismic data files not to have a specified CRS other than European Datum 1950. The transform from the standardised satellite based Global Positioning System defined in 1984 (WGS84) to European Datum 1950 was assumed to be a simple three parameter shift for all seismic data acquired prior to 1995 unless otherwise documented. Any data acquired after 1995 was assumed to use the updated seven parameter Bursa-Wolfe transform which came into effect in 1995 (UKOOA, 1999; IOGP, 2018). The uncertainty in location between the three parameter and the seven parameter transforms is approximately 30 metres, meaning accidentally using an incorrect transform would result in a minor mis-positioning which was considered acceptable for this regional study.

The loaded seismic lines were quality controlled internally within a survey and also externally against other surveys to ensure intersections of data were correct. Any required vertical correction, phase rotation (swapping of positive/negative convention of the data) or amplitude gain (brightness of the data) was applied in an attempt to yield a regionally consistent dataset. This process was challenging as many surveys lacked a definitive seabed reflector due to poor processing, meaning assessment of phase (positive/negative convention) was difficult. Several vintage

seismic lines were removed from the study as they demonstrated anomalous intersections with the remainder of the dataset and were likely significantly miss-positioned or had obvious errors within the seismic line (Figure 6-4). The relationship between the shotpoint and the resulting processed trace also had to be assigned manually in most of the vintage data. The relationship varied significantly within and between surveys. Several examples of increasing, decreasing or irregular shotpoint to trace relationships were found, specifically within the vintage dataset (Figure 6-4).

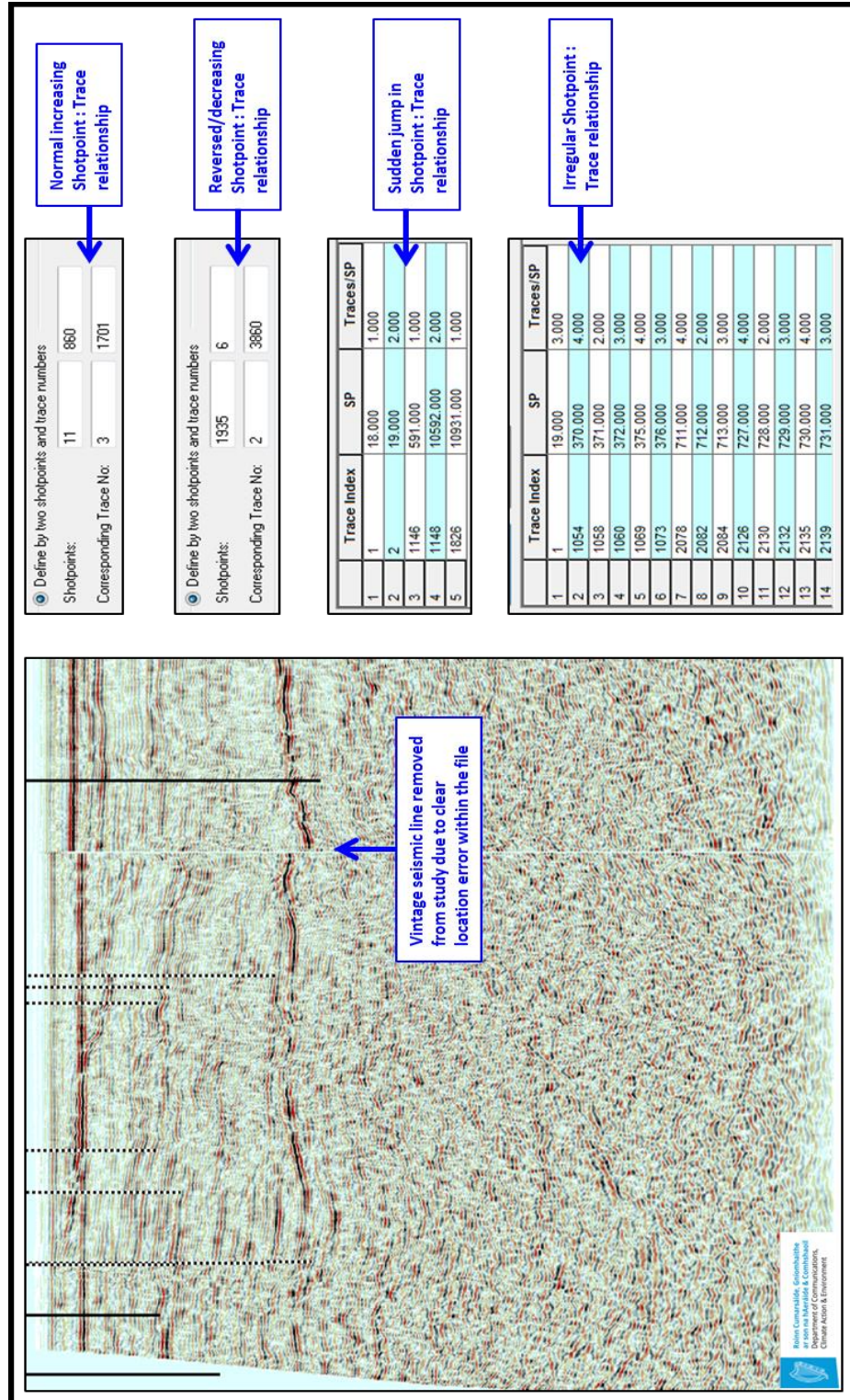


Figure 6-4. Examples of seismic loading issues encountered, note the vertical shift in seismic events on the displayed line and boxes illustrating 4 different shotpoint to trace relationships encountered.

6.4 Seismic Data Examples

The data quality from the Barryroe 3D survey is shown in Figure 6-5. While the dataset is limited in aerial extent, it provides the interpreter with full 3D visualisation and improved imaging due to 3D migration. Data quality is considered excellent given the hard water bottom environment. Clear primary data is visible down to the full 4.0 second two-way-time (TWT) record length, successfully imaging the entire Mesozoic sedimentary section.

The regional Fugro/TGS long offset SGC06 2D survey is presented as an example of modern 2D seismic data. Three dip lines are presented in Figure 6-6 to Figure 6-8. These lines show both the regional extent and data quality of the SGC06 survey. They image the entire extent of the NCSB and show primary data to a depth of beyond 4 seconds TWT.

Seismic lines NCS81-59 and NCS81-64, from the Merlin Profilers 1981 NCS 2D survey, are presented as examples of modern seismic reprocessing of vintage seismic data. Figure 6-9 and Figure 6-11 represents the original vintage product while Figure 6-10 and Figure 6-12 show the reprocessed product. These lines were reprocessed by Schlumberger Multiclient in 2014 with geological guidance and velocity QC provided by the author. The dataset demonstrates that modern processing techniques can yield valuable information from vintage data. The lines shown cross the entire NCSB and have good primary reflectivity down to 4 seconds TWT.

Vintage data quality varies significantly over the study area with some surveys being simply stacked data rather than migrated and stacked, as shown in Figure 6-13, the former having poorer imaging accuracy. Data of this poor quality can only be used reliably in the shallow section, less than one second two-way-time. In general, the vintage seismic data is of sufficient quality to follow seismic character and overall structural style identified on the modern seismic data, as discussed in Chapter 6.6.

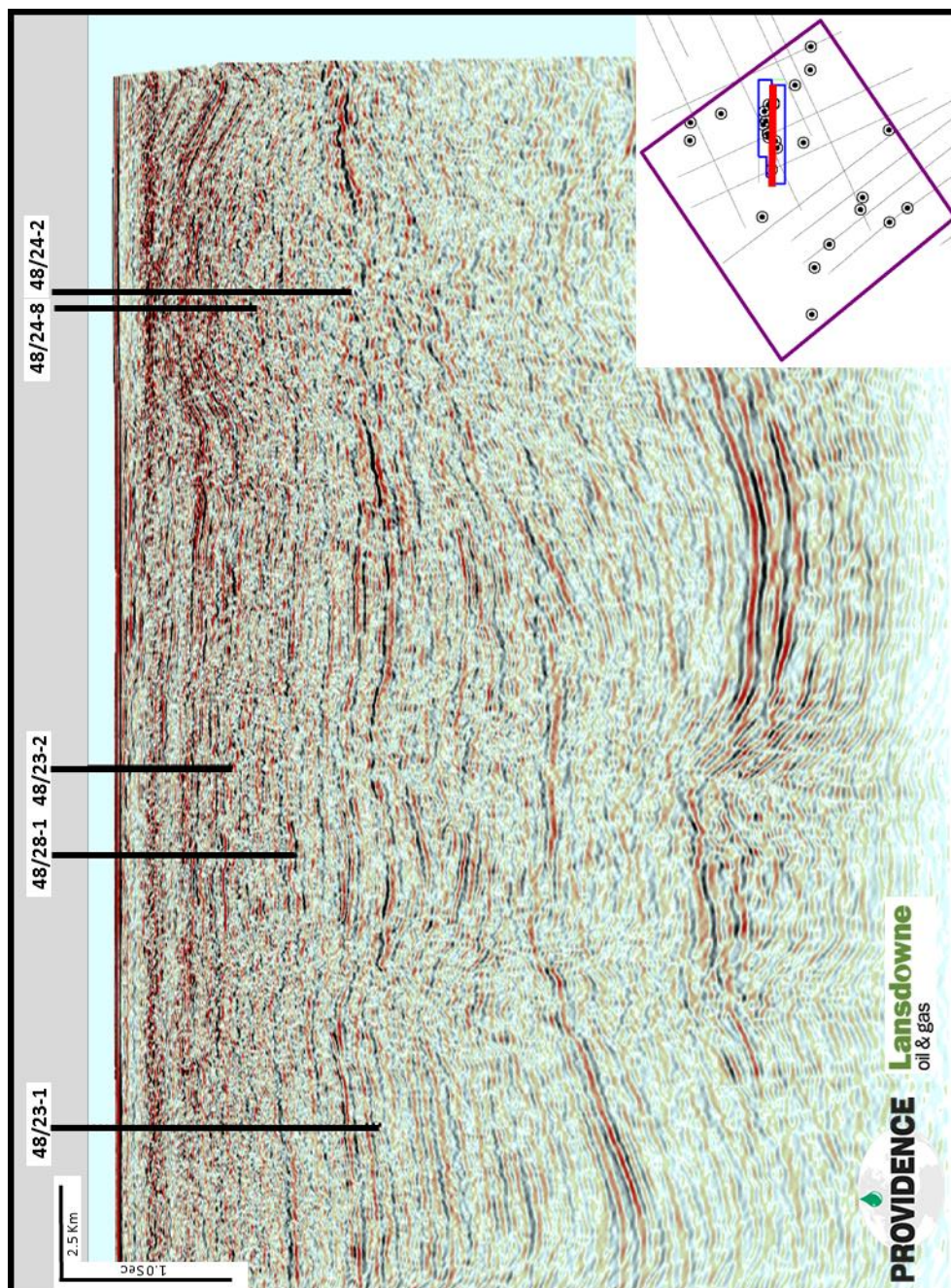


Figure 6-5. Barryroe 3D seismic data quality example, courtesy Providence Resources Plc and Lansdowne Oil and Gas Plc. Strong and continuous reflections can be identified throughout the seismic section.

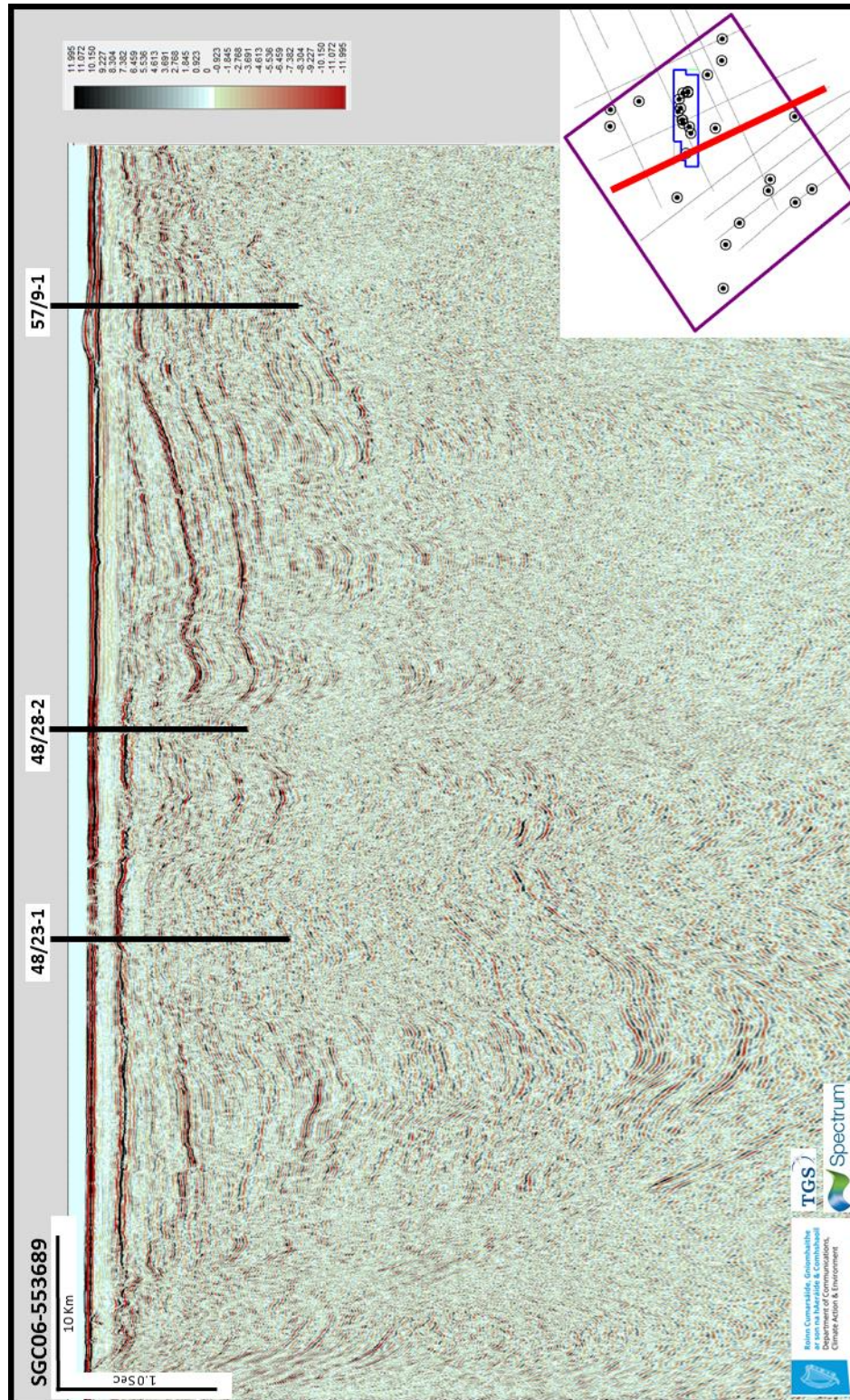


Figure 6-6. SGC06-553689 modern 2D seismic data quality example. Strong and continuous reflections can be identified throughout the seismic section.

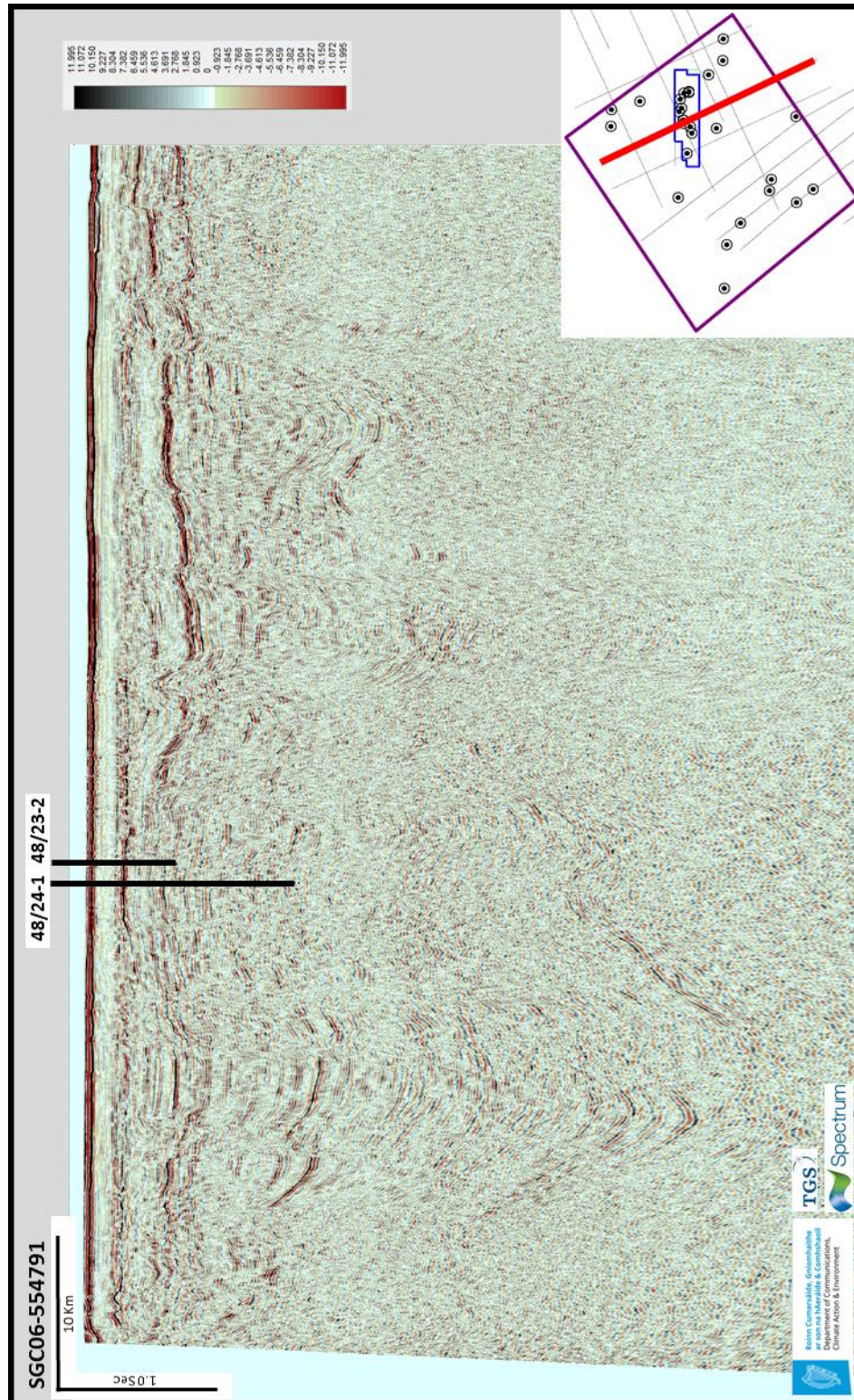


Figure 6-7. SGC06-554791 modern 2D seismic data quality example. Strong and continuous reflections can be identified throughout the seismic section.

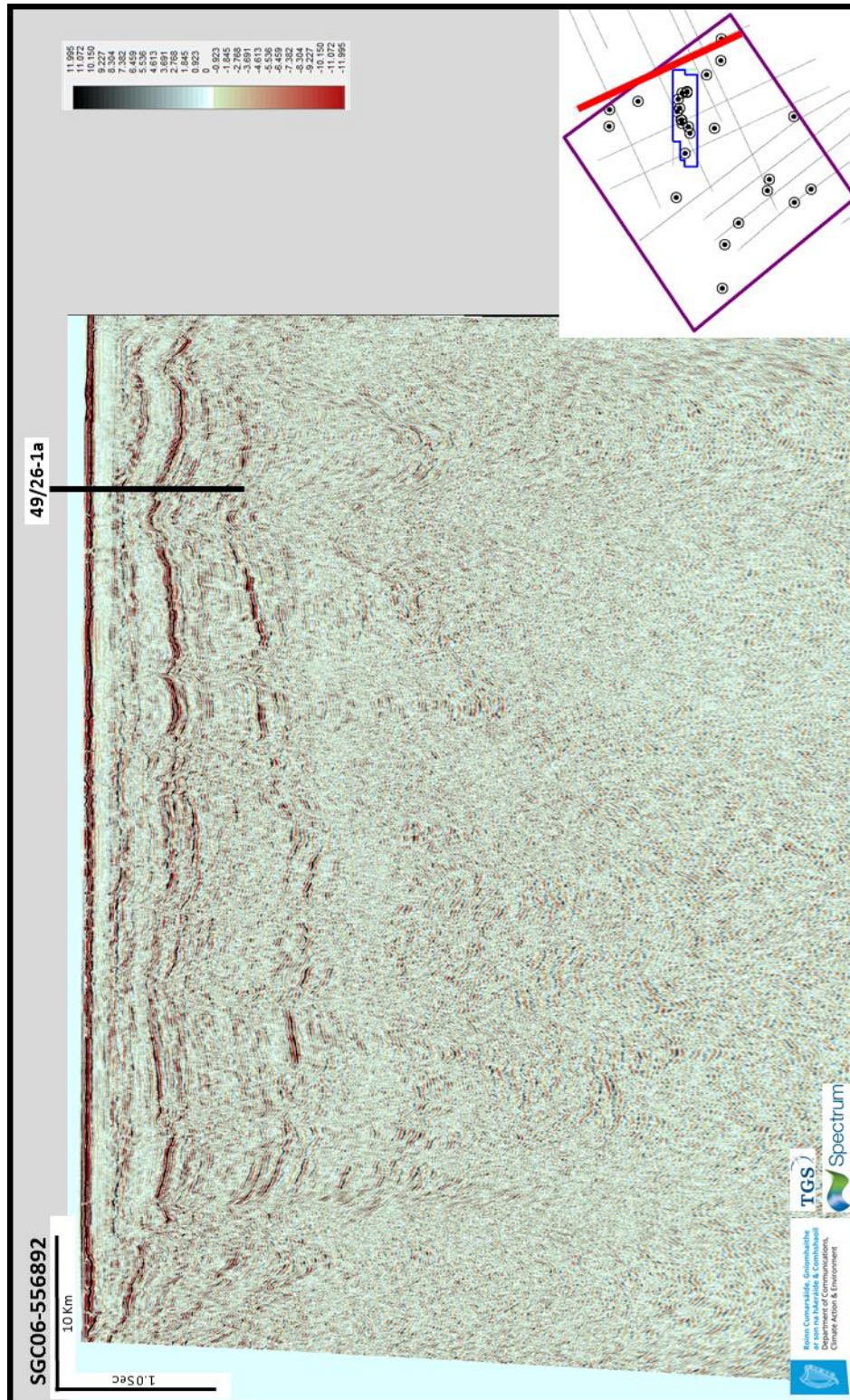


Figure 6-8. SGC06-556892 modern 2D seismic data quality example. Strong reflections can be identified, but are less continuous at this location.

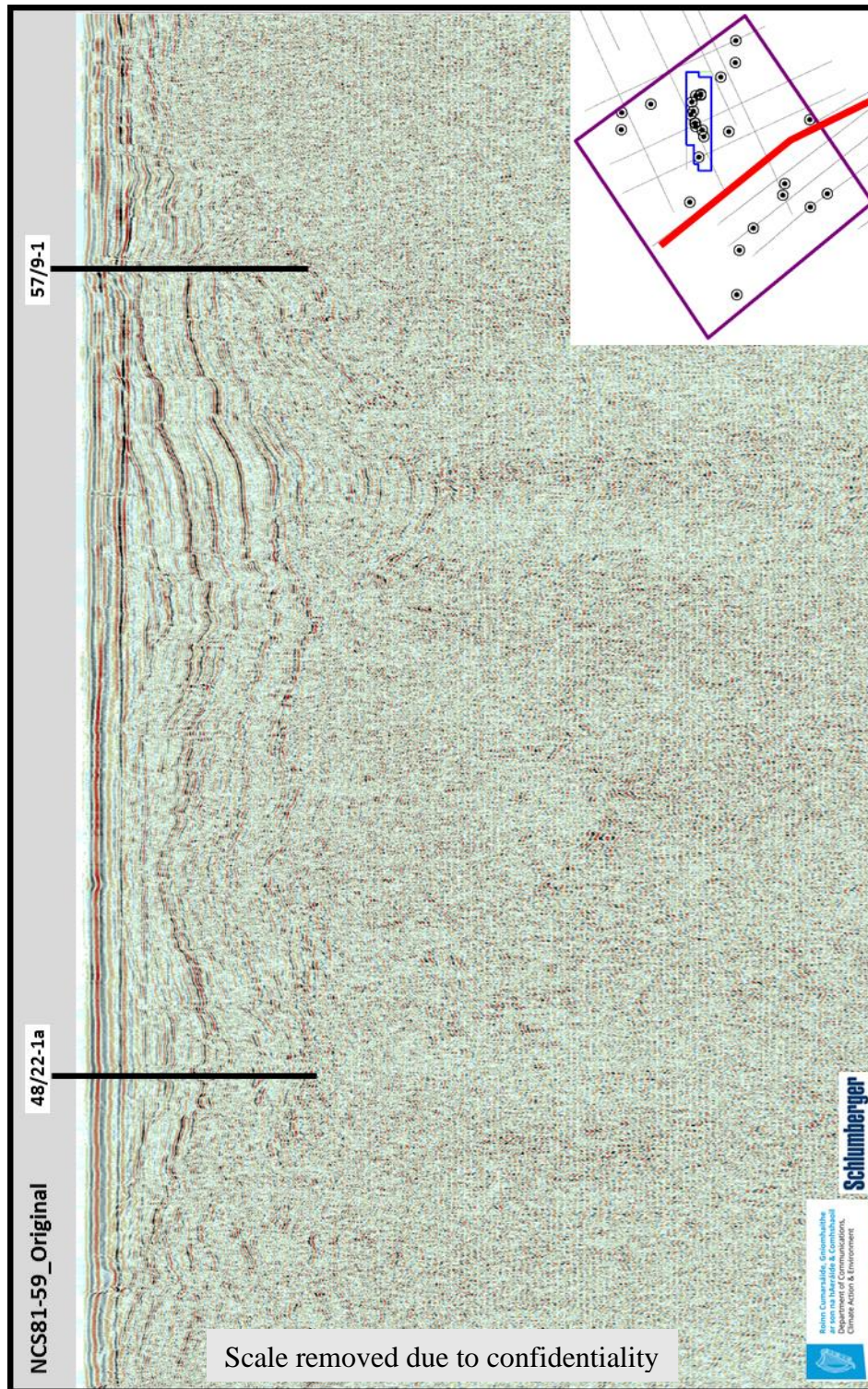


Figure 6-9. NCS81-59, original vintage processed product data quality example. Strong and continuous reflections can be identified in the shallow section only.

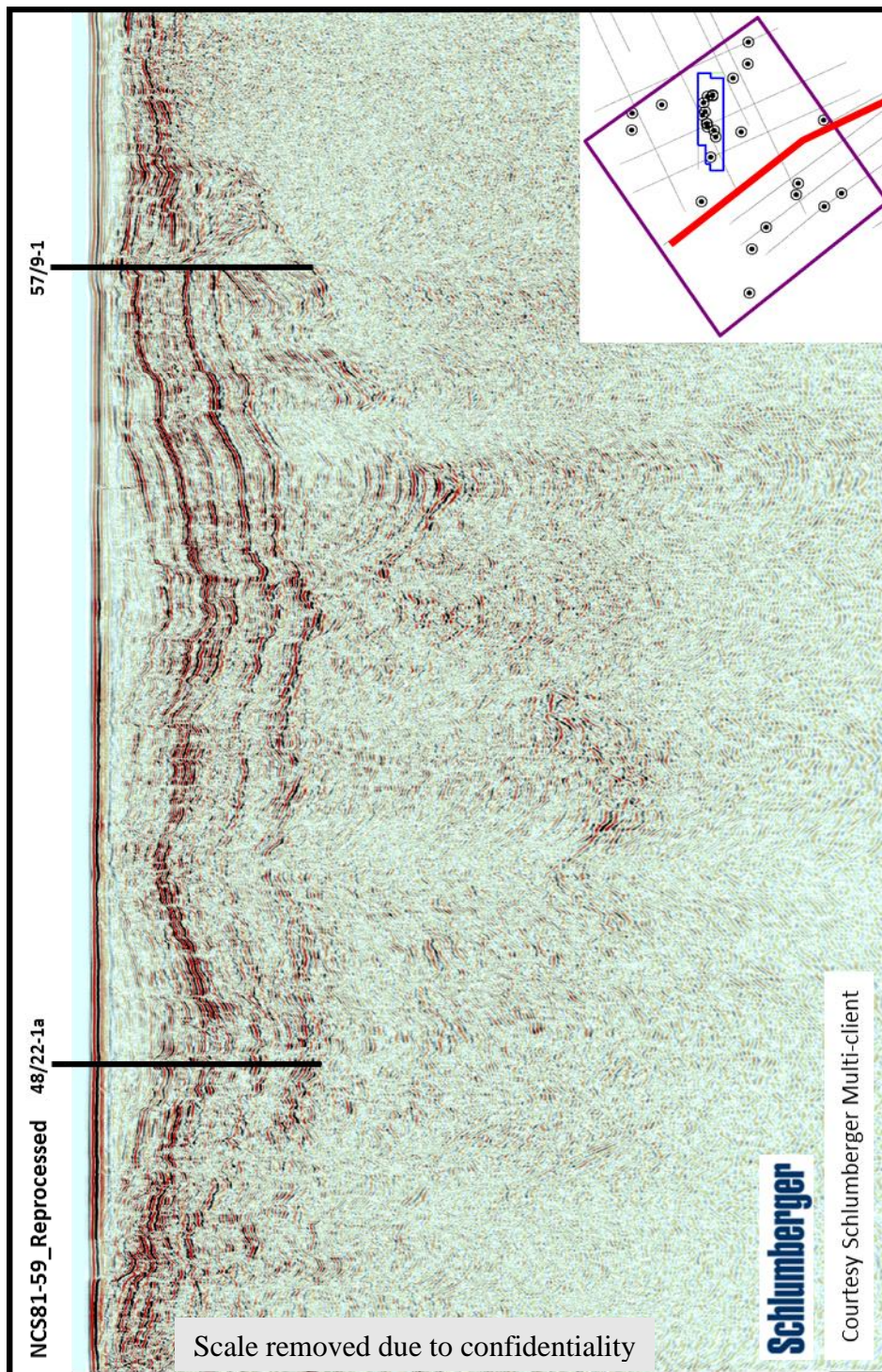


Figure 6-10. NCS81-59, reprocessed product data quality example. Strong reflections can be identified at depth that were not evident on the vintage processing.

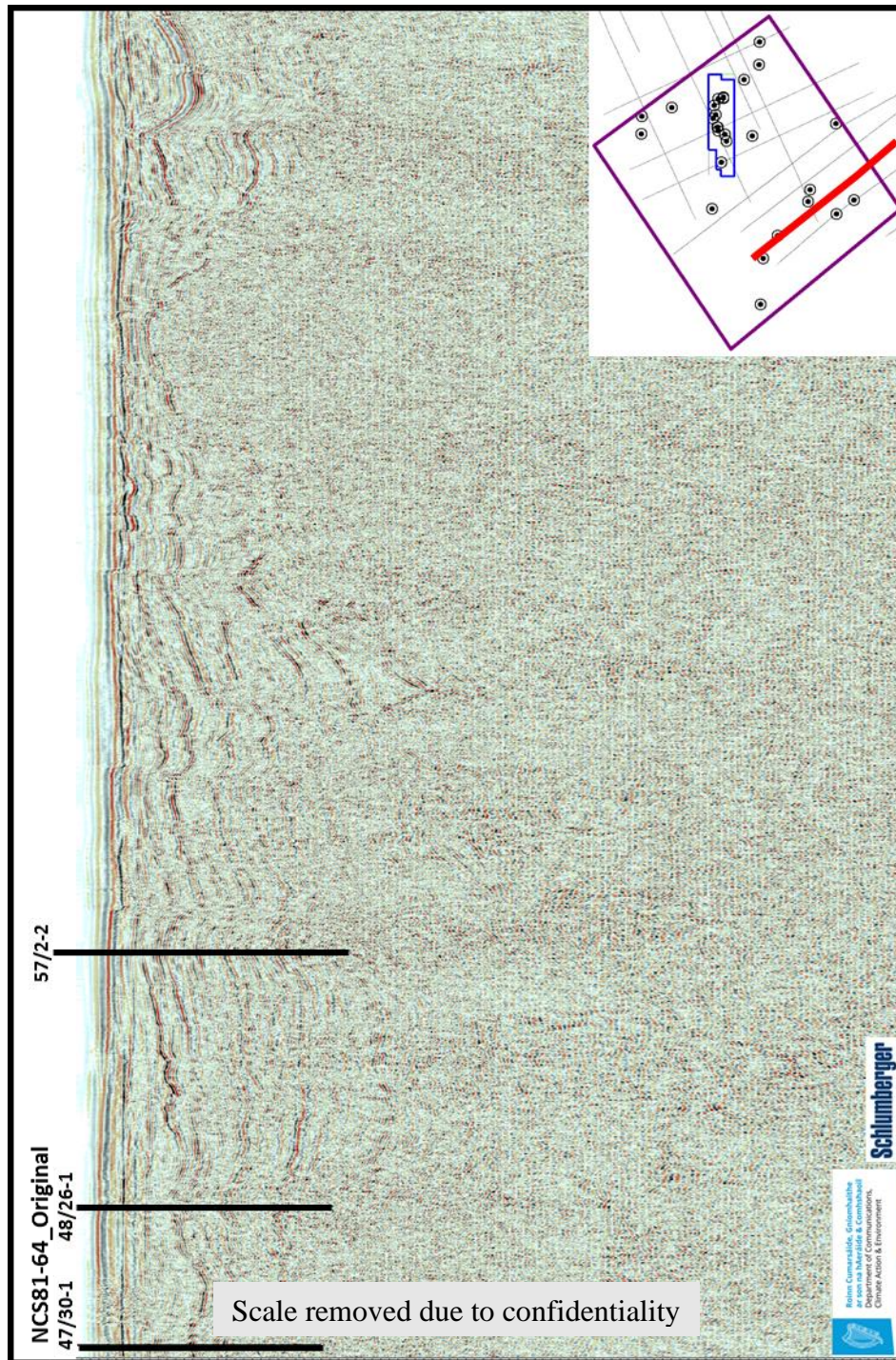


Figure 6-11. NCS81-64, original vintage processed product data quality example. Strong and continuous reflections can be identified in the shallow section only.

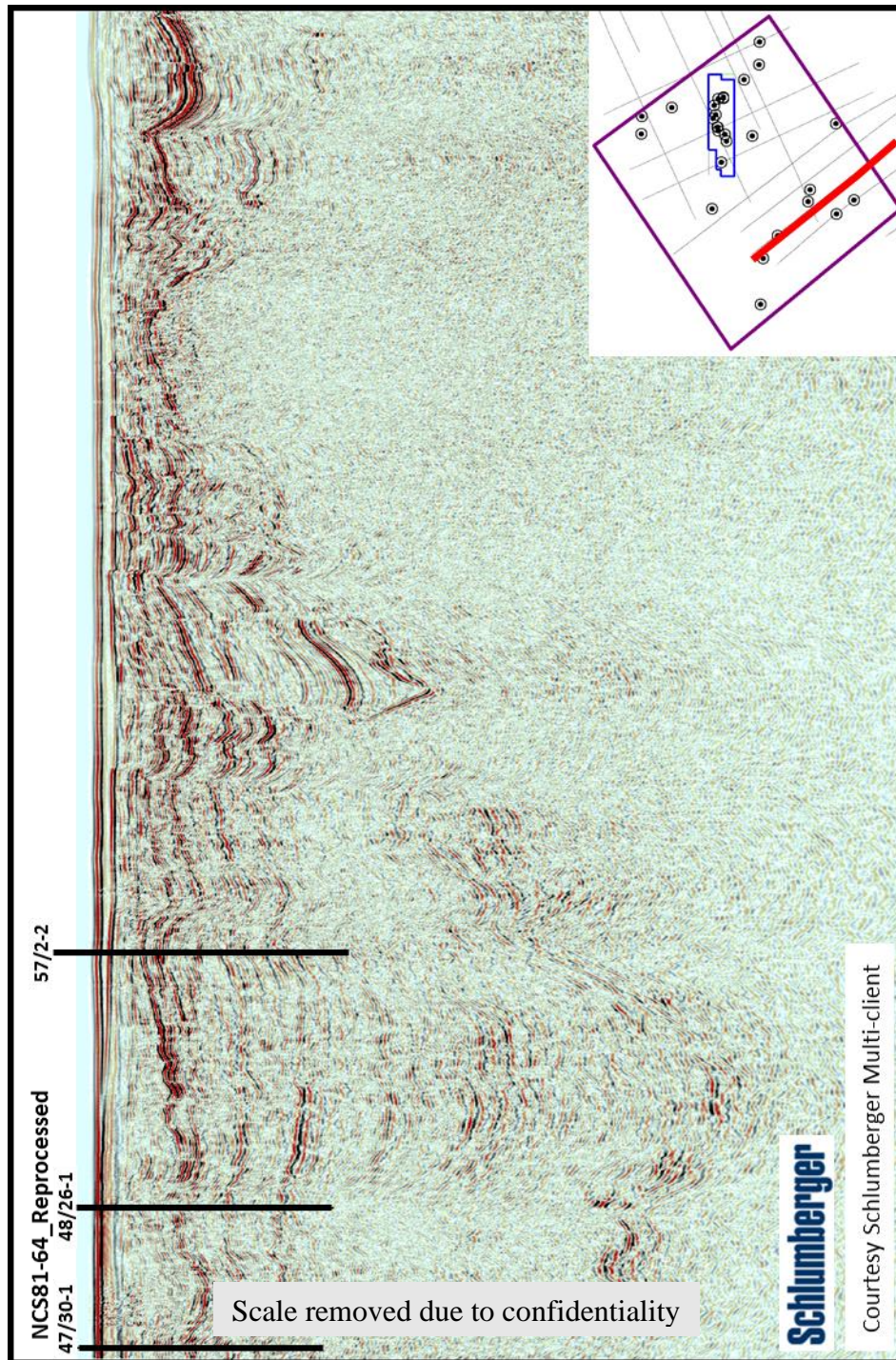


Figure 6-12. NCS81-64, reprocessed product data quality example. Strong reflections can be identified at depth that were not evident on the vintage processing.

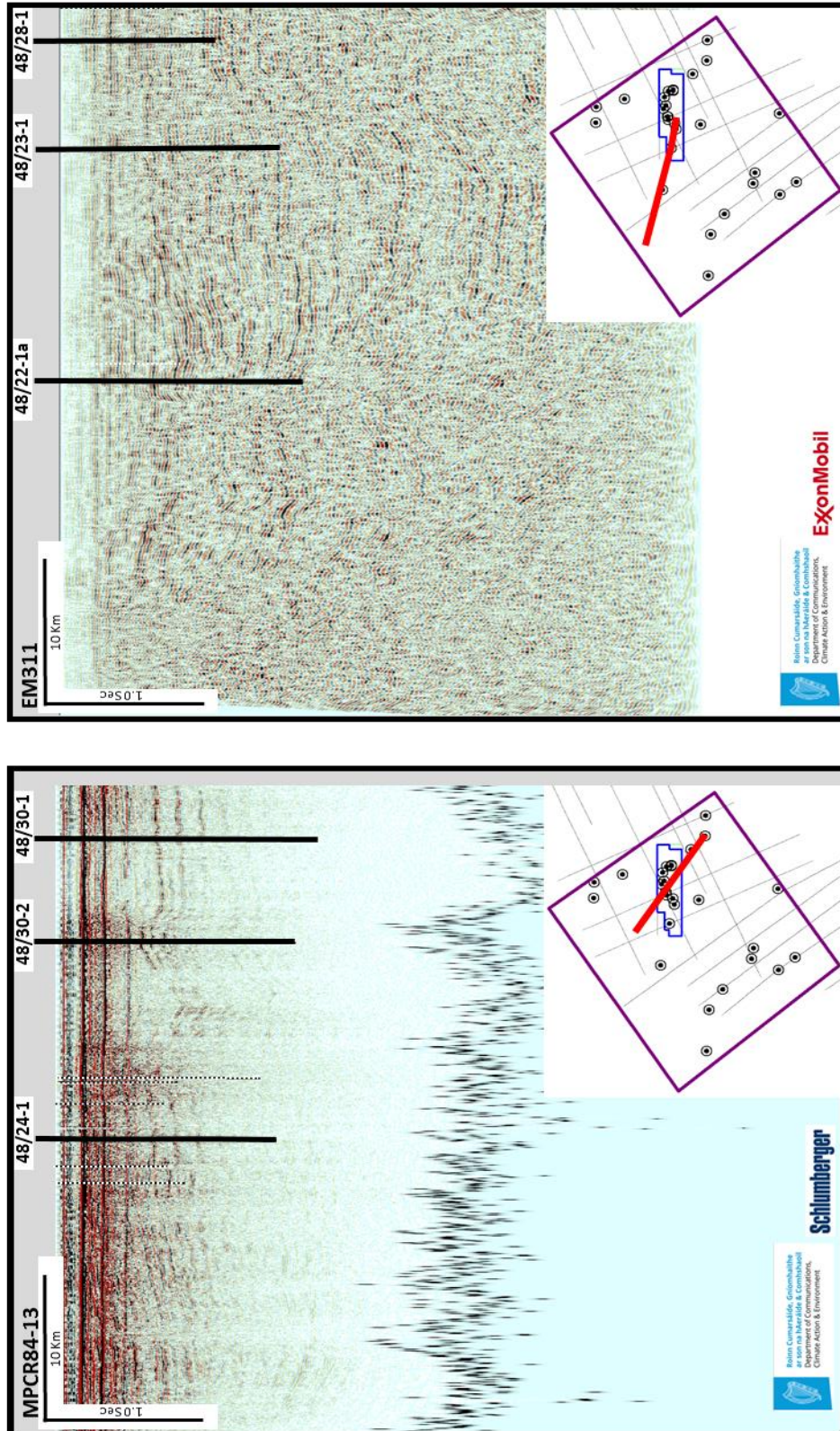


Figure 6-13. MPCR84-13 and EM311, poor data quality examples. Significant uncertainty in the reliability of seismic reflections on these sections.

6.5 Well database

As discussed in Chapter 6.1, the vertical domain of seismic data is not depth but is the time taken for an acoustic signal to travel through the subsurface and return back to the recording equipment. Well data is always measured as depth below a reference point on the drilling rig, which is a known distance above the seabed. To compare well data in depth with seismic data in time we rely on an acoustic survey conducted inside a drilled well, where the time an acoustic signal takes to arrive at multiple depth points within the well is measured, known as a checkshot survey or VSP survey (Brewer, 2000a; Brewer, 2000b). This acoustic survey allows for all data from a drilled well to be displayed in time on top of any collocated seismic data, for instance geological formation tops. It is also possible to use a sonic log (measures the acoustic slowness of rock adjacent to the tool in the well) recorded in a drilled well to create a pseudo seismic file at the well location. This file is known as a synthetic seismogram (Onajite, 2014). The synthetic seismogram shows the expected seismic response at the well location and can be compared against the actual recorded seismic data, ensuring the interpreter understands the exact seismic response for a lithological interface (Herron, 2011; Brown, 2011; Onajite, 2014; Robinson & Clark, 2017). Obtaining a good correlation between seismic data and a synthetic seismogram is difficult in the NCSB because of the level of residual multiple energy remaining within the seismic data (even after modern processing) that does not exist in the synthetic data. Also, the sonic logs in the NCSB are adversely affected by wellbore rugosity caused by shale instability (Kennedy, 2015).

Within the study area there are 30 exploration and appraisal wells (Figure 1-1). Released composite logs and final well reports were reviewed in detail for each well. Composite logs are one of the final geological reports compiled to document a drilled well, they contain all electrical logs acquired as well as geological interpretations of the operator (Evenick, 2008). The final well reports are an extended text report detailing the operations of the well and geological interpretations of the operator (Devereaux, 1998). Significant inconsistencies in formation top nomenclature exist with both local and company specific naming conventions common. Lithologic descriptions and biostratigraphic dating were taken from these documents and verified as appropriate by comparing regional well cross sections, Figure 6-14 and Figure 6-15. A revised and simplified set of formation tops were created across all the wells, paying particular attention to velocity breaks (which tend to be major lithological or structural boundaries) and cross referencing with the seismic database. These initial formation tops were updated later in the project to honour a new lithostratigraphic and biostratigraphic study of all wells offshore Ireland. This study was conducted by a consortium of companies on behalf of industry and the Department of Communications, Climate Action and Energy (Copestake *et al.*, 2018).

Wells 48/19-1, 48/23-1, 48/28-2, 48/22-1a, 57/07-1, 57/02-1 and 57/09-1 are close to the modern seismic dataset and provide stratigraphic control across these seismic datasets, Figure 6-3. This was critical to identifying the seismic character of the stratigraphy and providing a robust seismic interpretation. Other wells which

provided important ties to vintage 2D seismic data include 47/29-1, 47/30-1, 57/06-1, Figure 6-3.

From examination of the well and seismic data, a total of six distinct seismic markers could be identified regionally within the study area. These seismic markers represent the boundaries of major geological units in the Irish offshore and were also used by previous authors (Petrie *et al.*, 1989; Rowell, 1995; Naylor & Shannon, 2011).

- Top of the Cretaceous Chalk Group (referred to here as Chalk).
- Top Cenomanian (referred to here as Plenus Marl)
- Base Cretaceous (Intra Pollan Fm)
- Callovian-Oxfordian Unconformity (Top Peregrine Formation)
- Top Triassic (Top Penarth Formation)
- Top Palaeozoic Basement.

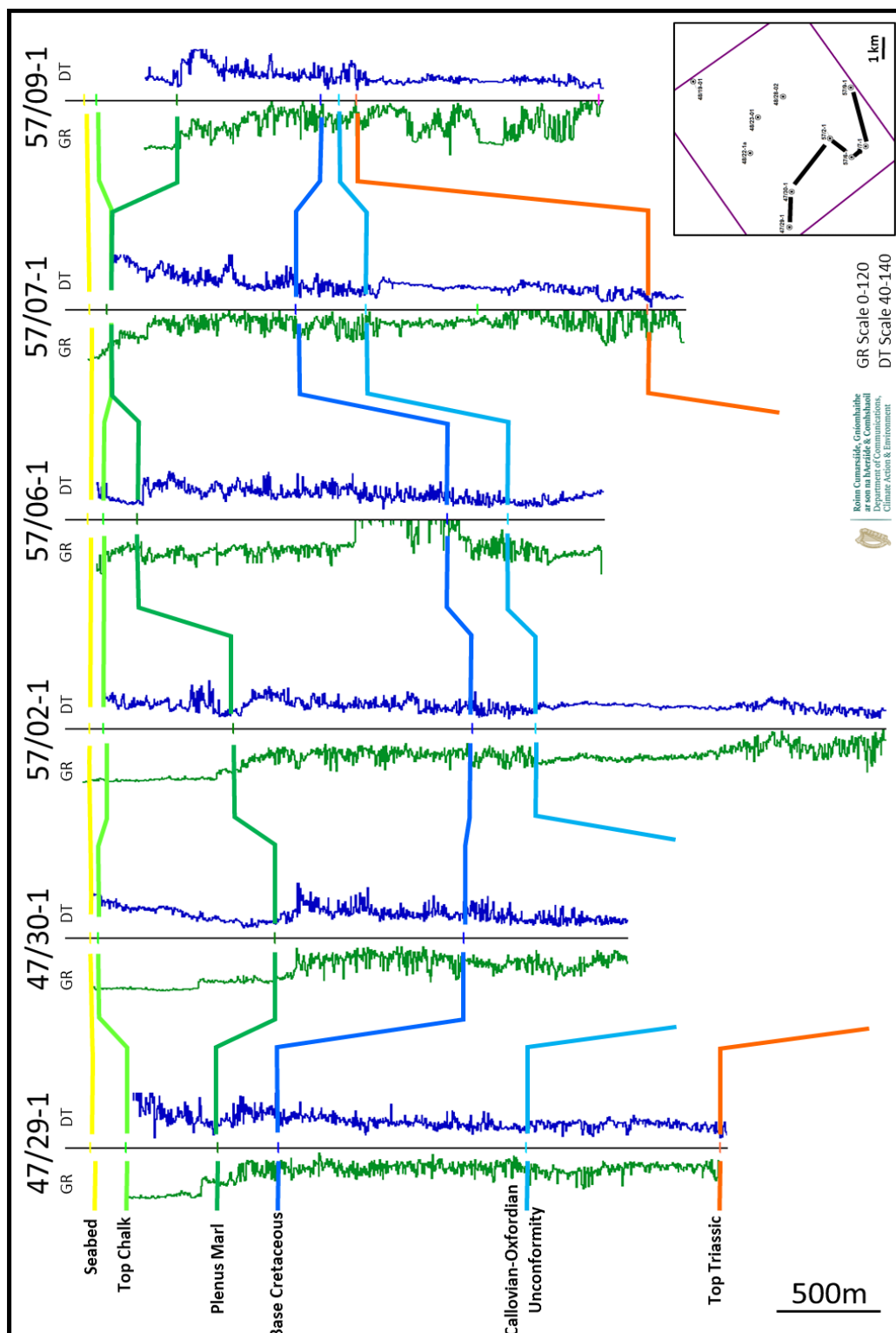


Figure 6-14. North – South correlation of Gamma Ray (GR) and Sonic (DT) logs from key wells on the west side of the study area, formation tops from Copestake *et al.*, 2018.

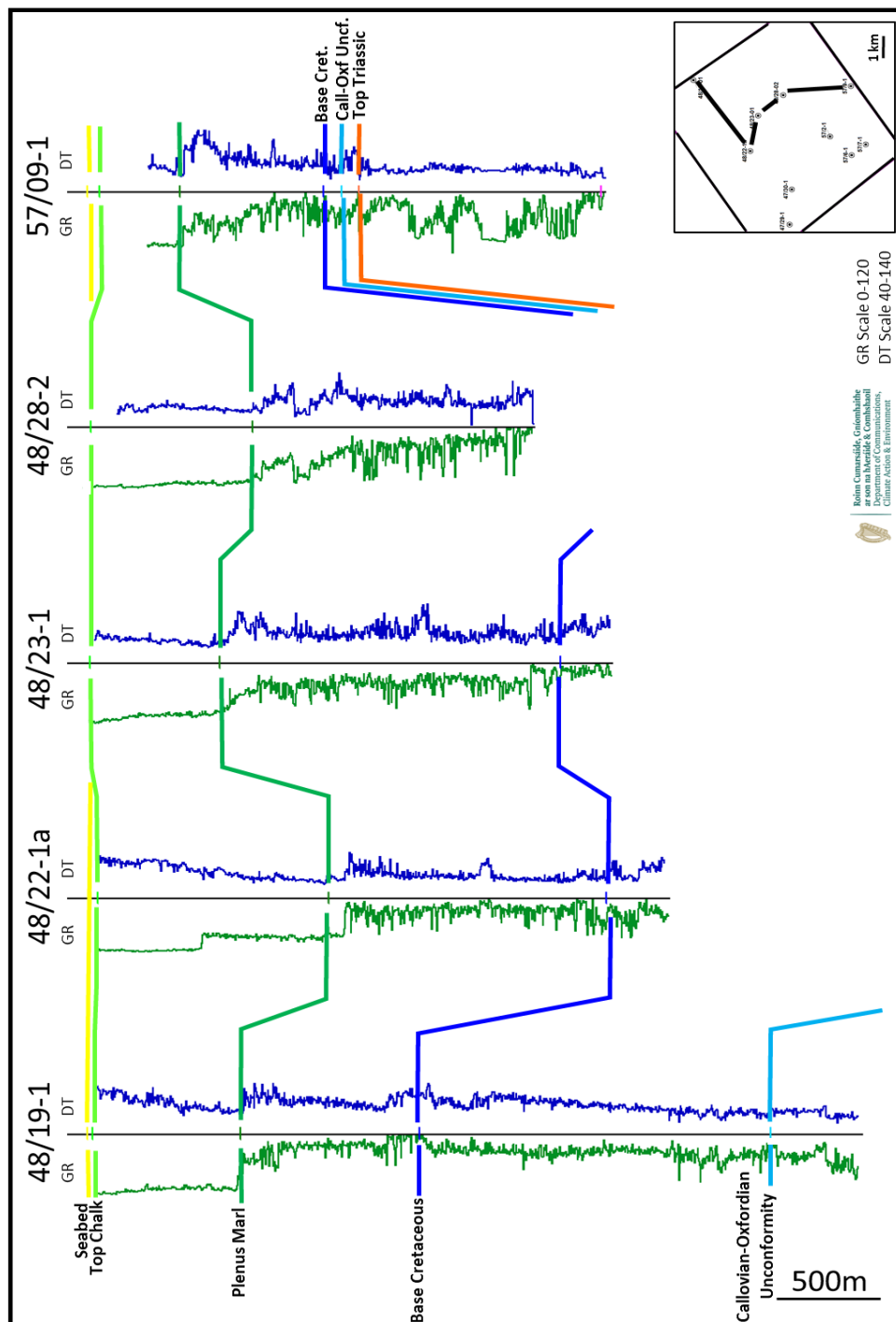


Figure 6-15. North – South correlation of Gamma Ray (GR) and Sonic (DT) logs from key wells on the east side of the study area, formation tops from Copestake *et al.*, 2018.

6.6 Seismic Interpretation

As discussed in Chapter 5, previous authors have described differing geometries for the NCSB, both of which are viable on the vintage seismic datasets available at the time and thus neither could be discounted. Modern seismic acquisition and processing techniques have yielded significant imaging improvements, particularly at depth, providing previously unseen structural detail which are incorporated within this study.

The common principles and practices of seismic interpretation have been followed, including recognising that seismic reflections represent changes in velocity and or density in the subsurface which can be diachronous or chronostratigraphic events (Herron, 2011). Interpretation relies on recognising regional dip as well as seismic character (continuous, discontinuous, chaotic, strong, weak etc.) and interpreting a geological rationale for these changes (faults, disconformities, lithological changes etc.) (Herron, 2011; Brown, 2011; Robinson & Clark, 2017; Ikelle & Amundsen, 2018). It is also critical to be aware of potential issues with seismic data and to avoid incorrect interpretations (Tucker & Yorston, 1973). A prior regional geological knowledge can be critical to a robust interpretation, ensuring the interpretation honours regional events such as tectonics, sea level changes and lithology changes. (Herron, 2011; Brown, 2011; Robinson & Clark, 2017; Ikelle & Amundsen, 2018).

The location and extent (6,000 km²) of the study area, shown in Figure 1-1, was based on the availability of modern seismic data, including the Barryroe 3D, parts of the SGC06 2D and the reprocessed NCS81 seismic surveys.

It is important to note that interpretation within the NCSB utilises both the well and seismic data from within the basin, but also extends and integrates interpretation from adjacent basins which have greater geological understanding due to good seismic data imaging, significantly more well control and more research. Basins on the NE Atlantic are all important, as are the conjugate Canadian basins however, the adjacent St. Georges Channel Basin, Fastnet Basin, South Celtic Sea Basin and East Irish Sea Basin are the most relevant and are discussed by several authors including Stuart, 1993; Barr *et al.*, 1981; Welch & Turner, 2000; Ruffell & Coward, 1992; Robinson *et al.*, 1981; Bulnes & McClay, 1998.

The interpretation process consisted of five stages which are outlined in detail in Chapters 6.6.1 to 6.6.5.

6.6.1 Interpretation Stage 1

A subset of modern 2D seismic data and the Barryroe 3D data were selected, as shown within Figure 6-2. This subset was observed at a zoomed-out scale to understand the full extent and regional context of each seismic line. The overall shapes, dip and geometry of the seismic reflectors were carefully noted, as were changes in these seismic reflectors along each line and between lines.

6.6.2 Interpretation Stage 2

The wells close to the subset of seismic data and with deep stratigraphic penetrations were overlain over the seismic data to show the vertical location of relevant formation tops within the wells. The wells were 48/19-1, 48/23-1, 48/28-2, 48/22-1a, 57/07-1, 57/02-1 and 57/09-1. A zoomed-in section of each seismic line to well intersection was analysed to recognise key geological stratigraphy and their associated seismic expression.

From examination of the well and seismic data, a total of six seismic markers could be identified regionally within the study area. These seismic markers represent the boundaries of major geological units in the Irish offshore and are also used by previous authors (Petrie *et al.*, 1989; Rowell, 1995; Naylor & Shannon, 2011) as well as being recently recognised in a regional biostratigraphic and lithostratigraphic review offshore Ireland (Copestake *et al.*, 2018).

The six seismic markers (described from shallow to deep) identified were:

- Top of the Cretaceous Chalk Group (referred to here as Chalk).

From the well control the Chalk is known to outcrop at the seabed extensively over the study area, with the exception of thin outliers of Cenozoic stratigraphy preserved in the southwest, see also Copestake *et al.* (2018). In these areas the top of the Chalk is represented by a significant

increase in acoustic impedance which is represented by a red seismic event (SEG normal polarity), Figure 6-16.

- Top Cenomanian (referred to here as Plenus Marl).

The Plenus Marl is one of the strongest and laterally continuous seismic markers within the study area. It is a significant lithological marker and a strong decrease in velocity (from high velocity chalk to the underlying lower velocity clastic material) and is clearly identifiable, Figure 6-16 and Figure 6-17. There is excellent stratigraphic control on the Plenus Marl with 30 exploration and appraisal well penetrations within the study area. These wells are dispersed within the study area but were fully utilised to provide a robust interpretation. The base of the Chalk Formation is at the base of the Cenomanian but does not have a consistent seismic character across the entire study area due to lateral changes in facies from chalk to sandstone within the Cenomanian. Some of these sands are known to be hydrocarbon bearing within the Celtic Sea.

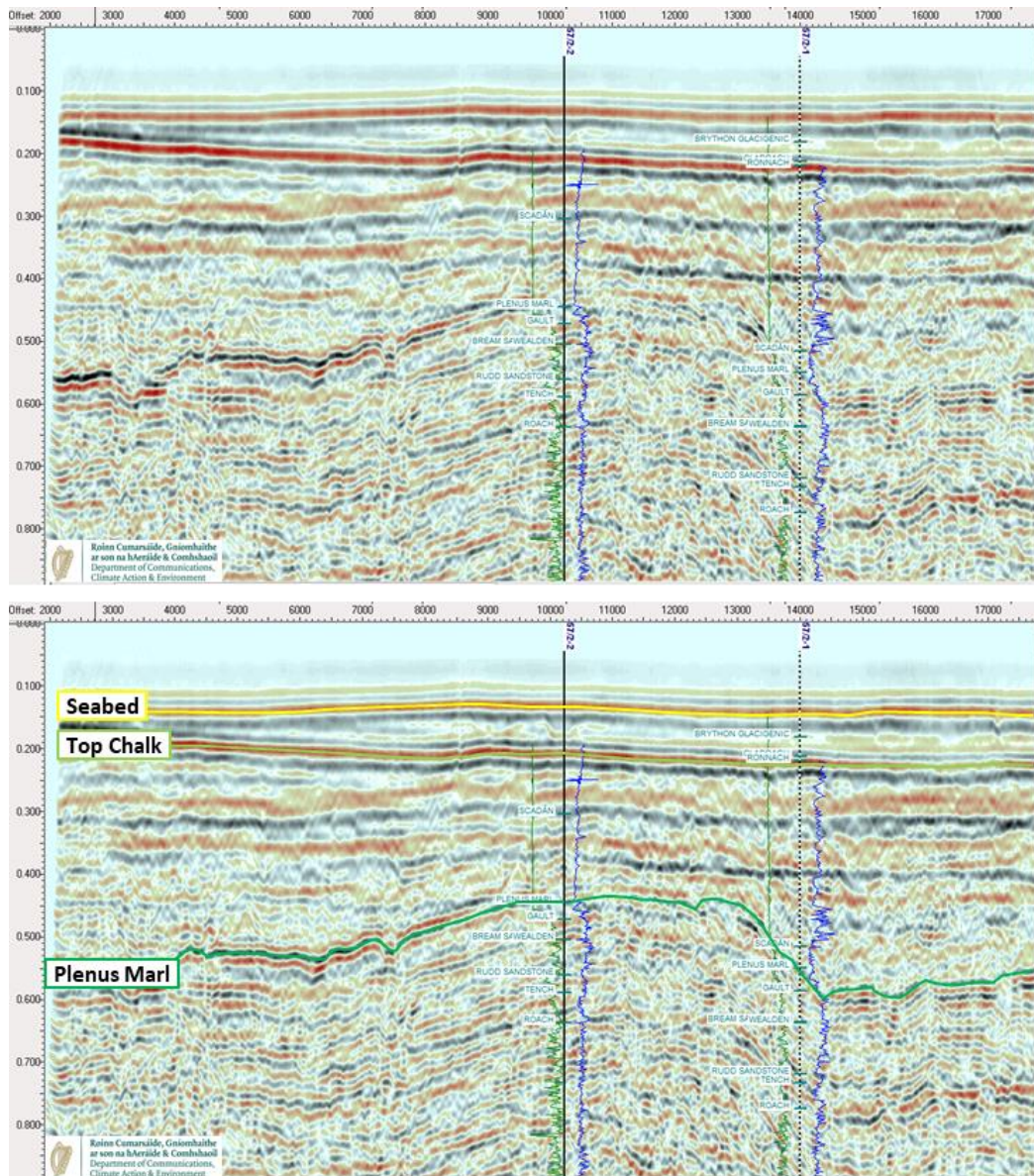


Figure 6-16. Seismic line ARC95-13 through wells 57/2-2 and 57/2-1 with GR log (green), Sonic log (blue) and formation tops (after Copestake et al., 2018). Presented with and without seismic interpretation.

- Base Cretaceous (Intra Perch Fm)

The base of the Cretaceous section is identified as a regionally extensive seismic marker being the upper of two parallel sets of reflectors within the basin centre, Figure 6-18. These two parallel events coalesce as the sedimentary package thins towards the basin margins. The seismic marker is described as Intra Perch Formation by Copestake *et al.* (2018) which is Berriasian in age, as they were unable to get a precise placement of the Base Cretaceous within the wells. This was primarily due to age uncertainty as the biostratigraphic data of the interval is dominated by non-marine micro-faunas and palynology. Regardless of the precise age of the seismic marker it can be considered as “near” Base Cretaceous and there is good stratigraphic control on the marker within the study area with 30 exploration and appraisal well penetrations. These wells are dispersed within the study area but were fully utilised to provide a robust interpretation.

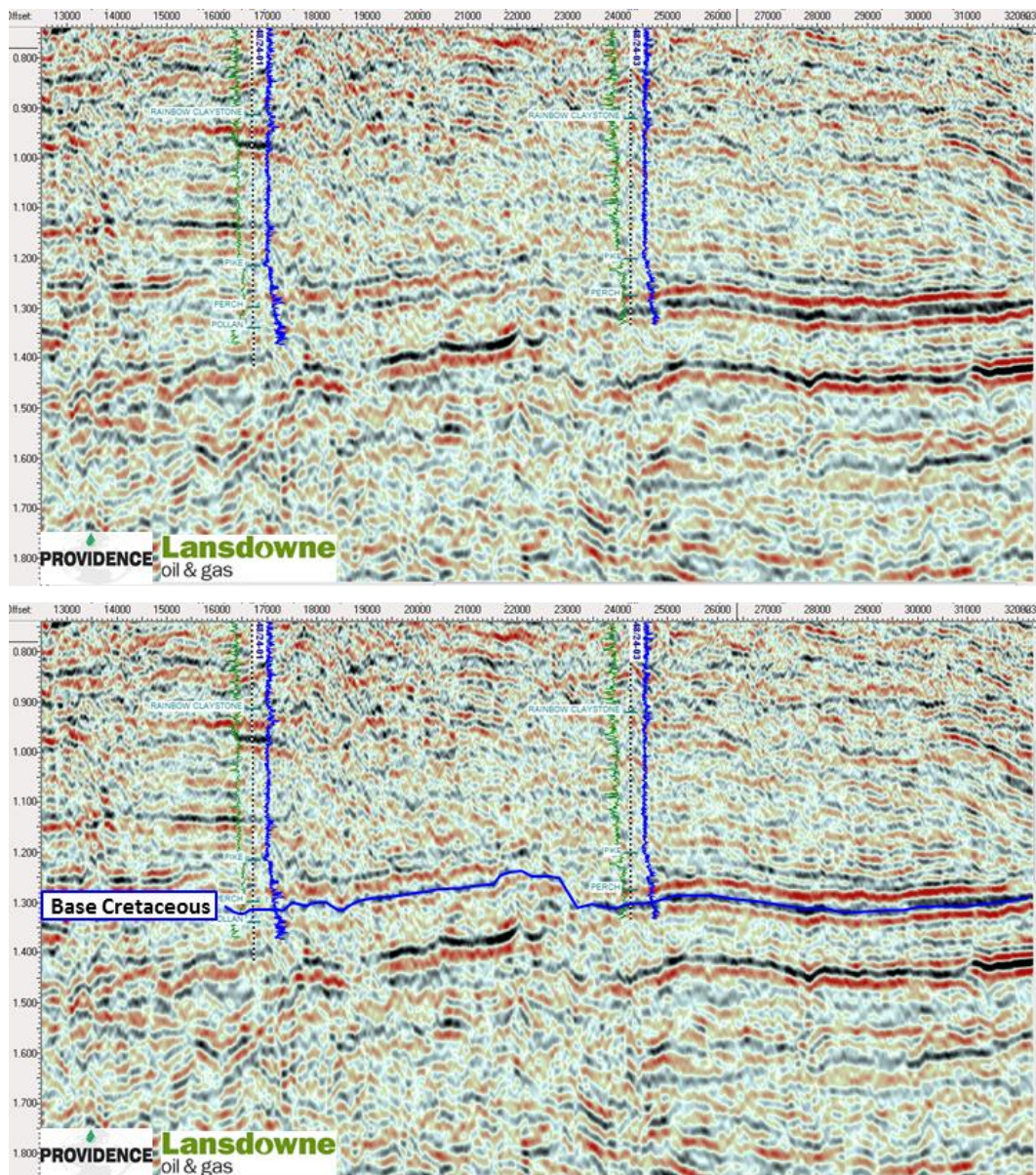


Figure 6-18. Barryroe 3D arbitrary seismic line through wells 48/24-1 and 48/24-3 with GR log (green), Sonic log (blue) and formation tops (after Copestake et al., 2018). Presented with and without Base Cretaceous seismic interpretation.

- Callovian-Oxfordian Unconformity (Top Peregrine Formation)

An intra-Jurassic unconformity is evident on seismic data within the Jurassic section in the basin centre with truncation of underlying seismic events, Figure 6-19. Well ties are also available to constrain the interpretation, Figure 6-20. This unconformity becomes difficult to interpret in areas of poor data quality or where there is little change in dip and no well control. In these areas, the interpretation is extended at a middle Jurassic level, honouring its relative position elsewhere on the seismic data. This interpretation is justified based on the regional extent of the unconformity both within the NCSB and adjacent basins (Stuart, 1993; Barr *et al.*, 1981; Welch & Turner, 2000; Ruffell & Coward, 1992; Robinson *et al.*, 1981; Bulnes & McClay, 1998). Coward & Trudgill (1989) describe a hiatus of Middle to Upper Jurassic in age. The recent biostratigraphic and lithostratigraphic study of wells offshore Ireland defined the unconformity more precisely as Callovian-Oxfordian in age and confirmed its regional extent across the NCSB (Copestake *et al.*, 2018). The unconformity event is often referred to as the Mid-Cimmerian tectonic event (Naylor & Shannon, 2011).

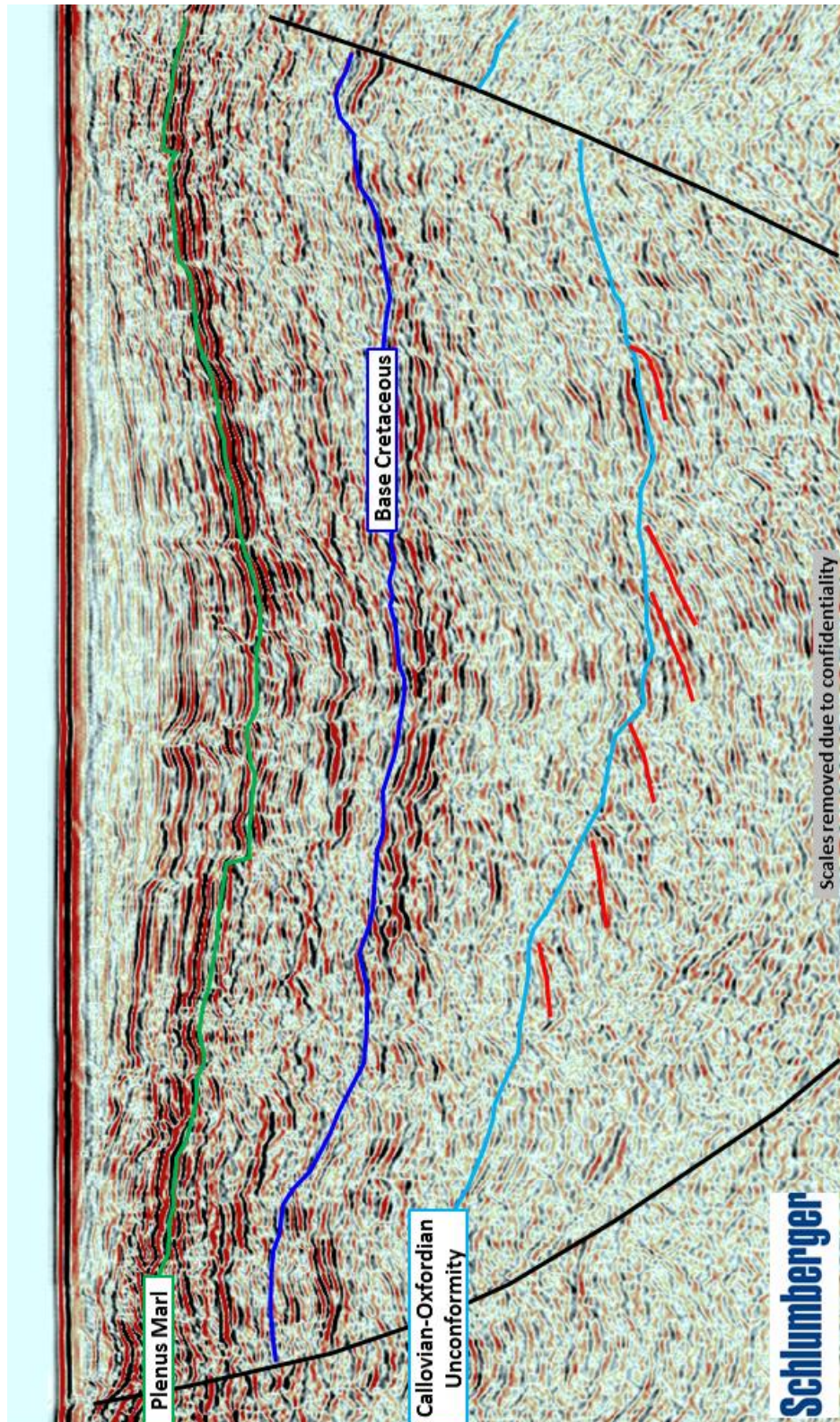


Figure 6-19. Seismic line NCS81-59 showing dipping reflectors (red) truncated by the Callovian-Oxfordian Unconformity.

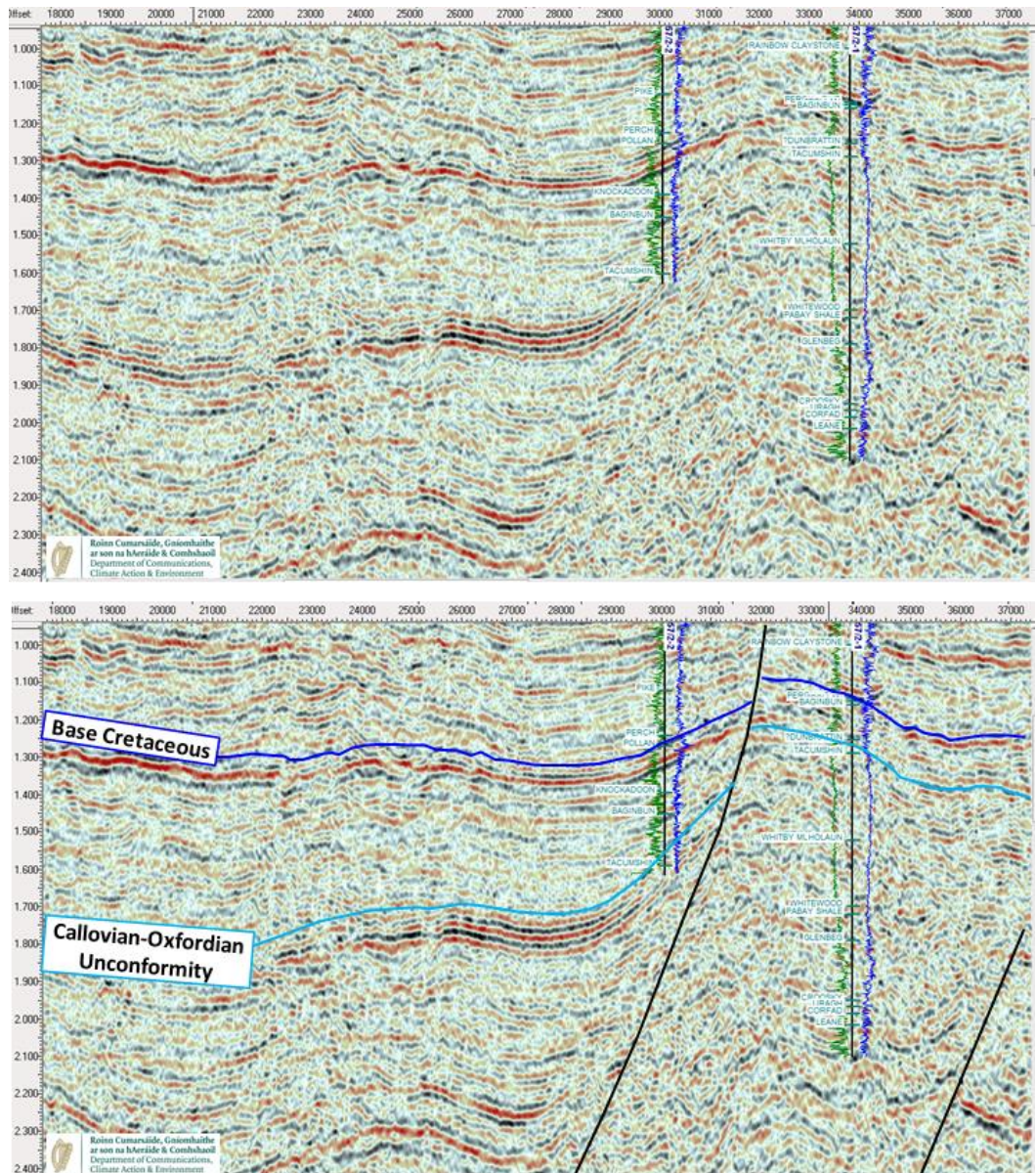


Figure 6-20. Seismic line ACS93-02 through wells 57/2-1 and 57/2-2 with GR log (green), Sonic log (blue) and formation tops (after Copestake et al., 2018). Presented with and without seismic interpretation.

- Top Triassic (Top Penarth Formation).

The Triassic interval is recognised primarily by the seismic character of the sequence, being a sequence of high amplitude reflectors overlying the basement. It is comprised of fluvial sandstones, mudstones and evaporites (Shannon, 1995). Well intersections are restricted to the basin margins, where the Triassic is shallowest, as shown in Figure 6-21. There are no Triassic well penetrations within the centre of the NCSB.

- Top Palaeozoic Basement.

The seismic expression of the top of the Palaeozoic basement is often a strong low frequency seismic event, Figure 6-21, however in the basin centre it is less distinct. This is due to its depth and the residual noise and multiple remaining even on the modern seismic data. The Palaeozoic basement is seen to be seismically opaque with some evidence of deep faults. This suggests the basement is predominantly homogeneous with little lithological change. Well 57/09-1 reports describe the Palaeozoic basement in this area as metamorphosed Carboniferous which is consistent with the characterless seismic response, often associated with a lack of regular density or velocity contrasts such as metamorphic or igneous rocks.

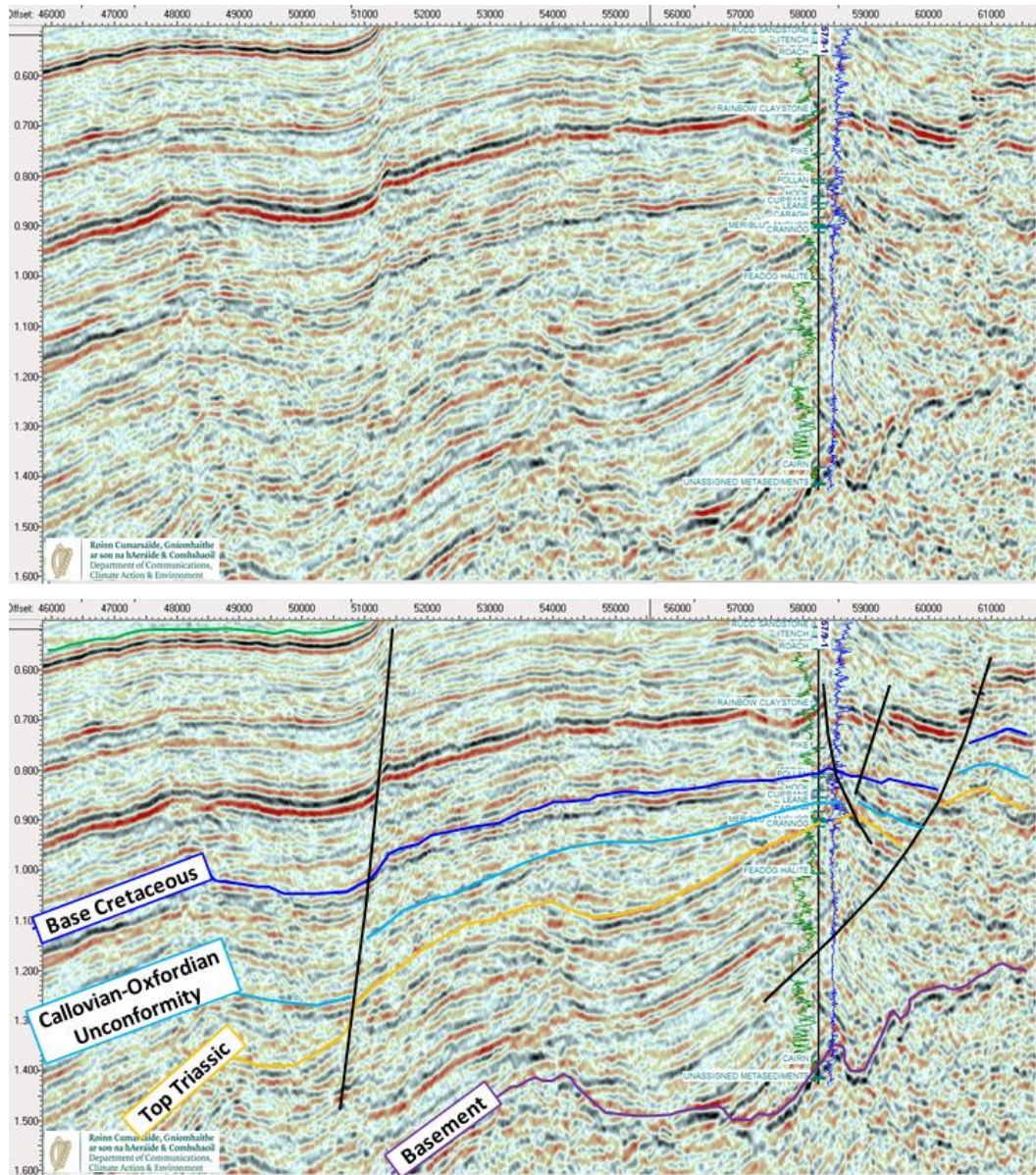


Figure 6-21. Seismic line ACS93-01 through well 57/9-1 with GR log (green), Sonic log (blue) and formation tops (after Copestake et al., 2018). Presented with and without seismic interpretation. Note the well encountered over 1000m (3281ft) of Triassic, containing approximately 250m (820ft) of massive halite.

6.6.3 Interpretation Stage 3

The third stage of the seismic interpretation is to create a framework interpretation of key faults and seismic markers which bounded the stratigraphy, taking into account the understanding of the data gained at the first stage. Regional geological knowledge, seismic character and termination of reflectors are the primary indicators utilised in the seismic interpretation away from well control. Major faults are picked based on offset of seismic reflectors or abrupt changes in dip. Minor or localised faulting was not incorporated into this regional study due to insufficient 3D seismic coverage. All six regional seismic markers were interpreted across each of the modern 2D seismic lines and the Barryroe 3D. The interpretation began at the well control points and extended away from the well control.

6.6.4 Interpretation Stage 4

The fourth stage was a thorough QC of the interpretation from stage three, ensuring the seismic marker interpretations honoured the well control and tied between all seismic line intersections. This is a critical stage in any seismic interpretation, the interpretation should be consistent and robust from any starting point, following a grid onto adjacent seismic data and back in a circular fashion to the starting point (Herron, 2011; Brown, 2011; Robinson & Clark, 2017; Ikelle & Amundsen, 2018). The fault interpretations were also reviewed, ensuring the fault plane orientation and throw was consistent and geologically sensible (Childs et al., 1996, 2009).

6.6.5 Interpretation Stage 5

Finally, using this framework of interpreted modern 2D and 3D seismic data, a robust interpretation could be extended using seismic character and overall structural style onto the poorer quality vintage 2D data, this was the fifth stage. The wells which provided important ties to the vintage 2D seismic data include 47/29-1, 47/30-1, and 57/06-1. Figure 6-22 shows a vintage Mil90 seismic line overlain on an adjacent modern SGC06 seismic line. Figure 6-23 shows a vintage CSN82 seismic line overlain on an adjacent reprocessed NCS81 seismic line. Examining Figure 6-22 and Figure 6-23 it is clear that the vintage data is of sufficient quality to successfully use seismic character and overall structural style to extend the interpretation from the modern seismic data to the vintage seismic data.

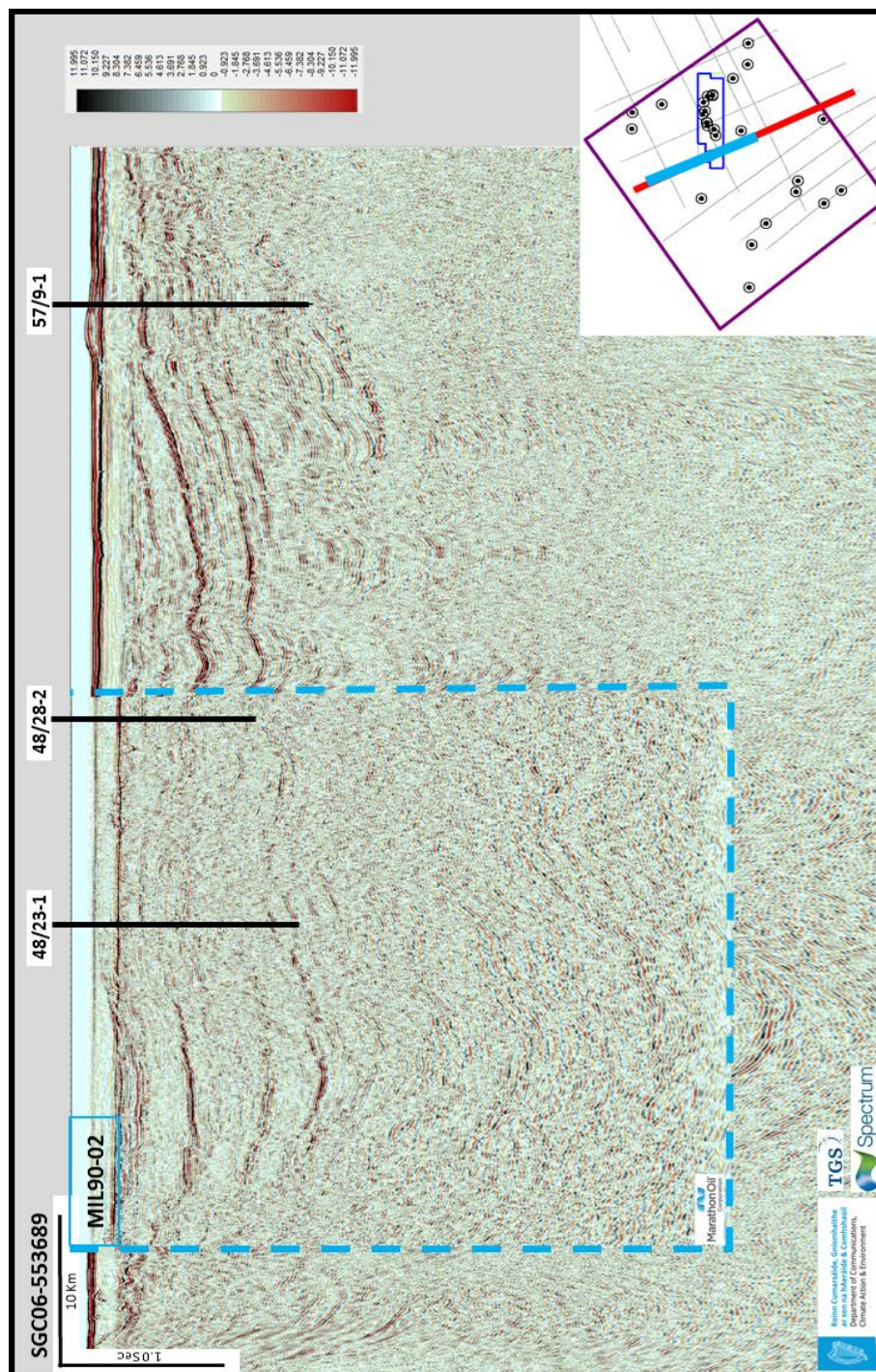


Figure 6-22. Vintage seismic line MIL90-02 overlain on adjacent SGC06-553689, demonstrating that the vintage seismic is of sufficient quality to successfully use seismic character and overall structural style to extend the interpretation from the modern seismic data to the vintage seismic data.

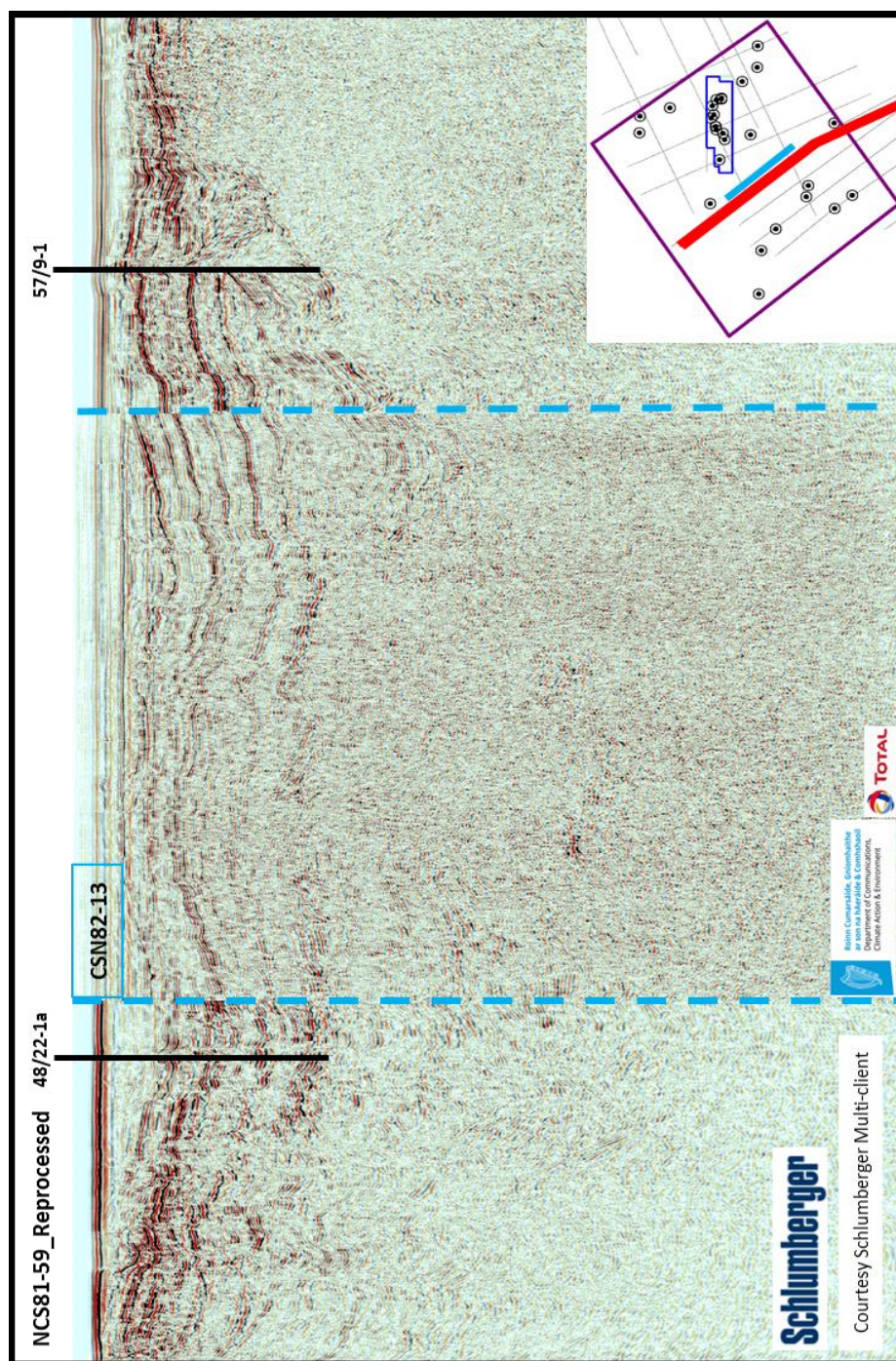


Figure 6-23. Vintage seismic line CSN82-13 overlain on adjacent reprocessed NCS81-59, demonstrating that the vintage seismic is of sufficient quality to successfully use seismic character and overall structural style to extend the interpretation from the modern seismic data to the vintage seismic data.

Maps of the structural interpretations were created for the six seismic markers over the study area in the time domain, from the vintage and modern seismic data. The maps were converted to the depth domain by using a layer by layer depth conversion process, using the velocity information from the primary wells (Marsden, 1989; Al-Chalabi, 2014; Francis, 2018a; Francis, 2018b). Seismic isochron maps were created for the interval between each seismic marker and crossplot against the associated sediment thickness of that interval in the wells. The dataset was well behaved and linear trends could be selected for each interval with a coefficient of determination ranging between 0.90 and 0.99, Figure 6-24. Using the linear trend per interval, the seismic isochron maps were converted to depth isopach maps (sediment thickness per interval). The interval velocity of each layer was calculated by dividing the depth isopach maps by the seismic isochron maps (depth / time), (Marsden, 1989; Al-Chalabi, 2014; Francis, 2018a; Francis, 2018b). The resultant interval velocity maps were then quality controlled against the seismic velocity from the modern dataset. Finally, the isopach maps were stacked as appropriate to create depth maps of the interpretation for each of the six seismic markers.

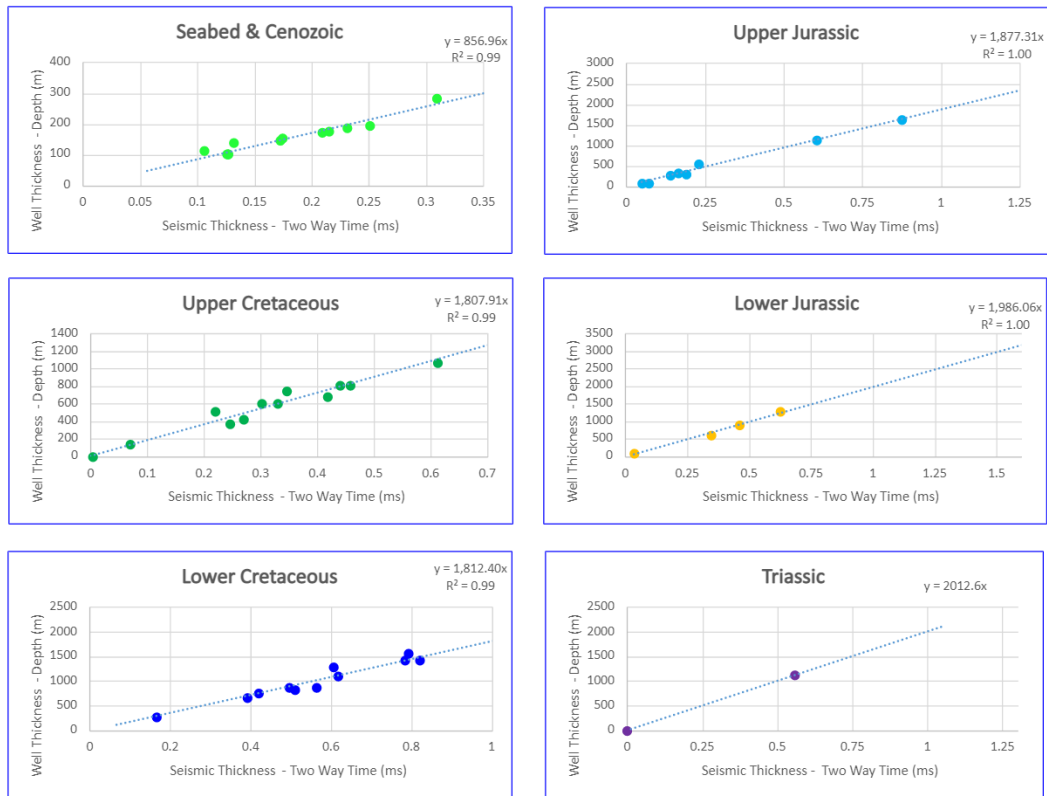


Figure 6-24. Cross-plots of seismic isochron versus well isopach used for layer by layer depth conversion, a coefficient of determination is presented for each layer.

7 Results

Representative seismic lines with and without interpretation are presented in Figure 7-1 to Figure 7-6 and reproduced in a larger scale in Appendix E. These figures highlight important results which are discussed in detail within this chapter.

The results are a suite of depth maps for the primary stratigraphic markers, a suite of isopach maps for the interval between each stratigraphic marker and the fault polygons for major basin scale faults associated with each map.

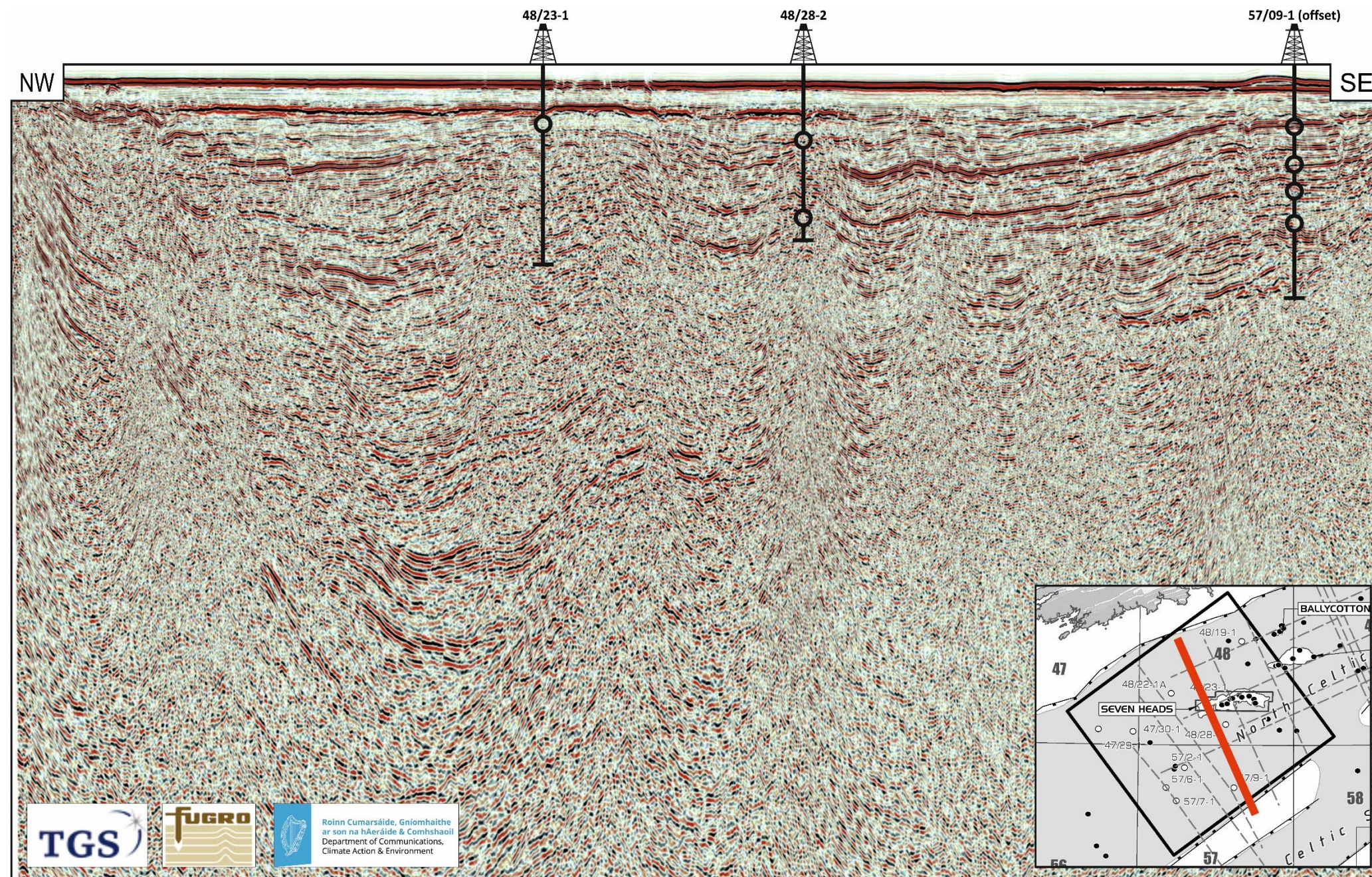


Figure 7-1. Seismic line SGC06-553689 imaging the entire NCSB, with hydrocarbon exploration well locations, without interpretation. Reproduced in a larger scale in Appendix E.1.

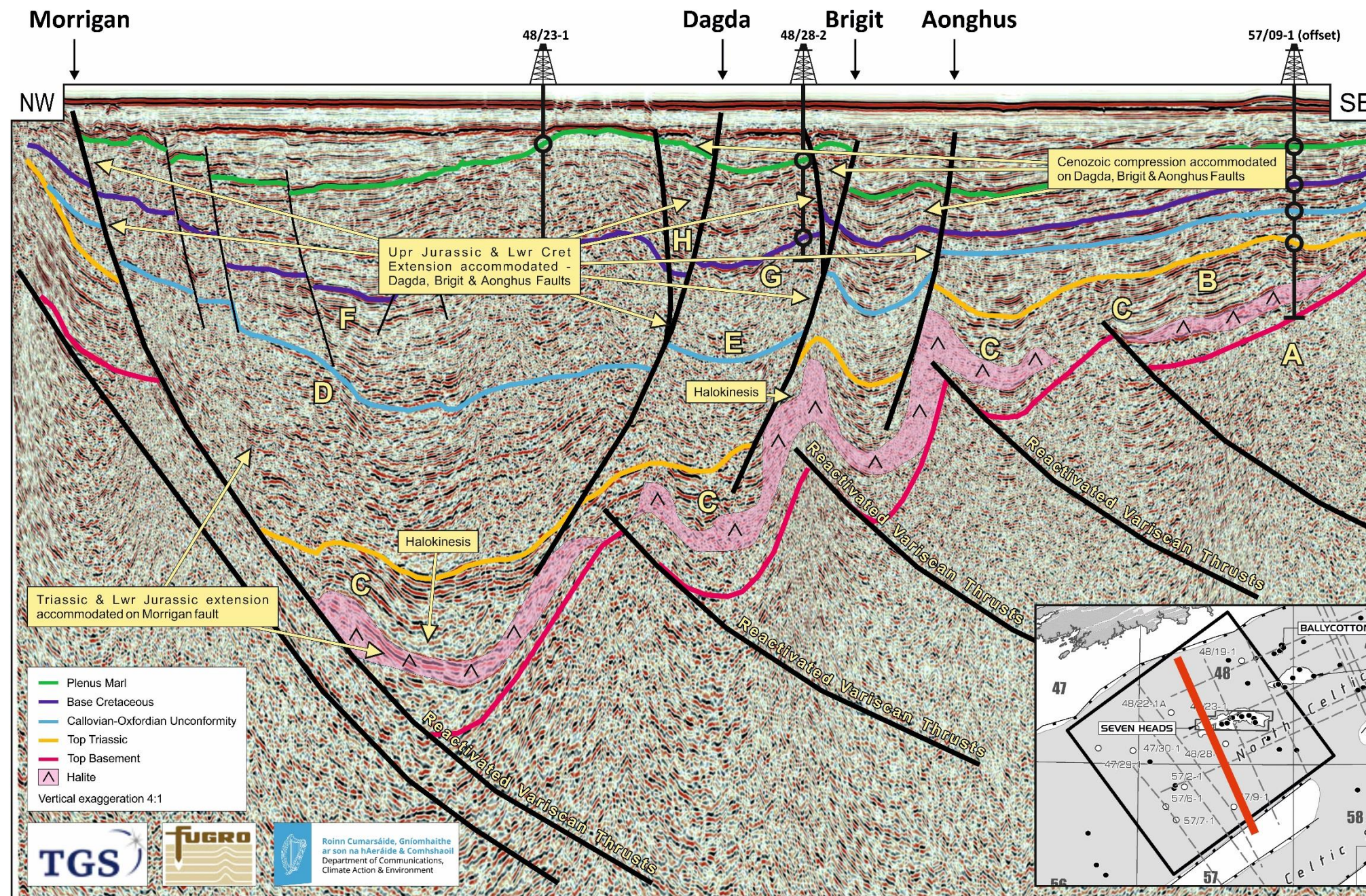


Figure 7-2. Seismic line SGC06-553689 imaging the entire NCSB with hydrocarbon exploration wells, major seismically definable stratigraphic markers and fault interpretation shown.

(A) represents the opaque seismic character of the Paleozoic Basement. (B) represents the high amplitude continuous character of the Triassic. (C) indicates areas of syn-sedimentary growth within the Triassic. (D) indicates subtle change in dip of seismic reflectors at the Callovian-Oxfordian unconformity. (E) indicates areas where the Callovian-Oxfordian Unconformity is interpreted and there is no change in dip or well control. (F) indicates the areas where the Base Cretaceous is represented by the upper of two parallel reflectors in the basin centre. (G) indicates where the reflectors at (F) have thinned and coalesced as one reflector. (H) indicates areas of syn-sedimentary growth within the Cretaceous. Reproduced in a larger scale in Appendix E.2.

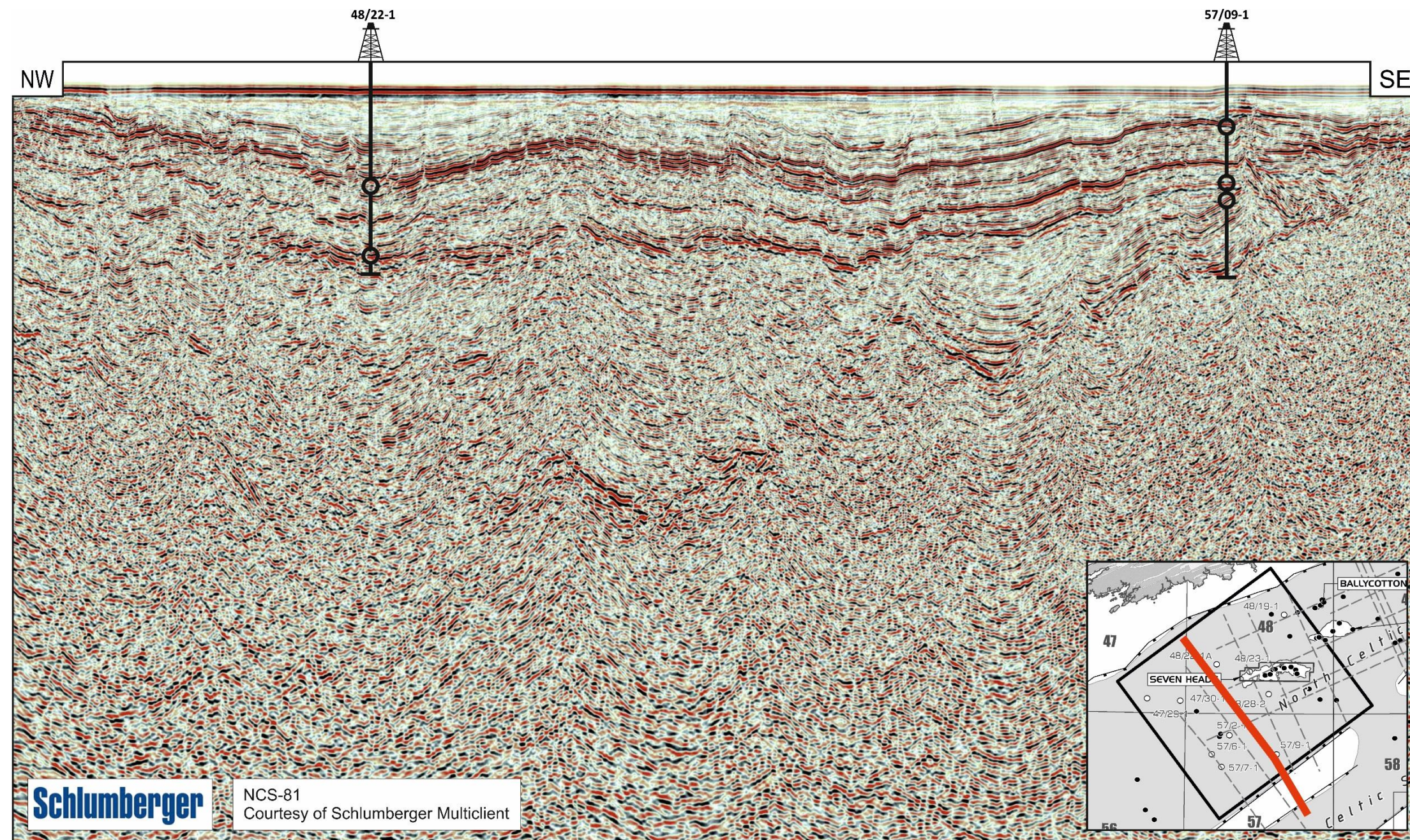


Figure 7-3. Northwest to southeast seismic line NCS81-59 imaging the entire NCSB, with hydrocarbon exploration well locations, without interpretation. Reproduced in a larger scale in Appendix E.3.

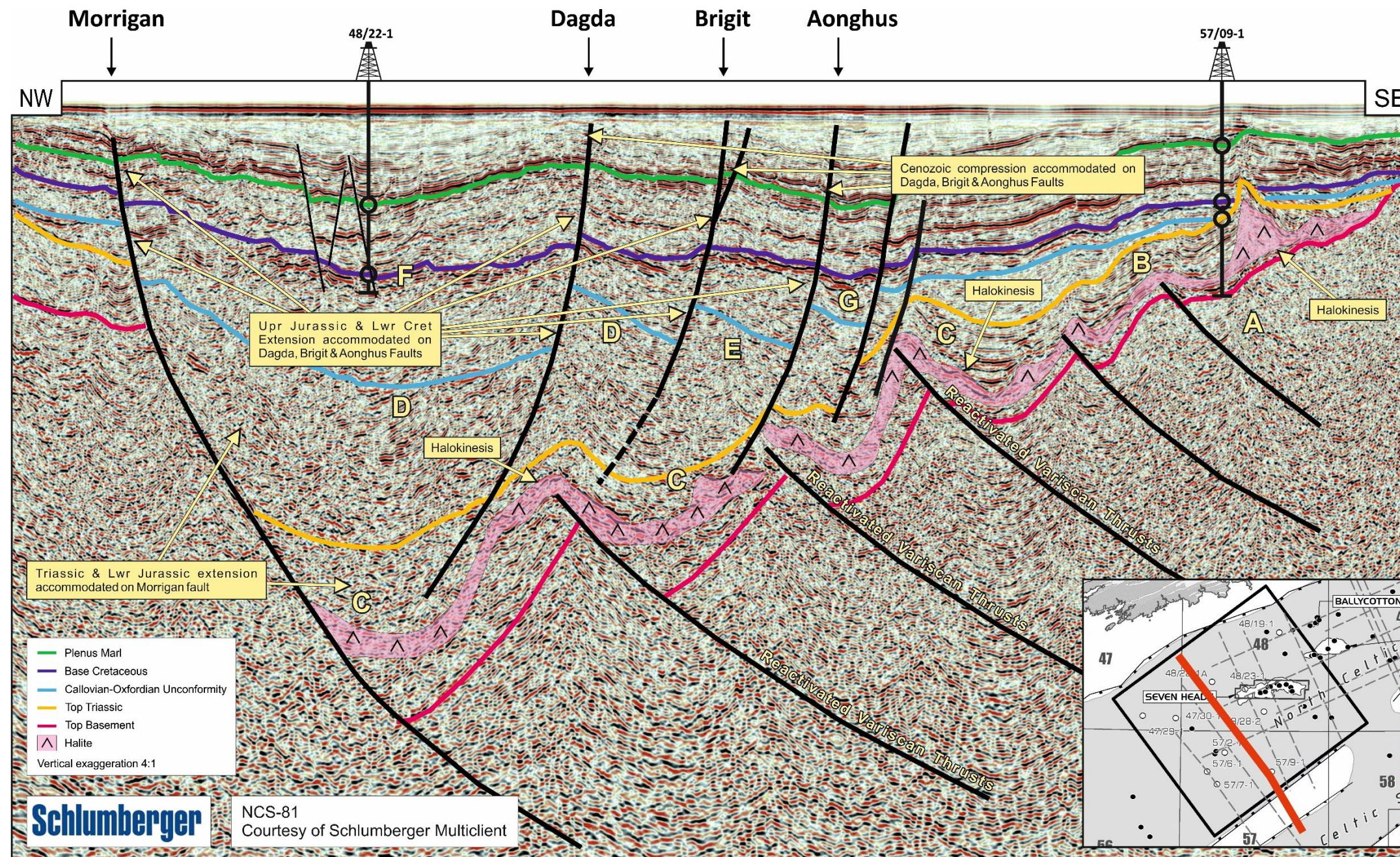


Figure 7-4. Northwest to southeast seismic line NCS81-59 imaging the entire NCSB, with hydrocarbon exploration wells, major seismically definable stratigraphic markers and fault interpretation shown, courtesy Schlumberger Multiclient. (A) represents the opaque seismic character of the Paleozoic Basement. (B) represents the high amplitude continuous character of the Triassic. (C) indicates areas of syn-sedimentary growth within the Triassic. (D) indicates subtle change in dip of seismic reflectors at the Callovian-Oxfordian unconformity. (E) indicates areas where the Callovian-Oxfordian Unconformity is interpreted and there is no change in dip or well control. (F) indicates the areas where the Base Cretaceous is represented by the upper of two parallel reflectors in the basin centre. (G) indicates where the reflectors at (F) have thinned and coalesced as one reflector. Reproduced in a larger scale in Appendix E.4.

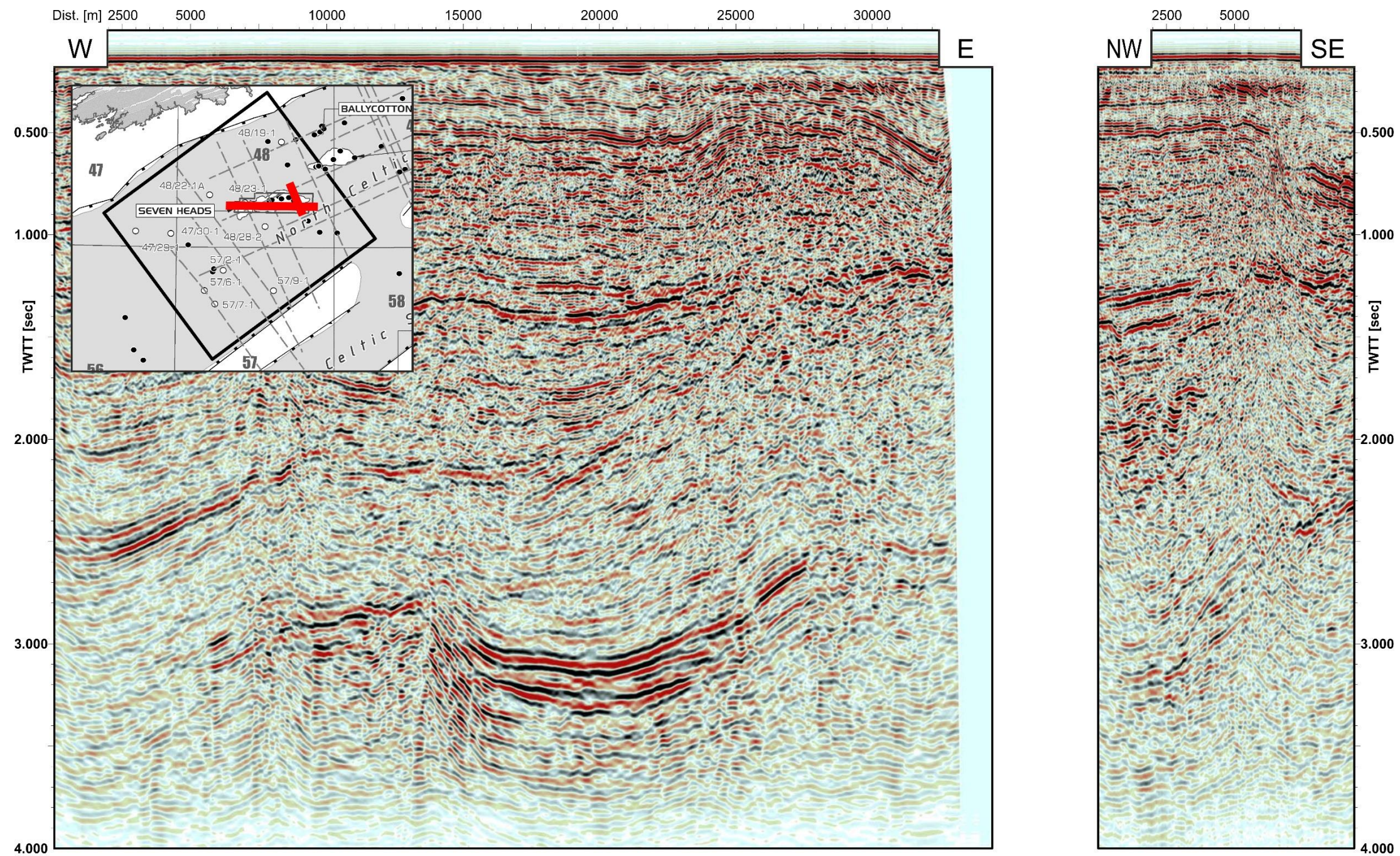


Figure 7-5. Barryroe 3D seismic data quality example, without interpretation. Courtesy Providence Resources Plc and Lansdowne Oil and Gas Plc. Reproduced in a larger scale in Appendix E.5.

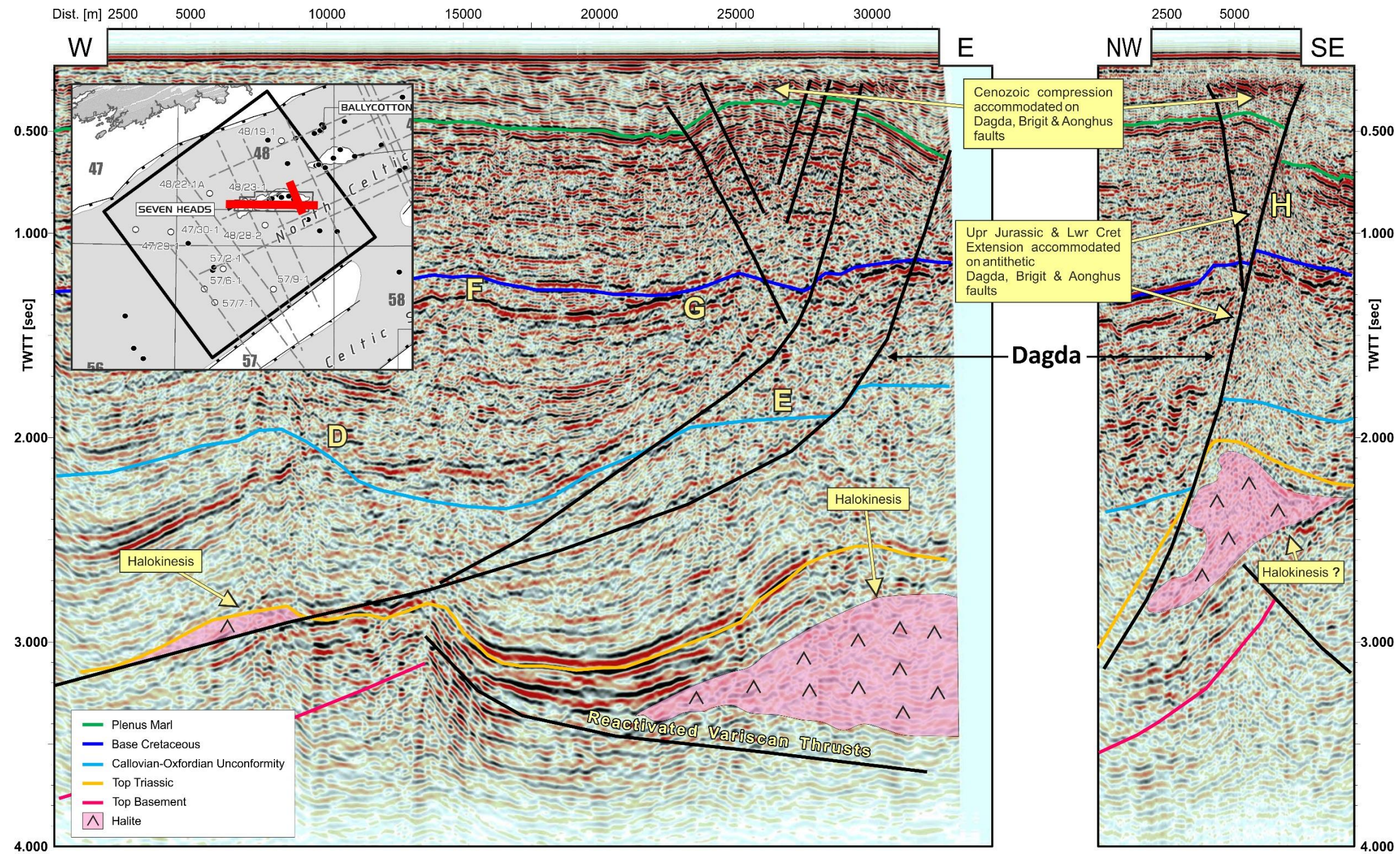


Figure 7-6. Barryroe 3D seismic data quality example, exhibiting imaging at depth and minor halokinesis. Courtesy Providence Resources Plc and Lansdowne Oil and Gas Plc. (D) indicates subtle change in dip of seismic reflectors at the Callovian-Oxfordian unconformity. (E) indicates areas where the Callovian-Oxfordian Unconformity is interpreted and there is no change in dip or well control. (F) indicates the areas where the Base Cretaceous is represented by the upper of two parallel reflectors in the basin centre. (G) indicates where the reflectors at (F) have thinned and coalesced as one reflector. (H) indicates areas of syn-sedimentary growth within the Cretaceous. Reproduced in a larger scale in Appendix E.6.

7.1 Stratigraphy

Six seismic markers could be identified regionally within the study area. These seismic markers represent the boundaries of major geological units in the Irish offshore. Resulting maps of the isopach and depth structure for each unit are presented in large scale format in Appendix F and Appendix G.

7.1.1 Palaeozoic Basement

The Palaeozoic basement is seen to be seismically opaque with a high amplitude, low frequency package overlying it (Figure 7-2 & Figure 7-4, Location A; Figure 7-7). This suggests the basement is predominantly homogeneous with little lithological change. Well 57/09-1 describes the Palaeozoic basement in this area as metamorphosed Carboniferous which is consistent with the opaque seismic response observed, (Figure 6-14 & Figure 7-7).

A depth map of the Top Paleozoic Basement is presented in Figure 7-8 and reproduced in Appendix F.1. It illustrates several reactivated Variscan thrust faults with a NE-SW strike and a southerly dip. The most northern of the faults is the Morrigan Fault (see Chapter 7.2) and exhibits the greatest throw with footwall depths of 3,000m (9,850ft) and hanging wall depths of up to 8,000m (26,300ft). The present-day depth of the basement within the study area varies from 1,000m (3,300ft) to over 9,000m (29,500ft) in the basin centre, adjacent to the Morrigan fault.

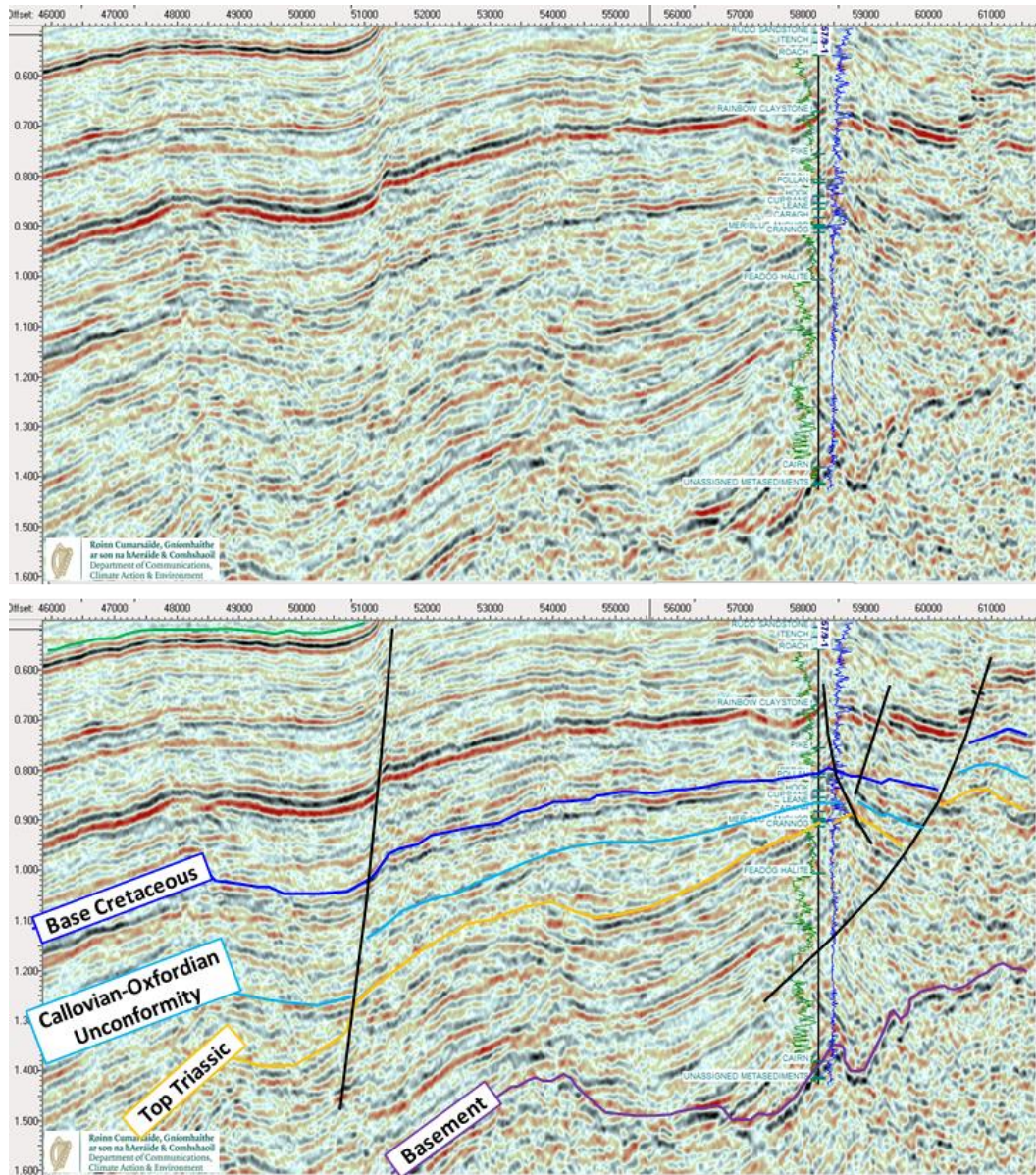


Figure 7-7. Seismic line ACS93-01 through well 57/9-1 with GR log (green), Sonic log (blue) and formation tops (after Copestake et al., 2018). Presented with and without seismic interpretation. The well encountered over 1000m (3281ft) of Triassic, represented as a high amplitude seismic package, containing approximately 250m (820ft) of massive halite. There is an opaque seismic character within the metamorphosed carboniferous basement encountered by the well.

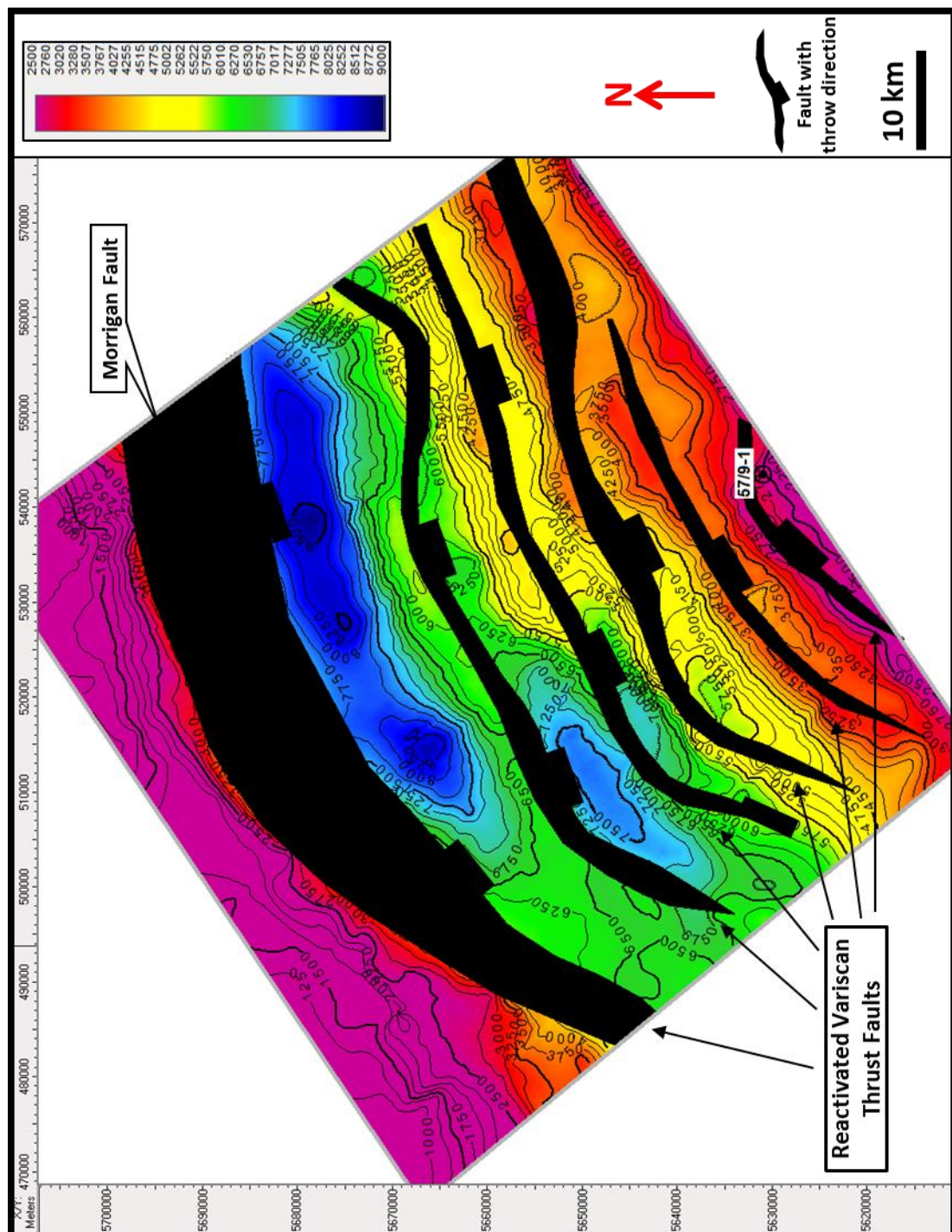


Figure 7-8. Depth map of Top Paleozoic Basement, interpreted within the study area, contour interval 250m (820ft), well control highlighted. Faulting has a NE-SW strike and a southerly dip. The fault labelled the Morrigan Fault exhibits the greatest throw.

7.1.2 Triassic

The high amplitude package overlying the basement (Figure 7-2 & Figure 7-4 Location B; Figure 7-7), is dated as Triassic, drilled at over 1000m (3281ft) in thickness and containing approximately 250m (820ft) of massive halite in well 57/09-1. The Triassic sedimentary section in the region can be divided into two groups. The lower Sherwood Sandstone Group (SSG) is dominantly fluvial sandstones while the upper Mercia Mudstone Group (MMG) is a red-bed mudrock and marly succession with variable amounts of evaporite (Naylor & Shannon, 2011). Well intersections are restricted to the basin margins, where the Triassic is shallowest. There are no Triassic well penetrations within the centre of the NCSB however Clayton *et al.* (1986) interpret a red bed sequence onshore southern Ireland as being potentially Triassic. A Triassic section has been proven on the basin margins (Shannon, 1995) and in adjacent basins (Bulnes & McClay, 1998; Evans *et al.*, 1990).

The depth map of the Triassic (Figure 7-10, Appendix F.2) shows the present-day depth varies from 1,500m (5,000ft) to the south to 7500m (24,600ft) adjacent to the Morrigan Fault. It should be noted that the depth map shows the location of Jurassic and Cretaceous extensional faults which sole out within the Triassic, but were not active during the Triassic, as discussed in Chapter 7.2 and are particularly evident within the Barryroe 3D survey (Figure 7-13 & Figure 7-14).

The location of significant Triassic syn-sedimentary extensional faults is interpreted within the Triassic on seismic data, with clear offset, sedimentary growth and

rotation evident (Figure 7-2 & Figure 7-4 – Location C) creating a series of half grabens. A zoom-in of one of these areas is shown in Figure 7-9 where the stratigraphy is seen to thicken to the NW above a low angle fault which dips to the SE.

The isopach of the Triassic interval is shown in Figure 7-11 & Appendix G.1 and illustrates the Triassic half grabens with extensional faults dipping to the southeast and strike-parallel to the northeast-southwest orientated northern basin bounding Morrigan Fault. These faults are interpreted to be reactivated Variscan structures, similar to the Morrigan Fault, which are known from regional geology to dip to the southeast (BIRPS & ECORS, 1986; McGeary *et al.*, 1987; Meere, 1995). Alternative interpretations were considered, specifically northerly dipping extensional faults (which would define a conventional graben with the Morrigan Fault). Due to subsequent faulting and halokinesis this alternative interpretation can appear valid on some seismic lines, however it was discounted as there were several locations of excellent seismic data quality where clear southerly dipping faults could be imaged on the seismic with growth of the sedimentary section evident above them, see Figure 7-9.

These reactivated Variscan thrust faults have significant thickening across the faults of up to 2,000m (6,600ft) (Figure 7-11 & Appendix G.1). Six half grabens can be identified within the study area, with up to 2500m (8200ft) of sediment deposited in the half grabens. It is also noted that there is considerable thickness variation along the strike of the half grabens which agrees with Musgrove *et al.* (1995) who

suggested the Triassic being partially controlled by paleo-topography. This variation in sediment thickness along the strike of the half grabens could also be associated with halokinesis. Triassic sediment is likely sourced from both the Variscan foreland to the north, being shed southward over the normal faults, and the Variscan uplands to the south, being shed northwards by fluvial and/or aeolian processes (Tyrrell *et al.*, 2012).

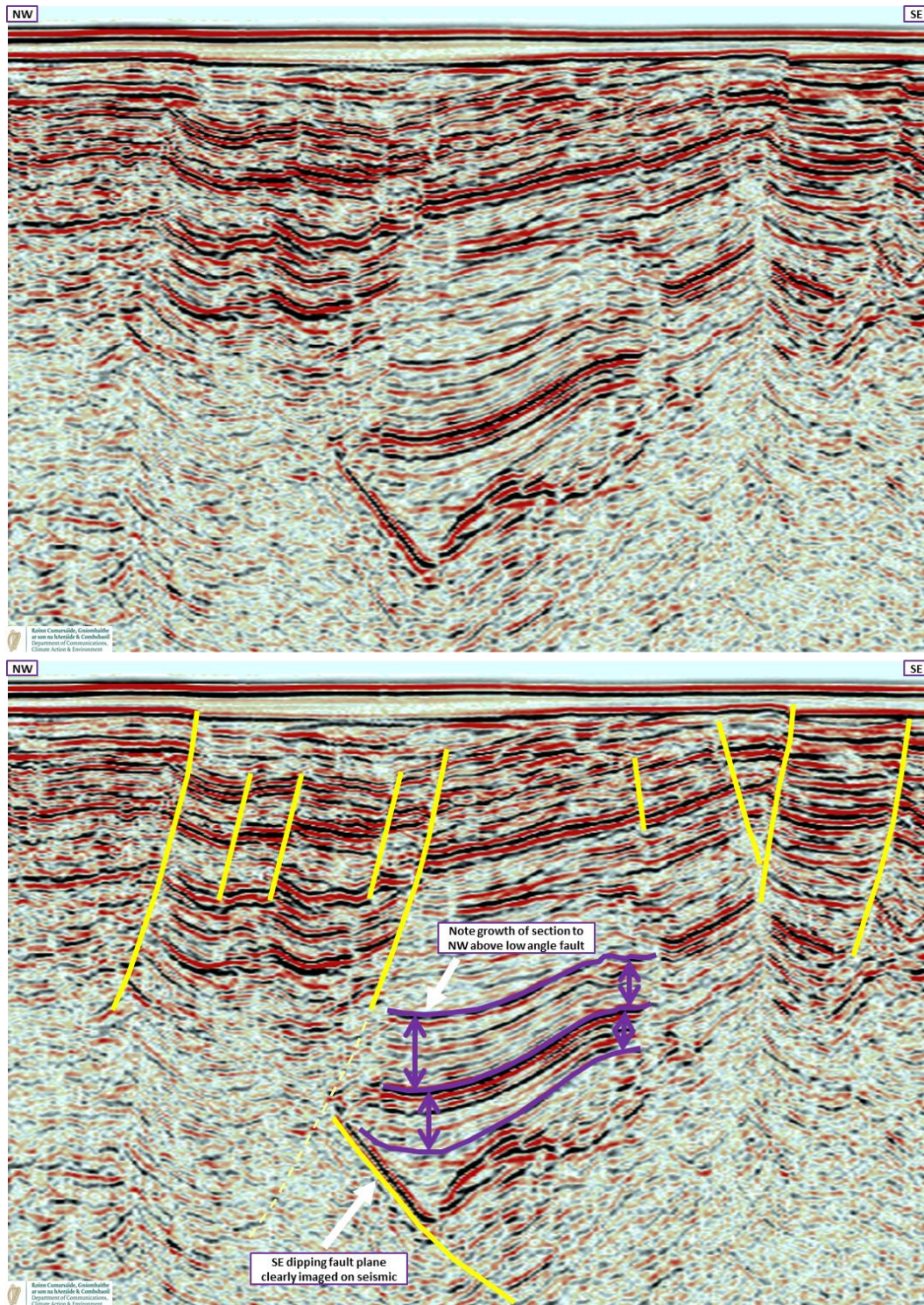


Figure 7-9. Seismic line NCS-84 with clearly identifiable faults in yellow and evidence of growth of stratigraphy to the NW above a low angle fault which dips to the SE. Presented with and without seismic interpretation.

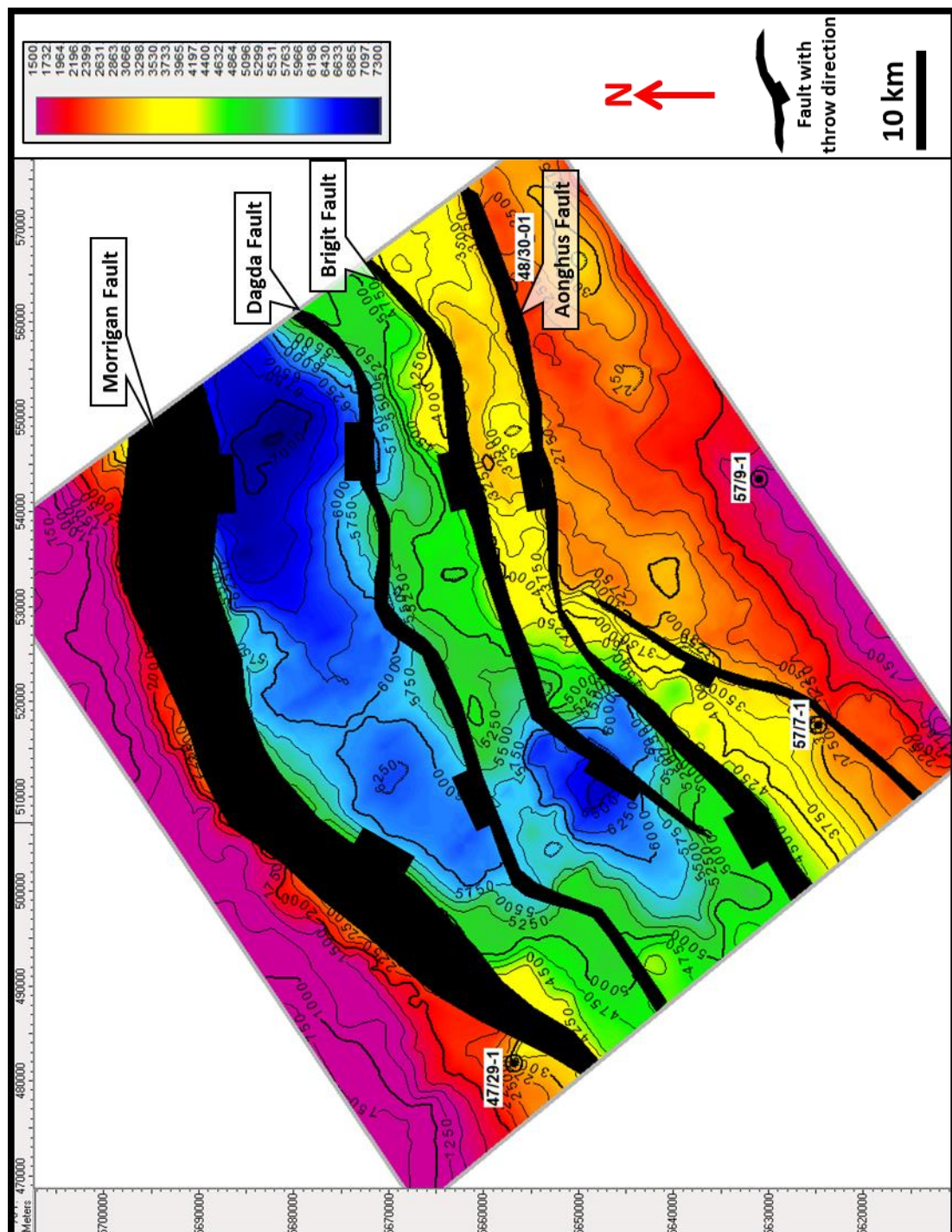


Figure 7-10. Depth map of Top Triassic, interpreted within the study area, contour interval 250m (820ft), well control highlighted. Faults which intersect the Top Triassic are younger faults with detach within the Triassic.

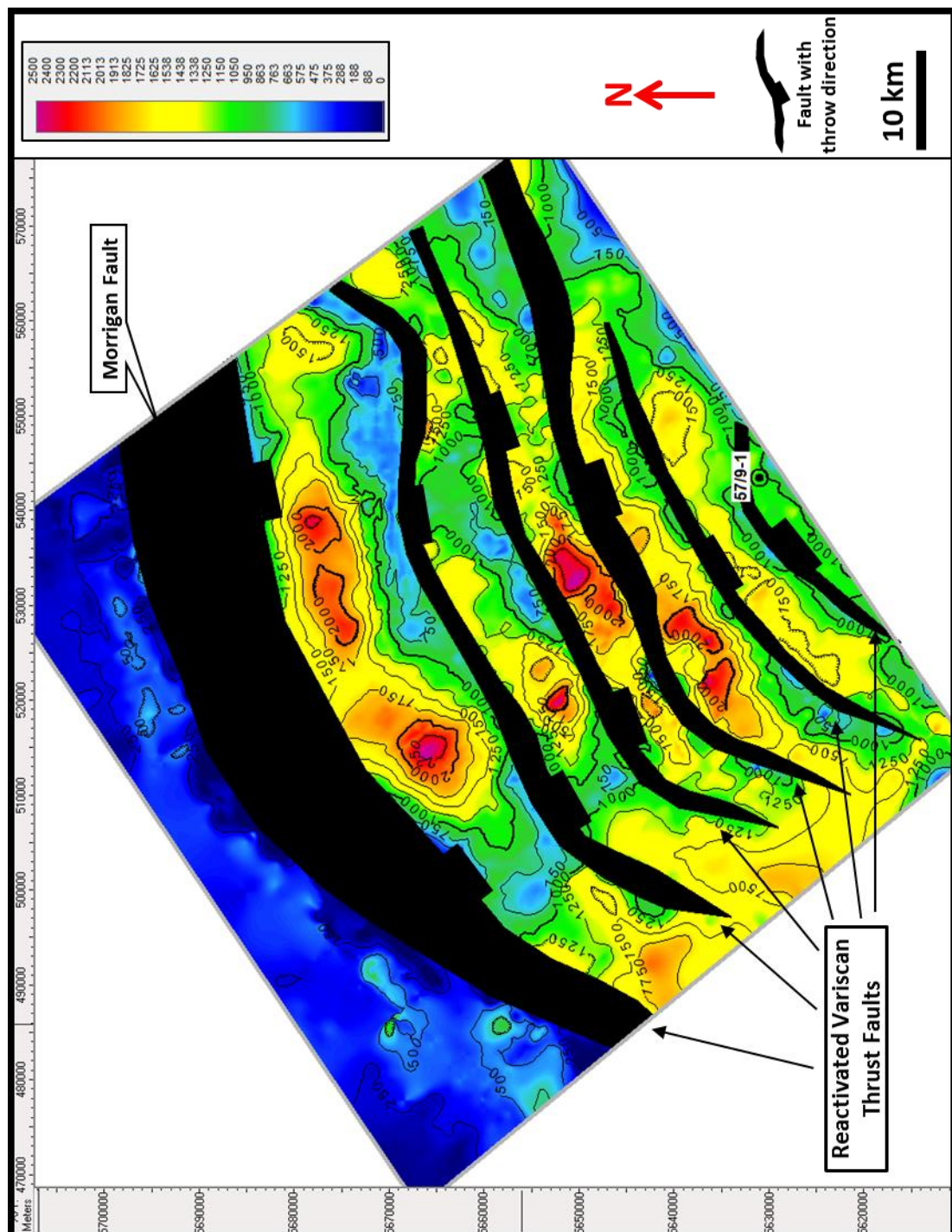


Figure 7-11. Isopach of the Triassic interpreted within the study area, contour interval 250m (820ft), well control highlighted. SW-NE reactivated Variscan faults accommodate Triassic extension creating 6 half grabens. Sediment thickness also changes along the strike of the half grabens suggesting both fault and paleo-topographic control on sedimentation.

Musgrove *et al.* (1995) postulate the presence of only thin Triassic sediments in the NCSB. The SSG is described as confined to existing paleo-topographic lows while the MMG is deposited during active rifting and is more extensive. Based on regional geology, Musgrove *et al.* (1995) predict the SSG will be present in areas where halite can be identified in the MMG. Naylor & Shannon (2011) and Shannon (1995) agree the Triassic was deposited in discrete fault bounded basins. These authors however suggest a mudstone and marl dominated MMG with thick Triassic halite restricted to the southern margin of the NCSB.

The modern seismic data shows features within the Triassic section which are consistent with minor halokinesis (Stewart, 2007; Herron, 2011; Brown, 2011; Robinson & Clark, 2017; Ikelle & Amundsen, 2018). Seismically opaque intervals with irregular shapes can be seen, commonly with parallel events below and distorted overlying intervals, particularly evident in Figure 7-12 at the 57/09-1 well location, this seismic character is consistent with Triassic salt (Stewart, 2007; Karlo *et al.*, 2014). The 57/9-1 well confirmed the Triassic as over 1000m (3281ft) in thickness and containing approximately 250m (820ft) of massive halite. The top of the opaque package is normally characterised by a bright amplitude, representing a change in velocity, consistent with evaporites.

Figure 7-13 to Figure 7-15 show further examples of interpreted halokinesis, with associated illustrations showing proposed salt movement. The seismic data also shows evidence of salt movement as early as the Lower Jurassic as the Callovian-

Oxfordian unconformity erodes uplifted/distorted Triassic (Figure 7-12) and evidence of salt withdrawal creating a Lower Jurassic depocenter (Figure 7-14).

This minor halokinesis is seen at several locations, including in the basin centre, as highlighted in Figure 7-2 to Figure 7-6 (Appendix E.1 to Appendix E.6). These modern data strongly suggest the presence of mobile evaporites (halites) within the Triassic across the NCSB. Based on the predictions of Musgrove *et al.* (1995), the thick package beneath the mobile evaporites is SSG. The modern seismic data therefore suggest extensive deposition of SSG across the NCSB rather than being thin or restricted (Musgrove, 1995; Naylor & Shannon, 2011). This interpretation is also supported by the presence of halite in adjacent basins (Bulnes & McClay, 1998; Evans *et al.*, 1990) and the interpretation of Triassic onshore southern Ireland (Clayton *et al.*, 1986).

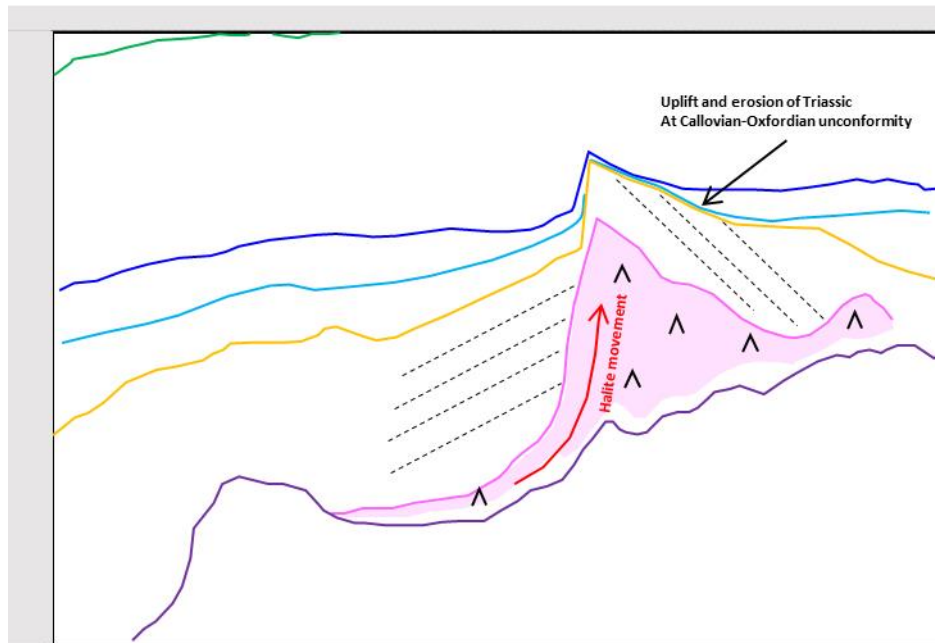
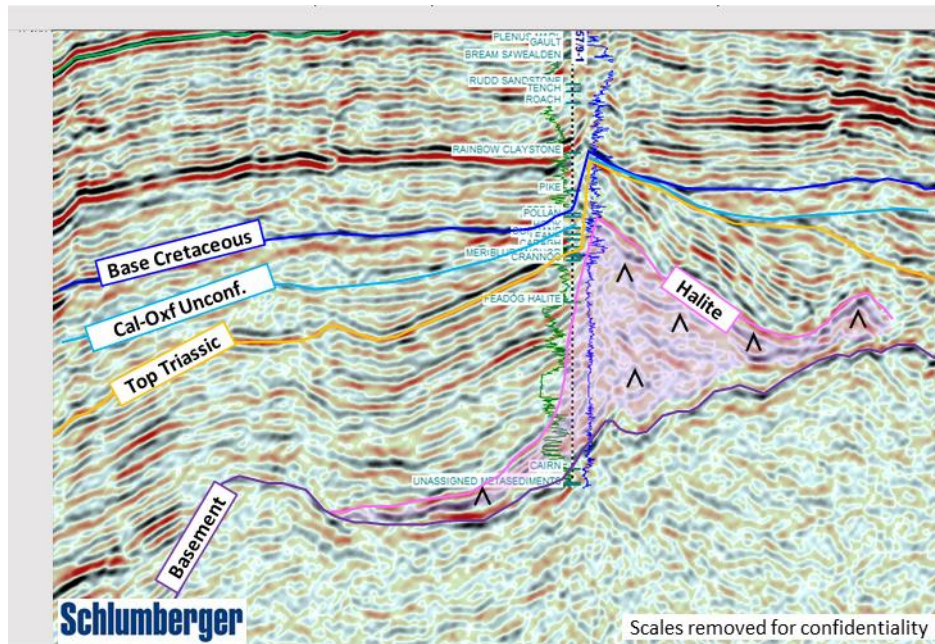


Figure 7-12. Seismic line NCS81-59 zoomed to 57/9-1 well, with area of halite movement (halokinesis) annotated and resulting erosion of Triassic section at the Callovian-Oxfordian unconformity which provides a date for onset of halokinesis as Lower Jurassic, courtesy Schlumberger Multiclient.

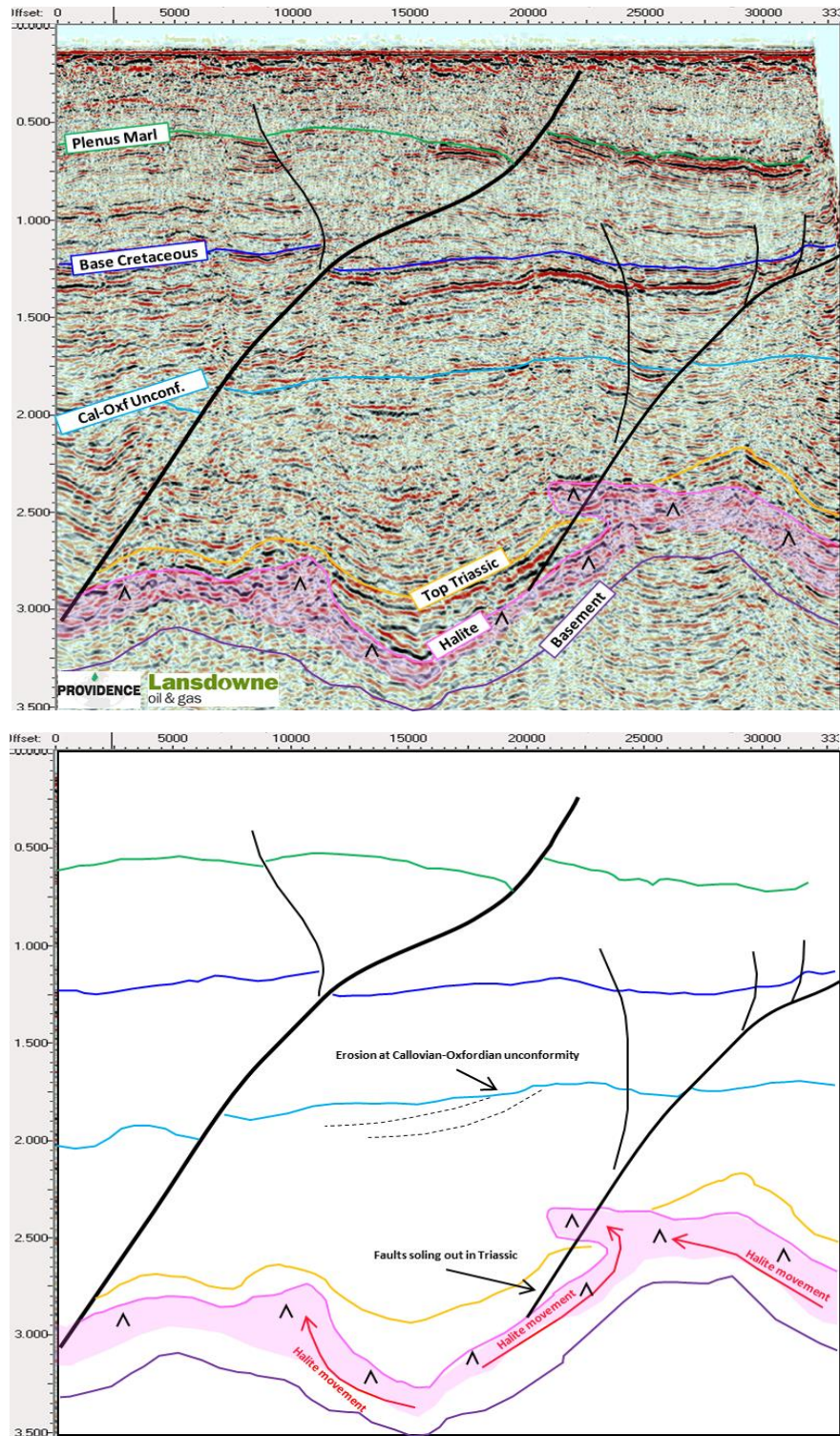


Figure 7-13. Barryroe 3D Inline 58, with area of halite movement (halokinesis) annotated. Overlying faults are seen to detach within the Triassic section. Note evidence of erosion of Lower Jurassic section by the Callovian-Oxfordian unconformity.

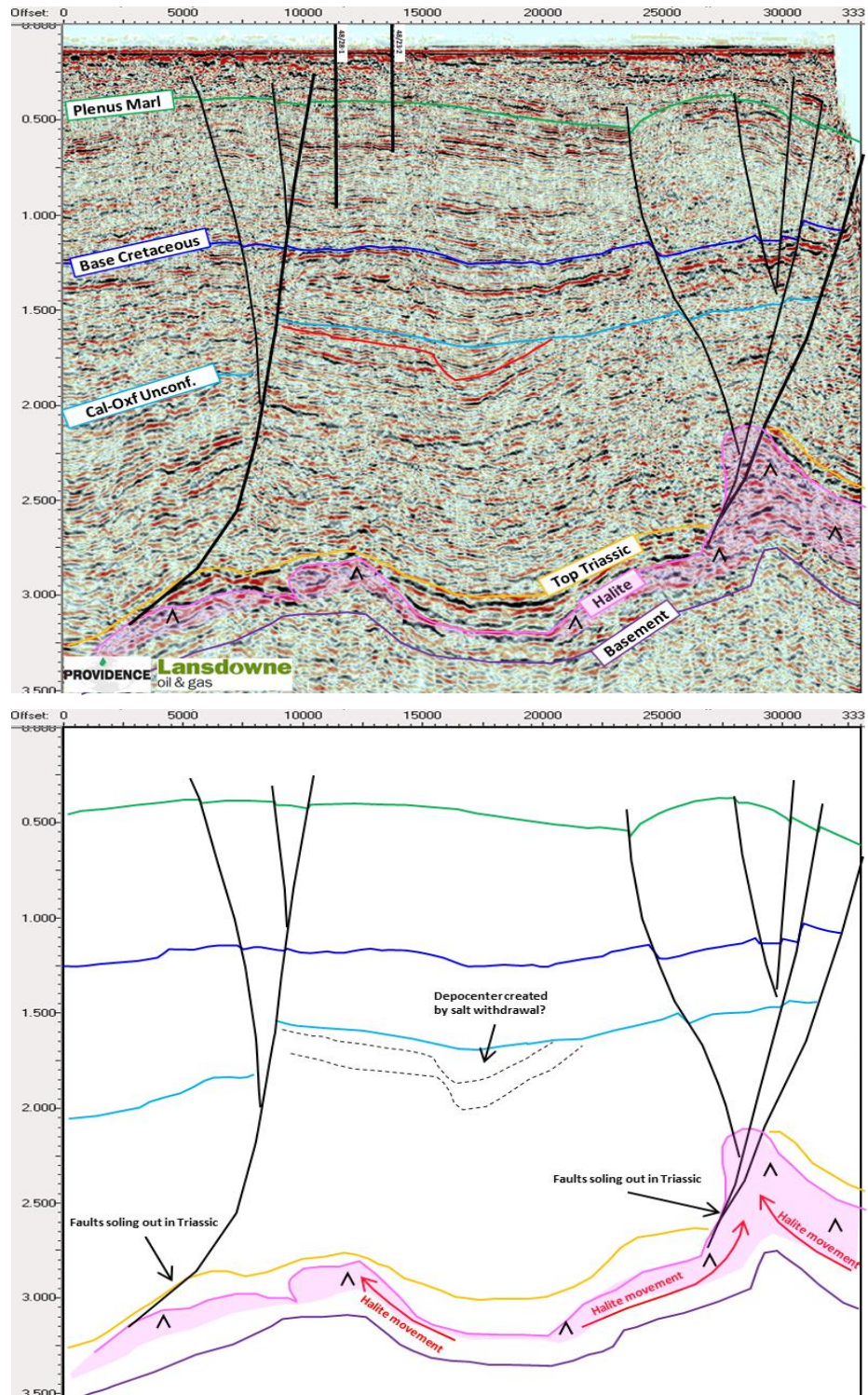


Figure 7-14. Barryroe 3D Inline 135, with area of halite movement (halokinesis) annotated. Salt withdrawal within the Lower Jurassic created a local depocenter. Overlying faults are seen to detach within the Triassic section.

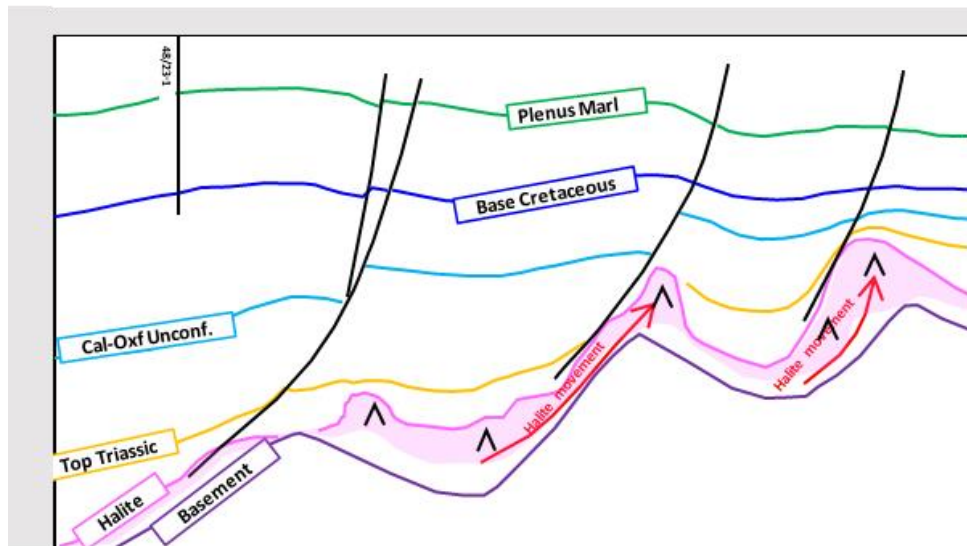
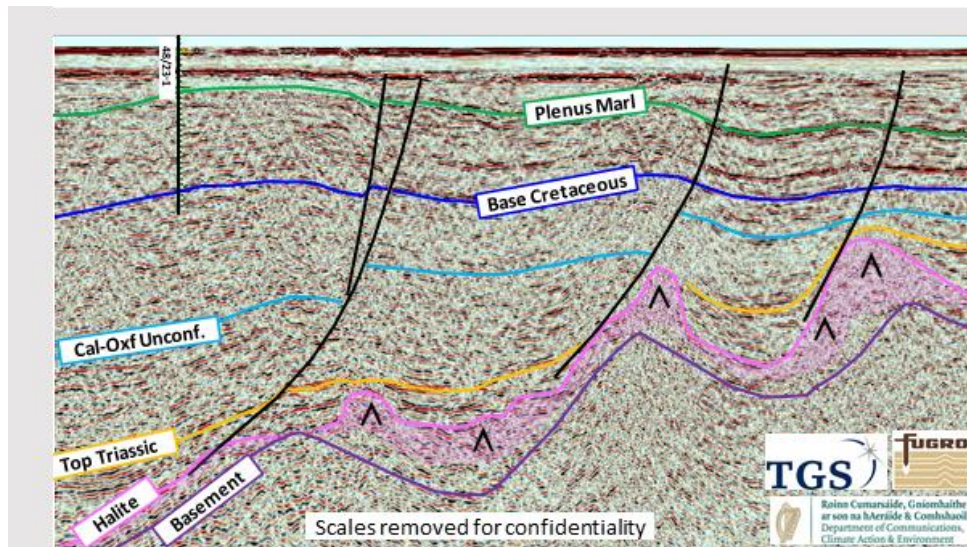


Figure 7-15. Seismic line SGC06-553689 zoomed to illustrate an area of halite movement (halokinesis). Overlying faults are seen to detach within the Triassic section.

7.1.3 Lower Jurassic

The transition from Triassic to Jurassic appears to be conformable with no evidence of an unconformity on the seismic or missing section within the wells. The Jurassic is the thickest succession in the NCSB with open marine conditions in the early Jurassic passing to shallow shelf, estuarine and non-marine deposits in the late Jurassic (Ewins & Shannon, 1995).

An unconformity is evident within the Jurassic section in the basin centre, on the left of seismic line SGC06-553689 and NCS81-59, with a subtle change in dip of seismic reflectors, Figure 7-2 & Figure 7-4, Location D. Evidence of an unconformity can also be seen on the Barryroe 3D data (Figure 7-13) and on vintage seismic data (Figure 7-16). Coward & Trudgill (1999) describe a hiatus of Middle to Upper Jurassic in age. The recent biostratigraphic and lithostratigraphic study of wells offshore Ireland defined the unconformity more precisely as Callovian-Oxfordian in age and confirmed its regional extent across the NCSB (Copestake et al., 2018). The unconformity event is often referred to as the Mid-Cimmerian tectonic event (Naylor & Shannon, 2011). It is particularly difficult to interpret this event in areas of poor data quality or where there is little change in dip and no well control, such as Figure 7-2 & Figure 7-4, Location E. In these areas the interpretation is extended at a middle Jurassic level, honouring its relative position elsewhere on the seismic data. This interpretation is justified based on the regional extent of the unconformity both within the NCSB and adjacent basins.

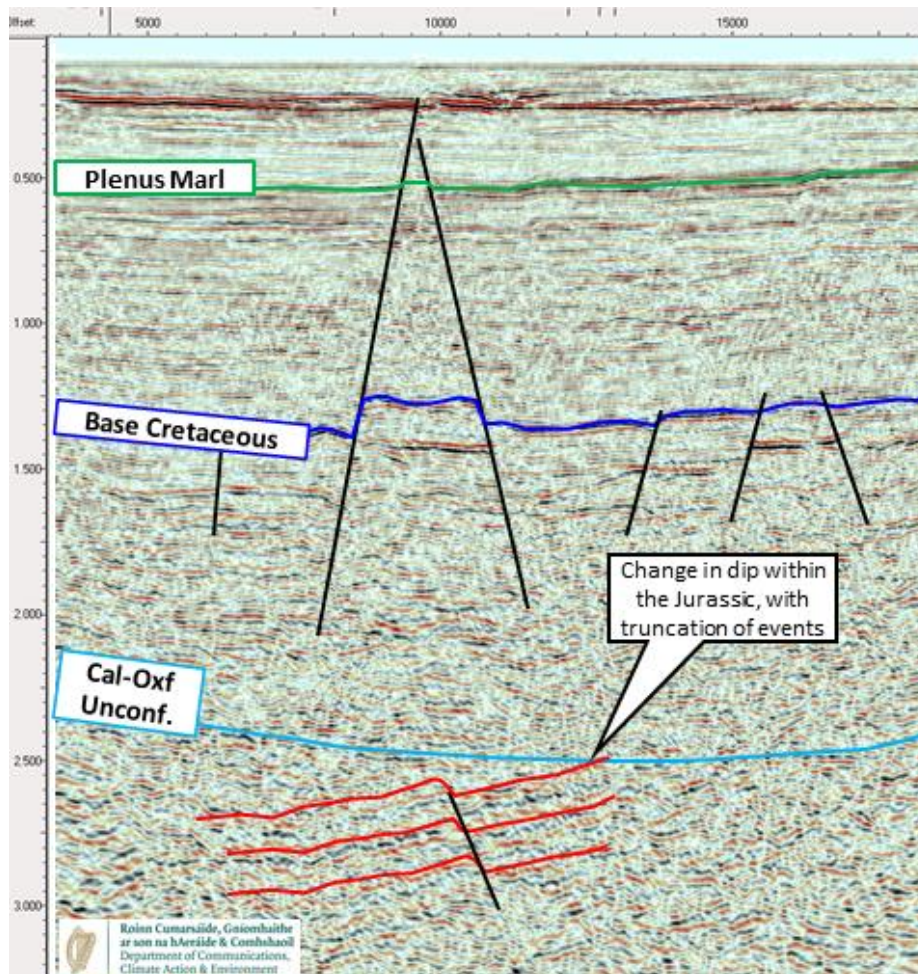


Figure 7-16. Seismic Line Mil90-16 illustrating evidence of Callovian-Oxfordian Unconformity in the basin centre on vintage seismic data.

A depth map of the Callovian-Oxfordian unconformity (top of the Lower Jurassic) is presented in Figure 7-17 & Appendix F.3. The present-day depth ranges from 4,700m (15,400ft) in the east between the Morrigan and Dagda Faults to 400m (1,300ft) on the basin margins to the north. There are local high areas of up to 2,800m (9,200ft) to the west against the Morrigan and Dagda Faults, the implications of these are discussed in Chapter 9.

The Lower Jurassic rifting appears to be accommodated by the Morrigan Fault in a half graben geometry, Figure 7-2 & Figure 7-4, Figure 7-18 & Appendix G.2. Due to later faulting complicating the seismic image it is difficult to be certain if the other southerly dipping faults (reactivated Variscan) were active at this time. The Morrigan Fault has accommodated up to 3,750m (12,300ft) of Lower Jurassic sediments as seen on the Lower Jurassic isopach map (Figure 7-18 & Appendix G.2) with two distinct areas of deposition to the west and east of the study area. The implications of these depocenters are discussed in Chapter 9.

Well 57/2-1 in the southwest of the study area drilled 1,500m (4,920ft) of Lower Jurassic shallow water marine limestones and shales, implying a significant section of Lower Jurassic remains undrilled. Caston (1995) suggests the shales of the Lower Jurassic to be the source of the 44° API oil tested at the Helvick Oil Field further east in the NCSB (Figure 1-1). The Lower Jurassic is also a possible source of the gas at the Kinsale Head Gas Field (Colley *et al.*, 1981).

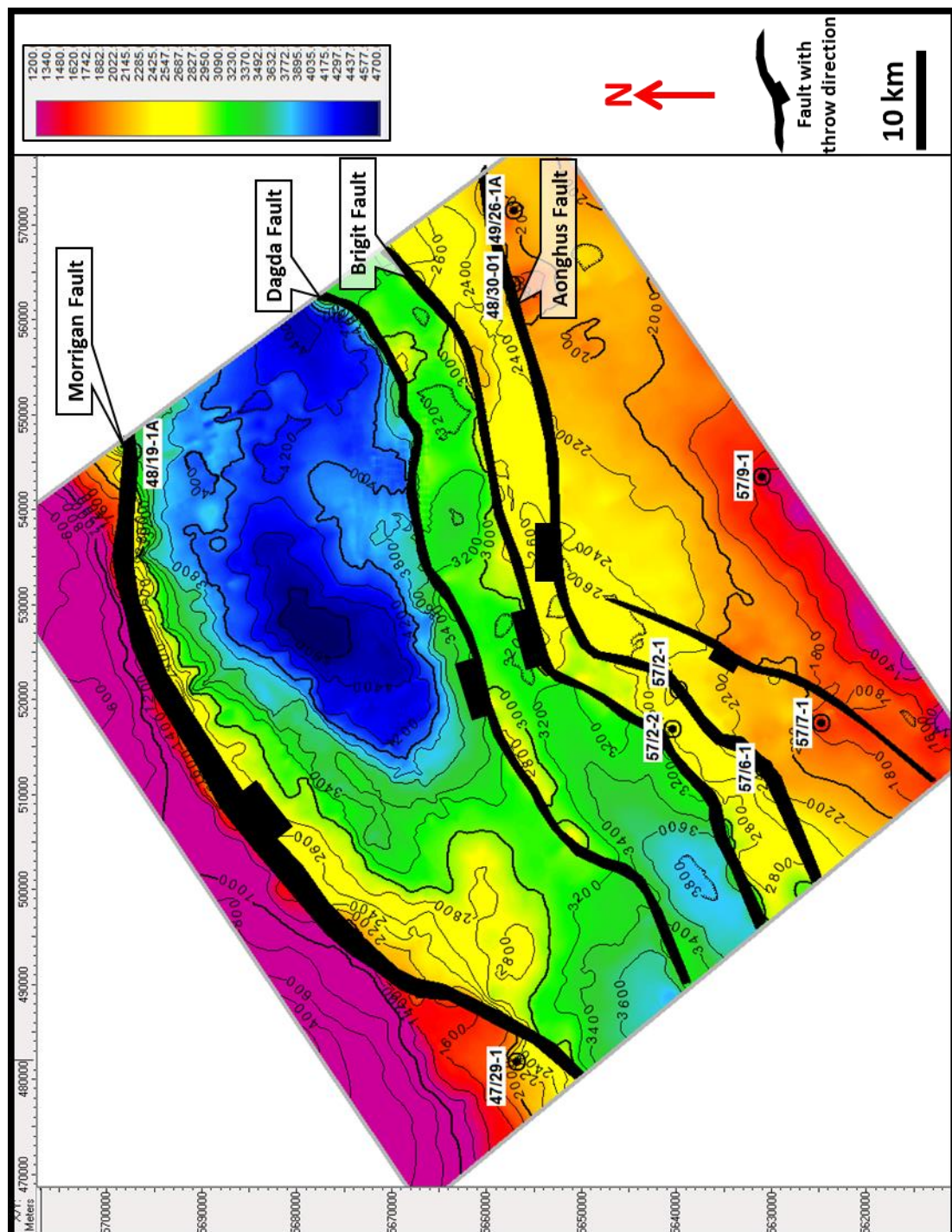


Figure 7-17. Depth map of Callovian-Oxfordian unconformity, interpreted within the study area, contour interval 200m (660ft), well control highlighted.

The deepest area of 4700m (15,400ft) is located to the NE between the Morrigan and Dagda faults. Local high areas of 2800m (9,200ft) exist to the west adjacent to the Morrigan and Dagda Faults.

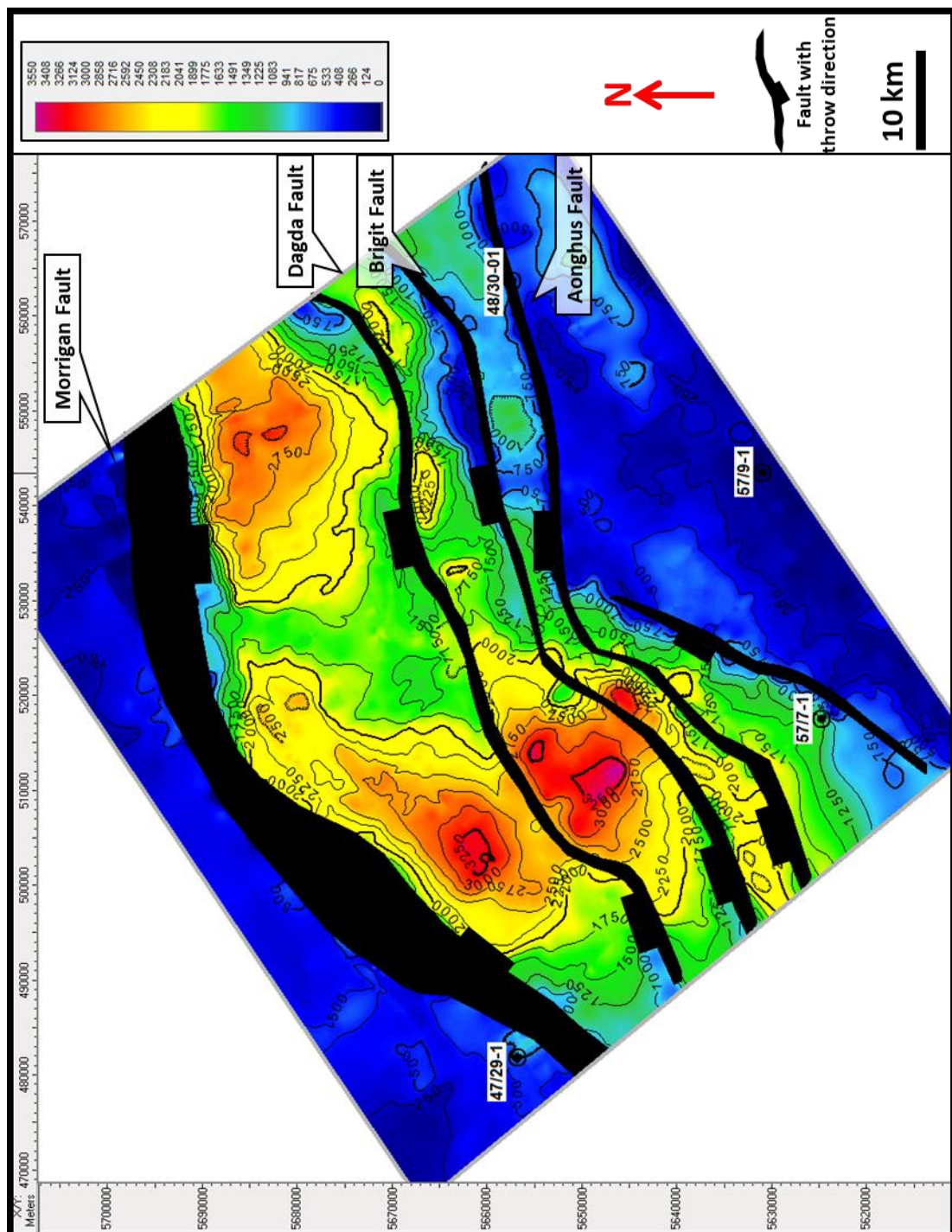


Figure 7-18. Isopach of the Lower Jurassic interpreted within the study area, contour interval 250m (820ft), well control highlighted. A western and Eastern isopach thick are readily identified. Note - faults are present day, any apparent thickness changes across northerly dipping faults may be an interpretation error on poor data.

7.1.4 Upper Jurassic

The Base Cretaceous (Intra Perch Fm) seismic marker is a regionally extensive event in the NCSB with good well control on the modern seismic lines presented in Figure 7-2 & Figure 7-4. The important wells for these lines are 48/23-1, 48/22-1a, 48/28-2 and 57/09-1. The Base Cretaceous seismic marker is the upper of two parallel reflectors within the basin centre, Figure 7-2 & Figure 7-4 Location F. These two parallel events coalesce as the sedimentary package thins towards the basin margins as shown in Figure 7-6 locations F & G. The event lies within the Purbeck Group with biostratigraphic data dominated by non-marine microfaunas and palynology which doesn't allow precise placement of a Base Cretaceous pick within the wells (Copestake et al., 2018). The Base Cretaceous seismic marker is thus correctly an Intra Perch Formation event of Berriasian age and is recognised by Copestake *et al.* (2018) as being unconformable to conformable across the NCSB. Given the strength of the seismic marker and the uncertainty in biostratigraphic picking within the wells it is reasonable to accept the Intra Perch Formation as the Base Cretaceous for the purposes of regional analysis.

A depth map for the Base Cretaceous event is presented in Figure 7-19. There is reduced throw evident on the Morrigan Fault than that observed for the older stratigraphy. Offset across the Dagda, Brigit and Aonghus Faults is barely discernible on the maps and is in the order of 0-100m (0-330ft). These northerly dipping faults are antithetic to the Morrigan Fault, the low throw values at the Base Cretaceous seismic event are due to reduced fault activity in the overlying Cretaceous and also Cenozoic compressional reactivation of these faults. The older

southerly dipping faults active in the Triassic terminate within the Lower Jurassic package and do not reach the Base Cretaceous seismic marker.

Figure 7-19 & Appendix F.4 illustrates two mid-basinal lows of up to 2600m (8500ft) depth separated by a local high in the region of the 47/30-1 and 48/26-1 wells. A subtle mid-basinal high is also evident following the 2200m (7200ft) contour against the Dagda fault, in the region of the 48/23-1, 48/24-1 and 48/24-3 wells; this is the Barryroe Oil Field.

The Upper Jurassic isopach is presented in Figure 7-20 & Appendix G.3 where a single dominant, and largely symmetrical, depocenter is evident to the northeast between the Morrigan and Dagda Faults of up to 2,200m (7,200ft). Syn-sedimentary growth is also evident across the Brigit and Aonghus Faults of 500m (1,650ft) and 300m (1,00ft) respectively. This suggests rifting in the Upper Jurassic was no longer accommodated primarily on the Morrigan Fault. Extension was now also accommodated by the southerly dipping Morrigan Fault and the antithetic northerly dipping Dagda, Brigit and Aonghus Faults; thus the Upper Jurassic extension is best described as having a conventional graben geometry. It is also noted that the antithetic Dagda, Brigit and Aonghus Faults which were active faults in the Upper Jurassic are detaching within the Triassic, as discussed in Chapter 7.2. Figure 7-21 illustrates both the syn-sedimentary growth across the Aonghus Fault and the detachment of the fault within the Triassic.

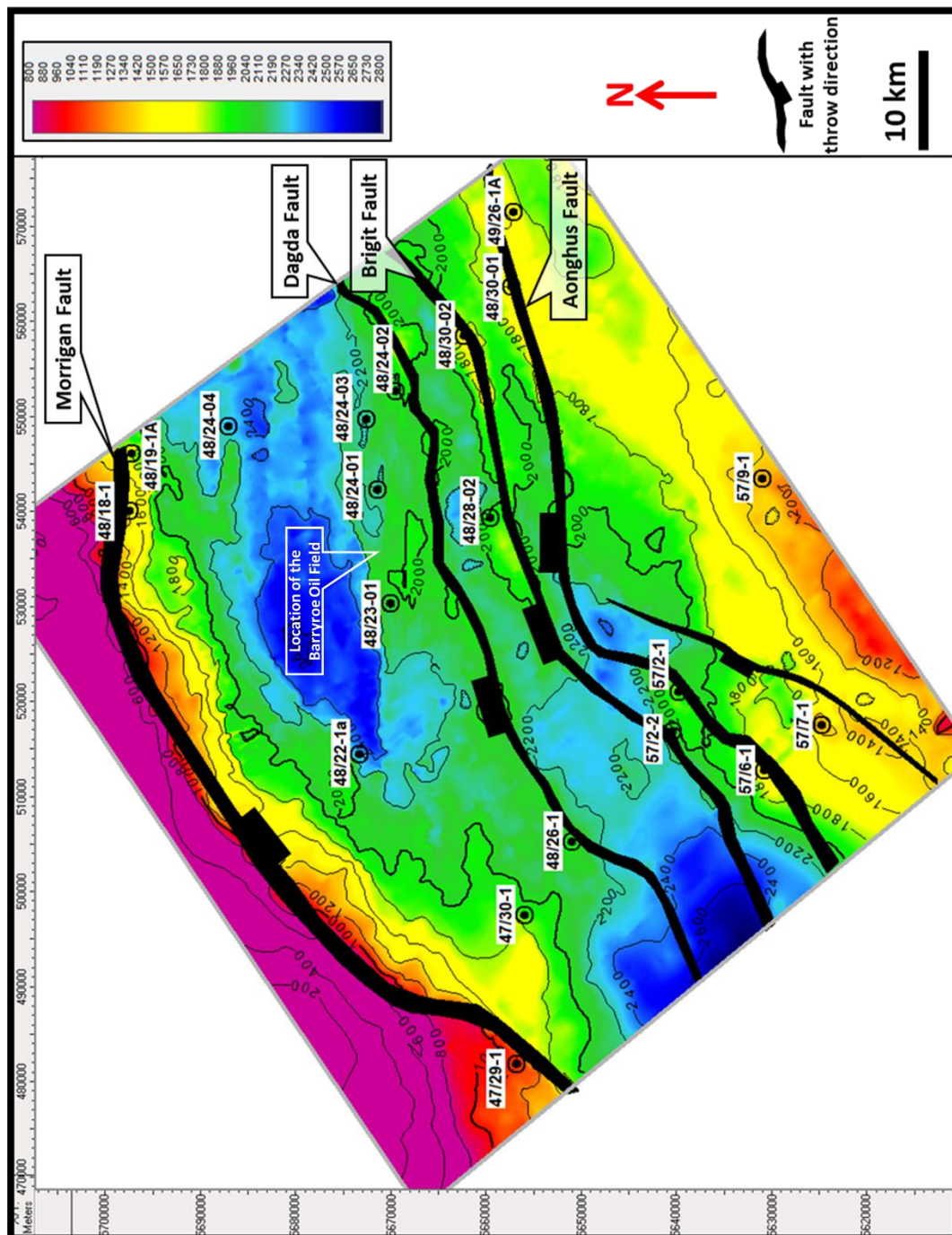


Figure 7-19. Depth map of Base Cretaceous interpreted within the study area, contour interval 200m (660ft), well control highlighted. There are two mid-basinal lows of up to 2600m (8500ft). A subtle mid-basinal high is also evident following the 2200m (7200ft) contour against the Dagda fault, in the region of the 48/23-1, 48/24-1 and 48/24-3 wells; this is the Barryroe Oil Field.

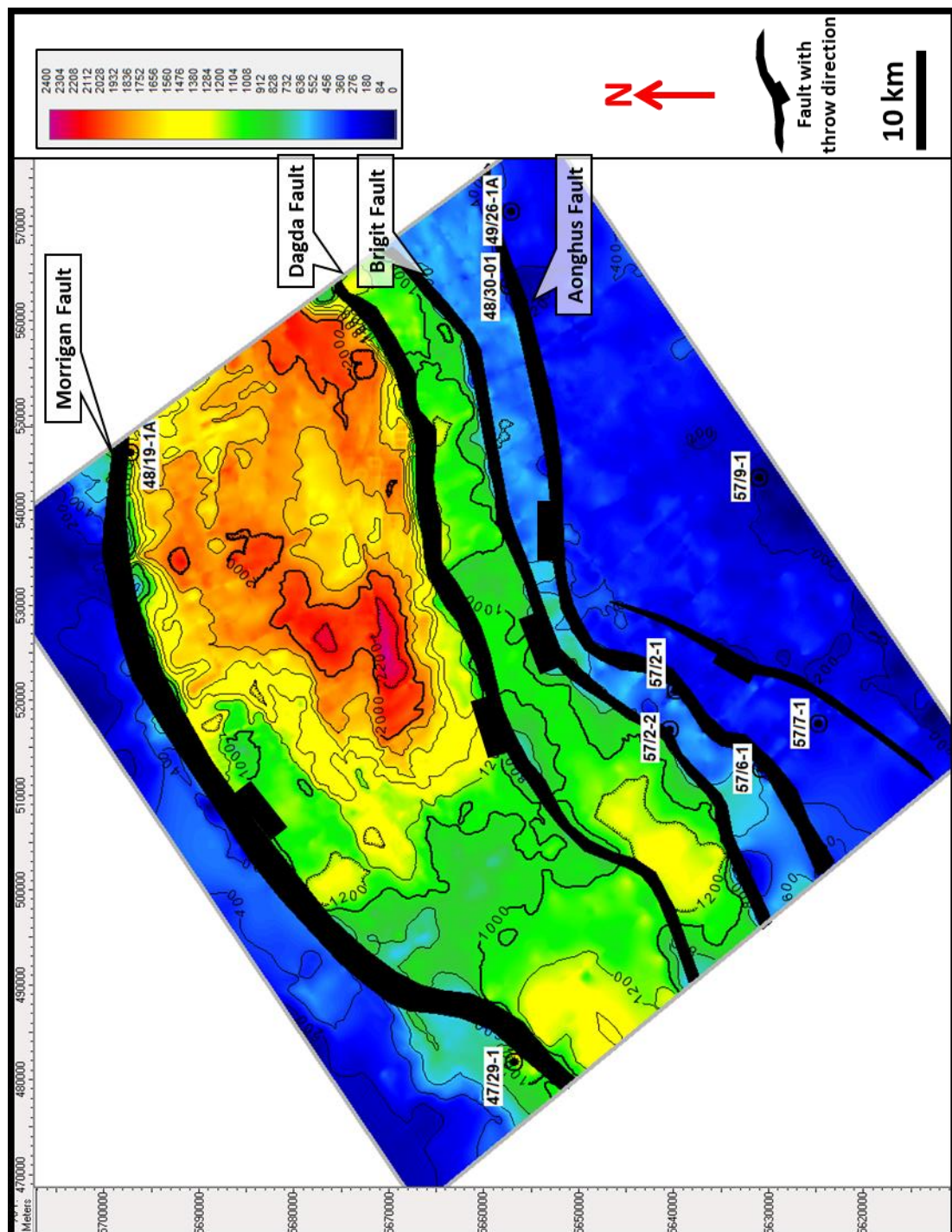


Figure 7-20. Isopach of the Upper Jurassic interpreted within the study area, contour interval 20m (660ft), well control highlighted. A primary depocenter is evident to the northeast between the Morrigan and Dagda Faults of up to 2,200m (7,200ft) thick. Syn-sedimentary growth is also evident across the Brigit and Aonghus Faults of 500m (1,650ft) and 300m (1,00ft) respectively.

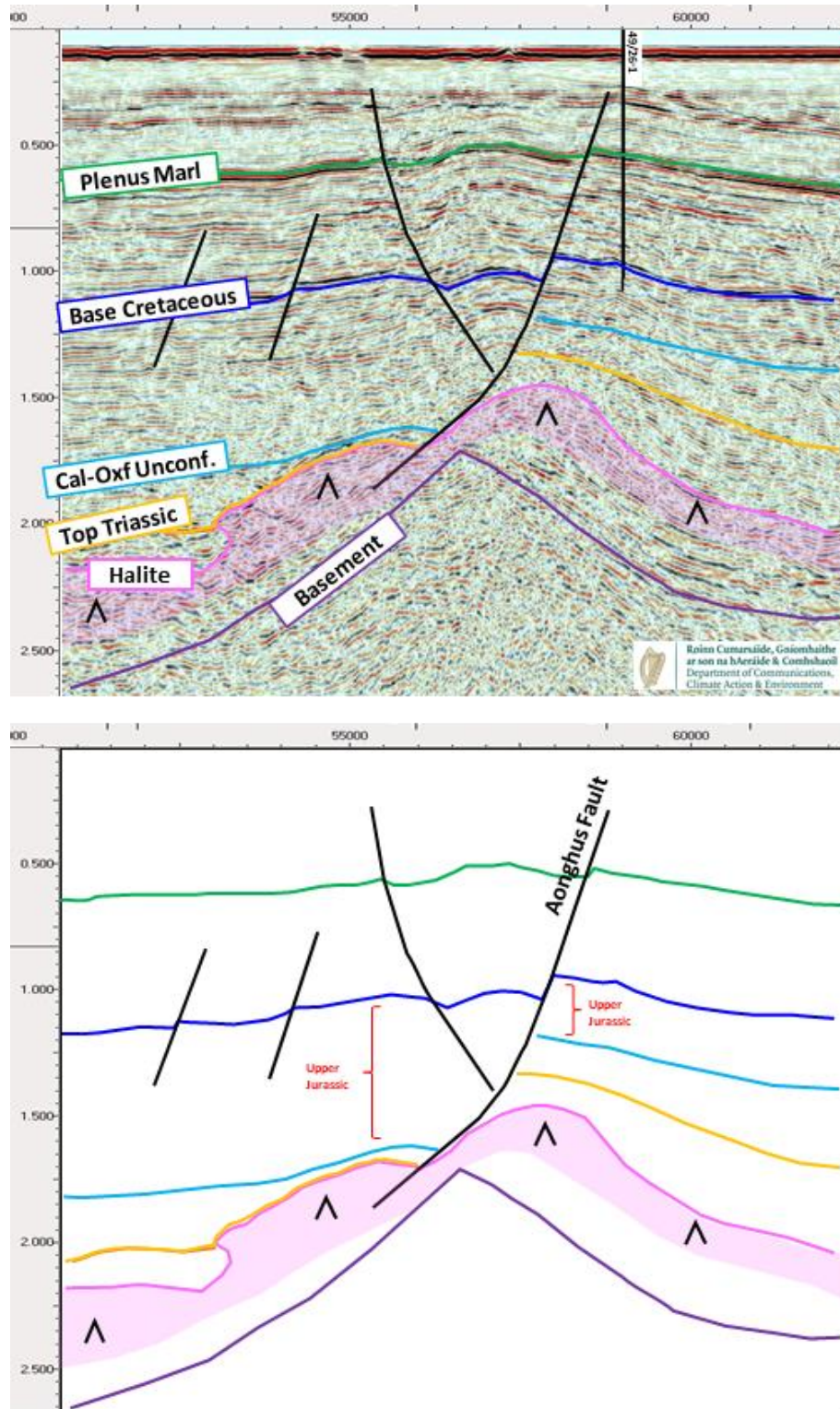


Figure 7-21. Seismic Line SGC06-556892 zoomed to illustrate growth of the Upper Jurassic section across the Aonghus Fault and the detachment within the Triassic section.

The adjacent Fastnet and South Celtic Sea Basins have limited Upper Jurassic sections due to either lack of deposition or later erosion (Naylor & Shannon, 2011). Shannon (1995) suggest this is due to Upper Jurassic hot spot related thermal doming, seen across much of northwest Europe (Underhill & Partington; 1993). An angular unconformity at the top of the Jurassic is not recognised on seismic data within the basin centre of the NCSB. This suggests a regional uplift event did not lead to sub-aerial exposure in the central NCSB. Some fault blocks against the basin margin, north and south, do show some evidence of the Late Jurassic or Early Cretaceous erosional event. The Helvick field 70 kilometres (43 miles) outside the study area to the northeast (Figure 1-1) is an example of this localised erosion at the basin margin (Caston, 1995). Erosion in this area is believed to be related to localised compression and block rotation at the basin flanks. It is possible that a regional uplift event, seen in adjacent basins, removed the access to the open marine environment during the latest Jurassic to earliest Cretaceous, creating a lacustrine environment (Purbeck Group) in the NCSB with continued sedimentation.

The thick lacustrine shales of the Purbeck Group deposited during this period are an important source rock for hydrocarbon generation. Composite logs show over 1,000m (3300ft) of Valanginian to Berriasian aged Purbeck Formation is encountered in the 48/19-1 and 48/25-1 wells to the east of the study area (Figure 6-15). This interval is the source rock for the Barryroe Oil Discovery (Howell & Griffiths, 1995).

Well 48/19-1 in the northeast of the study area drilled over 1,500m (4,920ft) of Upper Jurassic section containing lacustrine shales, restricted marine sandstones, limestones and silts.

7.1.5 Lower Cretaceous

The Plenus Marl (Top Cenomanian) is one of the strongest regional markers in the NCSB. It represents a significant decrease in acoustic impedance and is clearly identifiable on both modern and vintage seismic data. The underlying Selborne Group contains the Agone Sandstone Member (described as Greensand by previous authors), an Albian marine incursion depositing localised shallow marine glauconitic sand (Figure 3-3). The Agone Sandstone Member is the primary reservoir at the Kinsale Head Gas Field which has been producing dry gas since 1978. It was the target of several exploration wells with net sandstone thickness of up to 45m (140ft) and up to 40% porosity within the NCSB (Naylor & Shannon, 2011). Below the Selbourne Group the lower and middle Cretaceous is predominantly comprised of terrestrial fluvial lithologies termed the Wealden Group (Figure 3-3).

The Plenus Marl depth map (Figure 7-22 & Appendix F.5) shows some mid-basinal highs adjacent to the Dagda and Brigit Faults in the northeast of the study area. The larger of these against the Dagda Fault is the Seven Heads Gas Field and is the result of Cenozoic compressional reactivation.

The Lower Cretaceous isopach map shows clear evidence of thickening across the Morrigan, Dagda, Brigit and Aonghus Faults (Figure 7-23 & Appendix G.4) and up to 1800m (5900ft) of Lower Cretaceous was deposited within the study area. In the northeast of the study area the Morrigan, Dagda and Brigit Faults appear to accommodate most of the extension with on average 200m (660ft) syn-depositional growth each. In the southwest of the study area the Morrigan, Brigit and Aonghus Faults appear to accommodate most of the extension with on average 200m (660ft) syn-depositional growth each. The Dagda Fault therefore appears to be tipping out to the southwest with extension being accommodated on the other faults.

The isopach demonstrates syn-depositional growth across the Morrigan, Dagda, Brigit and Aonghus Faults demonstrating they were still active during Lower Cretaceous rifting following a conventional graben geometry. This thickening across the faults contradicts Naylor & Shannon (2011) who indicate there was little syn-rift faulting in the Cretaceous.

Figure 7-24 illustrates the thickening of the Lower Cretaceous section across the Dagda and Brigit Faults as well as reverse displacement of the Plenus Marl on the faults caused by later Cenozoic compression and uplift.

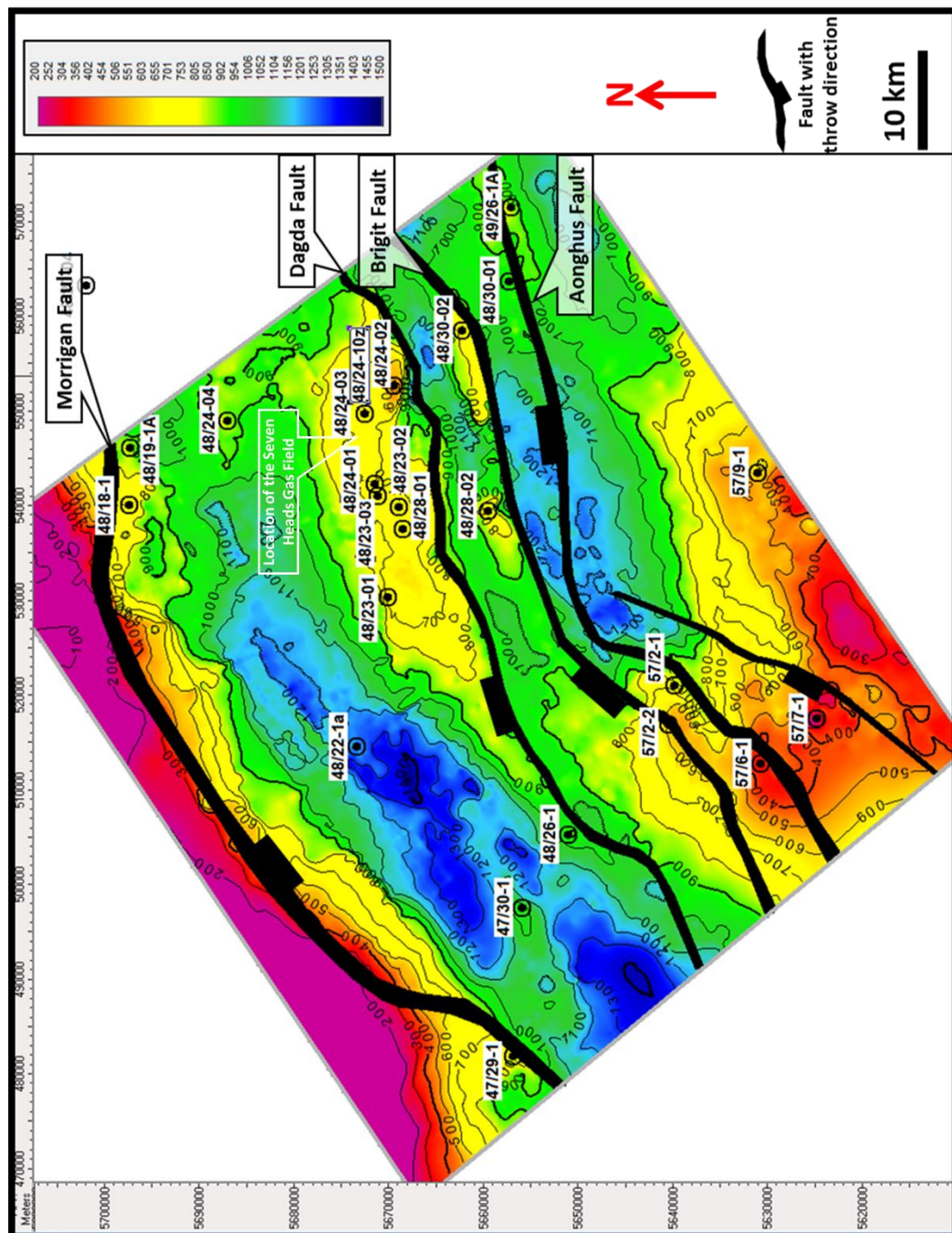


Figure 7-22. Depth map of Plenius Marl interpreted within the study area, contour interval 100 metres, well control highlighted. Note the mid-basinal highs adjacent to the Dagda and Brigit Faults in the northeast of the study area caused by Cenozoic compressional reactivation.

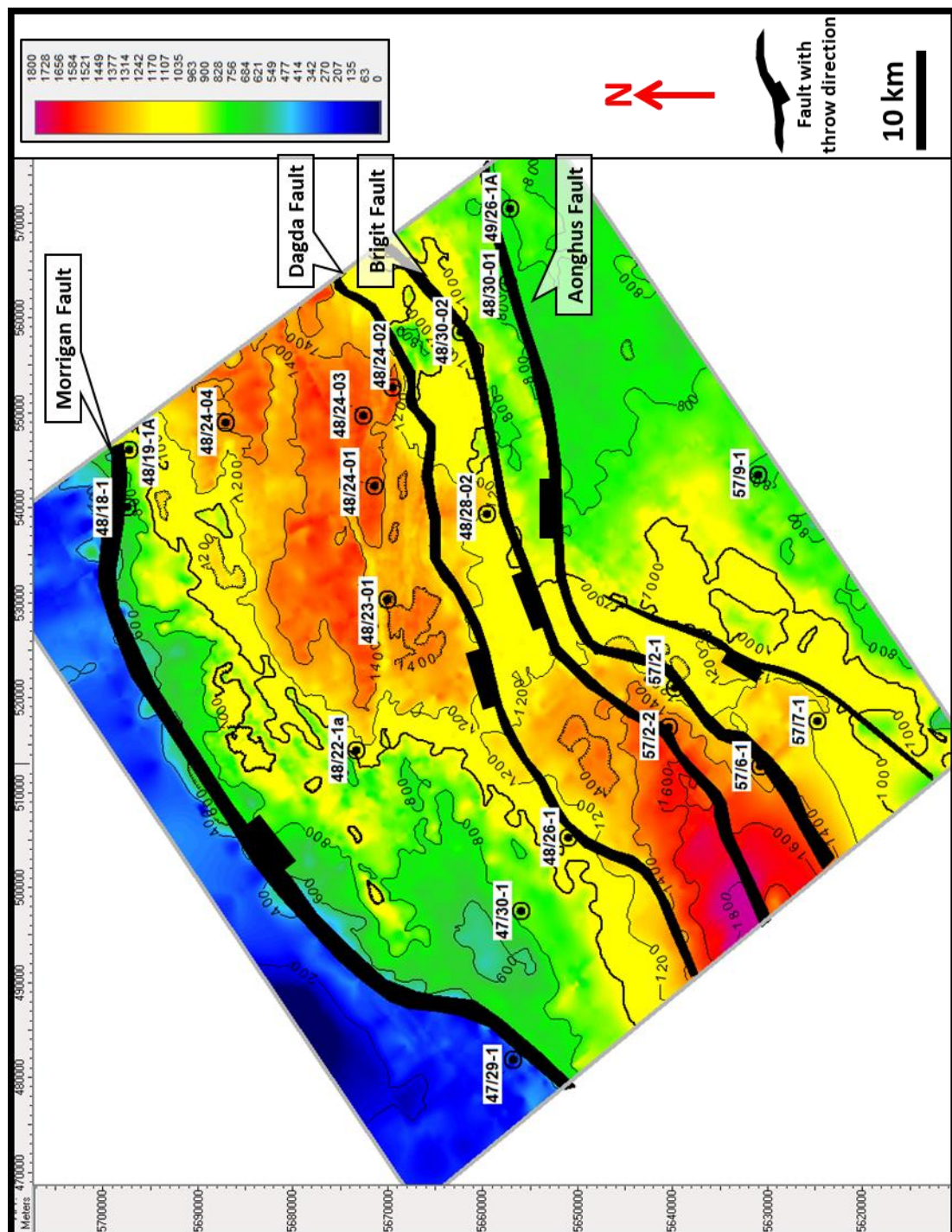


Figure 7-23. Isopach of the Lower Cretaceous interpreted within the study area, contour interval 200 metres, well control highlighted. Extension is accommodated primarily on the Morrigan, Dagda and Brigit Faults to the northeast and the Morrigan, Brigit and Aonghus Faults to the southwest.

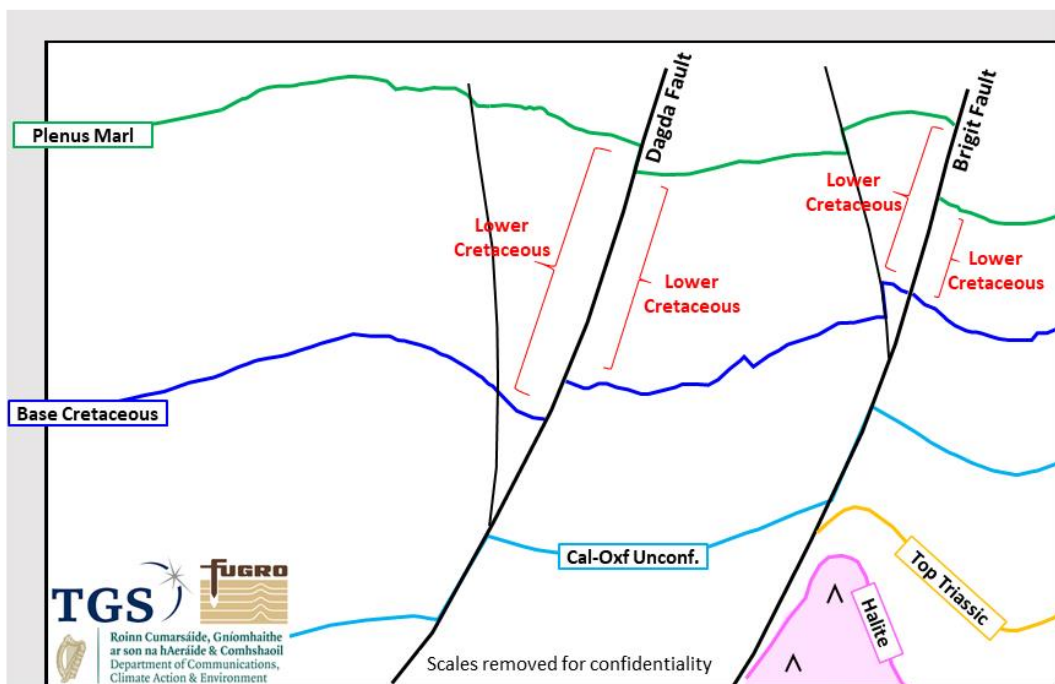
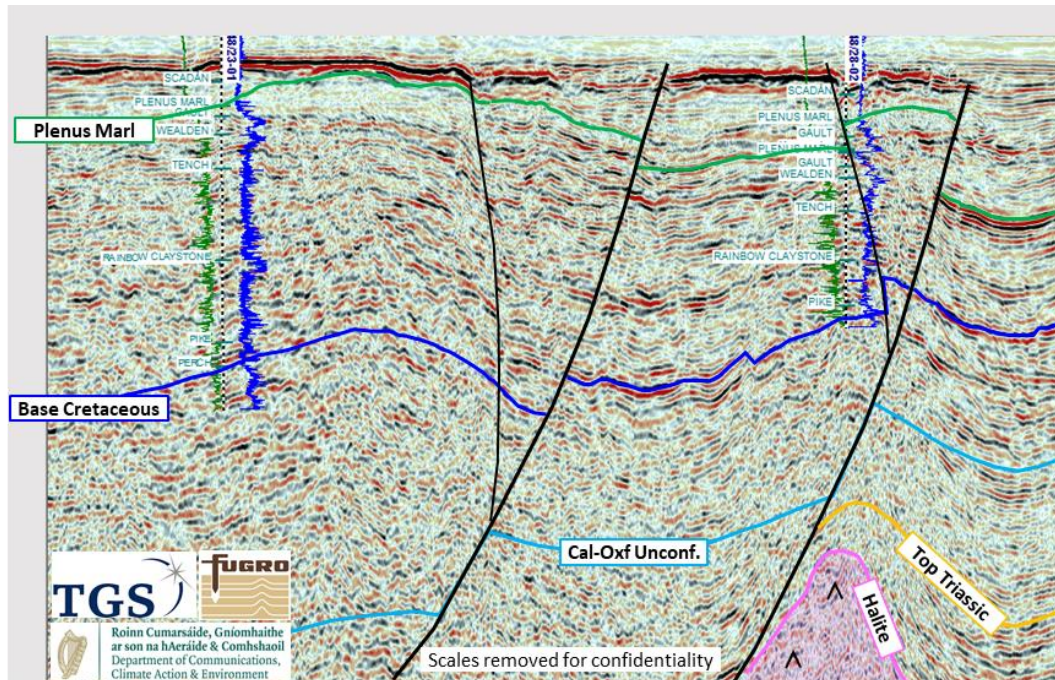


Figure 7-24. Seismic Line SGC06-553689 zoomed to illustrate reverse displacement at the Plenus Marl and growth of the Lower Cretaceous section across the Dagda and Brigit Faults.

7.1.6 Upper Cretaceous - Cenozoic

Over most of the NCSB, Cenozoic uplift has caused erosion of the Cenozoic strata and some of the Chalk. The Chalk therefore outcrops on the seabed extensively, with the exception of thin outliers of Cenozoic strata preserved in the southwest of the study area. A depth map for the top of the Upper Cretaceous is illustrated in Figure 7-25 & Appendix F.6 and shows where the Chalk outcrops on the seabed over most of the study area (100-130m / 330-430ft water depth) and the outliers of Cenozoic to the southwest of the study area. A complete section of Upper Cretaceous Chalk is thus only found in the southwest of the study area where it is up to 1,200m thick (3,950 feet) as shown in the Upper Cretaceous isopach map (Figure 7-26 & Appendix G.5).

The isopach of the Cenozoic and water column is illustrated in Figure 7-27 & Appendix G.6 where the Cenozoic is seen to be up to 200m thick (660 feet).

The Cenozoic uplift is dated by Murdoch *et al.* (1995) using apatite fission track analysis and vitrinite reflectance as a Paleocene regional uplift and an Oligo-Miocene compressive inversion. Murdock *et al.* (1995) also used seismic velocity analysis and vitrinite analysis to determine the extent of the inversion and describe a maximum uplift of 900m (2950ft) in the basin centre. Examination of the modern seismic shows uplift was concentrated along the Dagda, Brigit and Aonghus Faults, which are within the basin centre (Appendix E.1 to Appendix E.6) and thus is consistent with the results of Murdoch *et al.* (1995).

As discussed in Chapter 7.1.5 and Chapter 7.2, the Dagda, Brigit and Aonghus Faults were reactivated during Cenozoic compression. The associated uplift produced structural highs within the Lower Cretaceous stratigraphy (Appendix F.5) and also uplifted the overlying Upper Cretaceous and Cenozoic which was subsequently partially eroded. The Upper Cretaceous was deposited during a basin sag phase with extensive chalk facies across the entire NCSB and thus local variations in thickness would not be expected. The areas of thin Upper Cretaceous (<700m / 2300ft) adjacent to the Dagda and Brigit faults (Appendix G.5) are thus areas where Upper Cretaceous and Cenozoic section were eroded. The thinnest Upper Cretaceous section is 500m (1,650ft) thick adjacent to the 48/24-2 well and as mentioned above, the areas of complete Upper Cretaceous are up to 1,200m thick (3,950 feet). This suggests an eroded Upper Cretaceous section of approximately 700m (2,300ft). The Cenozoic outlier in the southwest of the study area is up to 200m thick (660 feet) and assuming a similar thickness existed over the entire NCSB prior to the uplift, the combined eroded section is estimated as up to 900m (2950ft). This is in agreement with the maximum uplift of 900m (2950ft) quoted by Murdock *et al.* (1995).

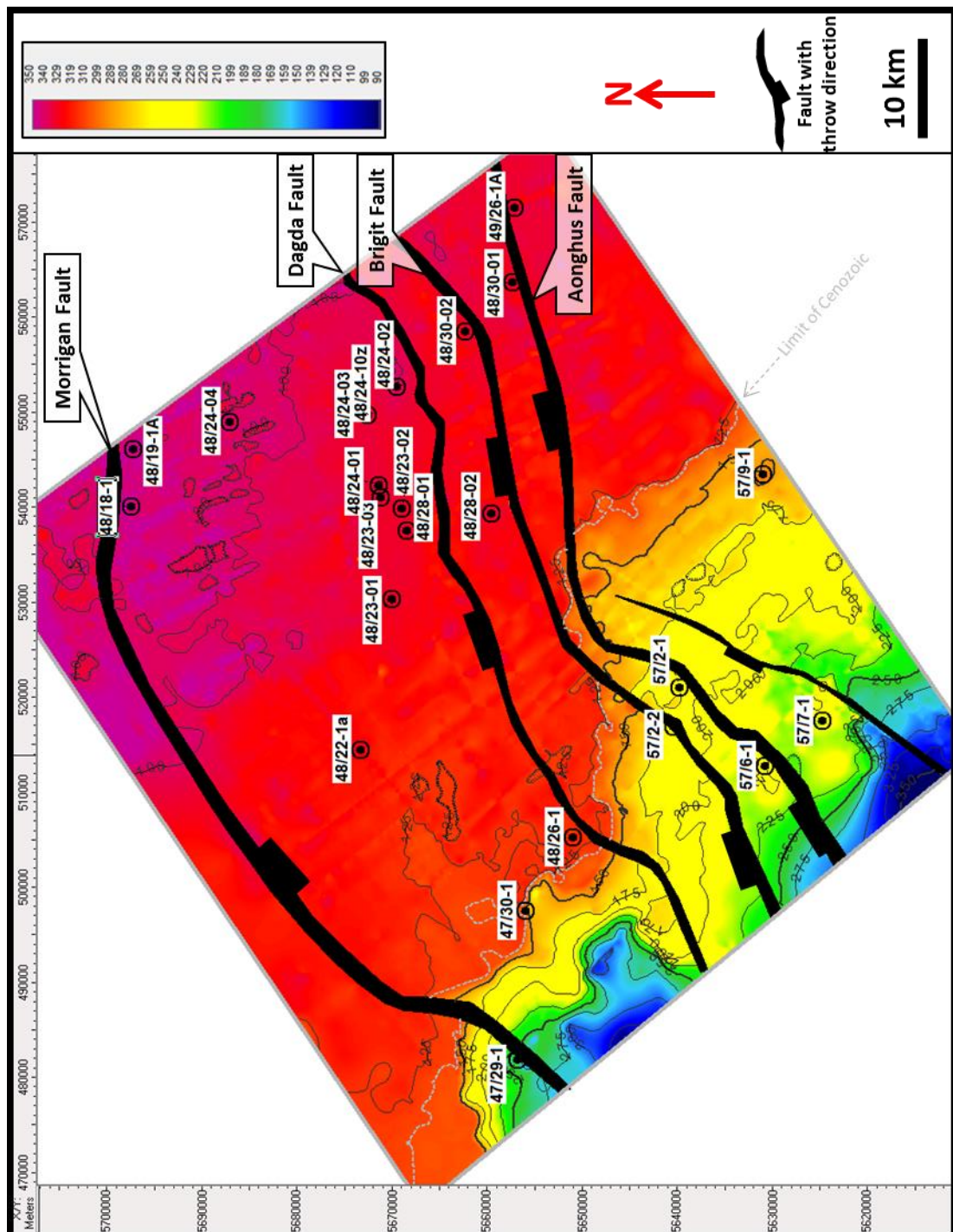


Figure 7-25. Depth map of Top Chalk (Seabed/ Base Cenozoic), interpreted within the study area, contour interval 25 metres, well control highlighted. A Cenozoic outlier is present to the southwest of the study area, to the northeast of this the Top Chalk outcrops at the seabed.

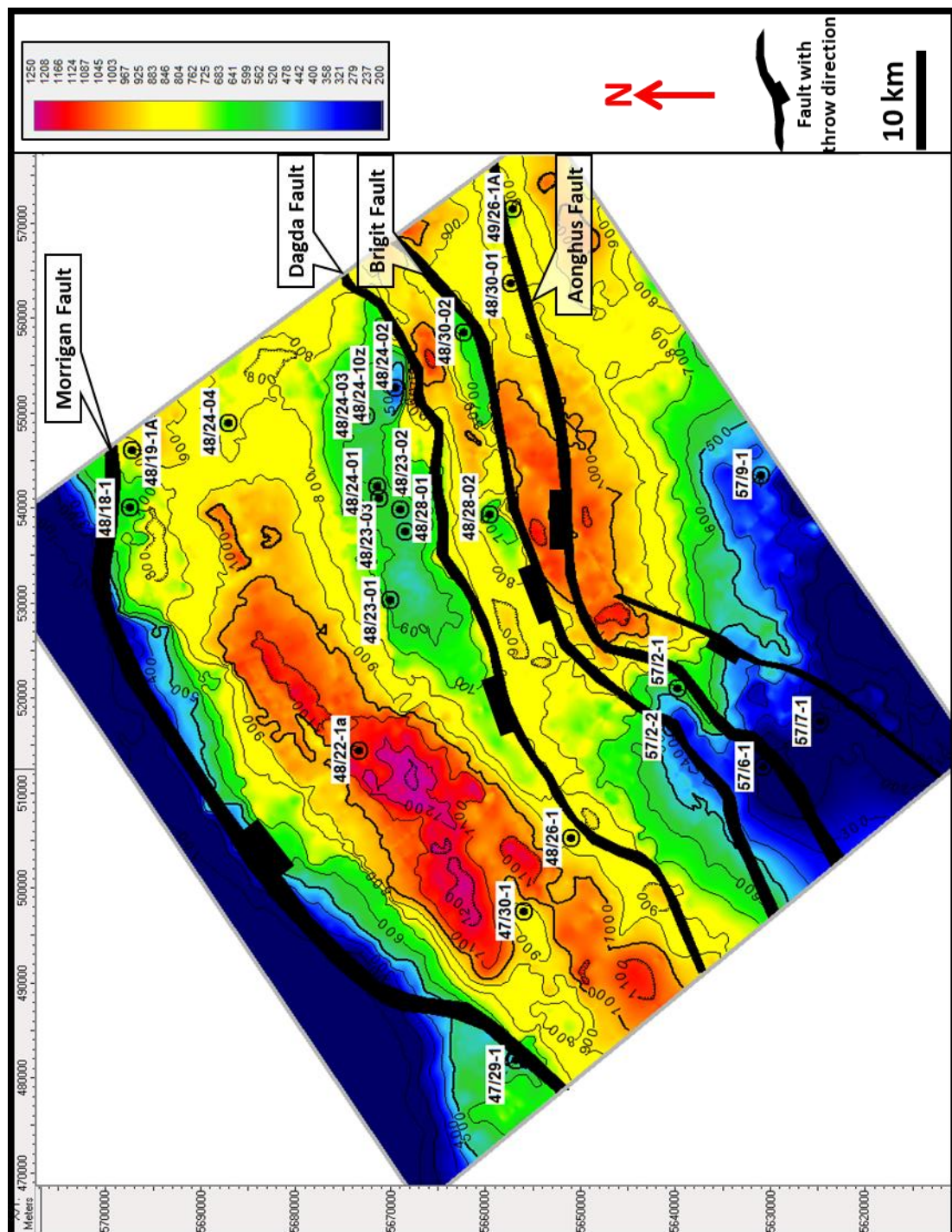


Figure 7-26. Isopach of the Upper Cretaceous (Chalk) interpreted within the study area, contour interval 100 metres, well control highlighted. Note isopach thins to the northeast against the Dagda and Brigit faults where Upper Cretaceous was eroded.

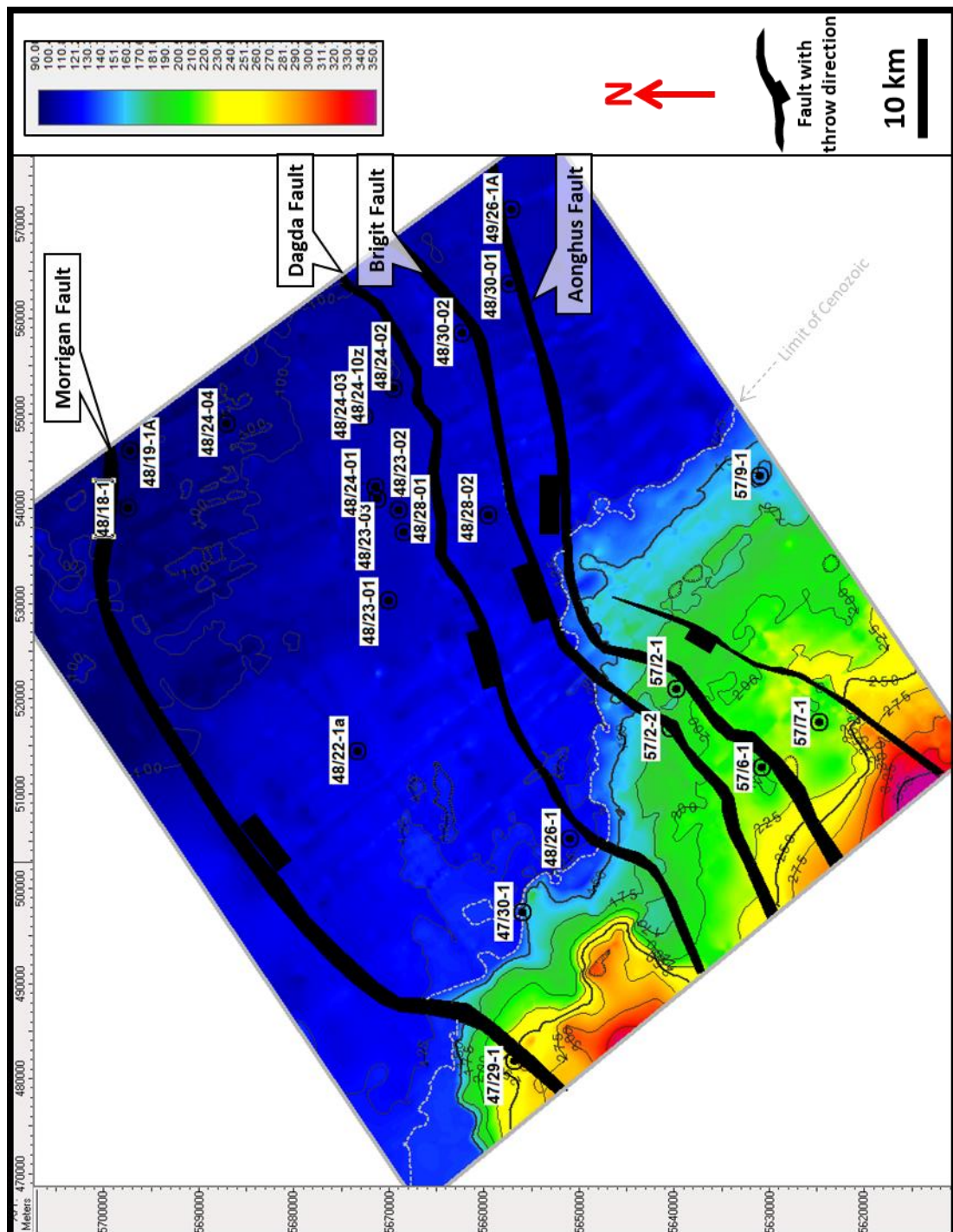


Figure 7-27. Isopach of Water Column and Cenozoic interpreted within the study area, contour interval 25 metres, well control highlighted. The water column is broadly consistent across the area at approximately 100-130m (330-430ft). The Cenozoic section is up to 200m (660ft) thick in the south west of the study area and absent to the north east.

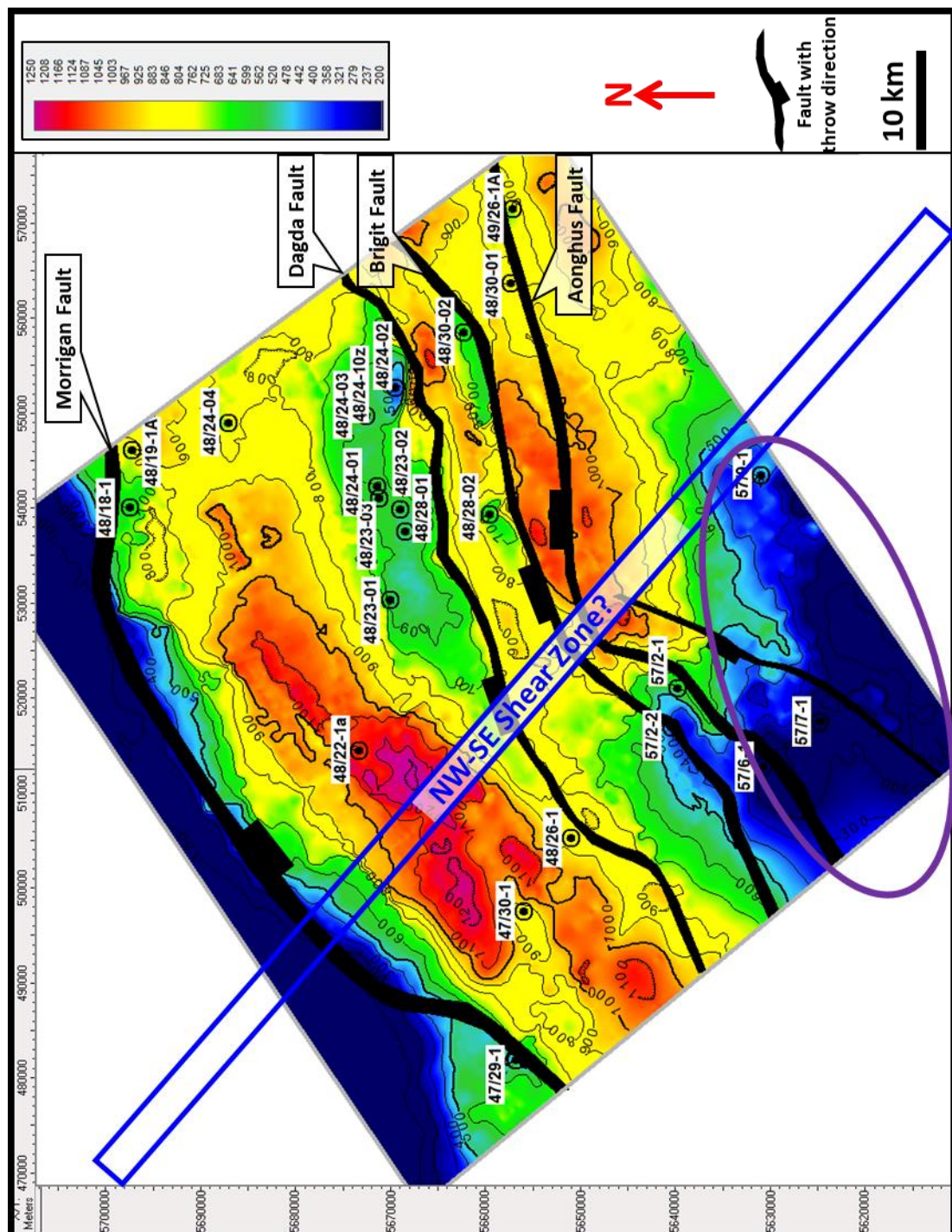


Figure 7-28. Isopach map of the Upper Cretaceous section, illustrating area of reduced thickness(circled in purple) which appears to be regional in nature and not reduced by later uplift and erosion. A NW-SE shear zone is postulated which would help explain regional variations in thickness during a basin sag phase..

7.2 Faults

Four primary faults were mapped within the study area and named after gods and goddesses from Celtic mythology. They represent significant structural elements within the NCSB and generally exhibit significant throw. At a regional level on 2D seismic data the faults appear to be extensive and slightly arcuate in nature. In reality, it is likely that each fault is made up of several smaller segments joined by breached ramp relay zones (Walsh et al., 2002).

The fault interpretation is supported by comparison with the freeair gravity data. Clear trends are evident within the gravity data in the NCSB basin which are highlighted in Figure 7-29 & Figure 7-30. These trends represent significant changes in the local freeair gravity caused by density variations within the subsurface. The strike of interpreted regional faults at the Triassic and Cretaceous follow the gravity trends and thus supports their interpretation as significant structural elements.

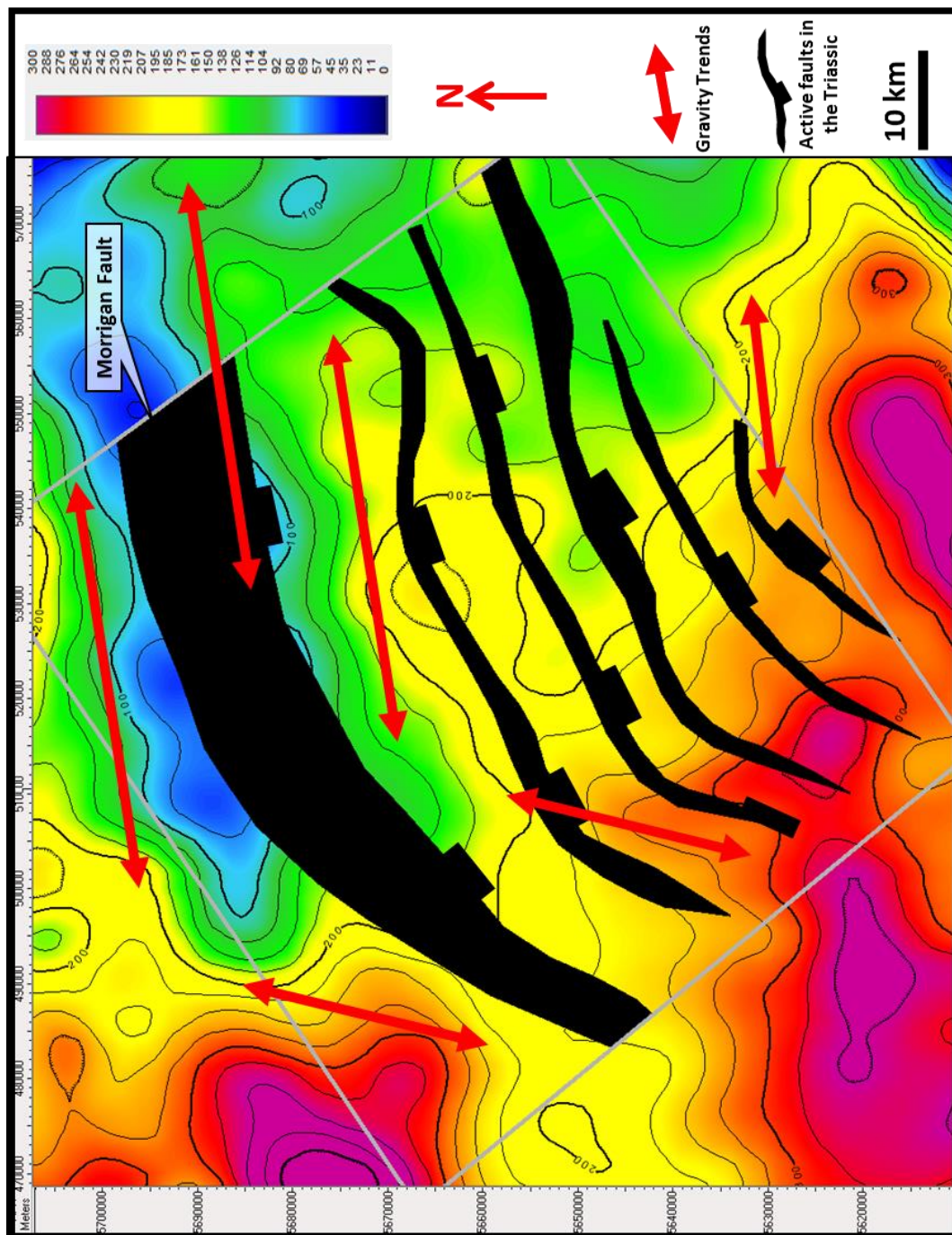


Figure 7-29. Map of the freeair gravity data in the study area. Gravity trends are indicated by red arrows and faults active within the Triassic are shown as black fault polygons. The strike of the faults appears to align with the gravity trends.

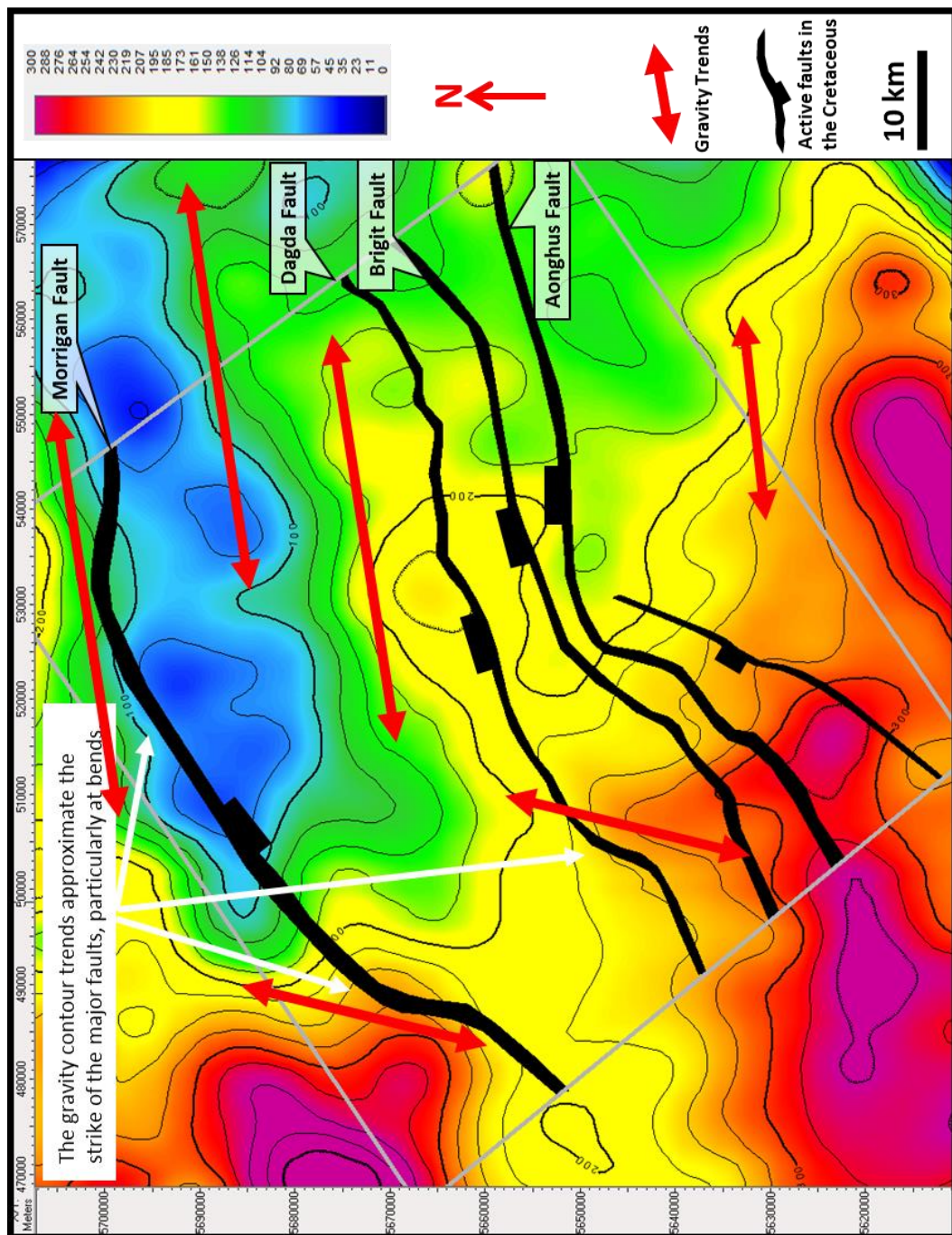


Figure 7-30. Map of the freeair gravity data in the study area. Gravity trends are indicated by red arrows and faults active within the Cretaceous are shown as black fault polygons. The strike of the faults appears to align with the gravity trends.

7.2.1 Morrigan Fault

The primary and longest living fault in the NCSB is a large fault which controls the northern extent of the NCSB Basin, named here as the Morrigan Fault (Figure 7-31). It appears to have initiated as an extensional fault in the Triassic, with significant offset and associated sediment deposition (Figure 7-31 & Figure 7-32). Throughout the Mesozoic it has acted primarily as a normal fault however localised minor Cenozoic inversion was observed outside the study area. The present-day maximum offset is in excess of 5,000m (15,000 ft) (Appendix F.1), with syn-depositional growth of 1,600m (5,250ft) in the Upper Jurassic (Appendix G.3). It strikes southwest-northeast and dips to the southeast, steeply in the shallowest section but becomes low angle quickly with depth (Figure 7-31). Structurally, a low angle extensional fault would generally be expected to have been originally a compressional feature. Looking at the regional context and the strike of the fault it is consistent with the Variscan trend, and indeed the earlier Caledonian trend (Robinson *et al.*, 1981; BIRPS & ECORS, 1986; McGeary *et al.*, 1987; Day *et al.*, 1989; Ruffell & Coward, 1992; McCann, 1996). A deep extension of the Morrigan Fault has also been mapped (Figure 5-4) by previous authors on deep refraction seismic data as a south-easterly dipping low angle detachment feature at 12-14 kilometres (7.5-8.5 miles) depth (BIRPS & ECORS, 1986; McGeary *et al.*, 1987; Petrie *et al.* (1989); O'Reilly *et al.*, 1991; Masson *et al.*, 1998) which is consistent with the significant extension it accommodates. It is thus interpreted that the Morrigan Fault is a reactivated Variscan thrust, there is no evidence to the contrary, and this is in agreement with previous authors.

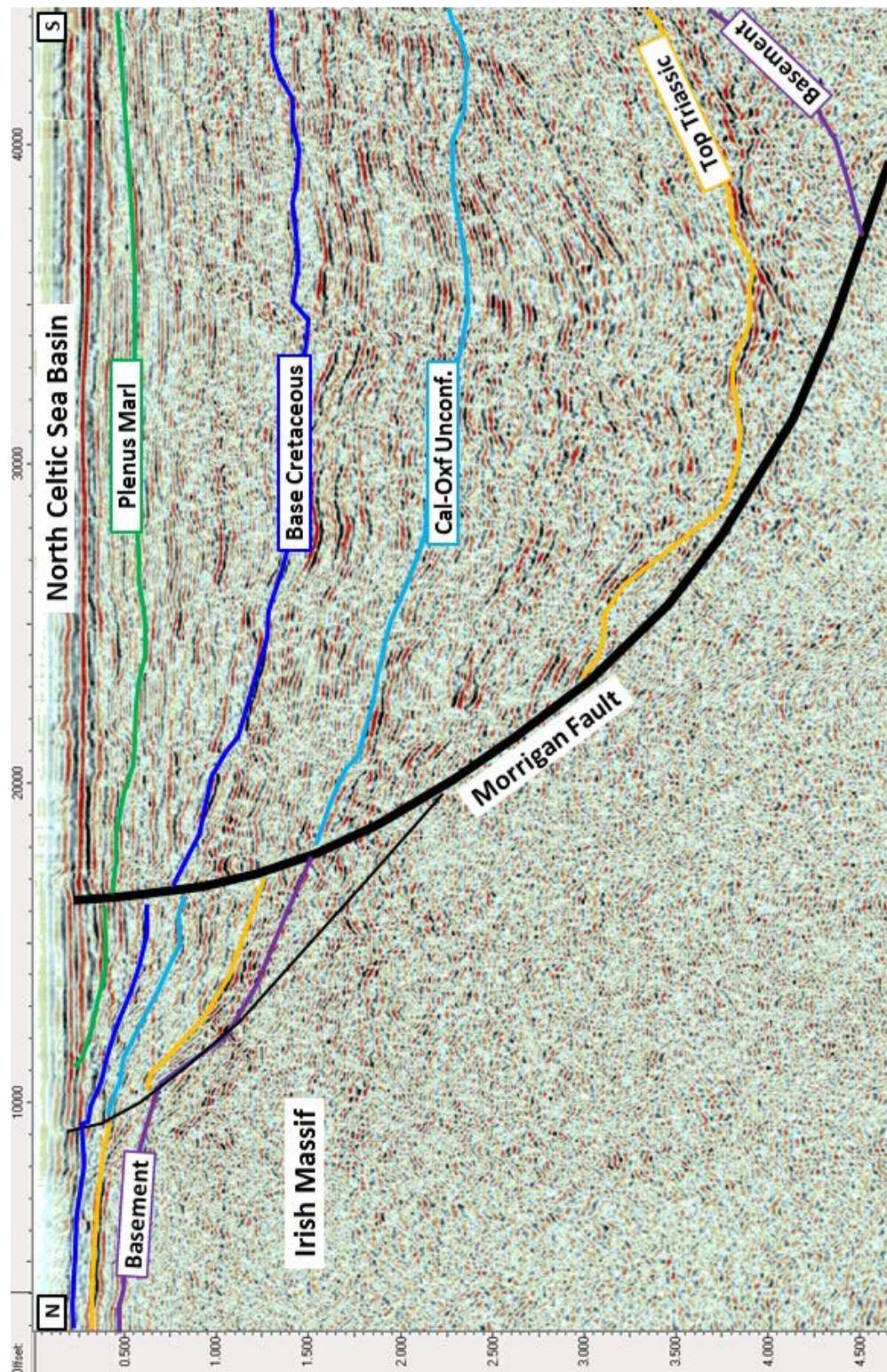


Figure 7-31. Seismic Line SWAT 5 with interpretation of the stratigraphy and the basin bounding Morrigan Fault. The fault becomes low angle with depth and exhibits significant offset and associated sediment deposition.

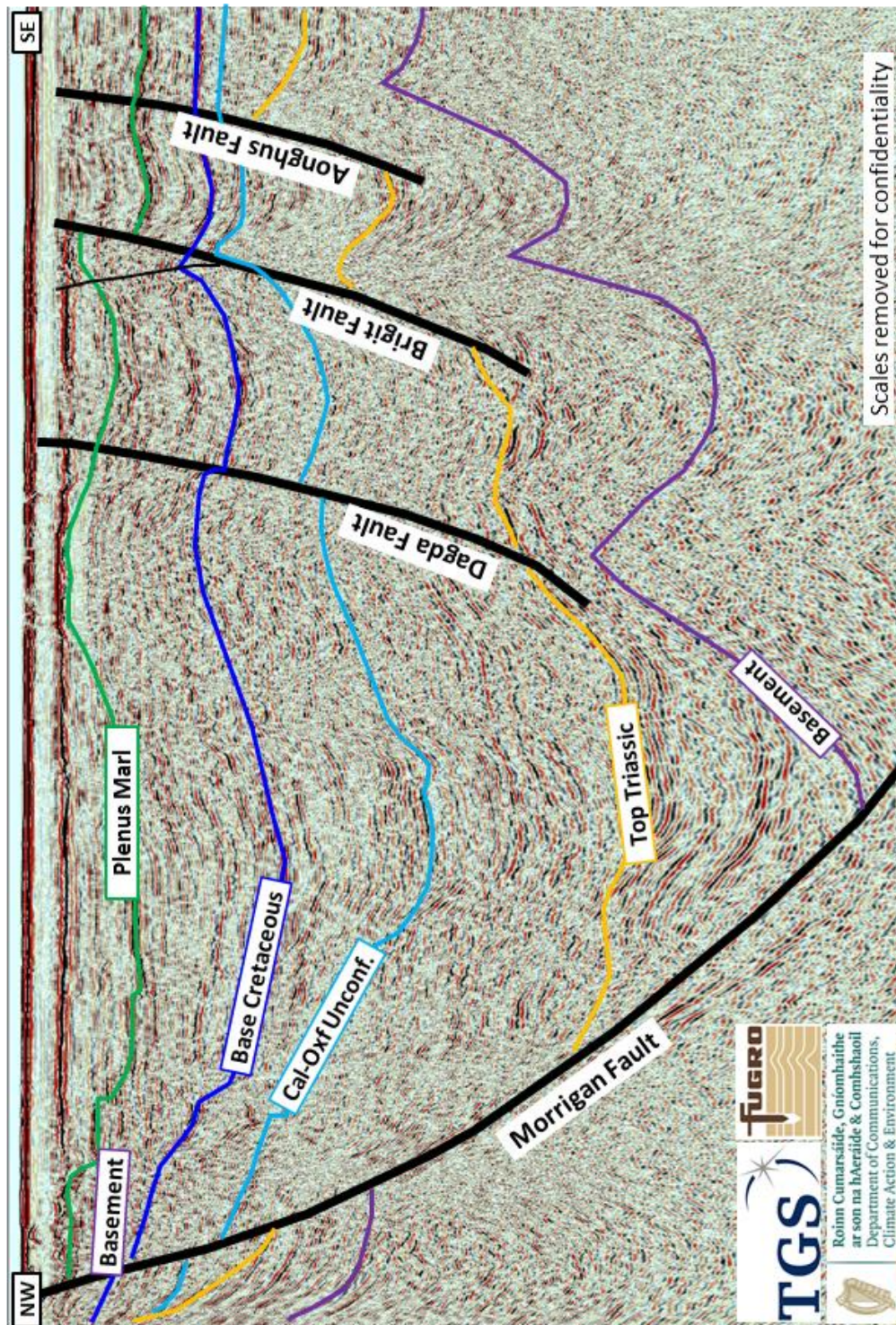


Figure 7-32. Seismic Line SGC06-553689 showing the interpretation of the major faults. The basin bounding Morrigan Fault becomes low angle with depth and was active from the Triassic to Cretaceous. The antithetic Dagda, Brigit and Aonghus Faults sole out within the rotated Triassic and are active from the Upper Jurassic to the Cretaceous.

7.2.2 Dagda Fault

The first large regional antithetic fault to the Murrigan Fault is named here as the Dagda Fault. It strikes southwest-northeast and dips to the northwest (Appendix F.4). It appears to initiate during Upper Jurassic rifting, soling out in the underlying and previously rotated Triassic sediments (Figure 7-32). The Dagda Fault, along with other antithetic faults, accommodates a significant portion of the extension in the Upper Jurassic and Cretaceous, Appendix E.1 to Appendix E.6, forming a conventional graben. Syn-depositional growth across the Dagda Fault in the Upper Jurassic is seen to be up to 1,200m (3,950 ft) (Appendix G.3). Cenozoic reactivation of this fault creates broad mid-basinal anticlines such as the structures at the Kinsale Head and Seven Heads gas fields (Appendix F.5).

7.2.3 Brigit Fault

The second largest antithetic fault is named here as the Brigit Fault. It is parallel to the Dagda Fault with consistent dip and strike (Appendix F.4). It has a similar history as the Dagda Fault, initiating as an extensional fault in the Upper Jurassic, soling out in the underlying Triassic, and with subsequent Cenozoic inversion (Figure 7-32). Syn-depositional growth across this fault in the Upper Jurassic is up to 500m (1,600 ft) (Appendix G.3). Cenozoic reactivation of this fault creates tight inversion structures as seen in Figure 7-2 (Appendix E.2), especially at locations where the Brigit Fault takes a left step/bend (at wells 57/2-2 & 48/30-2), likely to be breached relay zones (Appendix F.5). Similar inversion structures on left

stepping bends are evident on good quality 3D data in the Mizen Basin to the southeast (Rodriguez-Salgado *et al.*, 2020).

7.2.4 Aonghus Fault

The last of the primary faults mapped regionally within the study area is also antithetic to the Murrigan fault, the most southern of the three antithetic faults and named here the Aonghus Fault. The orientation and dip are consistent with the Dagda and Brigit Faults and syn-depositional growth in the Upper Jurassic is 300m (1,000 ft) (Appendix G.3). It has a similar history as the Dagda and Brigit Faults, initiating as an extensional fault in the Upper Jurassic, with subsequent Cenozoic inversion and soling out in the underlying Triassic (Figure 7-32).

7.3 Basin Evolution Observations

Appendix G.2 and Appendix G.3 show significant changes in sediment isopach between the Lower and Upper Jurassic, above and below the Callovian-Oxfordian unconformity. These changes in the isopach are believed to be related to changes in the active faulting as the antithetic Dagda, Brigit and Aonghus Faults initiated in the Upper Jurassic, marking a change in the structural development of the NCSB. This structural change is likely to have impacts on sediment provenance, input facies and distribution, with significant changes likely between the Lower and Upper Jurassic section.

Faults of opposite dip to a primary extensional fault, such as the Dagda, Brigit and Aonghus Faults, can form in response to gravitational instability of the sediments as they are rotated (Withjack *et al.*, 1990; Paton, 2006). Gibbs (1984) noted similar opposing listric faults detaching in low strength or over pressured zones, particularly within a half graben where there is roll-over in the hanging wall. This is particularly common where ductile rocks (such as halite) are present in the sedimentary package (Gibbs, 1984; Morley, 1995). There is clear evidence on the seismic data of the Dagda, Brigit and Aonghus Faults soling out within the Triassic as shown in Appendix E.1 to Appendix E.6.

The maximum thickness of the Upper Cretaceous is noted to be 1,200m (3,950 feet) and in areas of Cenozoic uplift and erosion adjacent to the Dagda and Brigit faults the remaining section and the uplift quoted by Murdock *et al.* (1995) agrees with a pre-erosion thickness of 1,200m (3,950 feet). However, in the extreme southwest of the study area, adjacent to the 57/7-1 well (Figure 7-33) the Upper Cretaceous thickness is 300-700m (1,000-2,300ft). Given the Upper Cretaceous was deposited during a basin sag phase significant local thickness changes would not be expected. This would suggest this thickness change is therefore a regional change. A NWSE shear zone is postulated which would be a sufficient regional structural feature that could impact the accommodation space created during the basin sag phase.

It is also noted that the Cenozoic inversion in the southwest of the study area appears to be concentrated on the Brigit and Aonghus Fault rather than on the Dagda Fault, this is most effectively demonstrated by the isopach of the Upper Cretaceous

(basin sag phase) as the Cretaceous chalk facies deposition would have little local thickness variations (Figure 7-33). The isopach illustrates several areas where the Upper Cretaceous is thinner than 800m (2550ft) indicating inversion on the underlying faults (Figure 7-33). This change in fault offset appears to be coincident with thickness changes within the Lower Cretaceous sediments (Figure 7-34).

It is postulated that the Dagda fault maybe tipping out to the southwest and the extensional strain was thus transferred to the Brigit and Aonghus Faults. It is also plausible that a transfer fault or shear zone exists, facilitating the transfer of extension between faults. This further supports the interpretation of a NW-SE shear zone or transfer fault in this location (Figure 7-33 & Figure 7-34).

The freeair gravity map also appears to support the interpretation of a transfer fault or shear zone (of unknown level or timing), Figure 7-35, where gravity values are consistently higher southwest of the possible shear zone, potentially indicating density changes within the basement either side of the proposed shear zone. Evidence of a NW-SE lineament within the NCSB is also discussed by O'Reilly *et al.* (1991) who recognise a transfer fault between different structural domains along Profile 7 of the COOLE refraction data (Figure 2-1). Similar large-scale transfer faults have been described by Kimbell *et al.* (2005) and Dore *et al.* (1999) and are interpreted to be reactivated Caledonian strike slip structures, they may also have served a similar kinematic function in the Variscan (Philcox, 1964). It is thus proposed that the presence of NW-SE shear zones that have influenced structural and stratigraphic development in the NCSB are inherited basement features of

Caledonian and/or Variscan age which were reactivated during Mesozoic extension. These NW-SE shear zones are likely to represent zones where extensional stress was transferred, for instance at the northeast end of the basin into the St. George's Channel Basin (Coward & Trudgill, 1989) and the southwest end of the basin into the Fastnet Basin (Robinson *et al.*, 1981). The presence of NW-SE shear zones in the NCSB is well established in the literature and are identified by Ziegler (1975 & 198), Naylor & Mounteney (1975), Pegrum & Mounteney (1978), Petrie *et al.* (1989), O'Reilly *et al.* (1991); Ruffel & Coward (1992) and McCann & Shannon (1993 & 1994).

In total, combining the maximum sediment isopachs for each section (Appendix G.1 to Appendix G.6), the seismic data, combined with the uplift described by Murdoch *et al.* (1995), supports up to 11 kilometres (36,000 feet) (present day thickness) of Mesozoic and Cenozoic sediment was deposited in the NCSB.

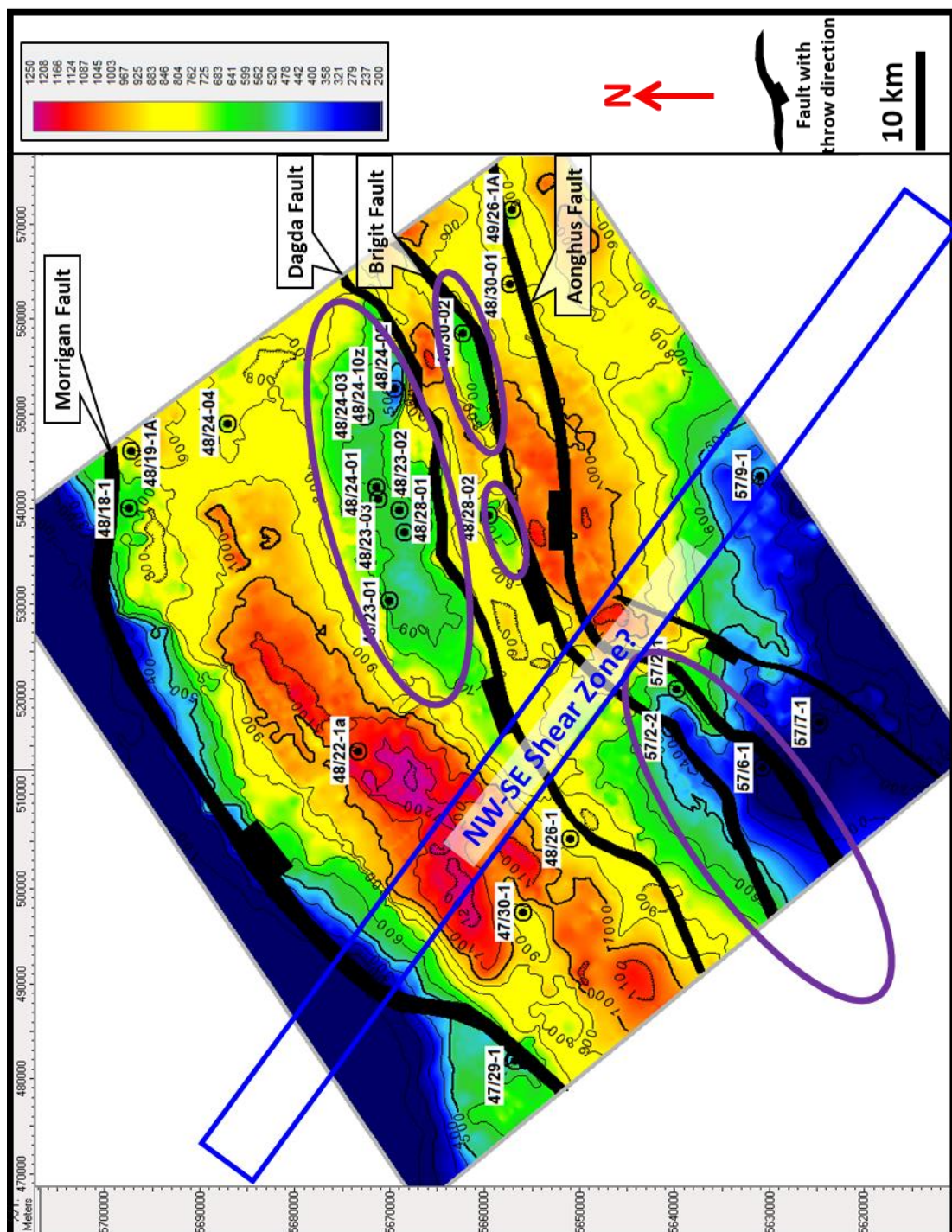


Figure 7-33. Isopach map of the Upper Cretaceous section, illustrating areas of inversion (circled in purple). The inversion is primarily accommodated on the Dagda Fault in the northeast and on the Brigit and Aonghus Faults to the southwest. A NW-SE shear zone is postulated which would facilitate the transfer of compression across faults.

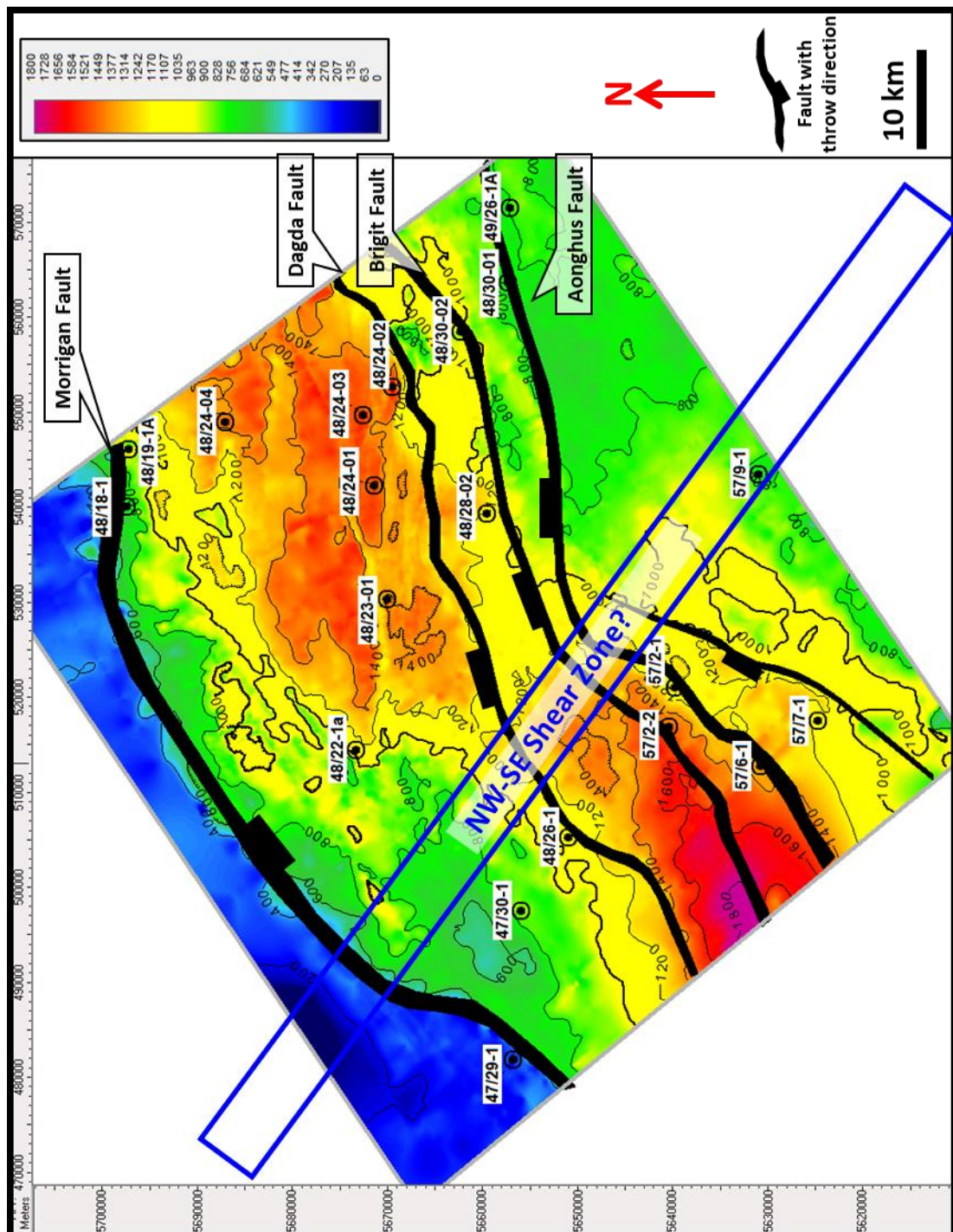


Figure 7-34. Isopach map of the Lower Cretaceous section, illustrating two discrete depocenters (in red). The depocenter locations suggest rift extension is being accommodated on the Dagda Fault in the northeast and on the Brigit and Aonghus Faults to the southwest. A NW-SE shear zone is postulated which would facilitate the transfer of extension across faults.

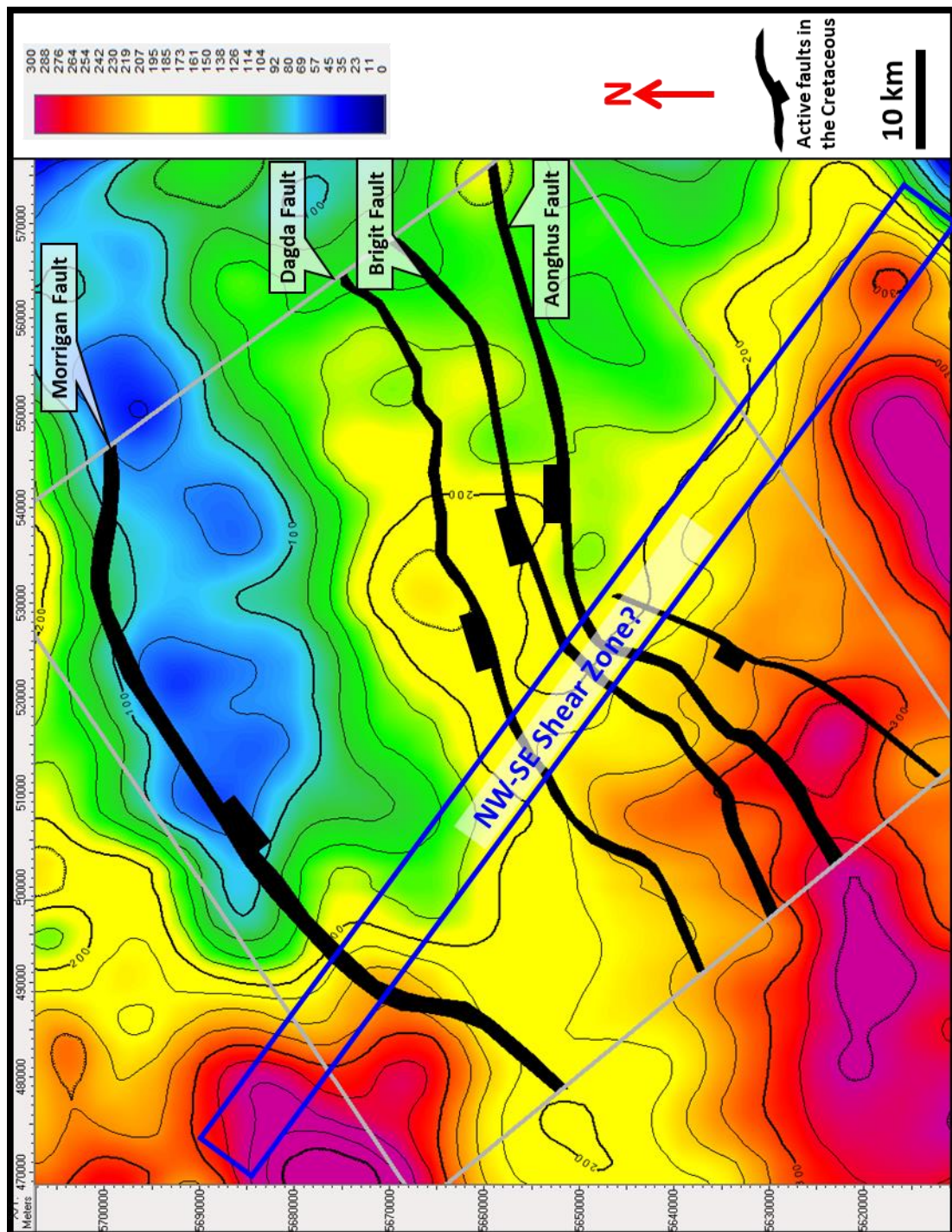


Figure 7-35. Smith and Sandwell (2015) freeair gravity map, overlain by Cretaceous fault polygons, showing potential NW-SE shear zone. Gravity values are higher to the west of the potential NW-SE shear zone indicating potential changes in basement density across the shear zone.

8 Revised Structural Model

Based on the interpretation of the available modern 2D and 3D seismic datasets a revised structural evolution is proposed for the NCSB (Figure 8-1) which complements and develops concepts from previous research.

A series of Variscan thrust bound blocks are presented in the pre-rift setting (Figure 8-2). This agrees with McCann (1996) who describes slivers of basement thrust over each other in an imbricate fashion. It is proposed that extension in the Triassic is accommodated by an asymmetric simple shear rift model (Wernicke, 1981) with pre-existing Variscan thrusts acting as a weak zone and creating a set of Triassic half grabens, Figure 8-2. These half grabens become listric with depth to a crustal boundary at a depth of 18-20 km (11-12.5 miles). Similar initial development was proposed by Dymant (1989), Dymant *et al.*, (1990); Dymant & Bano, (1991); Tappin *et al.*, (1994); and O'Reilly *et al.*, (1991). There are several examples in the Scandinavian Caledonides where thrusts are reactivated, rotated and new hinterland dipping extensional shear zones develop (Fossen, 2016).

Triassic syn-rift sediments are likely to have been transported from the Variscan foreland to the north and the Variscan hinterland to the south by aeolian and fluvial processes, as seen in adjacent basins (Tyrrell *et al.*, 2012). The Variscan hinterland to the south has been shown by Tyrrell *et al.* (2012) to be shedding sediment into the Wessex and East Irish Sea Basins further east. Shannon & MacTiernan (1993) present gravity data to support the Pembroke Ridge as being a large high level

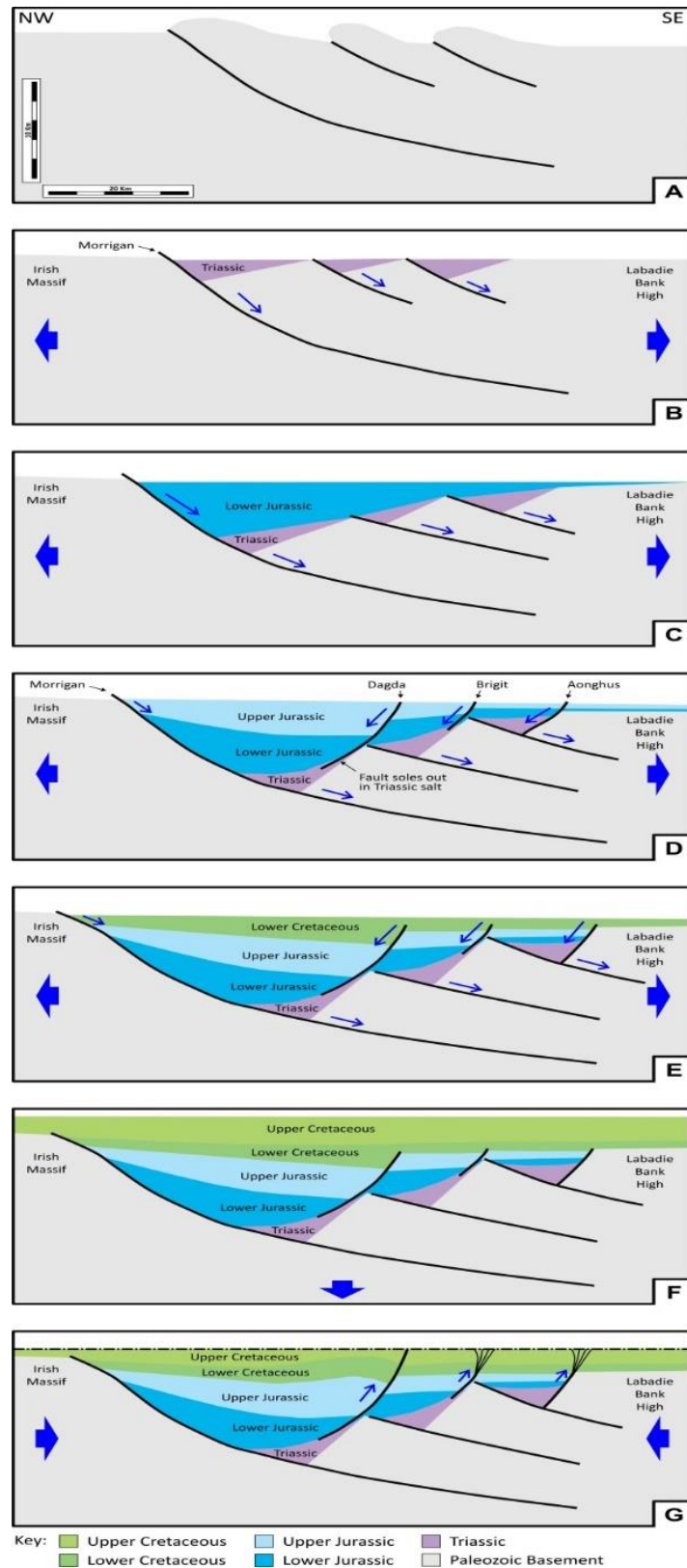


Figure 8-1. Revised structural evolution model of the NCSB. (A) Pre-rift setting of Variscan thrusts. (B) Triassic rifting accommodated by reactivated

Variscan thrusts as a series of half-grabens. (C) Rifting continued into the Lower Jurassic with a half-graben geometry. (D) Upper Jurassic rifting is accommodated by the northern basin bounding fault and new mid-basinal antithetic faults which detach within the underlying Triassic, forming a conventional graben geometry. (E) Lower Cretaceous extension continued as a conventional graben. (F) Upper Cretaceous basin sag. (G) Cenozoic compression accommodated by reactivating mid-basinal antithetic faults.

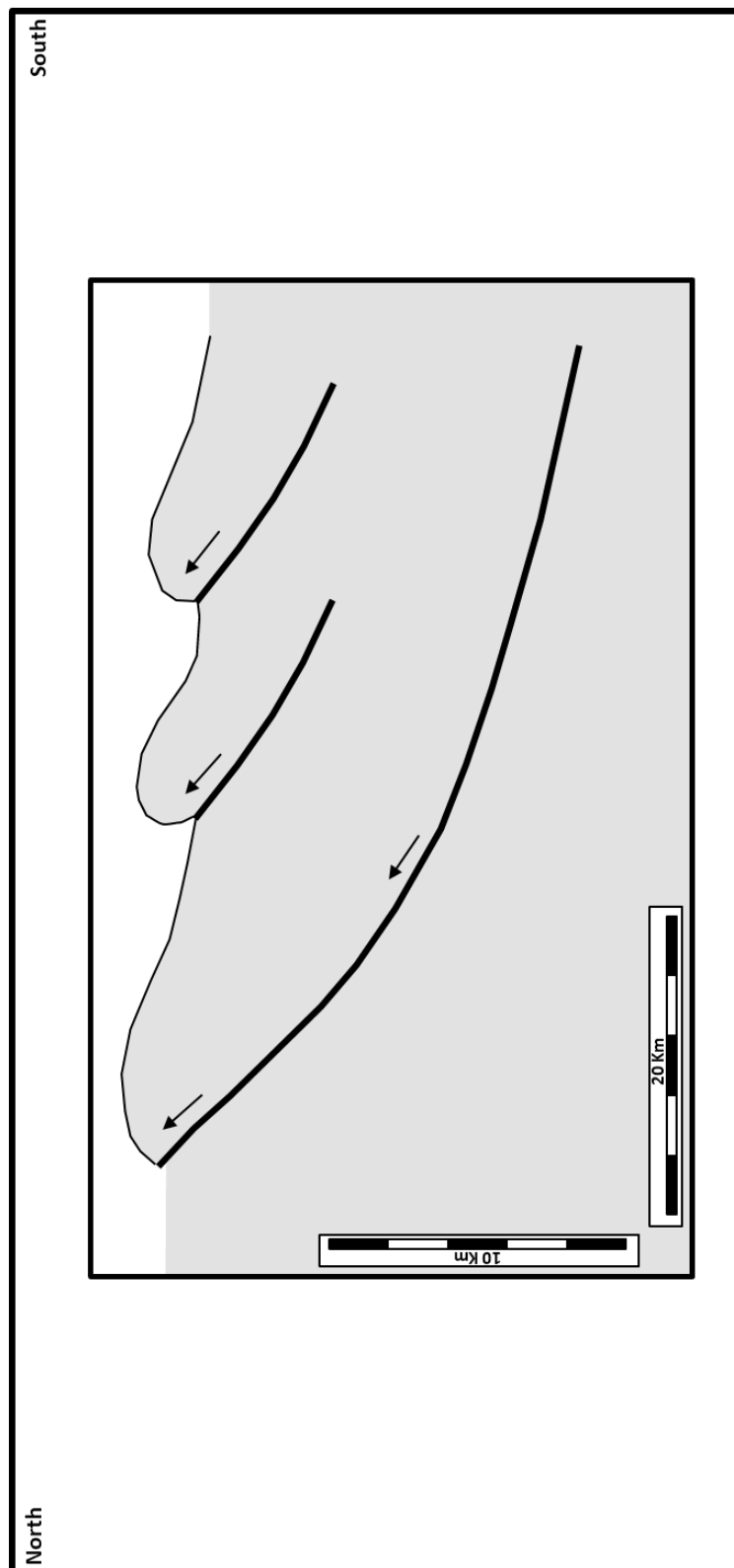


Figure 8-2. Structural evolution of the NCSB – Pre-rift setting showing a series of Variscan thrust bound blocks.

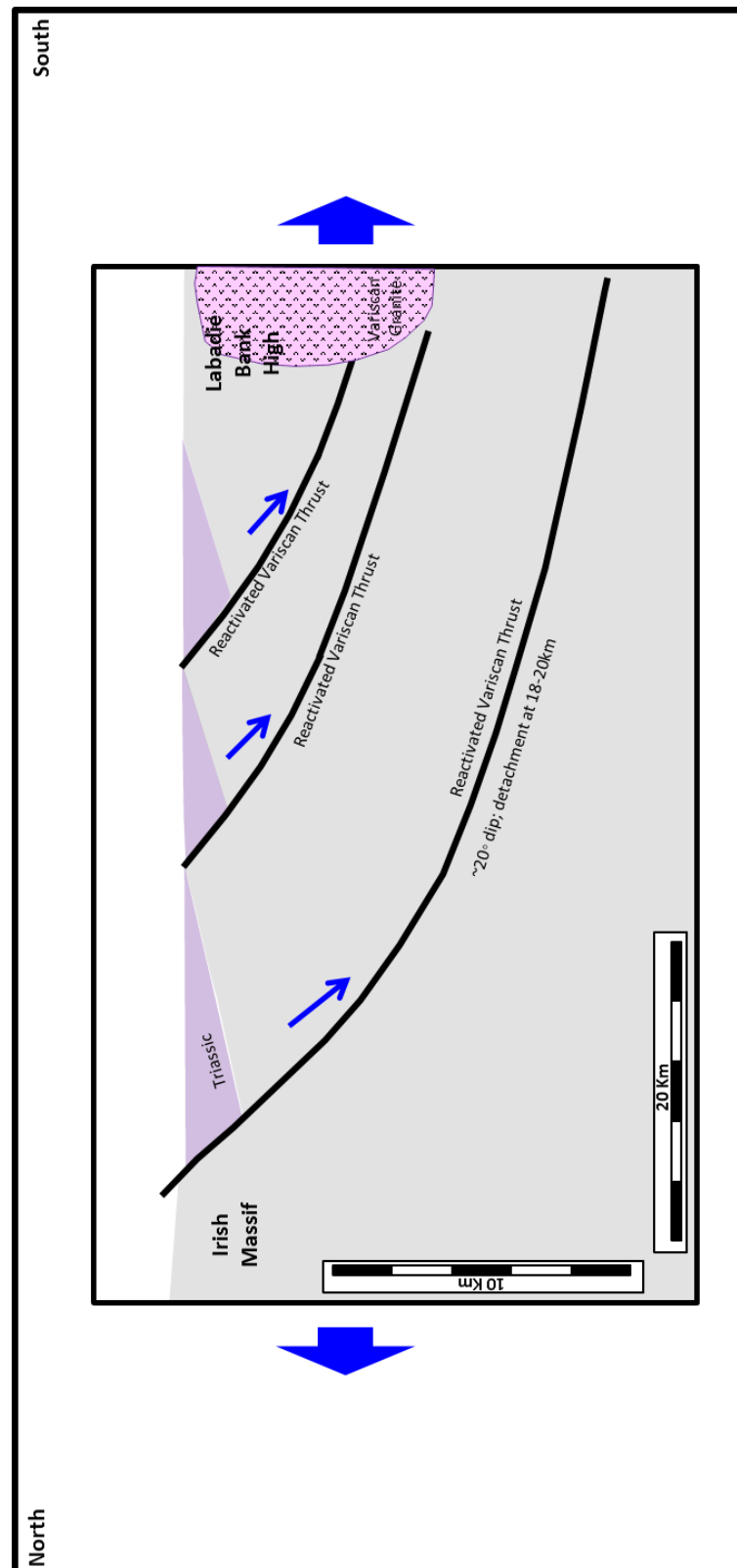


Figure 8-3. Structural evolution of the NCSB – Triassic cross section illustrating the proposed reactivation of Variscan thrusts to form a set of Triassic half grabens.

granite which may have been unroofed and provided a local sand source for the SSG. Musgrove *et al.* (1995) suggest the SSG is restricted to paleotopographic lows and associated with the presence of halite within the Triassic. The Triassic was confirmed as over 1000m (3281ft) in thickness and containing approximately 250m (820ft) of massive halite in well 57/09-1 (Figure 6-21). This well evidence and the evidence of halokinesis on the seismic data, annotated on Appendix E.1 to Appendix E.6, across the NCSB suggests evaporite deposition in the Triassic from regular saltwater influx and evaporation in a dominantly arid terrestrial environment. The interpreted half grabens were therefore likely to be linked, probably via reactivated Caledonian/Variscan northwest-southeast transfer faults (Figure 3-1– Location C), allowing regional access to the marine environment, particularly across the Labadie Bank High – Pembrokehire Ridge to the South Celtic Sea Basin (Shannon 1995).

Rifting continued through the Lower Jurassic and extension was accommodated primarily on the most northern of these reactivated Variscan thrusts, the Murrigan Fault (Figure 8-4). The other Variscan thrusts may have reduced movement as they became locked, possibly against the granites within the Labadie Bank High – Pembrokehire Ridge (Naylor & Shannon, 1982; Shannon & MacTiernan, 1993). The Murrigan Fault remained active, possibly because it is deeper in the section and may have propagated through the granite. A deep extension of the Murrigan Fault has been mapped (Figure 5-4) by previous authors on deep refraction seismic data as a south-easterly dipping low angle detachment feature at 12-14 kilometres (7.5-

8.5 miles) depth (BIRPS & ECORS, 1986; McGeary *et al.*, 1987; Petrie *et al.* (1989); O'Reilly *et al.*, 1991; Masson *et al.*, 1998). Halokinesis initiated within the Lower Jurassic, caused by movement on underlying faults (Tucker & Arter 1987) and differential loading of the overburden (Figure 7-12).

Throughout the Lower Jurassic the NCSB was a large half graben system with sediment thickening into the Morrigan Fault (Figure 8-4) and was predominantly a shallow marine environment (Ewins & Shannon, 1995). Vertical throw of over 2000m (6,600ft) on the Morrigan Fault (Appendix G.2) caused significant down dip rotation of the underlying Triassic sequence (Figure 8-4). Minor antithetic faults may have developed in the Lower Jurassic as salt halokinesis initiated (Tucker & Arter, 1987), similar to the fault model of Gibbs (1984).

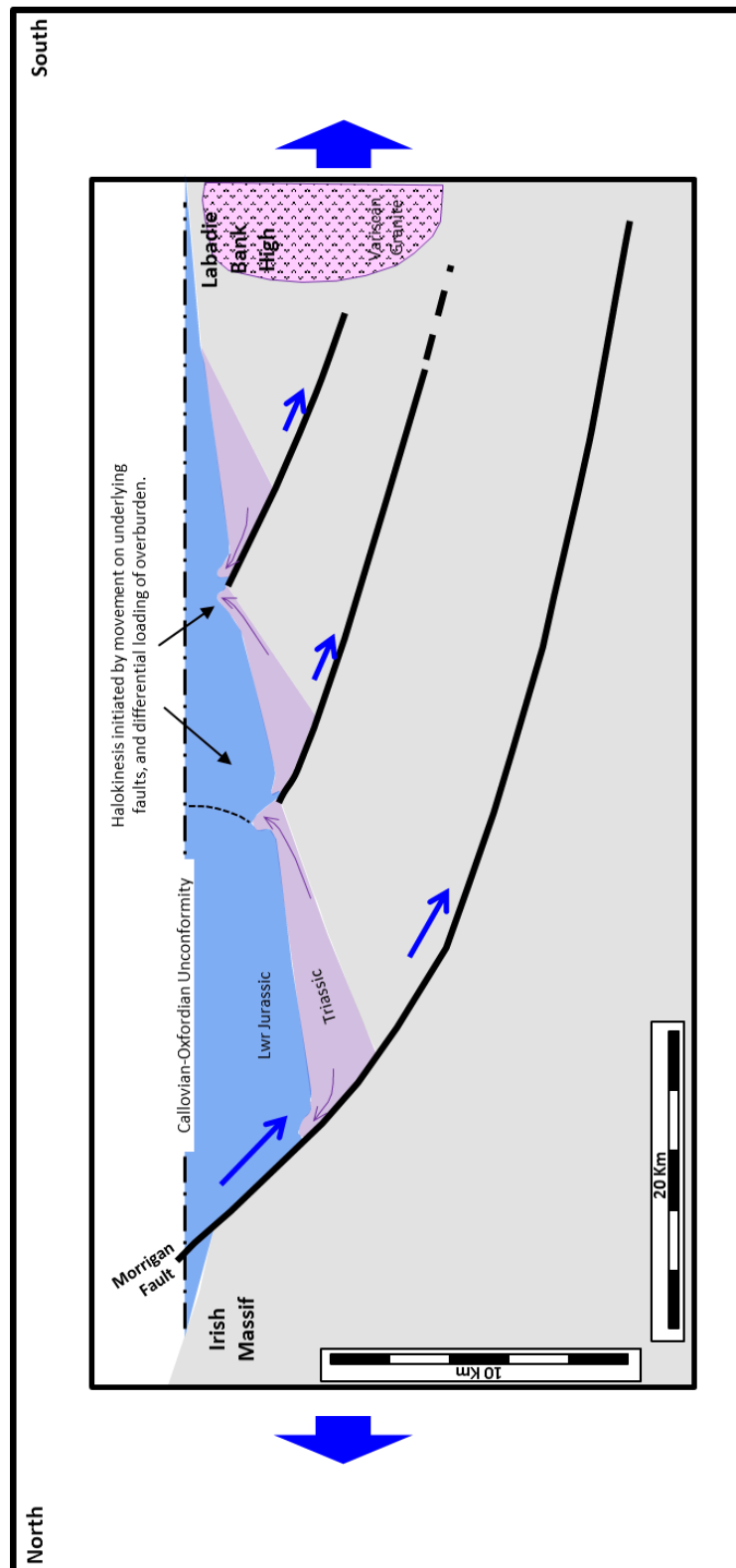


Figure 8-4. Structural evolution of the NCSB – Lower Jurassic cross section illustrating the continued extensional reactivation of Variscan thrusts to form a Lower Jurassic half graben. Minor halokinesis is also initiated.

A seismic line from the Goban Spur Basin (GSB), 300km to the southwest of the study area, is shown in Figure 8-5 compared with a seismic line from the NCSB study area. The GSB has several large half-grabens controlled by south-easterly dipping faults, creating significant rotation of early sediments. This striking similarity in deep structural style between the GSB and the NCSB further confirms the interpretation of regional reactivation of pre-existing Variscan thrust faults as half grabens. It is also noted that there are several examples of thrusts being reactivated as extensional faults within the Scandinavian Caledonides (Fossen, 2016) which further bolsters the interpretation, as does the understanding that structurally, a low angle extensional fault would generally be expected to have been originally a compressional feature.

The presence of a Callovian-Oxfordian Unconformity in the wells and locally on the seismic data suggests rifting may have stopped briefly, related to Mid-Cimmerian compression/uplift (Naylor & Shannon, 2011). Only a subtle change in dip of seismic reflectors can be seen locally on the modern data, suggesting this was a relatively minor event within the NCSB (Figure 7-16).

Rifting recommenced in the Upper Jurassic but the Morrigan Fault and underlying detachment accommodated significantly less rifting than previously, as extension was also accommodated on newly developed large mid-basinal faults, the Dagda, Brigit and Aonghus Faults, all of which are antithetic to the Morrigan Fault (Figure 8-6). Rifting was thus accommodated by a symmetric pure shear rift (McKenzie, 1978).

These antithetic faults initiated due to extension but may have been influenced by underlying halokinesis or simply by bed length extension and thinning of the hanging wall to the Murrumbidgee fault (Gibbs 1984). In both of these scenarios the underlying Triassic section had been rotated by up to 20 degrees in the previous rifting event and evaporites within the Triassic section became a detachment zone for mid-basinal normal faulting in the Upper Jurassic.

Pascoe *et al.* (1999) discuss how Triassic halite intervals have been noted as locally important as detachment zones during Jurassic rifting in the North Sea. Such structural style is common and noted by Withjack *et al.* (1990) and Paton (2006) where detachment faults of opposite dip to the primary fault can form in response to gravitational instability of the sediments as they are rotated. Morley (1995) notes this is particularly common where ductile rocks (such as halite) are present in the sedimentary package. Flip-Flop salt tectonics is an alternate method for the formation of the antithetic faults (Quirk & Pilcher, 2012; Quirk *et al.*, 2012). This is a process where salt halokinesis initiated in the foot-wall of an extensional fault, as the salt continues to move it may invert the hanging wall (or the salt wall may collapse), thus initiating an extensional fault in the opposing direction to the original fault in the old foot-wall (now a hanging-wall). This was considered however it was ruled out as there is no evidence of significant salt diapirism within the NCSB, only minor halokinesis is seen.

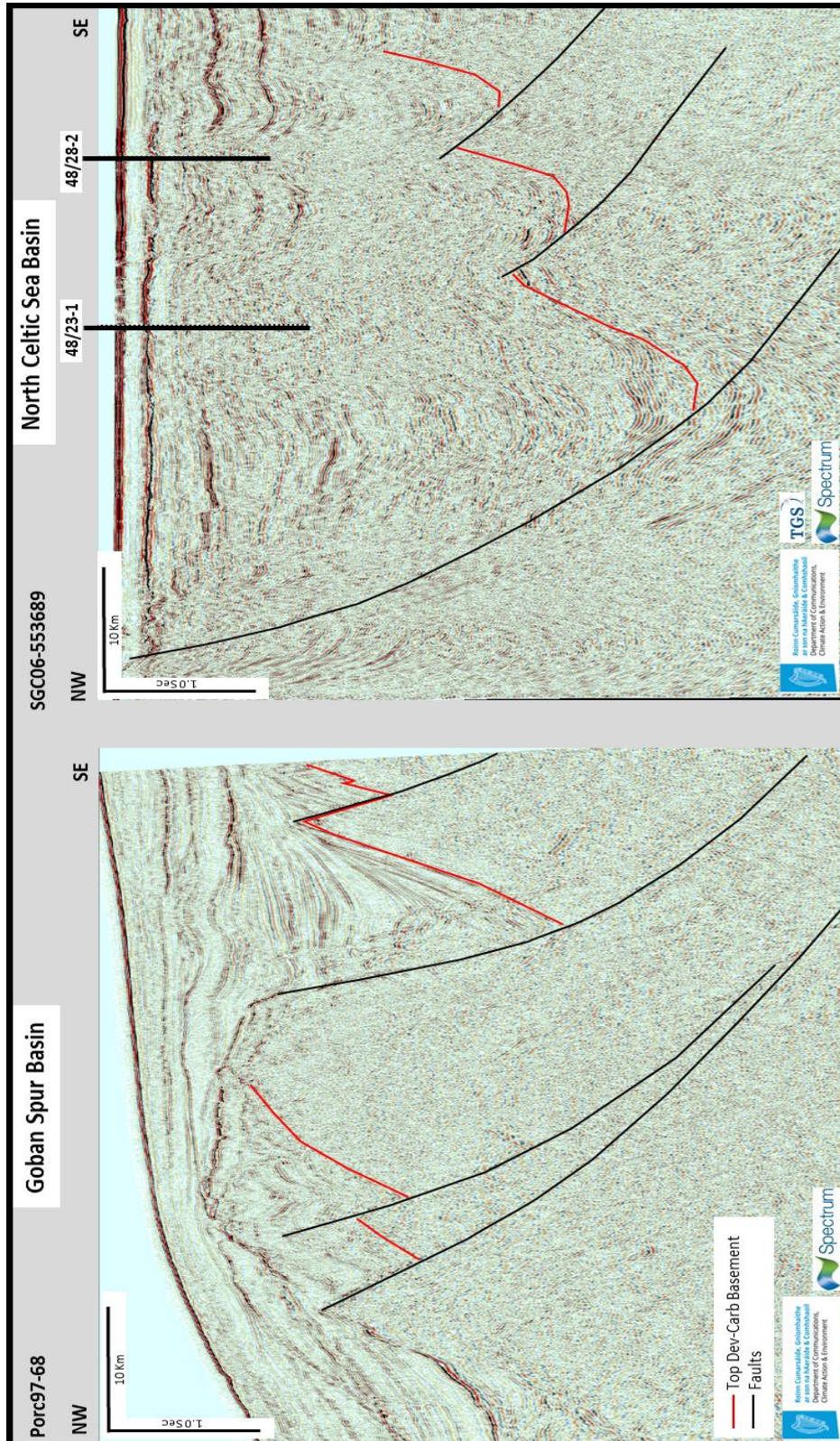


Figure 8-5. Seismic lines Porc97-68 from the Goban Spur Basin and SGC06-553689 from the NCSB, showing similar SE dipping fault style at depth.

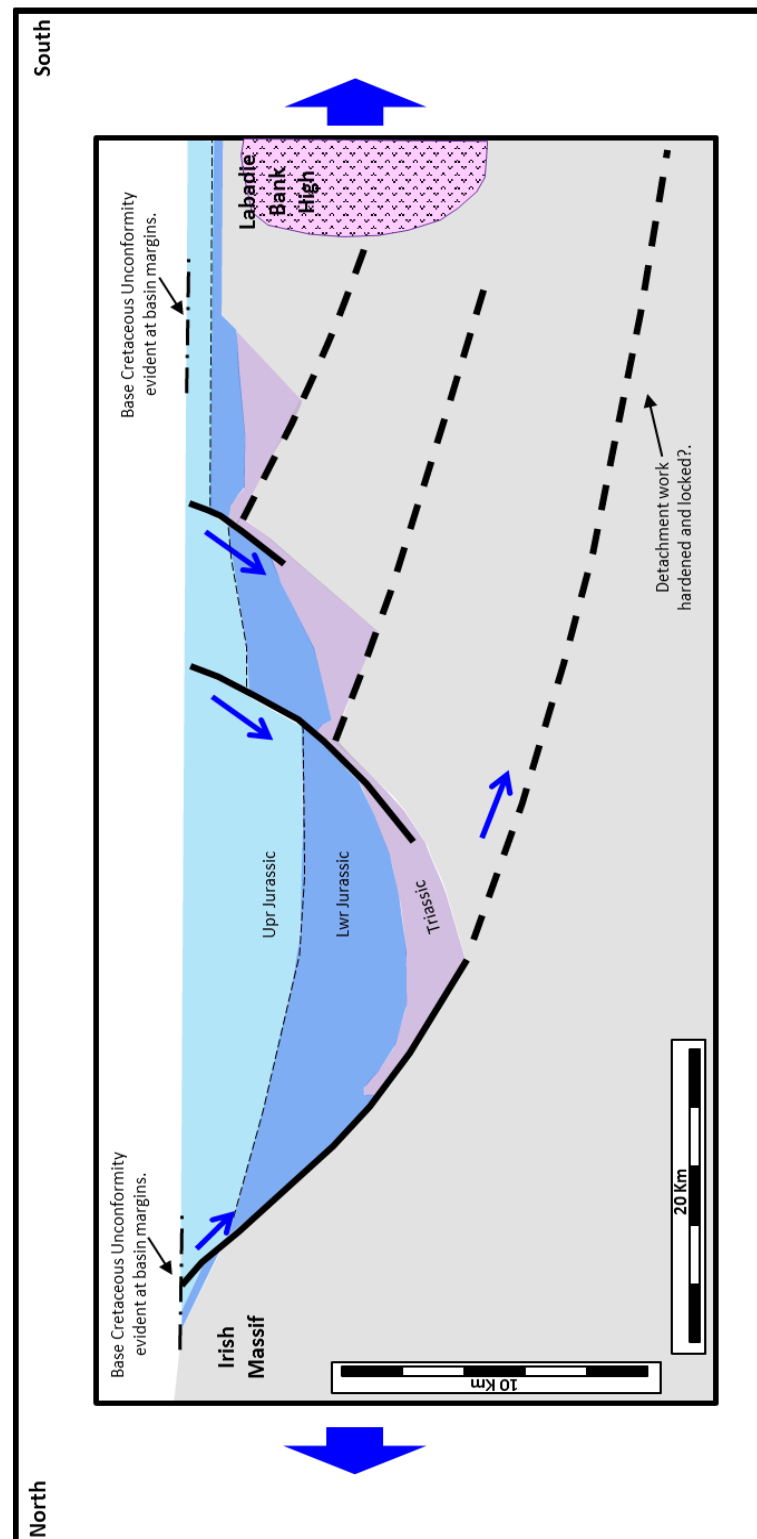


Figure 8-6. Structural evolution of the NCSB – Upper Jurassic cross section illustrating renewed rifting with extension accommodated on the northern basin bounding fault and on newly developed mid-basinal antithetic faults which detach within the underlying Triassic.

The NCSB did not experience a significant unconformity at the Base Cretaceous as seen in the adjacent Fastnet, South Celtic Sea, and Bristol Channel basins (Copestake et al., 2018) and indeed regionally across northwest Europe (Ziegler, 1982). Ruffell & Coward (1992) suggested that during the Upper Jurassic the Variscan Front may have been reactivated as a thrust, uplifting the areas to the east (Bristol Channel and northern Wessex Basins), while further west a thrust underlying the Labadie Bank High – Pembrokeshire Ridge was reactivated, uplifting the South Celtic Sea Basin, leaving the NCSB in the foreland and preserving the Upper Jurassic section. The NW-SE strike slip faults allowed this transfer of stress across pre-existing Variscan thrusts. The Upper Jurassic reactivation of a Variscan thrust under the South Celtic Sea Basin, but not the NCSB is again supportive of the Morrigan Fault having reduced throw, possibly as it started to become locked.

Some fault blocks on the basin margin, north and south, do show some evidence of the Late Jurassic or Early Cretaceous erosional event. The Helvick field 70 kilometres (43 miles) outside the study area (Figure 1-1) to the northeast is an example of this localised erosion at the basin margin (Caston, 1995). Erosion in this area is believed to be related to localised compression and block rotation at the basin flanks. It is possible that a regional uplift event, seen in adjacent basins, removed the access to the open marine environment during the latest Jurassic to earliest Cretaceous, creating a lacustrine environment (Purbeck Group) in the NCSB with continued sedimentation.

Rifting continued into the Lower Cretaceous with extension accommodated on the same faults as the Upper Jurassic, in a conventional graben geometry (Figure 8-7). Extensive well control in the basin supports a mud dominated terrestrial deposition with fluvial channels (Ewins & Shannon, 1995).

The post rift sag phase and regional sea level rise yielded a thick Chalk deposit in the Upper Cretaceous (Figure 8-8) which extended over the Labadie Bank High – Pembrokehire Ridge and also onshore Ireland as well as most Mesozoic basins in northwest Europe (Naylor & Shannon, 2011). This overstepping of the sag phase sediments beyond the basin bounding faults yields a classic “steer’s head” geometry and is similar to the model proposed by McMahon & Turner (1998) for the Cretaceous.

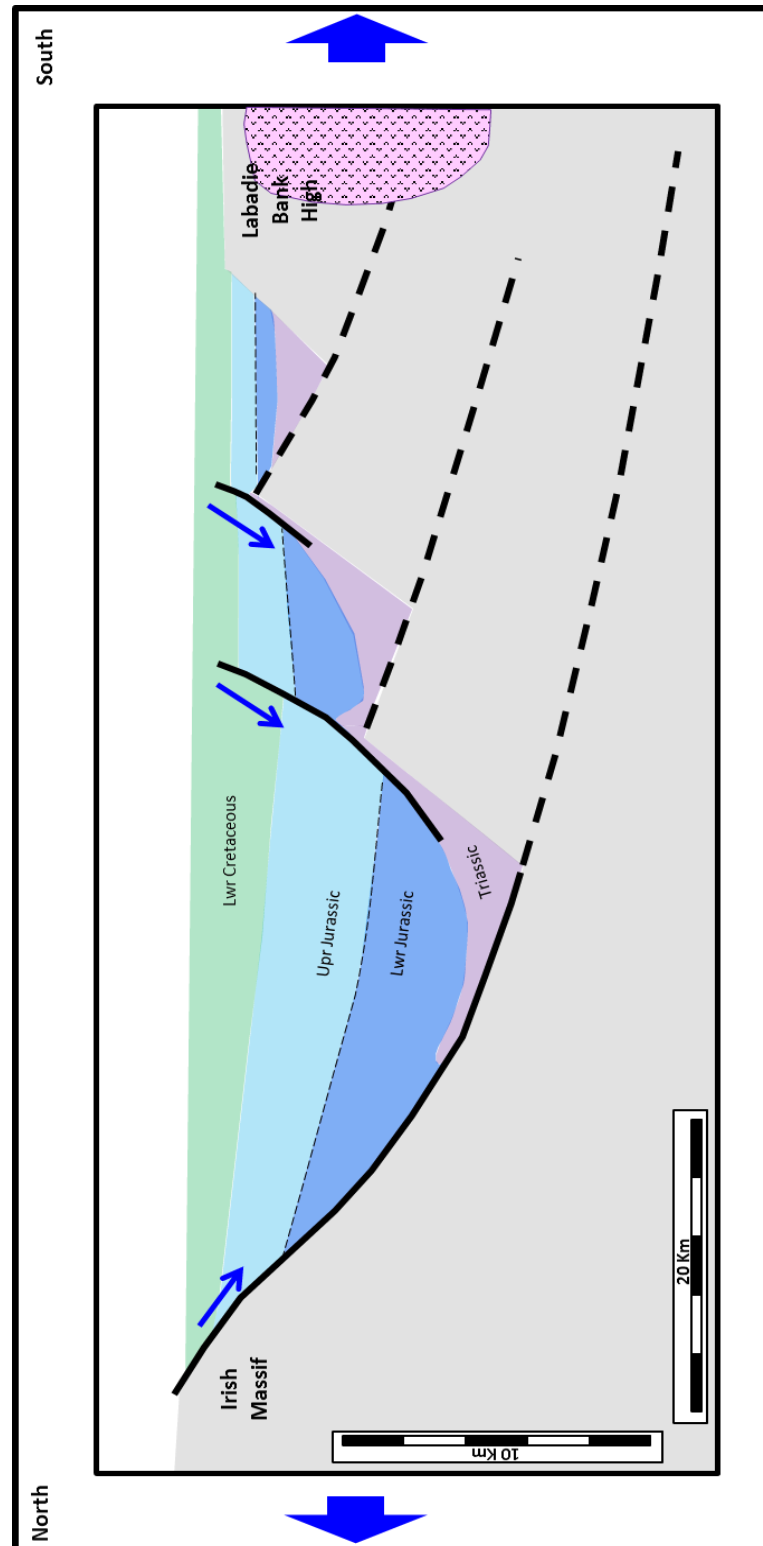


Figure 8-7. Structural evolution of the NCSB – Lower Cretaceous cross section illustrating continued rifting with extension accommodated on the northern basin bounding fault and on the mid-basinal antithetic faults which detach within the underlying Triassic.

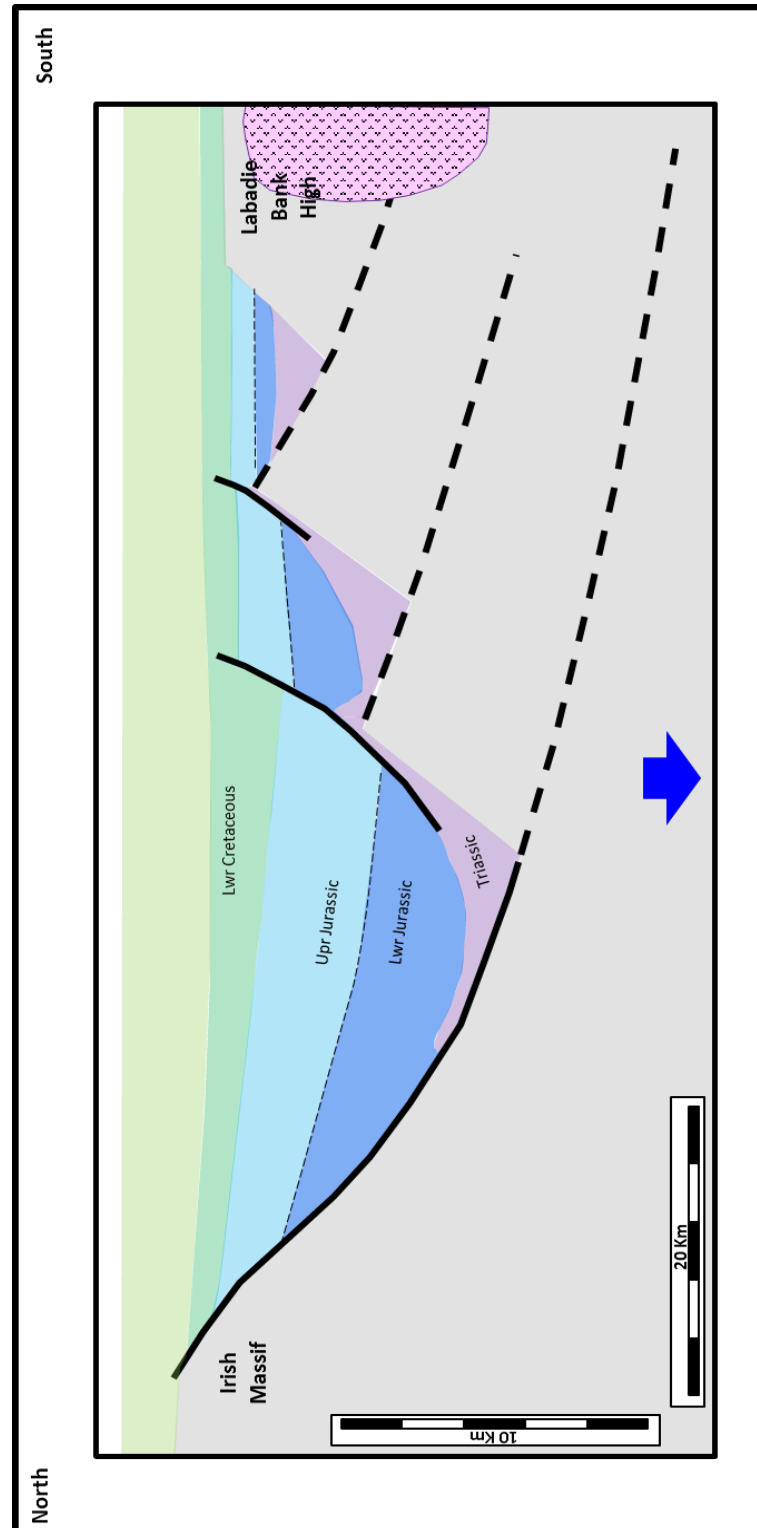


Figure 8-8. Structural evolution of the NCSB – Upper Cretaceous cross section illustrating a basin sag phase with Upper Cretaceous sediments overstepping the basin extents yielding a classic “steer’s head” geometry.

Post rift deposition continued into the Cenozoic however later Alpine compression in the Oligo-Miocene and uplift in the Paleocene (Murdoch *et al.*, 1995) has removed this section over much of the NCSB, in particular over the study area (Figure 8-9). The compression caused reactivation and reversal of the mid-basin antithetic faults creating broad mid-basinal anticlines (such as the Seven Heads and Kinsale Head Gas Fields) and flower structures (annotated on Appendix E.1 to Appendix E.6). It is likely uplift was concentrated in a mid-basin position as the Dagda, Brigit and Aonghus detached within Triassic halites and were preferentially reactivated by Cenozoic compression.

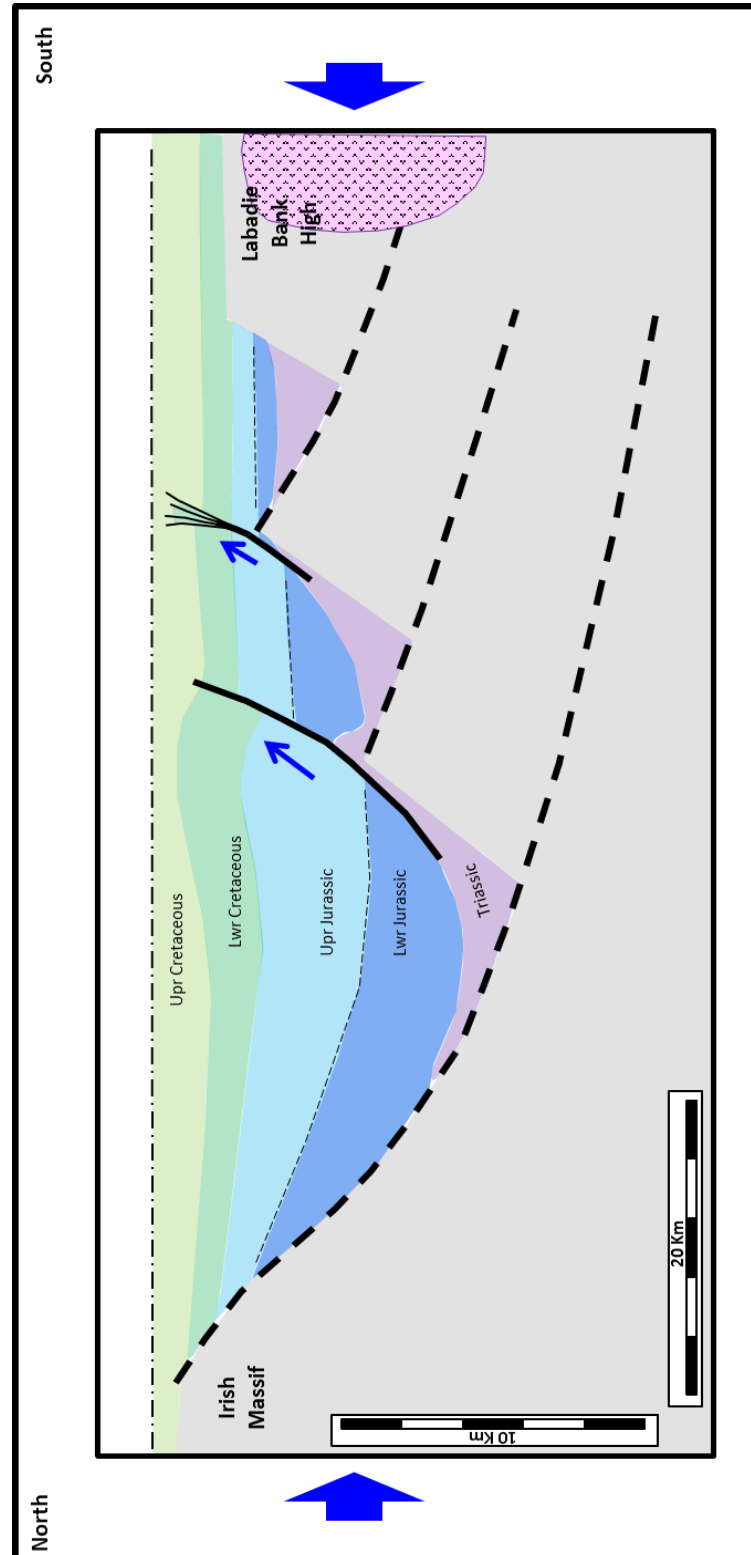


Figure 8-9. Structural evolution of the NCSB – Cenozoic cross section illustrating basin wide uplift and compressional reactivation of the mid-basinal faults to yield broad anticlines and flower structures.

9 Discussion

The revised structural evolution presented here from a half graben to a conventional graben geometry has significant implications for sediment deposition and current basin configuration. Several new tilted fault block structures are also likely to be recognised in the Triassic and Jurassic interval as more modern seismic data is acquired or vintage seismic data is reprocessed with modern demultiple processing techniques. Seismic evidence for the presence of extensive Triassic sediments with SSG and MMG overlying Palaeozoic basement is positive for hydrocarbon prospectivity at this level within the NCSB. This could open up a Triassic play in the NCSB, similar to the East Irish Sea (Stuart, 1993) or indeed the Wytch Farm oil field in Dorset, United Kingdom (Colter & Havard, 1981).

Recognising that Cenozoic inversion was focused on, and reactivated the mid-basin antithetic faults (Dagda, Brigit and Aonghus faults) is critical for hydrocarbon prospectivity. Source rocks within the Cretaceous and Jurassic will have reached their maximum hydrocarbon generation (greatest burial depth and temperature) just prior to Cenozoic inversion. Any early structures filled with hydrocarbon will thus be modified or potentially breached by the inversion, while late structures may receive no hydrocarbon charge.

The extent of the hydrocarbon prospectivity in the NCSB is put in context by the potential billion barrel Barryroe oil discovery and the producing 1 trillion cubic feet of gas at the Kinsale Head gas field, pers comm (Dr. John O'Sullivan, Providence Resources Plc).

9.1 Reservoir Potential

The revised structural evolution presented here has important implications for the prediction of coarse-grained clastic deposits within the NCSB. Existing paleogeography maps, such as those of Ziegler (1990), Stephenson (1983), and Ewins & Shannon (1995) require significant changes to reflect the revised structural evolution presented. Such revised interpretations will be critical in predicting both source rock and reservoir facies and dominant sediment input direction in the Triassic, Jurassic and Lower Cretaceous, reflecting the role of the primary syn-depositional faults.

An updated paleogeography is beyond the scope of this study, however it is relevant to briefly discuss some of the conceptional consequences of the revised structural development. Two broad intervals are chosen for discussion, the Lower Jurassic and the Upper Jurassic, as they represent active rifting in a half-graben and a conventional graben respectively. It is also noted that Ewins & Shannon (1995) considered the Lower Jurassic Sinemurian (LJ3) and Upper Jurassic Oxfordian-Early Kimmeridgian (UJ1) sequences as the intervals of best reservoir potential within the Jurassic and Cretaceous of the NCSB.

9.1.1 Lower Jurassic

The LJ3 of Ewins & Shannon (1995) was described as consisting of dominantly marine muds with shallow water marine bar sands developed in the shelfal environments surrounding the edge of the basin, adjacent to sediment supply,

particularly the Leinster Massif to the northeast, beyond the study area. In the adjacent Fastnet Basin deltaic sandstones are developed, possibly sourced from local highs surrounding the Fastnet Basin (Ewins & Shannon, 1995).

Within the study area there are Lower Jurassic depocentres of up to 3,500m (11,500ft) located on the northern side of the basin, in the hanging wall of the Morrigan Fault (Appendix G.2). There is limited well control in the areas of thickest Lower Jurassic in the NCSB to confirm the facies. Based on the adjacent Fastnet Basin, there is significant potential for deltaic sandstones within the NCSB Lower Jurassic depocentres, sourced from reworked Devonian sediments of the adjacent Irish Massif, controlled by extension along the Morrigan Fault.

An illustrative 3-D model is presented in Figure 9-1 to describe the potential structure and a cartoon of conceptual sedimentological processes and facies of the Lower Jurassic sequence.

The illustration (Figure 9-1) shows the Triassic depth surface (base Lower Jurassic), with present day depth contours within a half-graben geometry. The colour drape over the structure represents the thickness of the entire Lower Jurassic (up to the Callovian-Oxfordian Unconformity). A cartoon of conceptual sediment input points and submarine fan/delta deposits are overlain as an example of conceptual sediment patterns that might exist in response to the proposed structural model (Leader, 2011), although clearly significant additional well control or modern 3D seismic data would be required to review the potential for such sediment patterns.

Analysis of the hydrocarbon prospectivity of the Lower Jurassic would initially concentrate on the identification of valid structural highs coincident with potential reservoir facies. The Callovian-Oxfordian Unconformity depth map presented in Figure 9-2 highlights two structurally high areas. These two areas are coincident within a thick Lower Jurassic sequence, which could indicate a potential thick reservoir development, potentially of marine fan/delta deposits as discussed above and by Ewins and Shannon (1995).

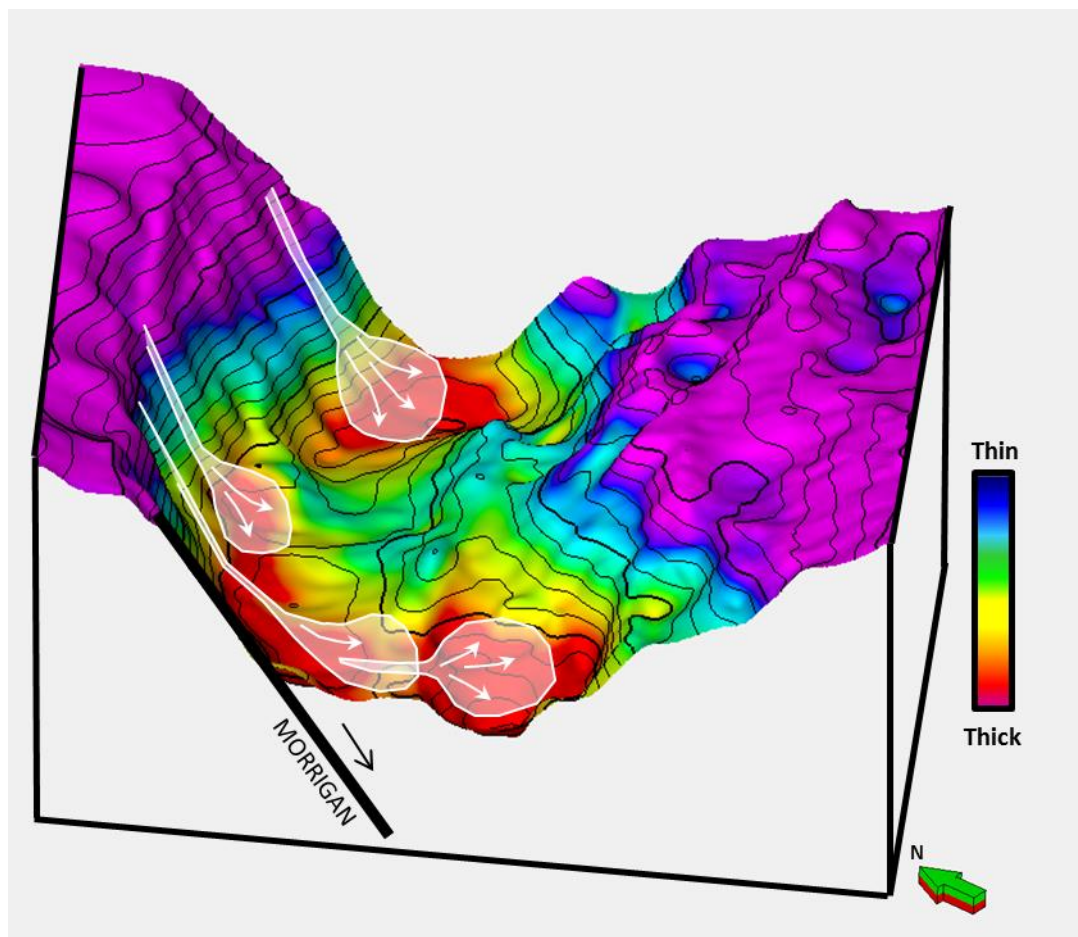


Figure 9-1. Triassic depth structure map (present day), coloured by overlying Lower Jurassic sediment thickness. Conceptual sediment patterns related to

the proposed structural model are proposed within the thickest sediment areas, with sediment controlled by the Morrigan Fault.

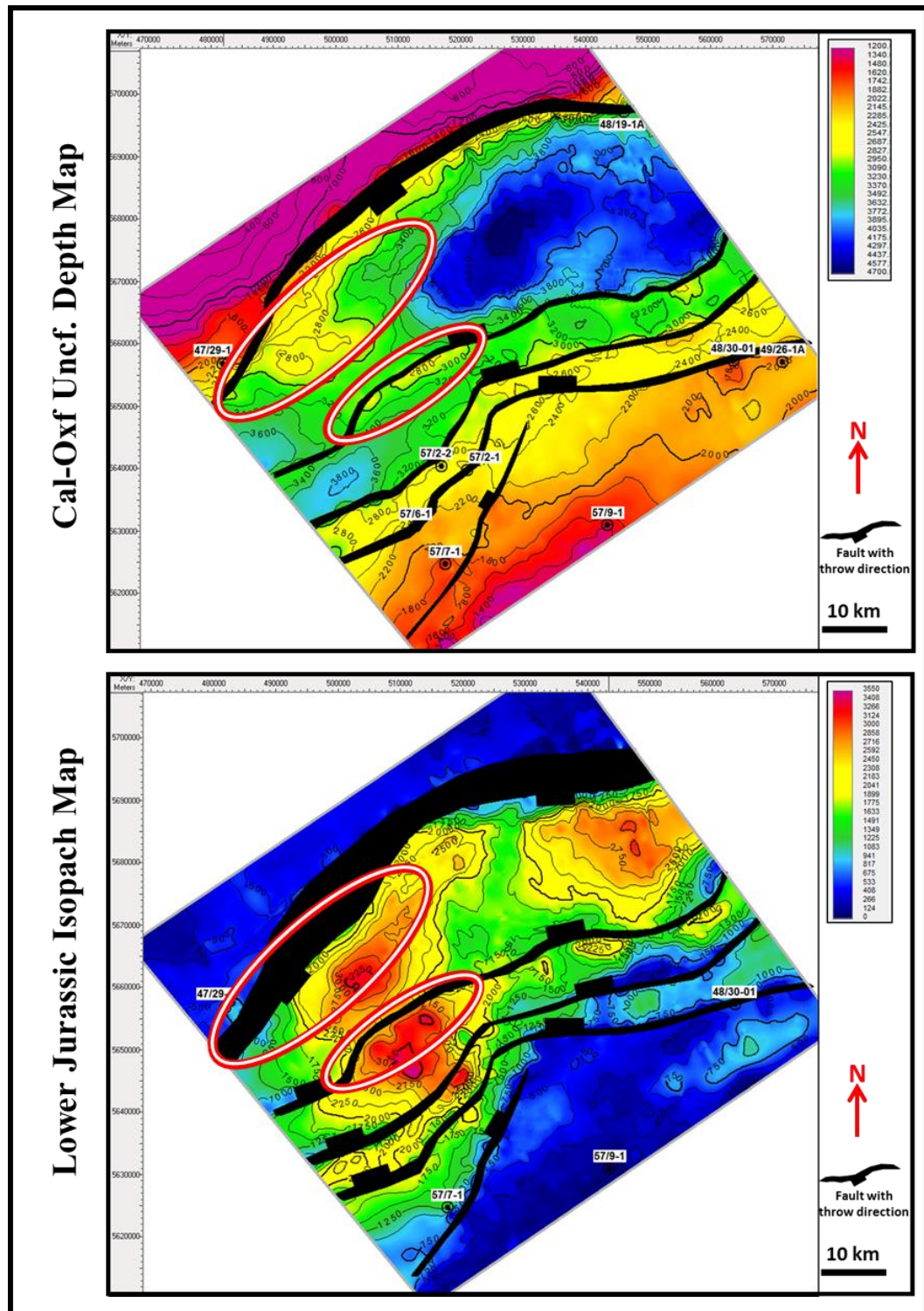


Figure 9-2. Depth map of the Callovian-Oxfordian Unconformity (top) and Lower Jurassic thickness (bottom). Structurally high areas which are

coincident with thick sediment are highlighted as areas of potential interest for Lower Jurassic hydrocarbon exploration. Note - faults are present day.

9.1.2 Upper Jurassic

The Upper Jurassic saw renewed rifting and the development of antithetic faults to the Morriggan Fault. Sedimentation was influenced strongly by regional tectonism producing a range of depositional environments from shallow marine, alluvial plain, fluvial deltaic and ultimately lacustrine (Ewins & Shannon, 1995). The UJ1 sequence of Ewins & Shannon (1995) is particularly well understood in the northeast of the basin (beyond the current study area) where there is well control. Non marine deltaics to shallow or restricted marine sediments are seen, particularly close to sediment input points. Closer to the study area, the Fastnet Basin and South Celtic Sea Basin were experiencing uplift and potentially providing coarse clastic sediments into the study area.

An illustrative 3-D model is presented in Figure 9-3 to describe the potential structure and a cartoon of conceptual sedimentological processes and facies of the Upper Jurassic sequence.

The illustration (Figure 9-3) shows the Callovian-Oxfordian depth surface (base Upper Jurassic), with present day depth contours within a conventional-graben geometry. The colour drape over the structure represents the thickness of the entire Upper Jurassic. A cartoon of conceptual sediment input points and submarine fan/delta deposits are overlain as an example of conceptual sediment patterns that might exist in response to the proposed structural model (Leader, 2011), although

clearly significant additional well control or modern 3D seismic data would be required to review the potential for such sediment patterns.

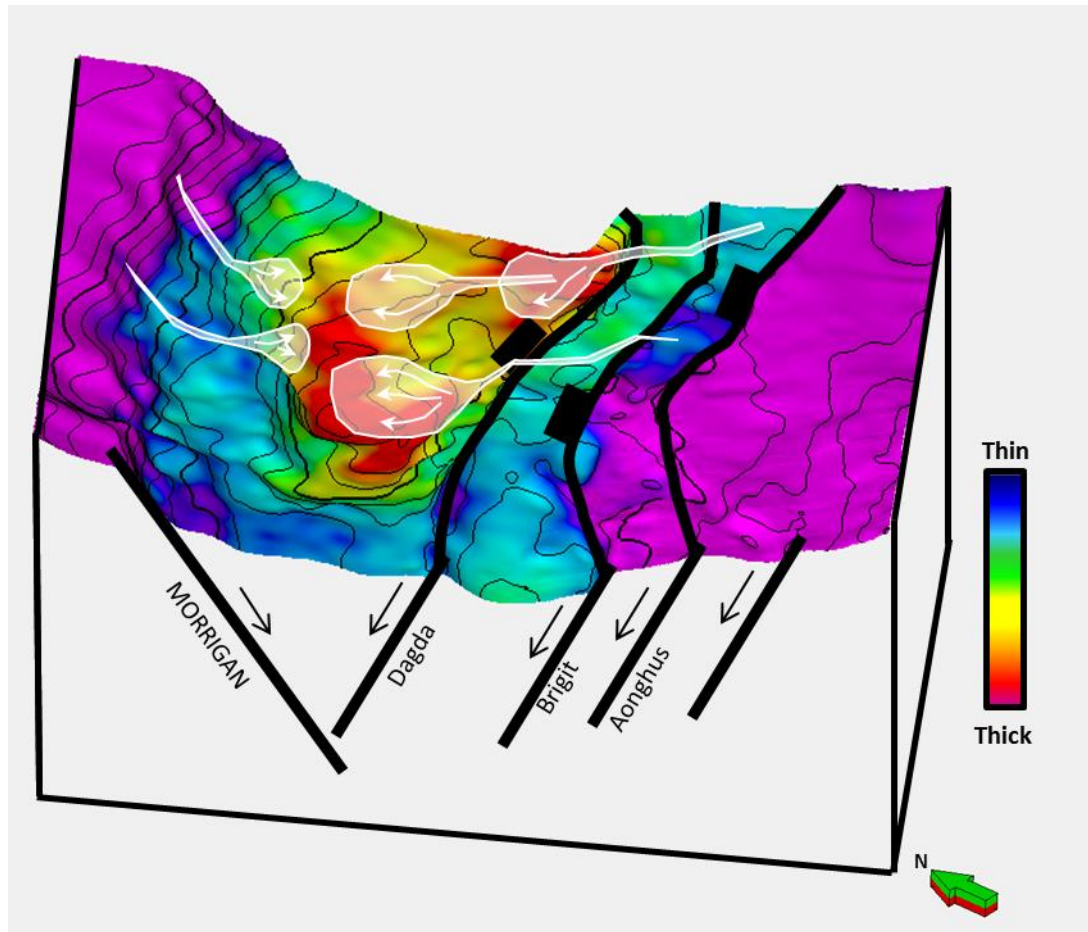


Figure 9-3. Callovian-Oxfordian Unconformity depth structure map (present day) with syn-depositional faults, coloured by overlying Upper Jurassic sediment thickness. Conceptual sediment patterns related to the proposed structural model are proposed within the thickest sediment areas. Note the conventional graben architecture, and the thickest sediment adjacent to the Dagda Fault.

Analysis of the hydrocarbon prospectivity of the Upper Jurassic would initially concentrate on the identification of valid structural highs coincident with potential

reservoir facies. The Base Cretaceous depth map presented in Figure 9-4 highlights a structurally high area. This area is coincident with a thick Upper Jurassic sequence, which could indicate a potential thick reservoir development, potentially of marine fan/delta deposits as discussed above.

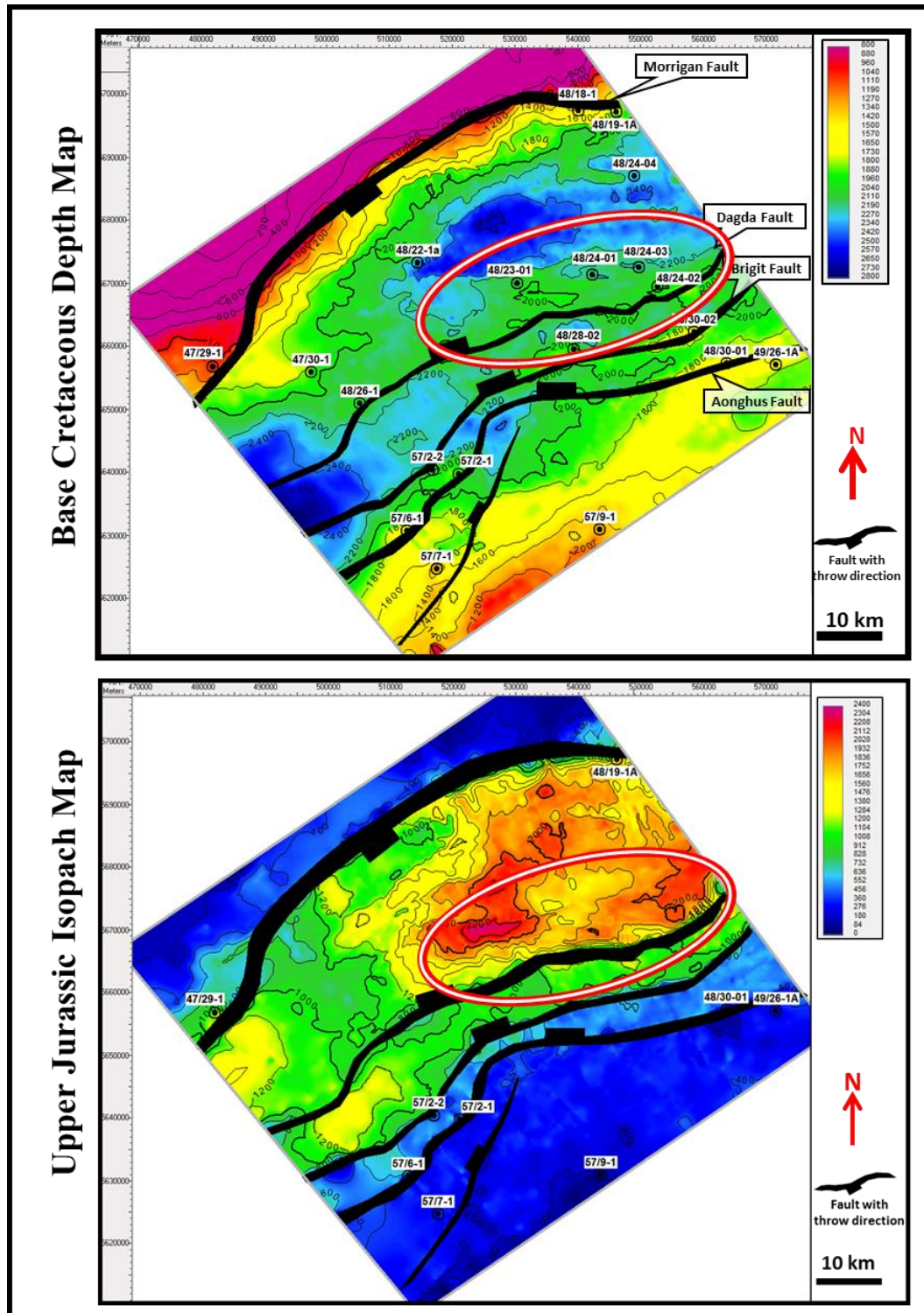


Figure 9-4. Depth map of the Base Cretaceous (top) and Upper Jurassic thickness (bottom). A structurally high areas which is coincident with thick sediment is highlighted as an area of potential interest for Upper Jurassic hydrocarbon exploration.

9.2 Source Potential

The shales of the Lower Jurassic unit are a possible source of the gas at the Kinsale Head Gas Field (Colley, 1981) and a source rock for the Helvick Oil Field (Caston, 1995). Thick lacustrine shales of Purbeck Formation (Tithonian-Valanginian) are the source rock for the Barryroe Oil Discovery (Howell & Griffiths, 1995). The presence, thickness and burial history of these intervals is important in reviewing any prospectivity believed to be sourced from these shales. The structural model proposed here would be a critical new input to future Petroleum Systems Models which assess potential hydrocarbon generation, expulsion and migration.

9.3 Renewed Interest

The NCSB has seen a renewed interest with modern multi-client seismic data acquired by Petroleum Geo-Services and GeoPartners (Chapter 4). It is generally accepted that multiclient surveys are not acquired without significant financial underwriting. The Petroleum Geo-Services and GeoPartners surveys represent a combined investment of approximately 10 million USD using standard industry metrics. This level of financial underwriting suggests major international oil and gas companies are once again actively reviewing the prospectivity of the NCSB, underwriting these seismic surveys. The extent of these surveys is shown in Figure 9-5.

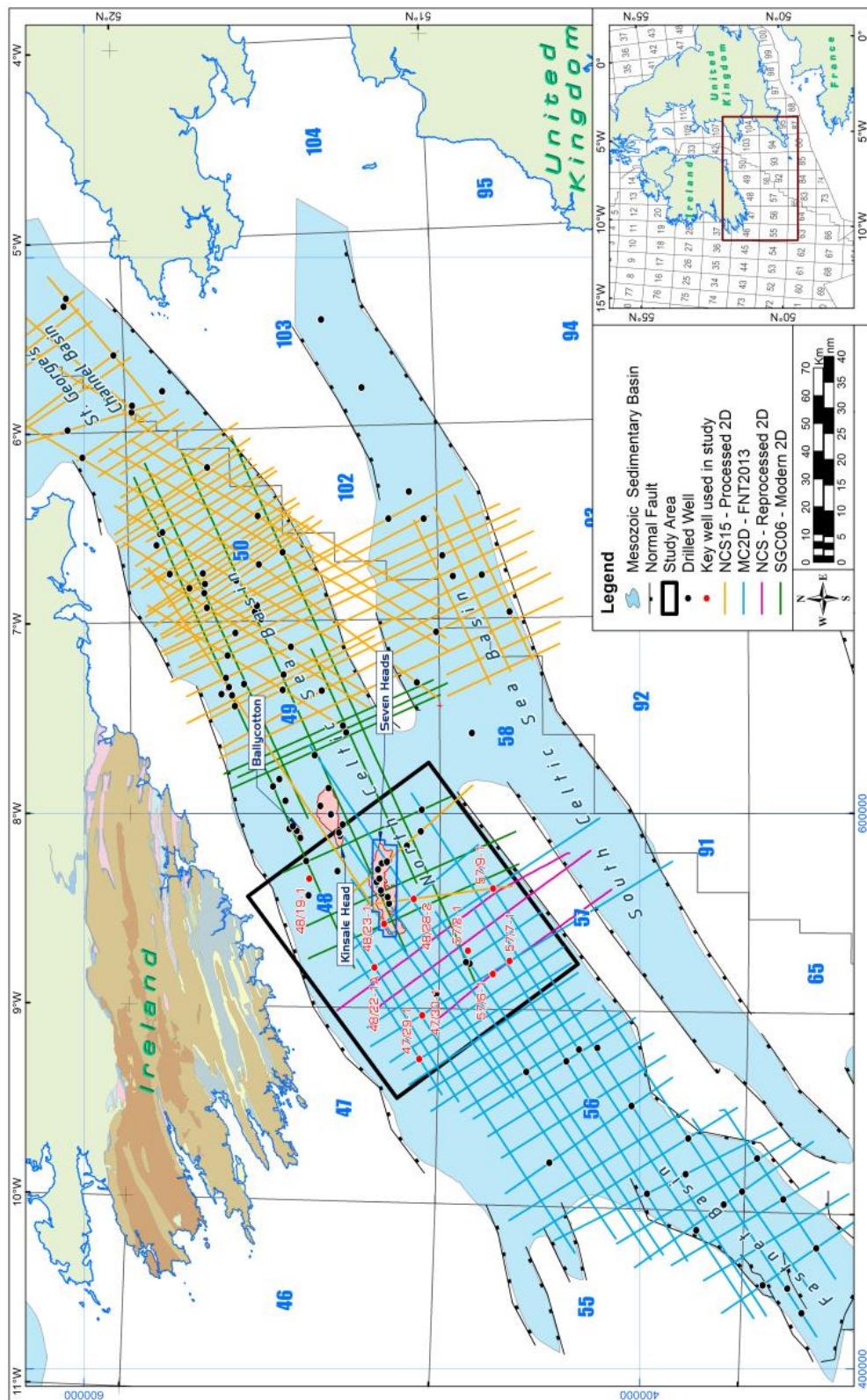


Figure 9-5. Regional multi-client seismic data recently acquired by Petroleum Geo-Services (blue) and GeoPartners (yellow).

This renewed interest may have been sparked by the Barryroe oil discovery, the shallow water environment and proximity to major European markets. The award of 17 blocks or part blocks to Eni S.p.A. in the adjacent basin St George's Channel Basin in 2014 is evidence of this. Comparing the issued hydrocarbon authorisations in the NCSB before the drilling of the 48/24-10z Barryroe oil well in 2011 (Figure 9-6) and the issued hydrocarbon authorisations in 2016 (Figure 9-7) also demonstrates the significant renewed interest in the hydrocarbon prospectivity of the NCSB.

In 2018 Providence Resources Plc and Lansdowne Oil & Gas Plc agreed to farm-out a 50% working interest in Barryroe to a Chinese consortium in return for funding 100% of drilling costs for 5 firm wells and 2 option wells, and a cash advance of \$19.5 million (Providence, 2018). This commercial deal once again shows the renewed interest in the NCSB and the significant investment it can attract.

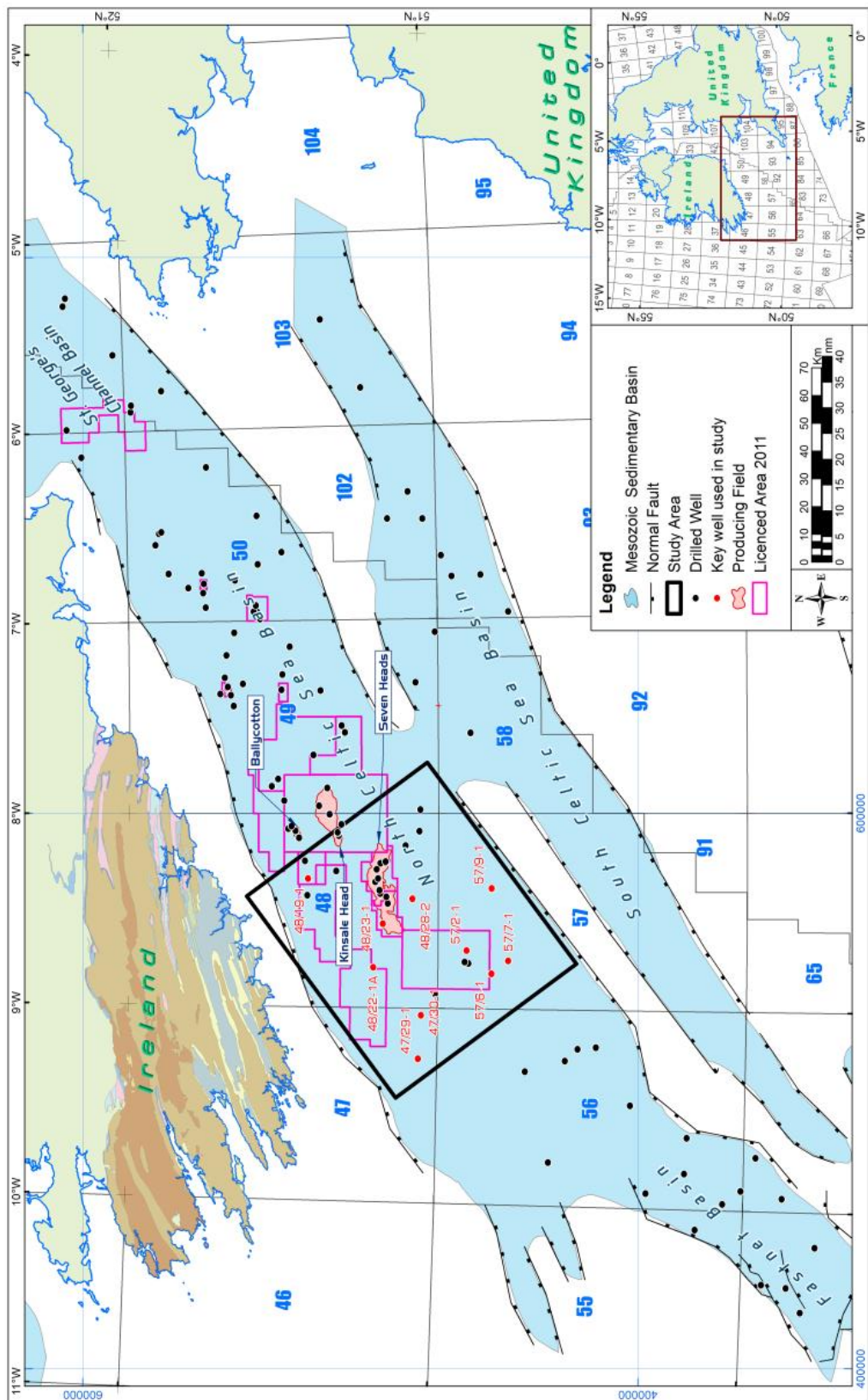


Figure 9-6. Licence authorisations in 2011.

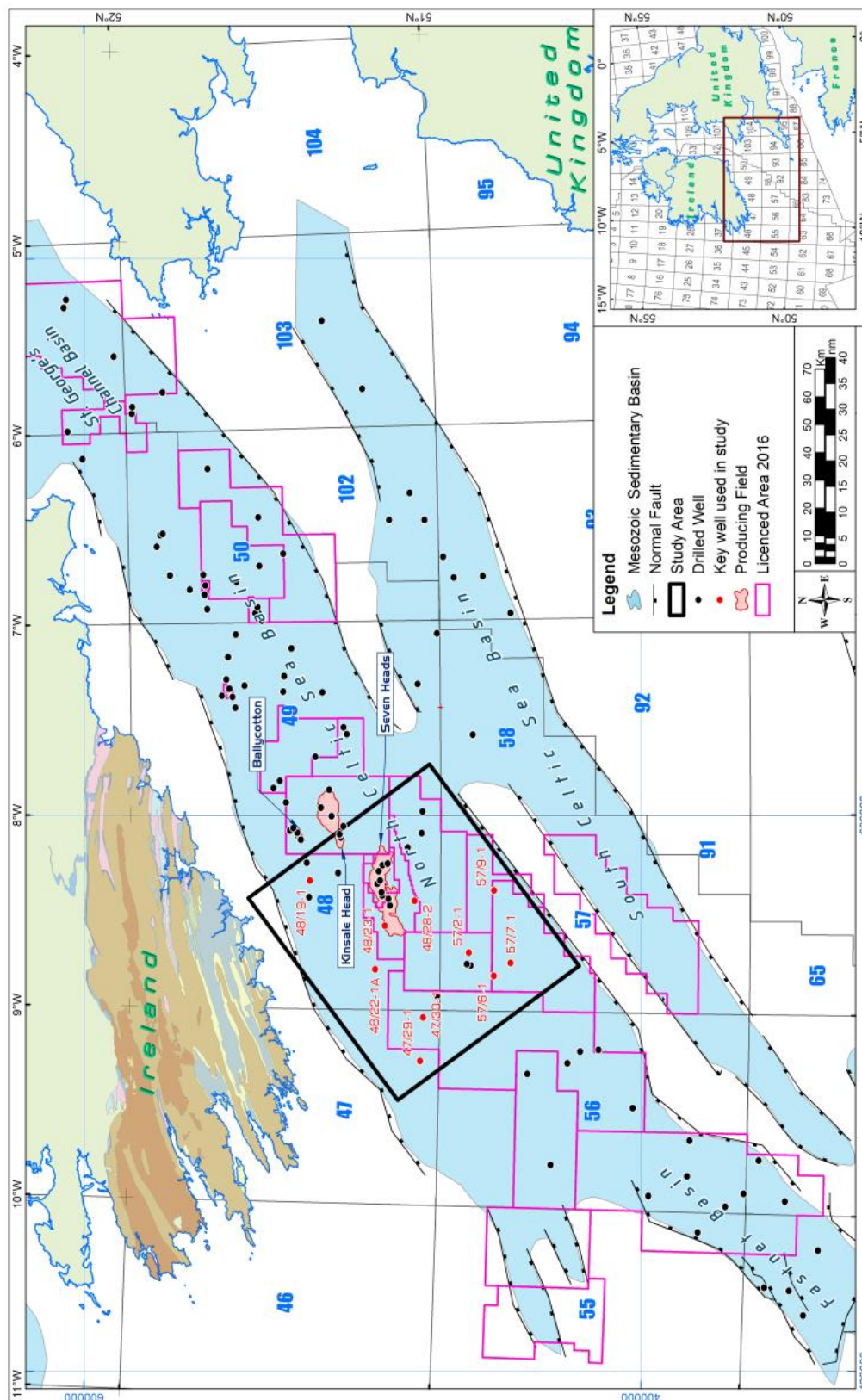


Figure 9-7. Licence authorisations in 2016.

10 Conclusions

The study has accessed the available modern 2D and 3D seismic data over a large portion of the NCSB. The historic models of structural development of the NCSB were compared against the modern seismic data, finding neither model accurately reflected the regional faults evident on the modern seismic data.

An updated interpretation of faults and major geological units was completed over the study area utilising the modern seismic data, with existing well control used to provide stratigraphic constraint. Regional knowledge from adjacent basins was integrated to ensure the interpretation fit within the regional stratigraphic and structural history.

The updated interpretation of the modern seismic data was used to propose an updated best fit structural evolution model for the NCSB.

The conclusions of the interpretation and the subsequent updated structural evolution model can be summarised as:

- Modern seismic acquisition and processing techniques provide images of the entire Mesozoic section in the North Celtic Sea Basin providing a new database to examine basin development.
- Triassic sediments are interpreted to be deposited in a series of half grabens across the entire basin, based on seismic character away from known well control and evidence of minor halokinesis.

- The modern seismic data suggests extensive deposition of SSG across the NCSB rather than being thin or restricted (Musgrove, 1995; Naylor & Shannon, 2011).
- Lower Jurassic sediments were controlled dominantly by the northern basin bounding “Morrigan” fault in a large half graben geometry.
- Seismic data supports over 6 kilometres (20,000 feet) of Triassic and Early Jurassic sediment was deposited in the NCSB.
- Evaporites within highly rotated Triassic half grabens is proposed as a decollement surface for the development of new antithetic faults to the Morrigan Fault, creating a conventional graben geometry throughout the Upper Jurassic and Lower Cretaceous rifting.
- Interpretation of the modern seismic data suggests Lower Cretaceous syn-rift faulting, which was not previously recognised.
- Cenozoic compression was preferentially accommodated on the antithetic faults due to their decollement in Triassic halites.
- Seismic data in this study combined with the uplift described by Murdoch *et al.* (1995) supports up to 11 kilometres (36,000 feet) of Mesozoic sediment was deposited in the NCSB.
- Improved exploration success in the NCSB is heavily dependent on accurate fault-controlled sediment facies distributions and predictions.

11 Recommendations For Further Study

- Sedimentological modelling of the Barryroe oil discovery describes the reservoir level within the Lower Wealden as a braid plain which is extensive over a large area. Further study to understand the paleogeographical and structural context for this depositional environment may be critical to discovering additional analogue prospects within the NCSB.
- Hydrocarbon exploration would benefit from a full suite of paleogeography maps for the entire NCSB taking into account this revised structural model and the recent biostratigraphic and lithostratigraphic nomenclature (Copestake et al., 2018). The current study area in isolation is insufficient to provide robust basin wide paleogeography maps.
- Due to the hard sea bottom seismic acquisition requires a large airgun. Large regional surveys should be encouraged rather than small localised surveys.
- Reprocessing of vintage 2D requires good demultiple techniques, often several passes, and a good understanding of the regional velocity.

References Cited

- Al-Chalabi, M. 2014. *Principles of Seismic Velocities and Time-to-Depth Conversion*.
- Anderson, E. 1951. *The Dynamics of Faulting and Dyke Formation with Applications to Britain.*, 2nd ed.. Edinburgh, Oliver and Boyd.
- Baker, B.M., Mohr, P.A. & Williams, L.A.J. 1972. Geology of the eastern rift system of Africa. *Geological Society of America Special Paper*, **136**, 67.
- Bancroft, J.C. 2007. *A Practical Understanding of Pre- and Poststack Migrations*. Society of Exploration Geophysicists.
- Barr, D. 1987. Lithospheric stretching, detached normal faulting and footwall uplift. *In: Geological Society, London, Special Publications*. 75–94.
- Barr, K.W., Colter, V.S. & Young, R. 1981. The geology of the Cardigan Bay-St. George's Channel Basin. *In: Illing, L. V. & Hobson, G. D. (eds) Petroleum Geology Conference Series Vol 2*. Geological Society of London, 432–443.
- Barton, N. 2006. *Rock Quality, Seismic Velocity, Attenuation and Anisotropy*.
- BIRPS. 1999. *The BIRPS Atlas II : A Second Decade of Deep Seismic Reflection Profiling*. Snyder, D. B. & Hobbs, R. W. (eds). Geological Society.
- BIRPS & ECORS. 1986. *Deep Seismic Reflection Profiling between England, France and Ireland*.
- Blundell, D.J. 1970. Interpretation of profiler records from the southern Irish Sea and the Celtic Sea. *Proceedings of the Geological Society*, 183–185.
- Blundell, D.J., Davey, F.J. & Graves, L.J. 1971. Geophysical surveys over the South Irish Sea and Nymphe Bank. *Journal of the Geological Society*, **127**, 339–375.

- Bois, C., Cazes, M., Hirn, A., Mascle, A., Matte, P., Montadert, L. & Pinet, B. 1988. Contribution of deep seismic profiling to the knowledge of the lower crust in France and neighbouring areas. *Tectonophysics*, **145**, 253–275.
- Bois, C., Lefort, J.P., Le Gall, B., Sibuet, J.C., Gariel, O., Pinet, B. & Cazes, M. 1990. Superimposed Variscan, Caledonian and Proterozoic features inferred from deep seismic profiles recorded between southern Ireland, southwestern Britain and western France. *Tectonophysics*, **177**, 15–37.
- Brewer, R.J. 2000. VSP Survey Meets Accuracy Demands. *AAPG Explorer*.
- Brewer, R.J. 2000. VSP is a Check Shot Step Up. *AAPG Explorer*.
- Brown, A.R. 2011. *Interpretation of Three-Dimensional Seismic Data*. Society of Exploration Geophysicists and American Association of Petroleum Geologists.
- Brun, J.P. & Beslier, M.O. 1996. Mantle exhumation at passive margins. *Earth and Planetary Science Letters*, **142**, 161–173.
- Bulnes, M. & McClay, K.R. 1998. Structural analysis and kinematic evolution of the inverted central South Celtic Sea Basin. *Marine and Petroleum Geology*, **15**, 667–687.
- Caine, J.S., Evans, J.P. & Forster, C.B. 1996. Fault zone architecture and permeability structure. *Geology*.
- Cameron, D.E., Carter, J. & McCallum, D. 2017. Structural and Depositional Characteristics of Mesozoic Rift Section-Jeanne d’Arc to Flemish Cap Graben, Offshore Newfoundland and Labrador, Canada. *In: AAPG International Conference and Exhibition*.
- Caston, V.N.D. 1995. The Helvick oil accumulation, Block 49/9, North Celtic Sea Basin. *In: Croker, P. F. & Shannon, P. M. (eds) Geological Society, London, Special Publications*. 209–225.

- Chadwick, R.A., Livermore, R.A. & Penn, I.E. 1989. Continental Extension in Southern Britain and Surrounding Areas and Its Relationship to the Opening of the North Atlantic Ocean. *In: Tankard, A. J. & Balkwill, H. R. (eds) Extensional Tectonics and Stratigraphy of the North Atlantic Margins.* American Association of Petroleum Geologists.
- Cheadle, M.J., McGeary, S., Warner, M.R. & Matthews, D.H. 1987. Extensional structures on the western UK continental shelf: A review of evidence from deep seismic profiling. *In: Geological Society, London, Special Publications.*
- Childs, C., Watterson, J. & Walsh, J.J. 1995. Fault overlap zones within developing normal fault systems. *Journal of the Geological Society*, **152**, 535–549.
- Childs, C., Watterson, J. & Walsh, J.J. 1996. A model for the structure and development of fault zones. *Journal of the Geological Society.*
- Childs, C., Holdsworth, R.E., Jackson, C.A.L., Manzocchi, T., Walsh, J.J. & Yielding, G. 2017. Introduction to the geometry and growth of normal faults. *In: Geological Society, London, Special Publications.* 1–9.
- Childs, C., Manzocchi, T., Walsh, J.J., Bonson, C.G., Nicol, A. & Schöpfer, M.P.J. 2009. A geometric model of fault zone and fault rock thickness variations. *Journal of Structural Geology.*
- Clayton, G., Sevastopulo, G.D. & Sleeman, A.G. 1986. Carboniferous (Dinantian and Silesian) and Permo-Triassic rocks in south County Wexford, Ireland. *Geological Journal*, **21**, 355–374.
- Colley, M.G., McWilliams, A.S.F. & Myers, R.C. 1981. Geology of the Kinsale Head gas field, Celtic Sea, Ireland. *In: Illing, L. V. & Hobson, G. D. (eds) Petroleum Geology Conference Series Vol 2.* Geological Society of London, 504–510.

- Colter, V.S. 1997. The East Irish Sea Basin-from caterpillar to butterfly, a thirty-year metamorphosis. *In*: Meadows, N. S., Trueblood, S. P., Hardman, M. & Cowan, G. (eds) *Petroleum Geology of the Irish Sea and Adjacent Areas*. Geological Society of London Spec Pub 124, 1–9.
- Colter, V.S. & Havard, D.J. 1981. The Wytch Farm Oil Field, Dorset. *In*: Illing, L. V. & Hobson, G. D. (eds) *Petroleum Geology Conference Series Vol 2*. Geological Society of London, 494–503.
- Copetake, P; Ainsworth, N. R.; Bailey, H. W.; Gallagher, L. T.; Gueinn, K.; Hampton, M.; Lavis, O. M.; Loy, T.; Riley, L. A.; Wright, T.D. 2018. A new standard lithostratigraphic framework for offshore Ireland. *In*: *Atlantic Ireland Conference*.
- Coward, M.P. & Trudgill, B. 1989. Basin Development and Basement Structure of the Celtic Sea Basins (SW Britain). *Bulletin de la Societe Geologique de France*, **V**, 423–436.
- Cowie, P.A., Gupta, S. & Dawers, N.H. 2000. Implications of fault array evolution for synrift depocentre development: Insights from a numerical fault growth model. *Basin Research*, **12**, 241–261.
- Curry, M.A.E., Barnes, J.B. & Colgan, J.P. 2016. Testing fault growth models with low-temperature thermochronology in the northwest Basin and Range, USA. *Tectonics*, **35**, 2467–2492.
- Davey, F.J. 1971. Bouguer Anomaly Map of the North Celtic Sea and Entrance to the Bristol Channel. *Geophysical Journal of the Royal Astronomical Society*, **22**, 277–282.
- Davis, G.H. & Hardy, J.J. 1981. The Eagle Pass detachment, southeastern Arizona: product of mid- Miocene listric(?) normal faulting in the southern Basin and Range. *Geological Society of America Bulletin*, **92**, 749–762.

- Davis, George H.; Reynolds, Stephen J.; Kluth, C. 2012. *Structural Geology of Rocks and Regions*. Wiley.
- Davison, I., Alsop, G.I., Evans, N.G. & Safaricz, M. 2000. Overburden deformation patterns and mechanisms of salt diapir penetration in the Central Graben, North Sea. *Marine and Petroleum Geology*, **17**, 601–618.
- Day, G.A. & Edwards, J.W.F. 1989. Influences of Variscan Structures Off Southwest Britain on Subsequent Phases of Extension. *In: European-African Margins*. AAPG Special Volumes, 425–432.
- Day, G.A. & Williams, C.A. 1970. Gravity compilation in the N.E. Atlantic and interpretation of gravity in the Celtic Sea. *Earth and Planetary Science Letters*, **8**, 205–213.
- DCCAE. 2019. Integrated Petroleum Affairs System.
<http://gis.dcenr.gov.ie/internetIPAS/servlet/internet/IPAS2IHome>.
- de Joussineau, G. & Aydin, A. 2009. Segmentation along Strike-Slip Faults Revisited. *In: Mechanics, Structure and Evolution of Fault Zones*. Birkhäuser Basel, 1575–1594.
- Delanty, L.J., Whittington, R.J. & Dobson, M.R. 1981. The Geology of the North Celtic Sea West of 7° Longitude. *Proceedings of the Royal Irish Academy. Section B: Biological, Geological, and Chemical Science*, **81**, 37–51.
- Devereaux, S. 1998. *Practical Drilling and Well Planning Manual*. PennWell Corporation.
- Dewey, J.F. 1982. Plate tectonics and the evolution of the British Isles. *Journal of the Geological Society*, **139**, 371.
- Doré, a G., Lundin, E.R., et al. 1999. Principal tectonic events in the evolution of the northwest European Atlantic margin. *In: Petroleum Geology Conference Series Vol 5*. Geological Society of London, 41–61.

- Driscoll, N.W. & Karner, G.D. 1998. Lower crustal extension across the Northern Carnarvon basin, Australia: Evidence for an eastward dipping detachment. *Journal of Geophysical Research: Solid Earth*.
- Dunbar, J.A. & Sawyer, D.S. 1988. Continental rifting at pre-existing lithospheric weaknesses. *Nature*, **333**, 450–452.
- Dyment, J. 1989. SWAT et les bassins celtiques: relations avec la croûte hercynienne, Moho neoforme. *Bulletin de la Societe Geologique de France*, **8**, 477–487.
- Dyment, J. & Bano, M.C. 1991. Deep crustal features of the Celtic Sea from complementary processing on the SWAT data. *Geophysical Journal International*, **105**, 71–83.
- Dyment, J., Sibuet, J.C. & Pinet, B. 1990. Deep structure of the Celtic Sea: a discussion on the formation of basins. *Tectonophysics*, **173**, 435–444.
- Ebinger, C.J., Rosendahl, B.R. & Reynolds, D.J. 1987. Tectonic model of the Malaŵi rift, Africa. *Tectonophysics*.
- Elliott, D. 1976. The Energy Balance and Deformation Mechanisms of Thrust Sheets. *Philosophical Transactions of the Royal Society A: Mathematical, Physical and Engineering Sciences*, **283**, 289–312.
- Etheridge, M.A., Symonds, P.A. & Lister, G.S. 1989. Application of the Detachment Model to Reconstruction of Conjugate Passive Margins Tankard, A. J. & Balkwill, H. R. (eds). *Extensional Tectonics and Stratigraphy of the North Atlantic Margins*, **46**.
- Evans, C.D.R., Hillis, R.R., Gatliff, R.W., Day, G.A. & Edwards, J.W.F. 1990. *The Geology of the Western English Channel and Its Western Approaches*. British Geological Survey.

- Evans, D., Graham, C., Armour, A. & Bathurst, P. 2003. *The Millennium Atlas: Petroleum Geology of the Central and Northern North Sea*. Geological Society of London.
- Evans, J.P. 1990. Thickness-displacement relationships for fault zones. *Journal of Structural Geology*.
- Evans, J.P., Forster, C.B. & Goddard, J. V. 1997. Permeability of fault-related rocks, and implications for hydraulic structure of fault zones. *Journal of Structural Geology*, **19**, 1393–1404.
- Evenick, J. 2008. *Introduction to Well Logs and Subsurface Maps*. PennWell.
- Ewins, N.P. & Shannon, P.M. 1995. Sedimentology and diagenesis of the Jurassic and Cretaceous of the North Celtic Sea and Fastnet Basins Croker, P. F. & Shannon, P. M. (eds). *Geological Society, London, Special Publications*, **93**, 139–169.
- Faulkner, D.R., Jackson, C.A.L., Lunn, R.J., Schlische, R.W., Shipton, Z.K., Wibberley, C.A.J. & Withjack, M.O. 2010. A review of recent developments concerning the structure, mechanics and fluid flow properties of fault zones. *Journal of Structural Geology*.
- Faulkner, D.R., Mitchell, T.M., Jensen, E. & Cembrano, J. 2011. Scaling of fault damage zones with displacement and the implications for fault growth processes. *Journal of Geophysical Research: Solid Earth*.
- Ferrill, D.A. & Morris, A.P. 2001. Displacement gradient and deformation in normal fault systems. *Journal of Structural Geology*, **23**, 619–638.
- Ferrill, D.A., Morris, A.P., McGinnis, R.N., Smart, K.J., Watson-Morris, M.J. & Wigginton, S.S. 2016. Observations on normal-fault scarp morphology and fault system evolution of the Bishop Tuff in the Volcanic Tableland, Owens Valley, California, U.S.A. *Lithosphere*, **8**, 238–253.

- Ferrill, D.A., Morris, A.P., McGinnis, R.N., Smart, K.J., Wigginton, S.S. & Hill, N.J. 2017. Mechanical stratigraphy and normal faulting. *Journal of Structural Geology*.
- Ferrill, D.A., Stamatakis, J.A. & Sims, D. 1999. Normal fault corrugation: Implications for growth and seismicity of active normal faults. *Journal of Structural Geology*, **21**, 1027–1038.
- Fort, X. & Brun, J.-P. 2012. Kinematics of regional salt flow in the northern Gulf of Mexico. *In: Geological Society, London, Special Publications*. 265 LP – 287.
- Fossen, H. 2016. *Structural Geology*, 2nd ed. Cambridge University Press.
- Francis, A. 2018a. A Simple Guide to Seismic Depth Conversion I. *GEO ExPro*, **15**.
- Francis, A. 2018b. A Simple Guide to Seismic Depth Conversion II. *GEO ExPro*, **15**.
- Funck, T., Geissler, W.H., Kimbell, G.S., Gradmann, S., Erlendsson, Ö., Mcdermott, K. & Petersen, U.K. 2017. Moho and basement depth in the NE Atlantic Ocean based on seismic refraction data and receiver functions. *In: Geological Society, London, Special Publications*. Geological Society of London, 207–231.
- Gardiner, P.R.R. & Sheridan, D.J.R. 1981. Tectonic framework of the Celtic Sea and adjacent areas with special reference to the location of the Variscan Front. *Journal of Structural Geology*, **3**, 317–331.
- Garfunkel, A. & Bartov, Y. 1977. Tectonics of the Suez rift. *Geological Survey of Israel Bulletin*, **71**, 44.

- Geluk, M. C.; Paar, W. A.; Fokker, P.A. 2007. Salt. *In*: Wong, T., Batjes, D. A. J. & de Jager, J. (eds) *Geology of the Netherlands*. Royal Netherlands Academy of Arts and Sciences, 283–294.
- Ghalayini, R., Homberg, C., Daniel, J.M. & Nader, F.H. 2017. Growth of layer-bound normal faults under a regional anisotropic stress field. *In: Geological Society, London, Special Publications*. Geological Society of London, 57–78.
- Gibbs, A.D. 1984. Structural evolution of extensional basin margins. *Journal of the Geological Society*, **141**, 609–620.
- Gibbs, A.D. 1989. Structural Styles in Basin Formation. *In*: Tankard, A. J. & Balkwill, H. R. (eds) *Extensional Tectonics and Stratigraphy of the North Atlantic Margins*. American Association of Petroleum Geologists.
- Gillis, E., Wright, R., McCallum, D., Stead, L. & Mitchell, V. 2018. New Insights on Prospectivity of the eastern Orphan Basin, Newfoundland and Labrador, Canada. *In: Conjugate Margins Conference*. Halifax.
- Gregory, J.W. 1921. *The Rift Valleys and Geology of East Africa*. Seeley, Service & Co. limited.
- Groshong, JR., Ri.H. & GROSHONG, R.H.J. 1988. Low-temperature deformation mechanisms and their interpretation. *Geological Society of America Bulletin*, **100**, 1329–1360.
- Hagelund, R. & Levin, S.A. 2017. *SEG-Y Revision 2.0 Data Exchange Format*.
- Harding, R. & Huuse, M. 2015. Salt on the move: Multi stage evolution of salt diapirs in the Netherlands North Sea. *Marine and Petroleum Geology*.
- Herron, D.A. 2011. *First Steps in Seismic Interpretation*. Society of Exploration Geophysicists.

- Hiscott, R.N. 1990. Comparative stratigraphy and subsidence history of Mesozoic rift basins of North Atlantic. *American Association of Petroleum Geologists Bulletin*, **74**, 60–76.
- Holdsworth, R.E. & Turner, J.P. 2002. *Extensional Tectonics: Regional-Scale Processes*. Geological Society of London.
- Howell, T.J. & Griffiths, P. 1995. A study of the hydrocarbon distribution and Lower Cretaceous Greensand prospectivity in Blocks 48/15, 48/17, 48/18 and 48/19, North Celtic Sea Basin Croker, P. F. & Shannon, P. M. (eds). *Geological Society, London, Special Publications*, **93**, 261–275.
- Hudec, M.R. & Jackson, M.P.A. 2007. Terra infirma: Understanding salt tectonics. *Earth-Science Reviews*, **82**, 1–28.
- Ikelle, L.T. & Amundsen, L. 2018. *Introduction to Petroleum Seismology*, 2nd ed. Society of Exploration Geophysicists.
- Illies, H. 1974. Intra-Plattentektonik in Mitteleuropa und der Rheingraben. *Oberrhein. Geol. Abh.*, **23**, 1–24.
- IOGP. 2018. *Geomatics Guidance Note 7, Part 2*.
- Jackson, C.A.-L., Bell, R.E., Rotevatn, A. & Tvedt, A.B.M. 2017. Techniques to determine the kinematics of synsedimentary normal faults and implications for fault growth models. *Geological Society, London, Special Publications*, **439**.
- Jackson, C.A.L. & Lewis, M.M. 2016. Structural style and evolution of a salt-influenced rift basin margin; the impact of variations in salt composition and the role of polyphase extension. *Basin Research*.
- Jackson, C.A.-L. & Rotevatn, A. 2013. 3D seismic analysis of the structure and evolution of a salt-influenced normal fault zone: A test of competing fault growth models. *Journal of Structural Geology*, **54**, 215–234.

- Jackson, M.P.A., Vendeville, B.C. & Schultz-Ela, D.D. 1994. Structural Dynamics of Salt Systems. *Annual Review of Earth and Planetary Sciences*, **22**, 93–117.
- Jackson, M. & Vendeville, B. 1994. Regional extension as a geologic trigger for diapirism. *Geological Society of America Bulletin*, **106**, 57–73.
- Jenyon, M.K. 1988. Overburden deformation related to the pre-piercement development of salt structures in the North Sea. *Journal of the Geological Society*, **145**, 445–454.
- Jenyon, M.K. 1985. BASIN-EDGE DIAPIRISM AND UPDIP SALT FLOW IN ZECHSTEIN OF SOUTHERN NORTH SEA. *American Association of Petroleum Geologists Bulletin*, **69**, 53–64.
- Jenyon, M.K. 1984. Seismic response to collapse structures in the Southern North Sea. *Marine and Petroleum Geology*, **1**, 27–36.
- Karlo, J.F., van Buchem, F.S.P., Moen, J. & Milroy, K. 2014. Triassic-age salt tectonics of the Central North Sea. *Interpretation*, **2**, 19–28.
- Kennedy, M. 2015. Practical Petrophysics. *Developments in Petroleum Science*, **62**.
- Kessler, L.G. & Sachs, S.D. 1995. Depositional setting and sequence stratigraphic implications of the Upper Sinemurian (Lower Jurassic) sandstone interval, North Celtic Sea/St George's Channel Basins, offshore Ireland. In: Croker, P. F.; Shannon, P. M. (ed.) *Geological Society, London, Special Publications*. Geological Society Special Publications, 171–192.
- Kim Welford, J., Shannon, P.M., O'Reilly, B.M. & Hall, J. 2010. Lithospheric density variations and Moho structure of the Irish Atlantic continental margin from constrained 3-D gravity inversion. *Geophysical Journal International*, **183**, 79–95.

- Kimbell, G.S., Ritchie, J.D. & Henderson, A.F. 2010. Three-dimensional gravity and magnetic modelling of the Irish sector of the NE Atlantic margin. *Tectonophysics*, **486**, 36–54.
- Kimbell, G.S., Ritchie, J.D., Johnson, H. & Gatliff, R.W. 2005. Controls on the Structure and Evolution of the NE Atlantic Margin Revealed by Regional Potential Field Imaging and 3D Modelling. *In: Petroleum Geology Conference Series Vol 6*. Geological Society of London, 933–945.
- Kockel, F. 1995. *Structural and Palaeogeographical Development of the German North Sea Sector*. Stuttgart, Germany, Schweizerbart Science Publishers.
- Koyi, H. 1988. Experimental modelling of role of gravity and lateral shortening in Zagros mountain belt. *American Association of Petroleum Geologists Bulletin*, **72**, 1381–1394.
- Koyi, H., Jenyon, M.K. & Petersen, K. 1993. The Effect Of Basement Faulting On Diapirism. *Journal of Petroleum Geology*, **16**, 285–312.
- Kusznir, N.J. & Egan, S.S. 1989. Simple-shear and pure-shear models of extensional sedimentary basin formation: application to the Jeanne d’Arc Basin, Grand Banks of Newfoundland. *Extensional tectonics and stratigraphy of the North Atlantic margins*.
- Kusznir, N.J., Marsden, G. & Egan, S.S. 1991. A flexural-cantilever simple-shear/pure-shear model of continental lithosphere extension: applications to the Jeanne d’Arc Basin, Grand Banks and Viking Graben, North Sea. *In: Geological Society, London, Special Publications*. Geological Society of London, 41–60.
- Kusznir, N.J. & Park, R.G. 1987. The extensional strength of the continental lithosphere: Its dependence on geothermal gradient, and crustal composition and thickness. *In: Geological Society, London, Special Publications*. 35–52.

- Landes, M., Prodehl, C., Hauser, F., Jacob, A.W.B. & Vermeulen, N.J. 2000. VARNET-96: influence of the Variscan and Caledonian orogenies on crustal structure in SW Ireland. *Geophysical Journal International*, **140**, 660–676.
- Lavier, L.L. & Manatschal, G. 2006. A mechanism to thin the continental lithosphere at magma-poor margins. *Nature*, **440**, 324–328.
- Leeder, M.R. 2011. *Sedimentology and Sedimentary Basins : From Turbulence to Tectonics*. Wiley-Blackwell.
- Lister, G.S., Etheridge, M.A. & Symonds, P.A. 1986. Detachment faulting and the evolution of passive continental margins. *Geology*, **14**, 246–250.
- Manatschal, G., Lavier, L. & Chenin, P. 2015. The role of inheritance in structuring hyperextended rift systems: Some considerations based on observations and numerical modelling. *Gondwana Research*, **27**.
- Marsden, D. 1989. Layer cake depth conversion. *The Leading Edge*, **8**.
- Masson, D.G. & Miles, P. 1986. Development and hydrocarbon potential of Mesozoic sedimentary basins around margins of North Atlantic. *AAPG Bulletin*, **86**, 721–729.
- Masson, F., Jacob, A.W.B., Prodehl, C., Readman, P.W., Shannon, P.M., Schulze, A. & Enderle, U. 1998. A wide-angle seismic traverse through the Variscan of southwest Ireland. *Geophysical Journal International*, **134**, 689–705.
- McCann, T. 1996. The North Celtic Sea reflector - A possible Caledonian basement structure, offshore southern Ireland. *Tectonophysics*, **266**, 361–377.
- McCann, T. & Shannon, P.M. 1993. Lower Cretaceous seismic stratigraphy and fault movement in the Celtic Sea Basin, Ireland. *First Break*, **11**, 335–344.
- McCann, T. & Shannon, P.M. 1994. Late Mesozoic reactivation of Variscan faults in the North Celtic Sea Basin, Ireland. *Marine and Petroleum Geology*, **11**, 94–103.

- McConnel, R.B. 1972. Geological development of the rift system of eastern Africa. *Geological Society of America Bulletin*, **83**, 2549–2572.
- McDonald, R.E. 1976. Tertiary Tectonics and Sedimentary Rocks Along the Transition: Basin and Range Province to Plateau and Thrust Belt Province, Utah. In: Hill, V. G. (ed.) *Symposium on Geology of Cordilleran Hingeline*. Rocky Mountain Association of Geologists, 281–318.
- McGeary, S., Cheadle, M.R., Warner, M.R. & Blundell, D.J. 1987. Crustal Structure of the continental shelf around Britain derived from BIRPS deep seismic profiling. In: Brooks, J. & Glennie, K. W. (eds) *Petroleum Geology Conference Series Vol 3*. Geological Society of London, 33–41.
- McKenzie, D. 1978. Some remarks on the development of sedimentary basins. *Earth and Planetary Science Letters*, **40**, 25–32.
- McMahon, N.A. & Turner, J.P. 1998. The documentation of a latest Jurassic-earliest Cretaceous uplift throughout southern England and adjacent offshore areas. In: Underhill, J. R. (ed.) *Geological Society, London, Special Publications*. 215–240.
- Meere, P.A. 1995. The structural evolution of the western Irish Variscides: an example of obstacle tectonics? *Tectonophysics*, **246**, 97–112.
- Meunier, J. 2011. *Seismic Acquisition from Yesterday to Tomorrow*. Society of Exploration Geophysicists.
- Millson, J. 1987. The Jurassic evolution of the Celtic Sea basins. In: Brooks, J. & Glennie, K. W. (eds) *Petroleum Geology Conference Series Vol 3*. Geological Society of London, 599–610.
- Mitchell, T.M. & Faulkner, D.R. 2009. The nature and origin of off-fault damage surrounding strike-slip fault zones with a wide range of displacements: A field study from the Atacama fault system, northern Chile. *Journal of Structural Geology*.

- Morley, C.K. 1995. Developments in the structural geology of rifts over the last decade and their impact on hydrocarbon exploration. *In: Geological Society, London, Special Publications*. 1–32.
- Morley, C.K. 2017. The impact of multiple extension events, stress rotation and inherited fabrics on normal fault geometries and evolution in the Cenozoic rift basins of Thailand. *Geological Society, London, Special Publications*, **439**, 413–445.
- Murdoch, L.M., Musgrove, F.W. & Perry, J.S. 1995. Tertiary uplift and inversion history in the North Celtic Sea Basin and its influence on source rock maturity. *In: Croker, P. F. & Shannon, P. M. (eds) Geological Society, London, Special Publications*. 297–319.
- Musgrove, F.W., Murdoch, L.M. & Lenehan, T. 1995. The Variscan fold-thrust belt of southeast Ireland and its control on early Mesozoic extension and deposition: a method to predict the Sherwood Sandstone. *In: Croker, P. F. & Shannon, P. M. (eds) Geological Society, London, Special Publications*. 81–100.
- Nance, R.D., Gutiérrez-Alonso, G., et al. 2012. A brief history of the Rheic Ocean. *Geoscience Frontiers*, **3**, 125–135.
- Naylor, D. (David) & Shannon, P. (Pat). 1982. *Geology of Offshore Ireland and West Britain*. Graham & Trotman.
- Naylor, D. & Mounteney, N. 1975. *Geology of the North-West European Continental Shelf*. Graham Trotman Dudley.
- Naylor, D. & Shannon, P.M. 2011. *Petroleum Geology of Ireland*. Dunedin Academic Press Ltd.
- Newman, P.J. & Worthington, M.H. 1982. In-Situ Investigation Of Seismic Body Wave Attenuation In Heterogeneous Media. *Geophysical Prospecting*, **30**, 377–400.

- Nicol, A., Childs, C., Walsh, J.J., Manzocchi, T. & Schöpfer, M.P.J. 2016. Interactions and growth of faults in an outcrop-scale system. *Geological Society, London, Special Publications*, **439**.
- Norris, D.K. 1958. *Structural Conditions in Canadian Coal Mines*.
- Onajite, E. 2014. Understanding Seismic Interpretation Methodology. In: Onajite, E. (ed.) *Seismic Data Analysis Techniques in Hydrocarbon Exploration*. 177–211.
- O'Reilly, B.M., Shannon, P.M. & Vogt, U. 1991. Seismic studies in the North Celtic Sea Basin: implications for basin development. *Journal of the Geological Society*, **148**, 191–195.
- O'Sullivan, J.M. 2001. The geology and geophysics of the SW Kinsale gas accumulation Shannon, P. M., Haughton, P. D. W. & Corcoran, D. V. (eds). *Geological Society, London, Special Publications*, **188**, 189–199.
- Otsuki, K. 1978. On the relationship between the width of shear zone and the displacement along fault. *The Journal of the Geological Society of Japan*, **84**, 661–669.
- Pascoe, R., Hooper, R.J., Storhaug, K. & Harper, H. 1999. Evolution of extensional styles at the southern termination of the Nordland Ridge , Mid-Norway : a response to variations in coupling above Triassic salt. In: *Petroleum Geology Conference Series Vol 5*. Geological Society of London, 83–90.
- Paton, D.A. 2006. Influence of crustal heterogeneity on normal fault dimensions and evolution: southern South Africa extensional system. *Journal of Structural Geology*, **28**, 868–886.
- Peacock, D.C.P. & Sanderson, D.J. 1994. Geometry and development of relay ramps in normal fault systems. *American Association of Petroleum Geologists Bulletin*, **78**, 147–165.

- Pegrum, R.M. & Mounteney, N. 1978. Rift basins flanking North Atlantic Ocean and their relation to North Sea area. *AAPG Bulletin*, **62**, 419–441.
- Peron-Pinvidic, G., Manatschal, G. & Osmundsen, P. 2013. Structural comparison of archetypal Atlantic rifted margins: A review of observations and concepts. *Marine and Petroleum Geology*, **43**, 21–47.
- Philcox, M.E. 1964. Compartmental deformation near Buttevant, County Cork, Ireland and its relation to the Variscan thrust front. *Scientific Proceedings of the Royal Dublin Society*, **2A**, 1–11.
- Polarcus. 2011. *Final Acquisition Report, Barryroe 2011 3D*.
- Price, N.J. 1966. *Fault and Joint Development in Brittle and Semi-Brittle Rock*. Elsevier.
- Prive, E. 1986. *Seismic Interpretation and Gravity Modelling of BIRPS SWAT Lines 5 and 6*.
- Proffett, J.M. 1977. Cenozoic geology of the Yerington district, Nevada, and implications for the nature and origin of Basin and Range faulting. *Bulletin of the Geological Society of America*.
- Providence. 2018. *Standard Exploration Licence 1/11 Barryroe, North Celtic Sea Basin*.
- Quennell, A.M. 1959. Tectonics of the Dead Sea rift. *Proceedings of the 20th International Geological Congress, Mexico*, 385–403.
- Quennell, A.M. 1958. The structural and geomorphic evolution of the dead sea rift. *Quarterly Journal of the Geological Society of London*, **114**, 1–24.
- Quirk, D.G. & Pilcher, R.S. 2012. Flip-flop salt tectonics Alsop, G. I., Archer, S. G., Hartley, A. J., Grant, N. T. & Hodgkinson, R. (eds). *Salt Tectonics, Sediments and Prospectivity*.

- Quirk, D., Schødt, N., Lassen, B., Ings, S., Hsu, D., Hirsch, K. & von Nicolai, C. 2012. Salt tectonics on passive margins: Examples from Santos, Campos and Kwanza Basins. *Geological Society, London, Special Publications*, **363**, 207–244.
- Ramsay, J.G. & Huber, M.I. 1983. *The Techniques of Modern Structural Geology*. Lisle, R. J. (ed.). Academic Press.
- Rank-Friend, M. & Elders, C.F. 2004. The Evolution and Growth of Central Graben Salt Structures, Salt Dome Province, Danish North Sea. *Geological Society, London, Memoirs*, **29**, 149–164.
- Ransome, Frederick. L.; Emmons, Willian H.; Garrey, G.H. 1910. *Geology and Ore Deposits of the Bullfrog District, Nevada*.
- Rehrig, W.A. & Reynolds, S.J. 1980. Geologic and geochronologic reconnaissance of a northwest-trending zone of metamorphic core complexes in southern and western Arizona. *Memoir of the Geological Society of America*, **153**, 131–157.
- Remmelts, G. 1996. Salt tectonics in the southern North Sea, the Netherlands. *In: Geology of Gas and Oil under the Netherlands*. Springer Netherlands, 143–158.
- Robein, E. 2010. *Seismic Imaging: A Review of the Techniques, Their Principles, Merits and Limitations*. EAGE.
- Robertson, E.C. 1982. Continuous Formation of Gouge and Breccia During Fault Displacement. *In: Proceedings - Symposium on Rock Mechanics*.
- Robinson, E.A. & Clark, D. 2017. *Basic Geophysics*. Society of Exploration Geophysicists.

- Robinson, K.W., Shannon, P.M. & Young, D.G.G. 1981. The Fastnet Basin: integrated analysis. *In: Illing, L. V. & Hobson, G. D. (eds) Petroleum Geology Conference Series Vol 2*. Geological Society of London, 444–454.
- Robson, D.A. 1971. Structure of the Gulf of Suez (Clysmic Rift), with special reference to the eastern side. *Quarterly Journal of the Geological Society of London*, **155**, 247–276.
- Rodríguez-Salgado, P., Childs, C., Shannon, P.M. & Walsh, J.J. 2020. Structural evolution and the partitioning of deformation during basin growth and inversion: A case study from the Mizen Basin Celtic Sea, offshore Ireland. *Basin Research*, **32**, 830–853.
- Rosendahl, B.R. 1987. Architecture of continental rifts with special reference to East Africa. *Annual review of earth and planetary sciences.*, **15**.
- Rosendahl, B.R., Reynolds, D.J., et al. 1986. Structural expressions of rifting: Lessons from Lake Tanganyika, Africa. *In: Geological Society, London, Special Publications*.
- Rowell, P. 1995. Tectono-stratigraphy of the North Celtic Sea Basin. *In: Croker, P. F.; Shannon, P. M. (ed.) Geological Society, London, Special Publications*, 101–137.
- Ruffell, A.H. 1995. Seismic stratigraphic analysis of non-marine Lower Cretaceous strata in the Wessex and North Celtic Sea Basins. *Cretaceous Research*, **16**, 603–637.
- Ruffell, A.H. & Coward, M.P. 1992. Basement tectonics and their relationship to Mesozoic megasequences in the Celtic Seas and Bristol Channel area. *In: Parnell, J. (ed.) Geological Society, London, Special Publications*. 385–394.
- Sandwell, D.T., Müller, R.D., Smith, W.H.F., Garcia, E. & Francis, R. 2015. Marine Gravity from Satellite Altimetry.
http://topex.ucsd.edu/grav_outreach/index.html.

- Sans, M.R. & Koyi, H. 2001. Modelling the role of erosion in diapir development in contractional settings. *Memoir of the Geological Society of America*, **193**, 111–122.
- Sato, H. & Fehler, M.C. 2009. Attenuation of High-Frequency Seismic Waves. *In: Seismic Wave Propagation and Scattering in the Heterogeneous Earth*. Berlin, Heidelberg, Springer Berlin Heidelberg, 109–148.
- Schultz-Ela, D.D., Jackson, M.P.A. & Vendeville, B.C. 1993. Mechanics of active salt diapirism. *Tectonophysics*, **228**, 275–312.
- Scourse, J., Uehara, K. & Wainwright, A. 2009. Celtic Sea linear tidal sand ridges, the Irish Sea Ice Stream and the Fleuve Manche: Palaeotidal modelling of a transitional passive margin depositional system. *Marine Geology*, **259**, 102–111.
- Selley, R.C. & Sonnenberg, S.A. 2015. *Elements of Petroleum Geology*.
- Shannon, P.M. 1991. Tectonic framework and petroleum potential of the Celtic Sea, Ireland. *First Break*, **9**.
- Shannon, P.M. 1995. Permo-Triassic development of the Celtic Sea region, offshore Ireland Boldy, S. A. R. (ed.). *Geological Society, London, Special Publications*, **91**, 215–237.
- Shannon, P.M. & MacTiernan, B. 1993. Triassic prospectivity in the Celtic Sea, Ireland - a case history. *First Break*, **11**, 47–57.
- Shipton, Z.K., Soden, A.M., Kirkpatrick, J.D., Bright, A.M. & Lunn, R.J. 2006. How thick is a fault? Fault displacement-thickness scaling revisited. *In: Abercrombie, R. (ed.) Earthquakes: Radiated Energy and the Physics of Faulting*. AGU, 193–198.

- Solheim, A., Riis, F., et al. 1996. Impact of glaciations on basin evolution: data and models from the Norwegian margin and adjacent areas Introduction and summary. *Global and Planetary Change*, **12**, 1–9.
- Soliva, R. & Benedicto, A. 2004. A linkage criterion for segmented normal faults. *Journal of Structural Geology*, **26**, 2251–2267.
- Stephenson, M.A. 1983. *50/12-2A Well Evaluation and Regional Palaeogeographic Reconstruction*.
- Stewart, S.A. 2007. Salt tectonics in the North Sea Basin: a structural style template for seismic interpreters. In: *Geological Society, London, Special Publications*.
- Stewart, S.A. & Coward, M.P. 1995. Synthesis of salt tectonics in the southern North Sea, UK. *Marine and Petroleum Geology*, **12**, 457–475.
- Stuart, I.A. 1993. The geology of the North Morecambe Gas Field, East Irish Sea Basin. In: Parker, J. R. (ed.) *Petroleum Geology Conference Series Vol 4*. Geological Society of London, 883–895.
- Taber, D.R., Vickers, M.K. & Winn Jr., R.D. 1995. The definition of the Albian ‘A’ Sand reservoir fairway and aspects of associated gas accumulations in the North Celtic Sea Basin. In: Croker, P. F.; Shannon, P. M. (ed.) *Geological Society, London, Special Publications*, 227–244.
- Tappin, D.R., Chadwick, R.A., Jackson, A.A., Wingfield, R.T.R. & Smith, N.J.P. 1994. *The Geology of Cardigan Bay and the Bristol Channel*. British Geological Survey.
- Tari, G., Dellmour, R., Rodgers, E., Sultan, S., Al Atabi, A., Daud, F. & Salman, A. 2014. Seismic expression of salt tectonics in the Sab’atayn Basin, onshore Yemen. *Interpretation*, **2**, 91–100.

- ten Veen, J., Gessel, S.F. & Dulk, M. 2012. Thin-and thick-skinned salt tectonics in the Netherlands; A quantitative approach. *Geologie en Mijnbouw*, **91**, 447–464.
- Tommasi, A. & Vauchez, A. 2001. Continental rifting parallel to ancient collisional belts: an effect of the mechanical anisotropy of the lithospheric mantle. *Earth and Planetary Science Letters*, **185**, 199–210.
- Torabi, A. & Berg, S.S. 2011. Scaling of fault attributes: A review. *Marine and Petroleum Geology*, **28**, 1444–1460.
- Trusheim, F. 1960. MECHANISM OF SALT MIGRATION IN NORTHERN GERMANY'. *Bulletin of the American Association of Petroleum Geologists*, **23**, 1519–1540.
- Tucker, P.M. & Yorston, H.J. 1973. *Pitfalls in Seismic Interpretation*. Society of Exploration Geophysicists.
- Tucker, R.M. & Arter, G. 1987. The tectonic evolution of the North Celtic Sea and Cardigan Bay basins with special reference to basin inversion. *Tectonophysics*, **137**, 291–307.
- Tyrrell, S., Haughton, P.D.W., Souders, A.K., Daly, J.S. & Shannon, P.M. 2012. Large-scale, linked drainage systems in the NW European Triassic: insights from the Pb isotopic composition of detrital K-feldspar. *Journal of the Geological Society*, **169**, 279–295.
- UKOOA. 1999. *Guidance Notes on the Use of Co-Ordinate Systems in Data Management on the UKCS*.
- Underhill, J.R. & Partington, M.A. 1993. Jurassic thermal doming and deflation in the North Sea: implications of the sequence stratigraphic evidence. In: Parker, J. R. (ed.) *Petroleum Geology Conference Series Vol 4*. Geological Society of London, 337–345.

- van der Zee, W. & Urai, J.L. 2005. Processes of normal fault evolution in a siliciclastic sequence: A case study from Miri, Sarawak, Malaysia. *Journal of Structural Geology*, **27**, 2281–2300.
- Vendeville, B. & Jackson, M. 1992. The fall of diapirs during thin-skinned extension. *Marine and Petroleum Geology*, **9**, 354–371.
- Vendeville, B. & Jackson, M. 1992. The rise of diapirs during thin-skinned extension. *Marine and Petroleum Geology*, **9**, 331–354.
- Vendeville, B. & Jackson, M. 1993. Rates of Extension and Deposition Determine Whether Growth Faults or Salt Diapirs Form. In: *Society of Economic Paleontologists and Mineralogists. Gulf Coast Section. Foundation 14th Annual Research Conference*. 5–8.
- Vermeulen, N.J., Shannon, P.M., Landes, M. & Masson, F. 1999. Seismic Evidence for Subhorizontal Crustal Detachments Beneath the Irish Variscides. *Irish Journal of Earth Sciences*, **17**, 1–18.
- Walsh, J.J., Nicol, A. & Childs, C. 2002. An alternative model for the growth of faults. *Journal of Structural Geology*, **24**, 1669–1675.
- Walsh, J.J., Watterson, J., Bailey, W.R. & Childs, C. 1999. Fault relays, bends and branch-lines. *Journal of Structural Geology*, **21**, 1019–1026.
- Walsh, J.J. & Watterson, J. 1991. Geometric and kinematic coherence and scale effects in normal fault systems. In: *Geological Society, London, Special Publications*. 193–203.
- Walsh, J.J. & Watterson, J. 1988. Analysis of the relationship between displacements and dimensions of faults. *Journal of Structural Geology*, **10**, 239–247.
- Watterson, J. 1986. Fault dimensions, displacements and growth. *Pure and Applied Geophysics*, **124**, 365–373.

- Weglein, A.B. & Dragoset, W.H. 2005. *Multiple Attenuation*. Society of Exploration Geophysicists.
- Weglein, A.B., Gasparotto, F.A., Carvalho, P.M. & Stolt, R.H. 1997. An inverse-scattering series method for attenuating multiples in seismic reflection data. *Geophysics*, **62**, 1975–1989.
- Welch, M.J. & Turner, J.P. 2000. Triassic-Jurassic development of the St. George's Channel basin offshore Wales, UK. *Marine and Petroleum Geology*, **17**, 723–750.
- Wells, S. 2004. *Review Of 2D Data And Parameter Determination Study For Proposed 3D Survey - Seven Heads*.
- Wernicke, B. 1985. Uniform-sense normal simple shear of the continental lithosphere. *Canadian Journal of Earth Sciences*, **22**, 108–125.
- Wernicke, B. 1981. Low-angle normal faults in the Basin and Range Province: Nappe tectonics in an extending orogen. *Nature*, **291**, 645–648.
- White, N.J. & McKenzie, D. 1988. Formation of the 'steer's head' geometry of sedimentary basins by differential stretching of the crust and mantle. *Geology*, **16**, 250.
- Wibberley, C.A.J., Yielding, G. & Di Toro, G. 2008. Recent advances in the understanding of fault zone internal structure: A review. *In: Geological Society, London, Special Publications*.
- Williams, G.D., Powell, C.M. & Cooper, M.A. 1989. Geometry and kinematics of inversion tectonics. *In: Geological Society, London, Special Publications*. 3–15.
- Wise, D. U. ; Dunn, D. E. ; Engelder, J. T. ; Geiser, P. A. ; Hatcher, R. D. ; Kish, S. A. ; Odom, A. L. ; Schamel, S. 1984. Fault-related rocks, suggestions from terminology. *Geology*, **12**, 391–394.

- Withjack, M.O., Olson, J. & Peterson, E. 1990. Experimental Models of Extensional Forced Folds. *AAPG Bulletin*, **74**, 1038–1054.
- Wright, L.A. & Troxel, B.W. 1973. Shallow-fault interpretation of Basin and Range structure, southwestern Great Basin. *In*: De Jong, K. A. & Scholten, R. (eds) *Gravity and Tectonics*. Wiley and Sons, 397–407.
- Yilmaz, Ö. 2001. *Seismic Data Analysis*. Society of Exploration Geophysicists.
- Youash, Y. 1969. Tension tests on layered rocks. *Bulletin of the Geological Society of America*, **80**, 303–306.
- Ziegler, P.A. 1982. *Geological Atlas of Western and Central Europe*, 1st ed. Shell International Petroleum Maatschopij B.V. The Hague.
- Ziegler, P.A. 1989. Geodynamic model for Alpine intra-plate compressional deformation in Western and Central Europe Cooper, M. A. & Williams, G. D. (eds). *Geological Society, London, Special Publications*, **44**, 63–85.
- Ziegler, P.A. 1975. *The Geological Evolution of the North Sea Area in the Tectonic Framework of North Western Europe*.
- Ziegler, P.A. 1987. Celtic Sea-Western Approaches area: an overview. *Tectonophysics*, **137**, 285–289.

Appendix A

List of Wells Drilled in the North Celtic Sea Basin

	Well	Year	Licence	Basin	Operator	Status	Released
PRODUCTION	<u>48/20-2</u>	1989	<u>PL01</u>	NCSB	Marathon	Gas Producer	Yes
	<u>48/25-3</u>	1995	<u>PL01</u>	NCSB	Marathon	Gas Producer	Yes
	<u>48/25-4</u>	2001	<u>PL01</u>	NCSB	Marathon	Gas Producer	Yes
	<u>48/25-5</u>	2001	<u>PL01</u>	NCSB	Marathon	Gas Producer	Yes
	<u>48/24-5A</u>	2001	<u>Seven Heads Gas LU</u>	NCSB	Ramco Oil Ltd	Gas Producer	Yes
	<u>48/25-6</u>	2003	<u>PL01</u>	NCSB	Marathon	Gas Producer	Yes
	<u>48/24-6</u>	2003	<u>Seven Heads Gas Lease</u>	NCSB	Ramco Seven Heads Ltd	Gas Producer	Yes
	<u>48/24-7A</u>	2003	<u>Seven Heads Gas Lease</u>	NCSB	Ramco Seven Heads Ltd	Gas Producer	Yes
	<u>48/24-8</u>	2003	<u>Seven Heads Gas Lease</u>	NCSB	Ramco Seven Heads Ltd	Gas Producer	Yes
	<u>48/24-9</u>	2003	<u>Seven Heads Gas Lease</u>	NCSB	Ramco Seven Heads Ltd	Gas Producer	Yes
EXPLORATION AND APPRAISAL	<u>48/25-1</u>	1970	<u>PL01</u>	NCSB	Marathon	P & A	Yes
	<u>48/25-2</u>	1971	<u>PL01</u>	NCSB	Marathon	P & TA	Yes
	<u>50/11-1</u>	1971	<u>PL02</u>	NCSB	Marathon	P & A	Yes
	<u>48/20-1A</u>	1972	<u>PL01</u>	NCSB	Marathon	P & TA	Yes
	<u>56/20-1</u>	1972	<u>PL04</u>	NCSB	Esso	P & A	Yes
	<u>49/11-1</u>	1972	<u>PL05</u>	NCSB	Marathon	P & A	Yes
	<u>49/16-1</u>	1973	<u>PL01</u>	NCSB	Marathon	P & A	Yes
	<u>49/16-2</u>	1973	<u>PL01</u>	NCSB	Marathon	P & TA	Yes
	<u>48/30-1</u>	1973	<u>PL06</u>	NCSB	Esso	P & A	Yes
	<u>48/24-1</u>	1973	<u>PL08</u>	NCSB	Esso	P & A	Yes
	<u>56/14-1</u>	1974	<u>PL04</u>	NCSB	Esso	P & A	Yes
	<u>48/28-1</u>	1974	<u>PL08</u>	NCSB	Esso	P & A	Yes
	<u>49/13-1</u>	1974	<u>PL09</u>	NCSB	Marathon	P & A	Yes
	<u>49/14-1</u>	1974	<u>PL10</u>	NCSB	Marathon	P & A	Yes
	<u>50/11-2</u>	1975	<u>PL02</u>	NCSB	Marathon	P & A	Yes
	<u>50/12-1</u>	1975	<u>PL02</u>	NCSB	Marathon	P & A	Yes
	<u>49/14-2</u>	1975	<u>PL10</u>	NCSB	Marathon	P & A	Yes
	<u>56/12-1</u>	1975	<u>PL11</u>	NCSB	Esso	P & A	Yes
	<u>47/30-1</u>	1975	<u>PL12</u>	NCSB	Esso	P & A	Yes
	<u>49/20-1</u>	1975	<u>PL13</u>	NCSB	Marathon	P & A	Yes

	<u>48/23-1</u>	1976	<u>PL08</u>	NCSB	Esso	P & A	Yes
	<u>50/3-1</u>	1976	<u>PL14</u>	NCSB	Marathon	P & A	Yes
	<u>57/6-1</u>	1976	<u>PL15</u>	NCSB	Esso	P & A	Yes
	<u>48/24-2</u>	1978	<u>PL08</u>	NCSB	Esso	P & A	Yes
	<u>48/22-1A</u>	1978	<u>PL18</u>	NCSB	Esso	P & A	Yes
	<u>49/17-1y</u>	1979	<u>PL19</u>	NCSB	Marathon	P & A	Yes
	<u>56/9-1</u>	1979	<u>PL20</u>	NCSB	Elf	P & A	Yes
	<u>50/12-2</u>	1981	<u>PL02</u>	NCSB	BP	P & A	Yes
	<u>49/9-1</u>	1983	<u>EL2/81</u>	NCSB	Gulf	P & A	Yes
	<u>49/9-2</u>	1983	<u>EL2/81</u>	NCSB	Gulf	P & TA	Yes
	<u>49/9-3y</u>	1983	<u>EL2/81</u>	NCSB	Gulf	P & TA	Yes
	<u>56/18-1</u>	1983	<u>EL2/82</u>	NCSB	Gulf	P & A	Yes
	<u>48/26-1</u>	1983	<u>EL3/82</u>	NCSB	Elf	P & A	Yes
	<u>57/7-1</u>	1983	<u>EL4/82</u>	NCSB	Burmah	P & A	Yes
	<u>57/2-1</u>	1983	<u>EL9/82</u>	NCSB	Total	P & A	Yes
	<u>57/9-1</u>	1984	<u>EL1/83</u>	NCSB	Conoco	P & A	Yes
	<u>49/10-1z</u>	1984	<u>EL2/81</u>	NCSB	Gulf	P & A	Yes
	<u>48/19-1</u>	1984	<u>EL2/82</u>	NCSB	Gulf	P & A	Yes
	<u>49/19-1</u>	1984	<u>PL10</u>	NCSB	Marathon	P & A	Yes
	<u>47/29-1</u>	1985	<u>EL3/82</u>	NCSB	Arco	P & A	Yes
	<u>50/6-1</u>	1985	<u>EL5/82</u>	NCSB	Gulf	P & A	Yes
	<u>48/18-1</u>	1985	<u>EL6/82</u>	NCSB	BP	P & A	Yes
	<u>49/15-1</u>	1985	<u>PL02</u>	NCSB	Esso	P & A	Yes
	<u>49/14-3</u>	1985	<u>PL10</u>	NCSB	Esso	P & A	Yes
	<u>42/21-1</u>	1986	<u>EL2/81</u>	NCSB	Gulf	P & A	Yes
	<u>50/7-1</u>	1986	<u>PL02</u>	NCSB	Marathon	P & A	Yes
	<u>49/13-2</u>	1986	<u>PL09</u>	NCSB	Marathon	P & A	Yes
	<u>50/3-2</u>	1986	<u>PL14</u>	NCSB	Enterprise Oil	P & A	Yes
	<u>49/9-4</u>	1987	<u>EL2/81</u>	NCSB	BP	P & A	Yes
	<u>50/6-2</u>	1987	<u>EL5/82</u>	NCSB	BP	P & A	Yes
	<u>57/2-2</u>	1987	<u>EL9/82</u>	NCSB	Total	P & A	Yes
	<u>49/9-5</u>	1989	<u>EL2/81</u>	NCSB	BP	P & A	Yes
	<u>48/20-3</u>	1989	<u>PL01</u>	NCSB	Marathon	P & A	Yes
	<u>48/20-4</u>	1989	<u>PL01</u>	NCSB	Marathon	P & A	Yes
	<u>48/20-5</u>	1989	<u>PL01</u>	NCSB	Marathon	P & A	Yes
	<u>50/13-1</u>	1990	<u>EL10/85</u>	NCSB	Conoco	P & A	Yes
	<u>48/24-3</u>	1990	<u>PL08</u>	NCSB	Marathon	P & A	Yes
	<u>48/24-4</u>	1990	<u>PL08</u>	NCSB	Marathon	P & A	Yes
	<u>50/3-3</u>	1991	<u>PL14</u>	NCSB	Marathon	P & A	Yes
	<u>48/19-2</u>	1992	<u>EL1/90</u>	NCSB	Bula	P & A	Yes
	<u>48/30-2</u>	1992	<u>PL06</u>	NCSB	Marathon	P & A	Yes

<u>50/12-3</u>	1993	<u>EL1/93</u>	NCSB	Mobil	P & A	Yes
<u>50/2-1</u>	1993	<u>EL3/93</u>	NCSB	Marathon	P & A	Yes
<u>48/28-2</u>	1993	<u>PL08</u>	NCSB	Marathon	P & A	Yes
<u>50/10-1</u>	1994	<u>EL1/94</u>	NCSB	Mobil	P & A	Yes
<u>56/15-1</u>	1995	<u>EL1/95</u>	NCSB	Chevron	P & A	Yes
<u>49/11-2</u>	1995	<u>EL10/95</u>	NCSB	Marathon	P & A	Yes
<u>50/6-3</u>	1995	<u>EL4/93</u>	NCSB	Marathon	P & A	Yes
<u>49/9-6z</u>	2000	<u>Helvick Lease</u>	NCSB	Providence Resources plc	P & TA	Yes
<u>49/9-6</u>	2000	<u>Helvick Lease</u>	NCSB	Providence Resources plc	Plugged Back	Yes
<u>48/24-5</u>	2001	<u>Seven Heads Gas LU</u>	NCSB	Ramco Oil Ltd	P & A	Yes
<u>48/23-2</u>	2003	<u>Seven Heads Gas Lease</u>	NCSB	Ramco Seven Heads Ltd	P & A	Yes
<u>48/24-7</u>	2003	<u>Seven Heads Gas Lease</u>	NCSB	Ramco Seven Heads Ltd	P & A	Yes
<u>49/26-1A</u>	2004	<u>LO03/1</u>	NCSB	Providence Resources plc	P & A	Yes
<u>49/23-1</u>	2006	<u>EL4/05</u>	NCSB	Island Oil and Gas Plc	P & TA	Yes
<u>48/23-3</u>	2006	<u>Seven Heads Gas Lease</u>	NCSB	Island Oil and Gas Plc	P & TA	Yes
<u>50/11-3</u>	2007	<u>EL2/07</u>	NCSB	Providence Resources Plc	P & TA	Yes
<u>49/23-2 2z</u>	2007	<u>EL4/05</u>	NCSB	Island Oil and Gas Plc	P & TA	Yes
<u>57/2-3</u>	2007	<u>EL5/05</u>	NCSB	Island Oil and Gas Plc	P & TA	Yes
<u>50/11-4</u>	2008	<u>EL2/07</u>	NCSB	Providence Resources Plc	P & A	Yes
<u>50/6-4</u>	2008	<u>EL2/07</u>	NCSB	Providence Resources Plc	P & TA	Yes
<u>48/24-10z</u>	2011	<u>EL1/11</u>	NCSB	Providence Resources	P & TA	Yes
<u>49/11-3</u>	2015	<u>EL4/07</u>	NCSB	PSE Seven Heads Limited	P & A	No

Appendix B

Seismic lines available which were fully or partially within the study area.

Count	Line Name	Year	Data Quality	Length(km)
1	EM311	1977	Poor Quality	48.97
2	EM312	1977	Poor Quality	29.149
3	EM313	1977	Poor Quality	27.816
4	EM314	1977	Poor Quality	24.698
5	EM315	1977	Poor Quality	24.938
6	EM316	1977	Poor Quality	27.246
7	EM317	1977	Poor Quality	20.166
8	NCS-116	1981	Average Quality	49.26
9	NCS-120	1981	Average Quality	72.177
10	NCS-122	1981	Average Quality	55.276
11	NCS-127	1981	Average Quality	72.789
12	NCS-132	1981	Average Quality	32.39
13	NCS-136	1981	Average Quality	84.726
14	NCS-202	1981	Average Quality	92.72
15	NCS-203	1981	Average Quality	65.166
16	NCS-204	1981	Average Quality	88.516
17	NCS-206	1981	Average Quality	64.356
18	NCS-33	1981	Average Quality	24.762
19	NCS-35	1981	Average Quality	25.098
20	NCS-36	1981	Average Quality	13.441
21	NCS-37	1981	Average Quality	25.171
22	NCS-38	1981	Average Quality	22.256
23	NCS-39	1981	Average Quality	25.377
24	NCS-40	1981	Average Quality	29.765
25	NCS-41A	1981	Average Quality	93.727
26	NCS-44	1981	Average Quality	21.004
27	NCS-45	1981	Average Quality	47.721
28	NCS-46	1981	Average Quality	62.883
29	NCS-46A	1981	Average Quality	23.218
30	NCS-50	1981	Average Quality	9.657
31	NCS-51	1981	Average Quality	45.658
32	NCS-52	1981	Average Quality	23.215
33	NCS-53	1981	Average Quality	9.867
34	NCS-54	1981	Average Quality	9.879
35	NCS-55	1981	Average Quality	47.758

36	NCS-56	1981	Average Quality	18.55
37	NCS-57	1981	Average Quality	17.237
38	NCS-58	1981	Average Quality	46.477
39	NCS-59	1981	REPROCESSED	101.321
40	NCS-60	1981	Average Quality	71.424
41	NCS-61	1981	Average Quality	9.799
42	NCS-61A	1981	REPROCESSED	83.338
43	NCS-62	1981	Average Quality	58.984
44	NCS-64	1981	REPROCESSED	82.802
45	NCS-65	1981	Average Quality	46.549
46	NCS-67	1981	REPROCESSED	77.973
47	NCS-70	1981	Average Quality	27.111
48	NCS-71	1981	Average Quality	15.86
49	NCS-73	1981	Average Quality	25.063
50	NCS-74	1981	Average Quality	23.771
51	82-48-01	1982	Average Quality	17.917
52	82-48-02	1982	Average Quality	21.162
53	82-48-03	1982	Average Quality	21.288
54	82-48-04	1982	Average Quality	16.29
55	82-48-05	1982	Average Quality	22.673
56	82-48-06	1982	Average Quality	36.277
57	82-48-07	1982	Average Quality	23.486
58	82-48-08	1982	Average Quality	19.902
59	82-48-09	1982	Average Quality	25.673
60	82-48-10	1982	Average Quality	36.337
61	82-48-11	1982	Average Quality	25.662
62	82-48-12	1982	Average Quality	21.899
63	82-48-13	1982	Average Quality	24.178
64	82-48-14	1982	Average Quality	36.267
65	82-48-15	1982	Average Quality	26.799
66	82-48-16	1982	Average Quality	21.659
67	82-48-17	1982	Average Quality	18.276
68	82-48-19	1982	Average Quality	25.41
69	82-48-21	1982	Average Quality	20.035
70	82-48-23	1982	Average Quality	24.907
71	82-48-25	1982	Average Quality	30.796
72	82-48-27	1982	Average Quality	23.785
73	82-48-29	1982	Average Quality	25.671
74	82-48-31	1982	Average Quality	23.782
75	82-48-33	1982	Average Quality	26.171
76	CSN82-09A	1982	Average Quality	27.707
77	CSN82-11	1982	Average Quality	50.488
78	CSN82-13	1982	Average Quality	39.583

79	CSN82-17	1982	Average Quality	17.486
80	CSN82-19	1982	Average Quality	47.04
81	CSN82-21	1982	Average Quality	35.439
82	CSN82-25	1982	Average Quality	17.672
83	CSN82-29	1982	Average Quality	36.025
84	CSN82-3	1982	Average Quality	41.15
85	CSN82-33	1982	Average Quality	33.38
86	CSN82-33 N	1982	Average Quality	25.695
87	CSN82-35	1982	Average Quality	29.028
88	CSN82-37A	1982	Average Quality	30.892
89	CSN82-37B	1982	Average Quality	10.501
90	CSN82-41	1982	Average Quality	28.3
91	CSN82-46	1982	Average Quality	24.475
92	CSN82-60	1982	Average Quality	20.412
93	CSN82-61	1982	Average Quality	7.902
94	CSN82-63	1982	Average Quality	11.692
95	CSN82-64	1982	Average Quality	21.906
96	CSN82-66	1982	Average Quality	22.482
97	CSN82-67	1982	Average Quality	14.203
98	CSN82-68	1982	Average Quality	24.117
99	CSN82-68A	1982	Average Quality	13.76
100	CSN82-69	1982	Average Quality	16.843
101	CSN82-71	1982	Average Quality	20.38
102	CSN82-73	1982	Average Quality	12.914
103	CSN82-75A	1982	Average Quality	15.57
104	CSN82-75B	1982	Average Quality	16.068
105	CSN82-76	1982	Average Quality	12.333
106	CSN82-83A	1982	Average Quality	10.541
107	CSN82-83B	1982	Average Quality	21.729
108	CSN82-91B	1982	Average Quality	18.22
109	CSN82-96B	1982	Average Quality	18.715
110	G83-57-02	1983	Good quality	22.838
111	G83-57-04	1983	Good quality	27.839
112	G83-57-05	1983	Good quality	15.291
113	G83-57-06	1983	Good quality	18.941
114	G83-57-07	1983	Good quality	14.793
115	G83-57-08	1983	Good quality	21.269
126	MP-84-02	1984	Poor Quality	21.32
127	MP-84-04	1984	Poor Quality	17.887
128	MP-84-04A	1984	Poor Quality	16.128
129	MP-84-06	1984	Poor Quality	25.468
130	MP-84-08	1984	Poor Quality	35.031
131	MP-84-10	1984	Poor Quality	17.174

132	MP-84-11A	1984	Poor Quality	26.07
133	MP-84-12	1984	Poor Quality	18.879
134	MP-84-13	1984	Poor Quality	23.392
135	MP-84-14	1984	Poor Quality	24.495
136	MP-84-15	1984	Poor Quality	26.675
137	MP-84-16	1984	Poor Quality	31.267
138	MP-84-17	1984	Poor Quality	16.233
139	MP-84-18	1984	Poor Quality	27.124
140	MP-84-19	1984	Poor Quality	14.697
141	MP-84-20	1984	Poor Quality	12.759
142	MP-84-21	1984	Poor Quality	10.783
143	MP-84-25	1984	Poor Quality	21.184
144	MP-84-27	1984	Poor Quality	21.786
145	MP-84-29	1984	Poor Quality	14.685
146	MP-84-31	1984	Poor Quality	18.901
147	MP-84-33	1984	Poor Quality	14.794
148	MP-84-35	1984	Poor Quality	18.759
149	MP-84-37	1984	Poor Quality	11.614
116	G85-48-01	1985	Good quality	17.188
117	G85-48-02	1985	Good quality	11.904
118	G85-48-03	1985	Good quality	18.8
119	G85-48-04	1985	Good quality	16.846
120	G85-48-04A	1985	Good quality	6.923
121	G85-48-05	1985	Good quality	18.539
122	G85-48-06	1985	Good quality	20.218
123	G85-48-07	1985	Good quality	18.083
124	G85-48-09	1985	Good quality	17.703
125	G85-48-15	1985	Good quality	15.982
150	BP87-48-22	1987	Good quality	19.986
151	BP87-48-32	1987	Good quality	6.464
152	sh88-02	1988	Poor Quality	7.413
153	sh88-03a	1988	Poor Quality	8.466
154	sh88-07	1988	Poor Quality	14.901
155	sh88-10	1988	Poor Quality	10.428
156	sh88-11	1988	Poor Quality	5.983
157	sh88-13	1988	Poor Quality	6.617
158	sh88-15	1988	Poor Quality	14.748
159	sh88-16	1988	Poor Quality	5.589
160	sh88-17	1988	Poor Quality	7.424
161	sh88-19	1988	Poor Quality	10.667
162	sh88-21	1988	Poor Quality	10.752
163	sh88-22	1988	Poor Quality	4.773
164	sh88-23	1988	Poor Quality	16.347

165	sh88-24	1988	Poor Quality	13.247
166	sh88-25	1988	Poor Quality	19.242
167	sh88-26	1988	Poor Quality	4.609
168	sh88-27b	1988	Poor Quality	8.086
169	sh88-29	1988	Poor Quality	8.055
170	sh88-30	1988	Poor Quality	4.626
171	sh88-31	1988	Poor Quality	36.23
172	sh88-33	1988	Poor Quality	17.5
173	sh88-35a	1988	Poor Quality	4.896
174	sh88-36	1988	Poor Quality	7.543
175	sh88-37	1988	Poor Quality	7.107
176	sh88-38	1988	Poor Quality	4.659
177	sh88-3a	1988	Poor Quality	8.457
178	sh88-5	1988	Poor Quality	4.568
179	sh88-7	1988	Poor Quality	14.873
180	sh88-72	1988	Poor Quality	15.547
181	sh88-9	1988	Poor Quality	6.63
182	MIL90_001	1990	Good quality	37.513
183	MIL90_002	1990	Good quality	37.513
184	MIL90_003	1990	Good quality	37.733
185	MIL90_004	1990	Good quality	37.21
186	MIL90_005	1990	Good quality	37.69
187	MIL90_006	1990	Good quality	45.625
188	MIL90_007	1990	Good quality	45.092
189	MIL90_008	1990	Good quality	45.092
190	MIL90_009	1990	Good quality	45.083
191	MIL90_010	1990	Good quality	45.134
192	MIL90_012	1990	Good quality	45.075
193	MIL90_013	1990	Good quality	44.987
194	MIL90_014	1990	Good quality	44.75
195	MIL90_015	1990	Good quality	43.87
196	MIL90_016	1990	Good quality	43.27
197	MIL90_017	1990	Good quality	42.632
198	MIL90_018	1990	Good quality	41.439
199	MIL90_019	1990	Good quality	45.499
200	MIL90_020	1990	Good quality	18.76
201	MIL90_021	1990	Good quality	39.317
202	MIL90_022	1990	Good quality	20.568
203	MIL90_086	1990	Good quality	28.795
204	MIL90_087	1990	Good quality	27.132
205	MIL90_105	1990	Good quality	48.949
206	MIL90_112	1990	Good quality	41.758
207	MIL90_113	1990	Good quality	40.334

208	MIL90_114	1990	Good quality	16.566
209	MIL90_115	1990	Good quality	26.961
210	MIL90_117	1990	Good quality	23.786
211	MIL90_119	1990	Good quality	20.248
212	MIL90_121	1990	Good quality	30.409
213	MIL90_122	1990	Good quality	41.511
214	MIL90_124	1990	Good quality	26.83
215	ACS-93-01	1993	Good quality	74.542
216	ACS-93-02	1993	Good quality	76.261
217	ACS-93-03	1993	Good quality	76.333
218	ACS-93-04	1993	Good quality	89.284
219	ARC95_001	1995	Good quality	19.087
220	ARC95_002_-02A	1995	Good quality	27.411
221	ARC95_003_03A	1995	Good quality	27.562
222	ARC95_004_04A	1995	Good quality	29.686
223	ARC95_005	1995	Good quality	31.137
224	ARC95_006	1995	Good quality	35.742
225	ARC95_007_07A	1995	Good quality	33.866
226	ARC95_008	1995	Good quality	30.316
227	ARC95_009_09A	1995	Good quality	33.307
228	ARC95_010	1995	Good quality	29.505
229	ARC95_011_-11A-11B	1995	Good quality	47.757
230	ARC95_012	1995	Good quality	23.627
231	ARC95_013	1995	Good quality	39.334
232	ARC95_014	1995	Good quality	21.646
233	ARC95_015	1995	Good quality	48.235
234	ARC95_016	1995	Good quality	21.262
235	ARC95_017	1995	Good quality	38.54
236	ARC95_018_18A	1995	Good quality	38.658
237	ARC95_019	1995	Good quality	27.579
238	ARC95_020	1995	Good quality	47.739
239	ARC95_021	1995	Good quality	47.862
240	ARC95_022_22C-22D	1995	Good quality	51.935
241	shds-97-12	1997	Poor Quality	18.449
242	shds-97-14	1997	Poor Quality	18.451
243	shds-97-16	1997	Poor Quality	18.438
244	shds-97-18	1997	Poor Quality	18.463
245	shds-97-20	1997	Poor Quality	18.45
246	shds-97-22	1997	Poor Quality	18.451
247	shds-97-24_24a	1997	Poor Quality	23.673
248	shds-97-26_26a	1997	Poor Quality	18.45

249	shds-97-28_28a	1997	Poor Quality	18.45
250	shds-97-31	1997	Poor Quality	12.274
251	shds-97-35	1997	Poor Quality	12.276
252	shds-97-37	1997	Poor Quality	12.274
253	shds-97-39	1997	Poor Quality	12.274
254	shds-97-41	1997	Poor Quality	12.276
255	shds-97-43	1997	Poor Quality	12.275
256	shds-97-45	1997	Poor Quality	12.277
257	shds-97-47	1997	Poor Quality	12.276
258	shds-97-49	1997	Poor Quality	12.277
259	shds-97-51	1997	Poor Quality	12.274
260	shds-97-53	1997	Poor Quality	12.276
261	shds-97-55_55a	1997	Poor Quality	12.276
262	shds-97-57_57a	1997	Poor Quality	12.283
263	shds-97-59a	1997	Poor Quality	12.275
264	shds-97-61	1997	Poor Quality	12.274
265	shds-97-63	1997	Poor Quality	12.274
266	shds-97-65	1997	Poor Quality	12.275
267	shds-97-82a	1997	Poor Quality	20.091
268	SGC06-139964	2006	MODERN PROCESSING	219.34
269	SGC06-140469	2006	MODERN PROCESSING	96.405
270	SGC06-141827	2006	MODERN PROCESSING	201.521
271	SGC06-143761	2006	MODERN PROCESSING	197.543
272	SGC06-553689	2006	MODERN PROCESSING	86.901
273	SGC06-554791	2006	MODERN PROCESSING	86.52
274	SGC06-556892	2006	MODERN PROCESSING	70.25
275	LOG08-2110-A009	2008	Good quality	15.951
276	LOG08-2111-A017	2008	Good quality	16.446
277	LOG08-2112-A011	2008	Good quality	15.929
278	LOG08-2113-A013	2008	Good quality	21.686
279	LOG08-2114-A010	2008	Good quality	21.122
280	LOG08-2115-A015	2008	Good quality	20.994
281	LOG08-2116-A012	2008	Good quality	20.926
282	LOG08-2117-A016	2008	Good quality	20.896
283	LOG08-2118-A018	2008	Good quality	21.161
284	LOG08-2119-A020	2008	Good quality	21.621
285	LOG08-2120-A024	2008	Good quality	21.828

286	LOG08-2121-A019	2008	Good quality	20.995
287	LOG08-2122-A021	2008	Good quality	21.023
288	LOG08-2123-A023	2008	Good quality	16.131
289	LOG08-2124-A025	2008	Good quality	14.243
290	LOG08-2125-A022	2008	Good quality	13.489
291	LOG08-2126-B026	2008	Good quality	18.516
292	LOG08-2127-A007	2008	Good quality	28.41
293	LOG08-2128-A001	2008	Good quality	30.988
294	LOG08-2129-A008	2008	Good quality	31.111
295	LOG08-2130-A002_B003	2008	Good quality	31.061
296	LOG08-2131-A004	2008	Good quality	30.87
297	LOG08-2132-A005	2008	Good quality	25.17
298	LOG08-2501-A030	2008	Good quality	17.09
299	LOG08-2502-A028	2008	Good quality	19.026
300	LOG08-2503-A029	2008	Good quality	18.983
301	LOG08-2504-A027	2008	Good quality	18.789
302	LOG08-2505-A006	2008	Good quality	19.956
303	LOG08-2506-A034	2008	Good quality	18.002
304	LOG08-2507-A032	2008	Good quality	23.298
305	LOG08-2508-A031	2008	Good quality	22.934
306	LOG08-2509-A033	2008	Good quality	21.436

Appendix C

List of Wells Available Within the Study Area

	Well	Year	Licence	Formation age at TD	Operator	Status
PRODUCTION	<u>48/24-5A</u>	2001	<u>Seven Heads Gas LU</u>	Barremian	Ramco Oil Ltd	Gas Producer
	<u>48/24-6</u>	2003	<u>Seven Heads Gas Lease</u>	Barremian	Ramco Seven Heads Ltd	Gas Producer
	<u>48/24-7A</u>	2003	<u>Seven Heads Gas Lease</u>	Barremian	Ramco Seven Heads Ltd	Gas Producer
	<u>48/24-8</u>	2003	<u>Seven Heads Gas Lease</u>	Barremian	Ramco Seven Heads Ltd	Gas Producer
	<u>48/24-9</u>	2003	<u>Seven Heads Gas Lease</u>	Barremian	Ramco Seven Heads Ltd	Gas Producer
EXPLORATION AND APPRAISAL	<u>47/29-1</u>	1985	<u>EL3/82</u>	Rhaetian	Arco	P & A
	<u>47/30-1</u>	1975	<u>PL12</u>	Tithonian	Esso	P & A
	<u>48/18-1</u>	1985	<u>EL6/82</u>	Tithonian	BP	P & A
	<u>48/19-1</u>	1984	<u>EL2/82</u>	Sinemurian	Gulf	P & A
	<u>48/22-1A</u>	1978	<u>PL18</u>	Tithonian	Esso	P & A
	<u>48/23-1</u>	1976	<u>PL08</u>	Tithonian	Esso	P & A
	<u>48/23-2</u>	2003	<u>Seven Heads Gas Lease</u>	Aptian-Barremian	Ramco Seven Heads Ltd	P & A
	<u>48/23-3</u>	2006	<u>Seven Heads Gas Lease</u>	Barremian	Island Oil and Gas Plc	P & TA
	<u>48/24-1</u>	1973	<u>PL08</u>	Tithonian	Esso	P & A
	<u>48/24-10z</u>	2011	<u>EL1/11</u>	Berriasian	Providence Resources	P & TA
	<u>48/24-2</u>	1978	<u>PL08</u>	Berriasian	Esso	P & A
	<u>48/24-3</u>	1990	<u>PL08</u>	Tithonian	Marathon	P & A
	<u>48/24-4</u>	1990	<u>PL08</u>	Tithonian	Marathon	P & A
	<u>48/26-1</u>	1983	<u>EL3/82</u>	Tithonian	Elf	P & A
	<u>48/28-1</u>	1974	<u>PL08</u>	Berriasian	Esso	P & A
	<u>48/28-2</u>	1993	<u>PL08</u>	Berriasian	Marathon	P & A
	<u>48/30-1</u>	1973	<u>PL06</u>	Carboniferous	Esso	P & A
	<u>48/30-2</u>	1992	<u>PL06</u>	Toarcian	Marathon	P & A
	<u>49/26-1A</u>	2004	<u>LO03/1</u>	Toarcian	Providence Resources plc	P & A
	<u>57/2-1</u>	1983	<u>EL9/82</u>	?Hettangian?	Total	P & A
	<u>57/2-2</u>	1987	<u>EL9/82</u>	?Pleinsbachian?	Total	P & A
	<u>57/6-1</u>	1976	<u>PL15</u>	?Bajocian?	Esso	P & A
	<u>57/7-1</u>	1983	<u>EL4/82</u>	Norian	Burmah	P & A
	<u>57/9-1</u>	1984	<u>EL1/83</u>	Carboniferous	Conoco	P & A

Appendix D

Formation Tops for Depth Conversion

Well	Layer 1 Water Column & Cenozoic			Layer 2 Upper Cretaceous			Layer 3 Lower Cretaceous		
	TWT (s)	TVDSS (m)	Int Vel	TWT (s)	TVDSS (m)	Int Vel	TWT (s)	TVDSS (m)	Int Vel
47/29-01	0.309	282.1	1825.7	0.578	705.5	3148.1	0.744	984.4	3360.8
47/30-1	0.174	154.1	1771.1	0.631	966.6	3555.8	1.126	1837.1	3517.2
48/19-1	0.106	112.9	2130.1	0.523	798.4	3287.8	1.032	1624.9	3247.5
48/22-1a	0.132	152.4	2309.1	0.744	1203.5	3434.9	1.349	2484.2	4233.6
48/23-1	0.126	103.9	1649.8	0.427	702.5	3977.0	1.219	2272.3	3964.2
48/28-2	0.127	104.2	1641.6	0.473	853.5	4331.0			
48/30-1	0.127	103.3	1627.2	0.567	918.4	3704.8	0.987	1670.9	3583.4
57/2-1	0.215	177.0	1646.5	0.545	776.5	3633.3	1.162	1877.0	3567.2
57/2-2	0.209	174.4	1669.2	0.429	685.4	4645.5	1.249	2119.9	3498.7
57/6-1	0.231	189.1	1636.8	0.301	332.1	4085.7	1.085	1762.8	3649.9
57/7-1	0.251	194.2	1547.8	0.255	194.2		0.818	1064.3	3090.6
57/9-1	0.172	145.9	1696.5	0.417	516.4	3024.5	0.808	1178.4	3386.1

Well	Layer 4 Upper Jurassic			Layer 5 Lower Jurassic			Layer 6 Triassic		
	TWT (s)	TVDSS (m)	Int Vel	TWT (s)	TVDSS (m)	Int Vel	TWT (s)	TVDSS (m)	Int Vel
47/29-01	1.347	2126.7	3788.7	1.806	3019.6	3890.5			
47/30-1									
48/19-1	1.908	3245.4	3699.8						
48/22-1a									
48/23-1									
48/28-2									
48/30-1	1.058	1752.3	2293.6	1.402	2358.9	3526.5			
57/2-1	1.351	2169.5	3095.4						
57/2-2	1.477	2659.1	4729.8						
57/6-1	1.223	2042.2	4049.0						
57/7-1	0.982	1386.9	3934.2	1.608	2685.7	4149.8			
57/9-1	0.857	1264.9	3531.6	0.894	1342.4	4189.2	1.45	2461.4	4025.2

Appendix E.1

Appendix E.2

Appendix E.3

Appendix E.4

Appendix E.5

Appendix E.6

Appendix F.1

Appendix F.2

Appendix F.3

Appendix F.4

Appendix F.5

Appendix F.6

Appendix G.1

Appendix G.2

Appendix G.3

Appendix G.4

Appendix G.5

Appendix G.6